

Supramolecular Hydrogels for Drug Delivery Applications

Anna Katherine Patterson

Doctor of Philosophy

University of York

Chemistry

July 2021

Abstract

Low molecular weight gelators (LMWGs) form gels through a series of non-covalent interactions, creating a network that traps solvent, preventing flow. Due to the reversible nature of the interactions, these materials are typically highly responsive to external stimuli, making them attractive for high-tech applications, particularly in the biomedical field.

Despite significant progress in this area, it is still challenging to design a gelator with the required properties for an application from scratch. This research therefore aims to develop novel materials, focussing on drug delivery applications, exploiting multiple strategies to achieve this.

We initially focussed on the dibenzylidene sorbitol derivative DBS-CONHNH₂, a hydrogelator capable of interaction with additives – but mechanically weak. This was therefore combined with a novel hydrogelator MBS-CO₂Me – which increased the robustness of the material. Both the mechanical and thermal properties could be tuned by varying the proportions of the two gelators. Additionally, the gel was capable of pH responsive release of naproxen, as well as encapsulation and release of atorvastatin.

The impact of sugar chirality on the behaviour of the gelators was then investigated, with DBS-CONHNH₂ synthesised using the L-sorbitol in place of the natural D sugar. This was shown to have the same properties as the D-DBS-CONHNH₂, as would be expected, with the exception of response to polarised light. The effect of encapsulating chiral additives within each enantiomer was then investigated, with small effects on the properties of the materials observed.

Finally, further characterisation of a previously reported gelator, based on glutamine amide, was carried out – with particular attention paid to the self-healing rheological properties of the gel. This investigation was carried out both for the gel alone, and for the gel with L-DOPA incorporated. As part of a collaboration, these gels were tested in early stage *in vivo*, for nasal delivery of L-DOPA to the brain, as a treatment for Parkinson's Disease. These early-stage tests indicated promise of these hydrogels as delivery vehicles for delivery of active agents to the brain.

Table of Contents

Acknowledgements	xxv
Declaration.....	xxvi
1. Chapter 1: Introduction	1
1.1 Introduction to Low Molecular Weight Gelators.....	1
1.2 Applications of Supramolecular Gels.....	3
1.2.1 Early Applications	3
1.2.2 Use of Supramolecular Gels as Antibiotic Agents	4
1.2.3 Use of Supramolecular Gels for Wound Healing.....	9
1.2.4 Supramolecular Gels for Cell Culture and Tissue Engineering	10
1.2.5 Use of Supramolecular Hydrogels for Drug Delivery.....	15
1.3 Modification of Gelator Molecules.....	24
1.3.1 Important Factors for Gelation.....	24
1.3.2 Common Types of Gelator Molecule.....	25
1.3.3 Design for Drug Delivery.....	35
1.3.1 Effects of Chirality on Self-Assembly	39
1.4 Two-Component Gel Systems.....	42
1.4.1 Development of Two-Component Systems.....	46
1.4.2 Chirality in Two-Component Systems	49
1.4.3 Mixtures of Enantiomers	51
1.4.4 Applications of Two-Component Gels	53
1.5 Hybrid Gel Systems	55
1.5.1 Polymer Gelators and LMWGs	55
1.5.2 Mixtures of LMWGs.....	61
1.6 Project Aims.....	66
2. Chapter 2: Hybrid Supramolecular Hydrogels	69
2.1 Synthesis of DBS-CONH ₂ and MBS-CO ₂ Me	69
2.2 Investigation of MBS-CO ₂ Me as a Hydrogel	73

2.2.1 Gelation and T_{gel} Testing of MBS-CO ₂ Me Hydrogels	73
2.2.2 Rheology of MBS-CO ₂ Me Hydrogels	76
2.2.3 Circular dichroism studies of MBS-CO ₂ Me.....	82
2.2.4 Imaging of MBS-CO ₂ Me.....	83
2.2.5 Release From MBS-CO ₂ Me Hydrogels.....	86
2.3 Development of Hybrid Hydrogels	88
2.3.1 Gelation and T_{gel} Testing of Hybrid Hydrogels	88
2.3.2 Imaging of Hybrid Hydrogels.....	91
2.3.3 Rheology of Hybrid Gels.....	92
2.3.4 NMR Studies for Hybrid Hydrogels	96
2.3.5 Drug Release from Hybrid Hydrogels.....	98
2.4 Conclusions.....	104
3. Chapter 3 – Development of Gel Beads for Statin Release	106
3.1 Development of DBS-CONHNH ₂ and Alginate Gel Beads.....	109
3.2 Development of DBS-CO ₂ H and Alginate Gel Beads	110
3.3 Development of DBS-CONHNH ₂ , DBS-CO ₂ H and Alginate Gel Beads.....	112
3.4 Properties of the Types of Bead	114
3.4.1 Rheology For the Different Materials	114
3.4.2 pH Responsiveness of Gel Beads.....	115
3.5 Release of Rosuvastatin from Hybrid Beads	116
3.5.1 Incorporation of Rosuvastatin.....	117
3.5.2 Release from Gel Beads	117
3.6 Conclusions and Future Work	123
4. Chapter 4 – Synthesis of Novel Sorbitol Derivatives	125
4.1 Synthesis of MBS Derivatives	128
4.1.1 General Procedure	128
4.1.2 Synthesis of MBS-Fur	130
4.1.3 Synthesis of MBS-CONHNH ₂	132

4.2 Gelation Screening of MBS Derivatives	133
4.2.1 Attempted Synthesis of DBS-Van	135
4.3 Gelation Studies for MBS-SMe	138
4.3.1 T_{gel} Studies for MBS-SMe	139
4.3.2 Rheology of MBS-SMe	140
4.3.3 Imaging of MBS-SMe	142
4.4 Synthesis of Non-symmetric DBS Derivatives.....	142
4.4.1 Synthesis of MBS-CO ₂ H.....	145
4.4.2 Further Reaction of MBS-CO ₂ H.....	146
4.4.3 Purification of DBS-CO ₂ H/CO ₂ Me	147
4.4.4 Synthesis of DBS-CO ₂ H/CONH ₂	149
4.4.5 Synthesis of DBS-CO ₂ Me/CONH ₂	149
4.5 Conversion of MBS Derivatives.....	150
4.5.1 Synthesis of MBS-CO ₂ Me/SMe.....	151
4.5.2 Synthesis of DBS-Van/CO ₂ Me.....	153
4.6 Improved ¹ H NMR Assignment of Protons in the Sugar Backbone	154
4.7 Conclusions and Future Work.....	156
5. Chapter 5 – Chirality of DBS-CONH ₂	158
5.1 L-DBS-CONH ₂	160
5.1.1 Synthesis of L-DBS-CONH ₂	160
5.1.2 Gelation Testing of L-DBS-CONH ₂	161
5.2 Comparison of the Two Enantiomers	163
5.2.1 Rheology of D-DBS-CONH ₂ and L-DBS-CONH ₂	163
5.2.2 Imaging of D-DBS-CONH ₂ and L-DBS-CONH ₂	164
5.2.3 Circular Dichroism Studies for D-DBS-CONH ₂ and L-DBS-CONH ₂	166
5.3 Mixtures of D-DBS-CONH ₂ and L-DBS-CONH ₂	168
5.3.1 Gelation Studies and Thermal Stability	168
5.3.2 Rheology of D-DBS-CONH ₂ and L-DBS-CONH ₂ Hydrogels	172

5.3.3 Imaging of the Mixed Hydrogels	175
5.3.4 Circular Dichroism for Mixed Samples	176
5.4 Incorporation of Chiral Additives	178
5.4.1 Gelation Studies with Chiral Additives	178
5.4.2 Rheology of Hydrogels with Chiral Additives	180
5.4.3 NMR Studies of the Hydrogels with Additives	182
5.4.4 Release of Chiral Additives.....	183
5.5 Biological Studies.....	185
5.5.1 Cytotoxicity Studies.....	185
5.5.2 Viability Studies.....	187
5.5.3 Alamar Blue Test	188
5.6 Conclusions.....	189
6. Chapter 6 – Glutamine Amide Derivatives	191
6.1 Release of L-DOPA from DBS-CONHNH ₂	193
6.1.1 NMR Studies for DBS-CONHNH ₂ Hydrogels with L-DOPA.....	194
6.1.2 Release of L-DOPA from DBS-CONHNH ₂ Hydrogels	194
6.2 Release of L-DOPA from MBS-CO ₂ Me	195
6.3 Development of Glutamine Amide Based Hydrogels.....	198
6.3.1 Rheology of Glutamine Amide Based Hydrogels	200
6.4 Glutamine Amide Hydrogels with L-DOPA	204
6.4.1 Rheology for Glutamine Amide Hydrogels with L-DOPA	205
6.4.2 Imaging of Glutamine Amide Hydrogels with L-DOPA.....	208
6.4.3 NMR Studies for Glutamine Amide Hydrogels with L-DOPA	210
6.5 Release of L-DOPA from Glutamine Amide Hydrogels.....	211
6.5.1 <i>In vitro</i> Release.....	211
6.5.2 <i>In vitro</i> Cytotoxicity Studies	212
6.5.3 <i>In vivo</i> Release and Biodistribution Studies	214
6.6 Conclusions.....	218

7. Conclusions and Future Work.....	221
8. Experimental.....	224
8.1 General Experimental Methods.....	224
8.2 Synthetic Procedures.....	225
8.2.1 Synthesis of DBS-CO ₂ Me.....	225
8.2.2 Synthesis of DBS-CONH ₂	226
8.2.3 Synthesis of MBS-CO ₂ Me.....	227
8.2.4 Synthesis of MBS-Van.....	227
8.2.5 Synthesis of MBS-Cin.....	228
8.2.6 Synthesis of MBS-SMe.....	229
8.2.7 Synthesis of MBS-Fur.....	230
8.2.8 Synthesis of MBS-CONH ₂	230
8.2.9 Synthesis of MBS-CO ₂ H.....	231
8.2.10 Synthesis of DBS-CO ₂ H/CO ₂ Me.....	232
8.2.11 Synthesis of DBS-CO ₂ Me/SMe.....	232
8.2.12 Synthesis of L-DBS-CO ₂ Me.....	233
8.2.13 Synthesis of L-DBS-CONH ₂	234
8.2.14 Synthesis of L-Boc glutamine dodecylamine.....	234
8.2.15 Synthesis of L-glutamine dodecylamine.....	235
8.3 Standard Procedures for Preparing Hydrogels in Sample Vials.....	236
8.3.1 DBS-CONH ₂ Hydrogels.....	236
8.3.2 MBS-CO ₂ Me Hydrogels.....	236
8.3.3 DBS-CONH ₂ and MBS-CO ₂ Me Hybrid Hydrogels.....	236
8.3.4 D-DBS-CONH ₂ and L-DBS-CONH ₂ Hydrogels.....	237
8.3.5 MBS-SMe Hydrogels.....	237
8.3.6 Glutamine Amide Hydrogels.....	237
8.4 Procedure for Determination of T_{gel} Values.....	237
8.5 Procedures for Rheology.....	237

8.6 Procedures for Preparing Hydrogel Samples for NMR.....	238
8.7 Variable Temperature NMR Experiments	238
8.8 Procedures for Preparing Gels for CD	238
8.9 CD Experiments	238
8.10 UV-vis Drug Release Experiments	239
8.11 HPLC Drug Release Experiments	239
8.12 TEM Sample Preparation.....	240
8.13 SEM Sample Preparation.....	240
8.14 Preparation of Buffers.....	241
8.14.1 Tris Buffer	241
8.14.2 HEPES Buffer	241
8.14.3 Phosphate Buffered Saline.....	241
8.14.4 pH 7.5 Phosphate Buffer	241
8.14.5 pH 7 Phosphate Buffer	241
8.14.6 pH 6.5 Phosphate Citrate Buffer	241
8.14.7 pH 5.5 Phosphate Citrate Buffer	241
8.14.8 Sodium Acetate Buffer	242
8.14.9 Sodium Citrate Buffer.....	242
9. Abbreviations.....	242
10. References	245

List of Figures

Figure 1. The general process for the formation of a self-assembled gel.	2
Figure 2. The tri-peptide gelator (left) used by Hartley and co-workers for the encapsulation and release of the antibiotic ciprofloxacin (right).	5
Figure 3. The tripeptide gelator developed for use with silver nanoparticles by Ko and co-workers.	5
Figure 4. Disc diffusion assay from work carried out by Smith and co-workers, showing the effect of the nanoparticle loaded gel beans on the growth of drug resistant vancomycin. (A) alginate gel; (B) alginate beads; (C) hybrid gel; (D) hybrid beads; (E) DBS-CONH ₂ gel.....	6
Figure 5. The (-)-menthol derivative used to gel solutions of antibiotic agents by Yi and co-workers.	6
Figure 6. The gelator developed by Banerjee and co-workers, which showed antibacterial properties.....	7
Figure 7. A modified NSAID gelator developed by Lavery and co-workers, using naproxen, two phenylalanine residues, and two lysine residues.	7
Figure 8. Dephosphorylation of compound 9 caused by phosphatase enzyme gives rise to compound 10 which self-assembles into a gel.	9
Figure 9. The glucosamine-based hydrogels developed by Xu et al. for use as aids in wound healing.....	10
Figure 10. The peptide amphiphile gelator developed by Stupp and co-workers, based on the five peptide sequence Ile-Lys-Val-Ala-Val, that was used in repair of spinal cord injuries. X indicates where the two halves of the structure join.	11
Figure 11. The Arg-Ala-Asp-Ala repeating peptide used by Schneider and co-workers as a scaffold for regeneration of optic nerves.....	12
Figure 12. The peptide-based gelators used by Gough and co-workers for cell proliferation and adhesion studies.	13
Figure 13. The gelator used by He and co-workers for the culture of mesenchymal stem cells.	14
Figure 14. The phenylalanine based gelator used by Feng and co-workers to determine the effects of nanostructure chirality on cell behaviour.....	14

Figure 15. A schematic to demonstrate the types of interaction possible between gel nanofibres and an additive. (a) No interactions; (b) Steric interactions; (c) Non-covalent interactions; (d) Additive part of the gel network.	16
Figure 16. The peptide used by Liu and co-workers as a dual drug delivery platform.	17
Figure 17. The bis-imidazolium based gelator used by Calpena and co-workers for encapsulation and release of ibuprofen and indomethacin.	18
Figure 18. The gelator (left) used by Hamachi and co-workers for triggered insulin release, and its breakdown products (right) following exposure to H ₂ O ₂	18
Figure 19. The peptide based gelator used by Wu and co-workers for encapsulation and release of doxorubicin.	19
Figure 20. The nucleoside based gelator used by Marlow and co-workers to study the rate of release of varied bioactive molecules.	20
Figure 21. Model prodrug gelator developed by Miravet and co-workers for triggered drug release. n=1 or 2.	21
Figure 22. The dipeptide based gelator used by He and co-workers to form a drug depot for release of DOX.	23
Figure 23. The azobenzene/sugar gelator investigated by Shinkai and co-workers.	26
Figure 24. The structures of D-sorbitol (31); dibenzylidene sorbitol (32); monobenzylidene sorbitol (33).	26
Figure 25. Common sites for modification of DBS. Blue circles: aromatic wings. Red circles: free alcohols.	27
Figure 26. The structure of DBS-CO ₂ H.	28
Figure 27. The structure of DBS-CONHNH ₂	28
Figure 28. Left: The MBS based gelator used by Feng and co-workers as an electrolyte. Right: The MBS derivative used by Niu and co-workers.	29
Figure 29. Early Fmoc-protected amino acid based gelators. Left: The Fmoc-Leu-Asp gelator reported by Jamney and co-workers, and used to encapsulate antiviral drugs. Right: The modified Fmoc-Phe gelator used by Xu and co-workers for detection of enzymes.	30
Figure 30. The gelators developed by Jia and co-workers - the general structure (40) and the R group present with (a) tryptophan; (b) methionine; (c) tyrosine.	31

Figure 31. Two of the phenylalanine based gelators studied by Banerjee and co-workers for proteolytic stability and release of DOX. Left: amino acid sequence DLL. Right: amino acid sequence LDD. The chiral centres are shown by the red circles.....	32
Figure 32. Left (blue box): Purines, adenosine and guanine. Right (red box): Pyrimidines, uracil, thymine and cytosine.....	33
Figure 33. The thymidine-based gelator reported by Shimizu and co-workers.	34
Figure 34. The bolaamphiphile thymine gelator developed by Barthélémy and co-workers, and tested as an injectable biomaterial.....	34
Figure 35. The β -galactosidase sensitive gelator precursor reported by Barthélémy and co-workers, with suggested applications in anti-cancer treatments. The cleavable lactose moiety is shown in purple.	35
Figure 36. The gelator, modified to include a model drug, developed by van Esch and coworkers. Green: gelator scaffold, blue: cleavable linker, red: model drug.	36
Figure 37. Three of the peptides used by Yang and co-workers to modify taxol to give self-healing hydrogelators.....	37
Figure 38. The acetaminophen based hydrogel developed by John and co-workers (left), and curcumin, the second drug encapsulated in the gel.....	38
Figure 39. The amino acid based gelators developed by Nanda and Banerjee, used for slow release of bioactive molecules.	38
Figure 40. The histidine based gelator (L form shown) developed by Koner and co-workers for stereospecific detection of amines (R forms shown).	39
Figure 41. The D-phenylalanine based gelators developed by Zhao and co-workers, both with (right) and without (left) the modification with ethylene glycol groups. Each gelator was also prepared using L-phenylalanine.....	41
Figure 42. The phenylalanine based hydrogelators developed by Maity and Maitra, which showed different rheological properties.....	42
Figure 43. The nucleotide based gelator used by Barthélémy and co-workers as a hydrogel in the study.....	43
Figure 44. The two gelators used by Feng and coworkers; the phenylalanine based gelator (63), the modified azobenzene (64) and its response to UV light.....	44

Figure 45. The Fmoc peptides used by Gough, Ulijn and co-workers to form hybrid hydrogels for cell culture.	45
Figure 46. The two components required for gel formation in the organogel reported by Shirai and co-workers, and the reversible interactions that lead to the gel formation.....	46
Figure 47. The gelation system developed by Hanabusa and co-workers.	47
Figure 48. The scheme for the reaction between lauric hydrazide and an aldehyde, resulting in the formation of the hydrazone gelator.	47
Figure 49. The bisaldehyde and a bisamine (top) used by van Esch and co-workers to form vesicles, that then assembled to form hydrogels (bottom).	48
Figure 50. Top: the peptide based gelator used by Guler and co-workers. Bottom: Glutaraldehyde, used for the formation of dynamic covalent bonds.	49
Figure 51. The bisurea based gelator (top) and non-gelling achiral additive (bottom) investigated by Miravet and co-workers. The (R) form of the gelator is shown, but the (S) form was also synthesised and investigated.	50
Figure 52. The bolaamphiphile gelator investigated by Liu and co-workers, and melamine, with which it can co-assemble to form hydrogels.....	51
Figure 53. The different modes of self-assembly possible on mixing two enantiomers of a gelator. (a) Self-sorting, with each fibre consisting of only one enantiomer; (b) racemic co-assembly, where each fibres contains an equal number of alternating enantiomers; (c) random co-assembly, with each fibre containing a random proportion of the two enantiomers, with no pattern.....	51
Figure 54. The two enantiomers of the glutamic acid based gelator investigated by Feng and co-workers.	52
Figure 55. The proposed interactions, shown for the L enantiomer, for the histidine and Zn ²⁺ hydrogels reported by Pal and co-workers.	53
Figure 56. The amino acid based gelators used by Ménard-Moyon and coworkers. The two component gels consisted of Fmoc-Tyr(Bzl) (89) with either Fmoc-Tyr (87) or Fmoc-Phe (88).	54
Figure 57. The NSAID and ammonium salt used by Dastidar and co-workers to form hydrogels with anti-inflammatory properties.	55
Figure 58. The two components used by Ulijn and co-workers for hydrogels for cartilage cell culture.....	55

Figure 59. The gelators used by Yang et al. to develop their hybrid hydrogels.....	57
Figure 60. The reaction used by Slavík and co-workers to determine optimum conditions for the Suzuki-Miyaura cross-coupling reactions using Pd loaded hybrid gels. Shown are the optimised conditions.....	59
Figure 61. An image of the shaped DBS-CONHNH ₂ /PEGDM hydrogel, showing the strip used for pH responsive drug release. Image taken from Reference 176.....	60
Figure 62. Schematic showing the shaped gel reactor developed by Chivers and co-workers.....	60
Figure 63. The dipeptide based gelators used by Adams and co-workers to form self-sorted gel networks.	62
Figure 64. The valine based gelators developed by Escuder and co-workers with 104 containing a carboxylic acid for catalysis, and 105 a proline residue. The reaction the gels catalysed is also shown.....	63
Figure 65. The gelators used by Hamachi and co-workers in a hybrid hydrogel.....	64
Figure 66. Two of the modified peptides used by Mata and co-workers in their multicomponent hydrogel. Top: the peptide containing the cell adhesion sequence, also modified with a cyclodextrin unit; Bottom: The peptide making up the majority of the nanofibres. Further modification of this gave the third component.....	66
Figure 67. General structure for the DBS and MBS derivatives that will be developed. R ₁ and R ₂ may be the same or different.	67
Figure 68. D-DBS-CONHNH ₂ (left) and L-DBS-CONHNH ₂ (right).....	68
Figure 69. Top: A ¹ H NMR spectrum for impure MBS-CO ₂ Me, highlighting the region 6.0-5.4 ppm. The peak at 5.64 ppm corresponds to the acetal proton. Bottom: A ¹ H NMR spectrum for pure MBS-CO ₂ Me.	71
Figure 70. An MBS-CO ₂ Me hydrogel, formed by a heat-cool cycle (at 0.85% wt/vol).	73
Figure 71. Change in appearance on melting, then cooling of MBS-CO ₂ Me hydrogels (left: gel before melting, right: gel after reforming).	75
Figure 72. Gel samples for rheological studies. Left: The sample once the bottomless vial has been removed. Right: a sample once it has been transferred to the rheometer.	78
Figure 73. Amplitude sweep (0.05%-100%) for MBS-CO ₂ Me hydrogels at 0.85% wt/vol. Temperature 25 °C, frequency 1 Hz.....	79

Figure 74. Frequency sweep (0.1 Hz-100 Hz) for MBS-CO ₂ Me hydrogels at 0.85% wt/vol. Temperature 25 °C, amplitude 0.158%.	80
Figure 75. Amplitude sweep (0.001%-100%) for reformed MBS-CO ₂ Me hydrogels at 0.85% wt/vol. Temperature 25 °C, frequency 1 Hz.	81
Figure 76. Frequency sweep (0.1 Hz-100 Hz) for reformed MBS-CO ₂ Me hydrogels at 0.85% wt/vol. Temperature 25 °C, amplitude 0.0019%.	82
Figure 77. CD spectrum, over a range of temperatures, for MBS-CO ₂ Me.	83
Figure 78. Left: TEM image of the MBS-CO ₂ Me hydrogel, scale bar 100 nm. Right: SEM image of an MBS-CO ₂ Me hydrogel, scale bar 1 μm.	85
Figure 79. Imaging for the thermally reformed MBS-CO ₂ Me hydrogels. Left: TEM image, scale bar 200 nm. Right: SEM image, magnification x20,000.	85
Figure 80. Breakdown of MBS-CO ₂ Me hydrogels on addition of aqueous media, over two hours.	86
Figure 81. The structure of naproxen.	87
Figure 82. Release of NPX from MBS-CO ₂ Me hydrogels (1 ml) into pH 7 buffer (6 ml), at 37 °C.	88
Figure 83. TEM (left) and SEM (right) images of DBS-CONH ₂ and MBS-CO ₂ Me hybrid hydrogels (a) 0.20% wt/vol and 0.10% wt/vol respectively, (b) 0.20% wt/vol and 0.80% wt/vol respectively, (c) 0.28% wt/vol and 0.10% wt/vol respectively, (d) 0.28% wt/vol and 0.80% wt/vol respectively. Scale bar for TEM 100 nm, for SEM 1 μm.	92
Figure 84. Amplitude sweep for hybrid hydrogels. Left: 'high' MBS-CO ₂ Me, 'low' DBS-CONH ₂ . Right: 'high' MBS-CO ₂ Me, 'high' DBS-CONH ₂	93
Figure 85. Amplitude sweep (0.05%-100%) for hybrid hydrogels. Left: 'low' MBS-CO ₂ Me, 'low' DBS-CONH ₂ . Right: 'low' MBS-CO ₂ Me, 'high' DBS-CONH ₂ . Temperature 25 °C, Frequency 1 Hz.	94
Figure 86. Amplitude sweeps (0.05%-100%) for MBS-CO ₂ Me hydrogel, DBS-CONH ₂ hydrogels, hybrid hydrogels with 'low' MBS-CO ₂ Me (0.10% wt/vol), 'low' DBS-CONH ₂ (0.24% wt/vol), and 'high' MBS-CO ₂ Me (0.80% wt/vol), 'low' DBS-CONH ₂ (0.24% wt/vol). Temperature 25 °C, frequency 1 Hz.	95
Figure 87. Amplitude sweep (0.01%-100%) for MBS CO ₂ Me and DBS CONH ₂ hybrid hydrogels, with a total gelator loading of 0.48% wt/vol, in different proportions of the two gelators. Temperature 25 °C, frequency 1 Hz.	96

Figure 88. The breakdown of the hybrid hydrogel with increasing temperature, monitored by ¹ H NMR spectroscopy.	98
Figure 89. Release of NPX from DBS-CONHNH ₂ and MBS-CO ₂ Me hybrid hydrogels (1 ml), into pH 7 buffer (6 ml) or pH 5.5 buffer (6 ml), at 37 °C.....	99
Figure 90. The hydrogen bonding interaction between the hydrazide groups of the gelator and the carboxylic acid group of NPX.	99
Figure 91. The structure of atorvastatin, a commonly prescribed statin.	100
Figure 92. Release of atorvastatin from hybrid hydrogels (1 ml), into pH 7 buffer (6 ml) at 37 °C, quantified by UV-vis.....	101
Figure 93. HPLC trace for a mixed sample of atorvastatin, DBS-CONHNH ₂ , and MBS-CO ₂ Me. The two gelators appear before 2 minutes, the atorvastatin at 14 minutes.	102
Figure 94. Amplitude sweep (0.01%-100%) for hybrid hydrogels containing 5 mg of atorvastatin. Temperature 25 °C, frequency 1 Hz.....	103
Figure 95. Release of atorvastatin from hybrid hydrogels (1 ml), into pH 7 buffer (6 ml, 1 ml replaced at each timepoint) at 37 °C, over 240 hours, quantified by HPLC.	104
Figure 96. The structures of the polymer gelators, PEGDM (left) and agarose (right) that have previously been combined with DBS-CONHNH ₂	106
Figure 97. Alginate, a natural biopolymer that can be combined with DBS-CONHNH ₂	107
Figure 98. A representation of the two types of network that can be formed in the alginate/DBS-CONHNH ₂ hybrid beads, depending on the order in which the stimuli for gel formation are applied.	108
Figure 99. Preparation of the hybrid alginate/DBS-CONHNH ₂ hydrogels in vials, and the hybrid core-shell beads. Reproduced from reference 216.	110
Figure 100. The structure of DBS-CO ₂ H.	111
Figure 101. Optical microscopy (left) and SEM (right) images for cross sections of DBS-CO ₂ H/alginate beads.	112
Figure 102. Optical microscopy (left) and SEM (right) images for cross sections of the 3-component gel beads.....	113
Figure 103. The structure of rosuvastatin, the API incorporated within the gel beads.	116

Figure 104. Release of rosuvastatin from gel beads (total 1 ml), into Tris HCl pH 7.4 buffer (6 ml) at 37 °C, over 24 hours.	118
Figure 105. Release of rosuvastatin from gel beads (total 1 ml) into pH 4.0 sodium acetate buffer (6 ml) at 37 °C.	119
Figure 106. Release of rosuvastatin from DBS-CONHNH ₂ /alginate gels, prepared either as beads (total 1 ml) or in vials (1 ml), into either Tris/HCl or sodium acetate buffers (6 ml) at 37 °C.	121
Figure 107. Release of rosuvastatin from DBS-CO ₂ H/alginate gels, prepared either as beads (total 1 ml) or in vials (1 ml), into either Tris/HCl, or sodium acetate buffer (6 ml) at 37 °C.....	122
Figure 108. The structures of dibenzylidene sorbitol and monobenzylidene sorbitol.....	125
Figure 109. DBS, with the key sites for modification marked. Blue circles - aromatic 'wings'. Red circle - free alcohols.....	126
Figure 110. Structure of MBS-iPr.....	138
Figure 111. Structure of MBS-SMe.....	138
Figure 111. Apparent hydrogel formed by MBS-SMe, following a heat/cool cycle (0.3% wt/vol).	139
Figure 112. Amplitude sweep (0.001%-100%) for MBS-SMe hydrogels (0.40% wt/vol). Temperature 25 °C, frequency 1 Hz.	141
Figure 113. Frequency sweep (0.1 Hz-100 Hz) for MBS-SMe hydrogels (0.40% wt/vol). Temperature 25 °C, frequency 1 Hz.	141
Figure 114. Images of the hydrogels formed by MBS-SMe (0.40% wt/vol). Left: SEM, scale bar 10 μm. Right: TEM, scale bar 5 μm.....	142
Figure 115. The structure of DBS-CO ₂ H/CONHNH ₂	143
Figure 116. The structure of DBS-CO ₂ H/CO ₂ Me.	143
Figure 117. Mass spectrum for the attempted synthesis of DBS-CO ₂ H/CO ₂ Me. The bottom half shows the predicted output, the top half the experimental spectrum.	144
Figure 118. (a) HPLC trace for the product of the DBS-CO ₂ H/CO ₂ Me reaction; (b) LC-MS trace for the reaction mixture, scanning at a mass of 461; (c) LC-MS trace for the reaction mixture, scanning at a mass of 474.....	148
Figure 119. The DBS derivatives that may be formed with MBS-CO ₂ Me and a second aldehyde.	151
Figure 120. DBS-CO ₂ Me, with labels for NMR assignment.....	154

Figure 121. The sugar region of the ^1H NMR for DBS- CO_2Me	155
Figure 122. The complex multiplet at 8.00-7.97 ppm in the 500 MHz ^1H NMR spectrum for DBS- CO_2Me	156
Figure 123. Different modes of assembly for a mix of two different enantiomers. (a) self-sorting; (b) true racemate; (c) pseudo racemate.....	158
Figure 124. Amplitude sweep (0.05%-100%) for D-DBS- CONHNH_2 and L-DBS- CONHNH_2 hydrogels, gelator concentration 0.28% wt/vol. Dark blue circles: D-DBS- CONHNH_2 G' , Light blue diamonds: D-DBS- CONHNH_2 G'' , Dark red squares: L-DBS- CONHNH_2 G' , Light red triangles: L-DBS- CONHNH_2 G'' . Temperature 25 °C, frequency 1 Hz.....	163
Figure 125. Frequency sweep (0.1 Hz-100 Hz) for D-DBS- CONHNH_2 and L-DBS- CONHNH_2 hydrogels, gelator loading 0.28% wt/vol. Dark red circles: D-DBS- CONHNH_2 G' , Light red diamonds: D-DBS- CONHNH_2 G'' , Dark blue squares: L-DBS- CONHNH_2 G' , Light blue triangles: L-DBS- CONHNH_2 G'' . Temperature 25 °C, amplitude 0.1%.	164
Figure 126. Imaging of L-DBS- CONHNH_2 (0.28% wt/vol) and D-DBS- CONHNH_2 (0.4% wt/vol) hydrogels. Top: SEM images, magnification x20,000, (left: L-DBS- CONHNH_2 , right: D-DBS- CONHNH_2). Bottom: TEM images, scale bar 100 nm, (left: L-DBS- CONHNH_2 , right: D-DBS- CONHNH_2).	165
Figure 127. The CD spectra for D-DBS- CONHNH_2 and L-DBS- CONHNH_2 . The highest temperatures are in red, and the lowest in blue.	167
Figure 128. T_{gel} values for D-DBS- CONHNH_2 and L-DBS- CONHNH_2 hydrogels, and the hydrogels formed from mixtures of the two enantiomers.	171
Figure 129. ^1H NMR spectra for L-DBS- CONHNH_2 (top) and D-DBS- CONHNH_2 and L-DBS- CONHNH_2 (bottom) hydrogels. Total loading for both hydrogels is 0.24% wt/vol.....	172
Figure 130. Amplitude sweep (0.01%-100%) for racemic DBS- CONHNH_2 hydrogels. Total gelator loading 0.28% wt/vol. Temperature 25 °C, frequency 1 Hz.....	174
Figure 131. Frequency sweep (0.1 Hz-100 Hz) for racemic DBS- CONHNH_2 hydrogels. Total gelator loading 0.28% wt/vol. Temperature 25 °C, amplitude 0.05%.....	175
Figure 132. SEM (x20,000) (top) and TEM images (scale bar 100 nm) (bottom) for racemic hydrogels (left) and L-DBS- CONHNH_2 hydrogels (right). Total gelator loading for both samples - 0.28% wt/vol.	176

Figure 133. Ellipticity, measured at 272 nm, for mixed D-DBS-CONHNH ₂ and L-DBS-CONHNH ₂ hydrogels, total gelator loading 0.1% wt/vol.	177
Figure 134. (S)-naproxen (118a) and (R)-naproxen (118b).	178
Figure 135. Amplitude sweep (0.01%-100%) for D-DBS-CONHNH ₂ hydrogels with (R)- or (S)-NPX. Gelator loading 0.28% wt/vol, one equivalent NPX. Temperature 25 °C, frequency Hz.	180
Figure 136. Amplitude sweep (0.01%-100%) for L-DBS-CONHNH ₂ hydrogels with (R)- or (S)-NPX. Gelator loading 0.28% wt/vol, one equivalent NPX. Temperature 25 °C, frequency 1 Hz.	181
Figure 137. Release of (R)-NPX and (S)-NPX from D-DBS-CONHNH ₂ hydrogels (1 ml), into pH 7 buffer (6 ml) at 37 °C. Gelator loading is 0.28% wt/vol, with one equivalent of NPX.....	184
Figure 138. Release of (R)-NPX and (S)-NPX from L-DBS-CONHNH ₂ hydrogels (1 ml), into pH7 buffer (6 ml) at 37 °C. Gelator loading is 0.28% wt/vol, with one equivalent of NPX.....	184
Figure 139. Hydrogels of L-DBS-CONHNH ₂ (top) and D-DBS-CONHNH ₂ (bottom), prepared in a 6 well plate. Gelator concentration for all hydrogels is 0.4% wt/vol.	186
Figure 140. The plate after 48 hours, following treatment with crystal violet methanol solution. Purple indicates viable cells. Top: L-DBS-CONHNH ₂ ; Bottom: D-DBS-CONHNH ₂	186
Figure 141. Cell viability for D-DBS-CONHNH ₂ and L-DBS-CONHNH ₂ hydrogels (0.3% wt/vol) at days 0, 3, 6, 10.	187
Figure 142. Impact of different amino acids, and glucose, on the reduction of Alamar Blue. Absorbance measured following incubation of gels with Alamar Blue at 37 °C for 4 hours. Solution was then removed, and absorbance measured.	189
Figure 143. The structure of carbidopa, the additive administered with L-DOPA.	192
Figure 144. The potential interaction between L-DOPA and the DBS-CONHNH ₂ gel fibres.....	193
Figure 145. Release of L-DOPA from DBS-CONHNH ₂ hydrogels (1 ml), into pH 5.5 or pH 6.5 buffer (6 ml) at 37 °C. Gelator loading 0.28% wt/vol, L-DOPA one molar equivalent.	195
Figure 146. UV-vis spectra for release from MBS-CO ₂ Me hydrogels, both with and without L-DOPA.....	197
Figure 147. The Schiff base gelator formed from glutamine amide and benzaldehyde.	200
Figure 148. Amplitude sweep (0.001%-100%) for glutamine amide gels (0.3% wt/vol) formed with benzaldehyde (1 equivalent). Temperature 25 °C, frequency 1 Hz.	201

Figure 149. Frequency sweep (0.1 Hz-100 Hz) for glutamine amide (0.35 wt/vol) hydrogels with benzaldehyde (1 equivalent). Temperature 25 °C, amplitude 0.0078%.....	202
Figure 150. Left: Glutamine amide and benzaldehyde hydrogel (0.5 ml, 0.35% wt/vol, 1 equivalent benzaldehyde) formed in a syringe. Centre: The solution immediately after injection of the hydrogel into a vial. Right: The reformed hydrogel, following standing overnight.....	202
Figure 151. Shear viscosity of glutamine amide hydrogels (0.35% wt/vol, 1 equivalent benzaldehyde) with changing frequency. Blue: frequency is 2 Hz. Red: frequency is 100 Hz. Temperature 25 °C, shear strain 0.012%.	203
Figure 152. G' and G'' for the reformation of glutamine amide hydrogels (0.35% wt/vol, 1 equivalent benzaldehyde). The gap at 200-230 s is the time at which the frequency was increased. Temperature 25 °C, shear strain 0.012%.	204
Figure 153. Amplitude sweep for glutamine amide and benzaldehyde hydrogels (0.35% wt/vol, 1 equivalent benzaldehyde) with L-DOPA (1 equivalent). Temperature 25 °C, frequency 1 Hz.	206
Figure 154. Shear viscosity of glutamine amide and benzaldehyde hydrogels (0.35% wt/vol, 1 equivalent benzaldehyde) with L-DOPA (1 equivalent). Blue: frequency is 2 Hz. Red: Frequency is 100 Hz. Temperature 25 °C, shear strain 0.012%.	207
Figure 155. The G' and G'' for the reformation of glutamine amide hydrogels with L-DOPA (0.35% wt/vol, 1 equivalent benzaldehyde, 1 equivalent L-DOPA). The gap at 200-230 s is when the frequency was increased. Temperature 25 °C, shear strain 0.012%.....	207
Figure 156. TEM (left) and SEM (right) images for glutamine amide hydrogels with L-DOPA. (a) benzaldehyde:L-DOPA 1:1 (b) benzaldehyde:L-DOPA 1:4 (c) benzaldehyde:L-DOPA 1:10. All scale bars 5 µm.	209
Figure 157. Release of L-DOPA (0.8 mM) from glutamine amide hydrogels (1 ml, 0.35% wt/vol) with benzaldehyde (1 equivalent), into pH 7 buffer (6 ml).	211
Figure 158. Cytotoxicity of the glutamine amide hydrogel alone, and with L-DOPA, in human nasal septum tumour RPMI 2650 cells. Cells were incubated with culture media, containing up to 10% gel alone, gel with L-DOPA, or L-DOPA solution for 24 and 48 h.....	213
Figure 159. Viability of cells with varying concentrations of the glutamine amide hydrogel, Tween® 80 and CTAB for 24 and 48 h.....	213
Figure 160. Uptake of [³ H] L-DOPA from hydrogel or solution in (a) the brain, (b) the nasal cavity, (c) the blood and (d) the liver, at 10 minutes, 20 minutes and 1 hour after administration. Results	

are %ID per tissue, with data expressed as the mean \pm SD. Statistical significance is compared between each timepoint. * $p < 0.05$, ** $0.01 < p < 0.05$, *** $p < 0.01$ (one-way ANOVA)..... 215

Figure 161. Distribution of L-DOPA in selected organs, following delivery by either intranasal hydrogel formulation, intranasal solution, or intravenous solution. Results are %ID per tissue, with data expressed as the mean \pm SD. Statistical significance is compared between each timepoint. * $p < 0.05$, ** $0.01 < p < 0.05$, *** $p < 0.01$ (one-way ANOVA)..... 216

Figure 162. Distribution of [^3H] L-DOPA in the brain, 10 minutes from intranasal delivery of the hydrogel formulation. (a) View of a mouse brain, with different sections indicated. (b) [^3H] L-DOPA uptake in different brain sections. 218

Figure 163. Calibration curve for the quantification of atorvastatin. 240

List of Schemes

Scheme 1. Hydrolysis of glucono- δ -lactone to form gluconic acid.....	3
Scheme 2. Synthesis of DBS-CO ₂ Me.	70
Scheme 3. Synthesis of DBS-CONHNH ₂	70
Scheme 4. Synthesis of MBS-CO ₂ Me	72
Scheme 5. The synthesis of DBS-CO ₂ Me.....	126
Scheme 6. The conversion of DBS-CO ₂ Me (116) to give DBS-CONHNH ₂ (35) or DBS-CO ₂ H (34)....	127
Scheme 7. General scheme for the synthesis of MBS derivatives.....	128
Scheme 8. Ring opening polymerisation of furfural.	131
Scheme 9. Synthesis of MBS-Fur (124).	131
Scheme 10. Synthesis of MBS-CONHNH ₂	132
Scheme 11. The first proposed method for the synthesis of DBS-Van.....	136
Scheme 12. The second proposed method for synthesis of DBS-Van.....	137
Scheme 13. The synthesis of DBS-CO ₂ H/CO ₂ Me from DBS-CO ₂ Me. Although only one product is shown in the scheme, it is possible that hydrolysis could occur at either ester group.....	144
Scheme 14. The proposed two-step route for the synthesis of DBS-CO ₂ H/CO ₂ Me.	145
Scheme 15. The conversion of MBS-CO ₂ Me to give MBS-CO ₂ H.	145
Scheme 16. Synthesis of DBS-CO ₂ H/CO ₂ Me from MBS-CO ₂ H.....	146
Scheme 17. The synthesis of DBS-CO ₂ H/CONHNH ₂ from DBS-CO ₂ H/CO ₂ Me.	149
Scheme 18. Synthesis of DBS-CO ₂ Me/CONHNH ₂ from DBS-CO ₂ Me.....	150
Scheme 19. General scheme for the reaction of MBS-CO ₂ Me with a further aldehyde, for the formation of a non-symmetric DBS derivative.	151
Scheme 20. The reaction of MBS-CO ₂ Me with 4-(methylthio)benzaldehyde to form a DBS derivative.	152
Scheme 21. The synthesis of DBS-Van/CO ₂ Me. Although only one product is shown in the scheme, a number of different substitutions might be possible.	153
Scheme 22. Synthesis of L-DBS-CO ₂ Me.....	160

Scheme 23. Synthesis of L-DBS-CONHNH ₂	161
Scheme 24. Reduction of resazurin (weakly fluorescent) to give resorufin (highly fluorescent). .	188
Scheme 25. Conversion of L-DOPA to dopamine, that occurs in vivo, by the action of DOPA decarboxylase.....	191
Scheme 26. Synthesis of glutamine amide.....	198
Scheme 27. Formation of the Schiff base responsible for gelation, from glutamine amide and 4-nitrobenzaldehyde.	199

List of Tables

Table 1. Optimisation of the synthesis of MBS-CO ₂ Me, varying the equivalents of sorbitol. The 'extra' peak integrations are for peaks in the acetal region that do not correspond to MBS-CO ₂ Me, that were still present after purification steps.	72
Table 2. Gelation tests for MBS-CO ₂ Me hydrogels in buffer solutions.....	74
Table 3. T _{gel} values for MBS-CO ₂ Me hydrogels at a range of gelator concentrations.	75
Table 4. Comparison of T _{gel} values for initial gels, and reformed gels.....	76
Table 5. Selected concentrations of DBS-CONH ₂ and MBS-CO ₂ Me tested for gelation in the hybrid hydrogel.	89
Table 6. T _{gel} values for hybrid hydrogels, with varying concentrations of the two gelators. For all the gels, total gelator concentration is 0.48% wt/vol. Note: at 65% MBS-CO ₂ Me, no gel was formed.	90
Table 7. Selected T _{gel} values for hybrid hydrogels, with varying total concentrations, and varying proportions of the two gelators.....	91
Table 8. G' values for gels formed from DBS-CONH ₂ , DBS-CO ₂ H and alginate.	114
Table 9. Aldehydes investigated for formation of MBS derivatives, using the standard Dean-Stark conditions. Yield quoted is relative to the aldehyde. Trace indicates a small amount of product could be observed in ¹ H NMR, but not isolated.	129
Table 10. Screening for gelation of MBS-Van and MBS-Cin. All used 0.5 ml of water. S=solution, V=viscous liquid, C=crystals.	133
Table 11. Gelation screening for MBS-Van and MBS-Cin, in water/DMSO and water/ethanol mixes. S=solution, C=crystals. All samples were at 0.3% wt/vol.....	134
Table 12. Solvent screen for MBS-Cin and MBS-Van. All samples at 1% wt/vol.....	135
Table 13. Gelation screening for MBS-SMe. Each sample used 0.5 ml water. Results: P=precipitate, I=insoluble, C=crystals, G=gel, WG=weak gel.	139
Table 14. T _{gel} values for MBS-SMe hydrogels, formed at a range of concentrations.	140
Table 15. Gelation screen for L-DBS-CONH ₂	162

Table 16. Thermal stability of L-DBS-CONH ₂ and D-DBS-CONH ₂ . Note: T _{gel} values are only monitored up to 100 °C for hydrogels - above this, it would not be possible to determine if the loss of the gel is due to the breakdown of the network or the evaporation of the solvent.	162
Table 17. Gelation screen for mixtures of D-DBS-CONH ₂ and L-DBS-CONH ₂ . The percentage of each gelator shown is the proportion of the total gelator, at a loading of 0.28% wt/vol. G=Gel.	169
Table 18. T _{gel} values for D-DBS-CONH ₂ and L-DBS-CONH ₂ hydrogels. Total gelator loading 0.28% wt/vol.....	170
Table 19. G' values for mixes of D-DBS-CONH ₂ and L-DBS-CONH ₂ hydrogels (total concentration 0.28% wt/vol).....	174
Table 20. Gelation testing for different combinations of DBS-CONH ₂ and naproxen enantiomers. Gelator loading is 0.28% wt/vol, with one equivalent of NPX.	179
Table 21. T _{gel} values for D-DBS-CONH ₂ and L-DBS-CONH ₂ hydrogels, with (S)-NPX or (R)-NPX. Hydrogels have gelator loading of 0.28% wt/vol, with 1 equivalent of NPX.....	179
Table 22. The effect of the addition of NPX to the DBS-CONH ₂ hydrogels. Gelator concentration 0.28% wt/vol, with one equivalent of NPX.....	182
Table 23. The percentage of (R)-NPX and (S)-NPX not bound to the gel network, as determined by use of a DMSO internal standard. Gelator loading 0.28% wt/vol, with one equivalent of NPX. ...	183
Table 24. T _{gel} values for MBS-CO ₂ Me hydrogels with and without L-DOPA.	196
Table 25. Gelation testing for glutamine amide hydrogels (0.35% wt/vol, 1 equivalent benzaldehyde) with L-DOPA. Equivalentents are molar equivalentents. G=Gel, P=Precipitate.	205

Acknowledgements

There are many people to thank, who have supported me throughout my PhD. Firstly, my supervisor, Professor David Smith, for his valuable advice, guidance, and encouragement. I have always enjoyed my work as part of the research group, and his ideas and enthusiasm have been a huge part of that.

I would also like to thank all the technical staff who have helped me out over the course of the project, including Heather Fish (NMR), Karl Heaton (MS), Scott Hicks (HPLC), Andrew Leech (CD), and Meg Stark and Karen Hodgkinson (Imaging).

I also need to thank members of the DKS group, both past and present! There are too many to list, but some special mentions - thank you to Phill, for all your help when I started, for making the lab such a fun and welcoming place to work. Jack, thank you for always having a smile on your face, and making us all laugh so much. Carmen, thank you for all your support and guidance, which has been invaluable! Thank you also for putting up with my teasing about what might be fun to try on pizza. Kirsten, thank you for being a better friend than I could have hoped for – for your endless encouragement and company on walks and pub trips.

Others who need a mention are Saikiran, for her friendship and company on tea breaks, and Athanasia – I miss our long walks along the Ouse! Also Sam, for being so welcoming at the beginning, Nik and Maggie, for always having time for a chat, and Pavan, for all the cricket talk. Thanks to Chris, for your friendship, for always being there to offer advice, and the many hours spent in the pub. Special mentions also to the Wentworth Squash Team and everyone at UYWCC – for providing some of the best fun I had in York. Thank you also to David, Kirstin, and Shona, for being there throughout my time at York.

Thank you also to Steph, Charlotte, and Lucie (along with Chris, Arthur, and Joel), who have always been there to offer encouragement, from the very beginning. A particular thank you is required for keeping me accountable during the writing stage! It is impossible to imagine life without you!

Finally, thank you to all my family, who have supported me throughout my PhD. Thanks to my brothers Will and George, who can always make me laugh. The biggest thanks to my Mum and Dad, who have supported me throughout my whole education, and especially over the last year. I couldn't have done it without you!

Declaration

I declare that this thesis is a presentation of original work. The work presented is entirely my own, except where otherwise indicated in the text. This work has not previously been presented for an award at this, or any other, University. All sources are acknowledged as References. Aspects of this work have been published in the following journal articles: *Chem. Commun.*, 2020, **56**, 11046-11049; *Adv. Sci.*, 2021, 2101058; *Chem. Eur. J.*, 2021, **27**, 13203-13210.

1. Chapter 1: Introduction

1.1 Introduction to Low Molecular Weight Gelators

Gels are soft materials that are typically composed of over 99% liquid – with the remainder being made up of gelator.¹ The gelator forms a solid-like network that immobilises the solvent and prevents flow. Therefore gels, despite the high solvent content, do not flow, and behave as viscoelastic materials.²

All gels have this characteristic in common – however, they can be classified in a number of ways – most commonly by the type of solvent, and the type of gelator. Gels formed with organic solvents are known as organogels, and those formed from water are hydrogels. The molecules that form these materials are known as organogelators and hydrogelators respectively. Some gelators may be capable of gelling both organic solvent and water, although these are rarer.^{3,4} Other molecules can gel ionic liquids (ionogels)^{5,6} or deep eutectic solvents (eutectogels).^{7,8}

The second key distinguishing point is the type of gelator, determined by the interactions between them. Polymer gelators (PGs) are comprised of monomers held together by covalent bonds - giving extended polymer chains. These polymer chains can then interact with one another either through the formation of covalent cross-linking bonds to give ‘chemical gels’ or via non-covalent interactions to give ‘physical gels’.⁹ These materials have been known for many years – indeed gels formed from natural polymers were being investigated in academic science as early as 1861.¹⁰

The other major class of gelators are low molecular weight gelators (LMWGs). Gels formed from such gelators rely entirely on non-covalent interactions for self-assembly (as such they can also be classified as ‘physical gels’). Each individual gelator molecule, typically with a molecular weight of under 3000 Da, interacts with others through a mix of hydrogen bonding, π - π stacking, solvophobic interactions, van der Waals forces and other intermolecular interactions. This typically results in extended fibrils (supramolecular polymers). The gel fibrils, consequently bundle into fibres as a result of different non-covalent interactions and hence form an entangled network. As such, these hierarchical materials are formed entirely as a result of non-covalent interactions.¹¹ In principle, this makes gels based on LMWGs more dynamic and reversible than polymer gels, as unlike polymer gels, they can be disassembled to give small highly-mobile low-molecular-weight species.

Although supramolecular gels can be formed from a variety of different classes of molecule, they follow the same general pattern for self-assembly. First, the individual molecules start to interact with each other, through non-covalent interactions. This leads to the formation of fibrils, which then bundle into larger fibres. These fibres then further interact to form the sample-spanning network – this is what traps the solvent molecules (Figure 1).¹²

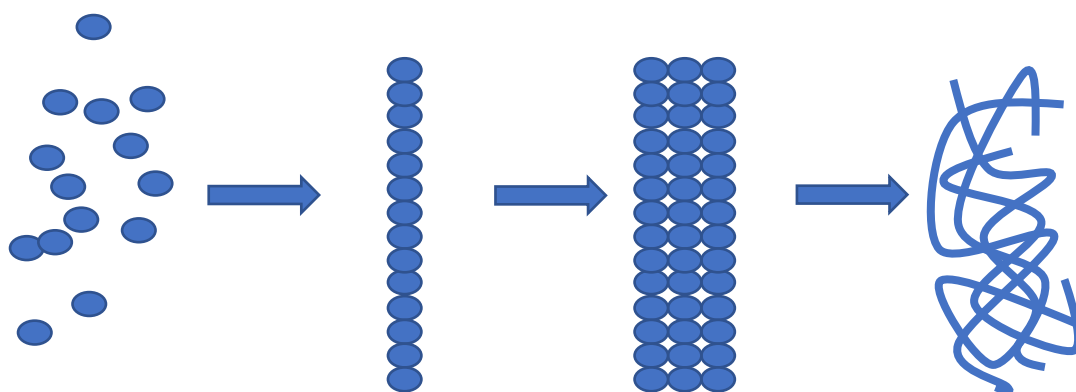
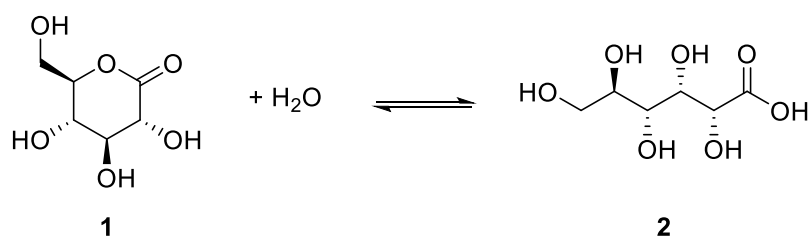


Figure 1. The general process for the formation of a self-assembled gel.

This process can be triggered in a number of ways. Typically, there is a move from an environment in which the gelator molecule is soluble, to one in which it is not.¹³ This change can be achieved by changing a number of conditions. One of the most common methods is heating then cooling – on heating, the gelator dissolves in the solvent, and the gel then forms once the temperature falls below the temperature of gelation (T_{gel}), the point at which the gelator is no longer soluble.¹ A change in pH is another commonly used method to trigger self-assembly, especially for gelators which contain a carboxylic acid group.^{14,15} The gelator is initially dissolved in a solution at a pH higher than the pK_a of the gelator – the carboxylic acid group is deprotonated and the molecule is therefore more soluble. The pH of the solution is then decreased, the gelator is protonated, and becomes increasingly insoluble, eventually forming a gel. This pH change can be achieved by addition of aqueous acid, but in these cases, protonation can occur at a faster rate than diffusion, leading to inhomogeneous gels. It is now more common to utilise a slow change in pH, using an acid that slowly hydrolyses in water (Scheme 1) – a technique first developed by Adams et al.¹⁶ This approach leads to more gradual protonation of the gelator, and therefore the formation of more homogenous gels. Other common methods for triggering gelation include sonication,¹⁷ photoinitiation,¹⁸ and enzyme activation¹⁹ – again, all of these methods have the potential to change how soluble the gelator is in the chosen environment and set up a situation where slow precipitation can give rise to controlled fibril formation and subsequent gel assembly.



Scheme 1. Hydrolysis of glucono- δ -lactone to form gluconic acid.

Evidently, different classes of gel will have different general properties, making each type suitable for different applications. Polymer gels tend to be fairly mechanically robust due to the covalent linkages between monomer units – but at the expense of responsiveness to external stimuli. In contrast, supramolecular gels are mechanically weaker, but have much greater responsiveness to external stimuli.²⁰ It is for this reason that supramolecular gels have become of increasing interest.

The mechanical weakness of supramolecular gels is a result of these materials being reliant on only non-covalent forces. However, these weaker interactions are also what give supramolecular gels a key advantage. They tend to be very responsive to external stimuli, such as a change in temperature or pH, as the interactions are much more reversible than the covalent bonds formed by polymer gelators. As noted above, supramolecular gels can be fully reversed to give a low viscosity aqueous solution by disassembling the self-assembled network into its constituent low-molecular-weight building blocks. This means that LMWGs assemble into highly responsive materials.

1.2 Applications of Supramolecular Gels

As noted above, the responsiveness of gels based on LMWGs has led to the hugely increased interest in supramolecular gels.²¹ These materials have potential in applications as diverse as environmental remediation,²² as electrolytes,²³ and in catalysis.²⁴ There has been particular growth in biomedical applications, particularly for supramolecular hydrogels,²⁵ as a result of the generally good biocompatibility of this type of material, and the focus of this introduction is on the use of these materials in biomedicine.

1.2.1 Early Applications

Early applications of gels generally focussed on exploiting the ability of gelators to trap large volumes of solvent. One early use of polymer hydrogels in a medical application was the use of the PG glycolmonomethacrylate, which was used to develop the chemically cross-linked polymer

gel soft contact lens in 1960 – it's combination of biocompatibility, permeability to gases, and ability to support a high water content led to its use in this application.²⁶ Other early applications of polymer gelators include the use of agar and similar gels for use in microorganism culture – here gelators were useful for the ability to immobilise growth medium.²⁷

However, as the field of supramolecular gels has grown, so have their potential applications in biomedical settings. These applications aim to use not just the ability of the gelator to hold large volumes of solvent, but to tune the properties of the gelator to design high-tech, responsive materials. Desirable features include the ability to hold large volumes of water, but also the potential to be biodegradable, interact with additives, and break down in response to certain stimuli. Hydrogels are therefore being investigated as solutions in a range of biomedical applications.

1.2.2 Use of Supramolecular Gels as Antibiotic Agents

Antibiotic resistance is an increasing and significant problem for modern healthcare, as more strains of antibiotic bacteria develop, and discovery of new antibiotics cannot keep pace.²⁸ Hydrogels for antibiotic applications fall into three main categories – the antibiotic agent being incorporated within the gel, the use of gelators with inherent antibiotic properties, or causing the death of bacteria via gel formation.

Peptide based gelators are especially common for use in antimicrobial applications. Hartley and co-workers reported the use of a tripeptide hydrogelator (**3**) (Figure 2), capable of forming in the presence of the antibiotic ciprofloxacin (CIP) (**4**).²⁹ The formation of the hydrogel was triggered by a change in pH, and the gel was found to be more stable, and more resistant to strain when CIP was also incorporated. This was thought to be a result of the presence of CIP in the hydrophobic pockets of the hydrogel. Imaging also indicated that the nanostructure of the hydrogels was impacted by the addition of the antibiotic.

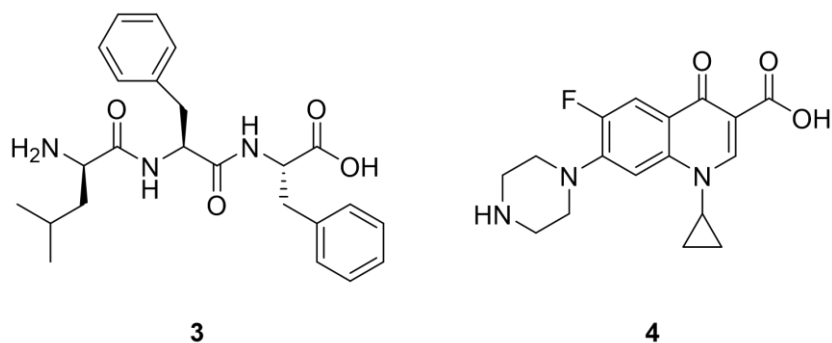


Figure 2. The tri-peptide gelator (left) used by Hartley and co-workers for the encapsulation and release of the antibiotic ciprofloxacin (right).

These drug-loaded hydrogels were then capable of releasing CIP (*in vitro*) over the course of 2-3 days, with the most rapid release over the first 8 hours. Following this, inhibition tests indicated that the CIP-loaded gel showed reasonable antibiotic activity, with the gelator alone also showing some mild antibiotic activity. The authors suggested that the relatively sustained release, over the course of a couple of days, could mean that these hydrogels are suitable for use in wound dressings.

As well as antibiotics, the incorporation of nanoparticles into a hydrogel can also lead to a material with antimicrobial properties. Silver nanoparticles typically have good antibiotic properties, and therefore it is desirable to keep them at the site of potential infection – this may be achieved by use of a hydrogel. In 2016, Ko *et al.* reported a naphthalene protected tripeptide hydrogel (Figure 3), capable of acting as a scaffold for the formation of silver nanoparticles.³⁰ The hydrogel was formed following a pH change, and Ag⁺ ions added. These were then reduced to form nanoparticles.

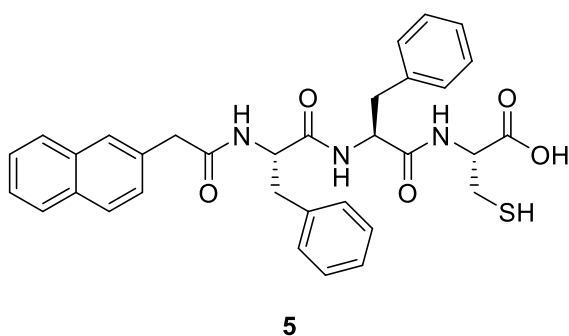


Figure 3. The tripeptide gelator developed for use with silver nanoparticles by Ko and co-workers.

Once the nanoparticles had been formed, IR studies indicated that these were interacting strongly with the gel nanofibres. The nanoparticle loaded hydrogels showed good antibacterial activity, against both gram-positive and gram-negative bacteria. Additionally, there was good

biocompatibility observed when tested with HeLa cells. This gives the potential of these materials for applications in wound dressing.

Progress is also being made in shaping gels containing nanoparticles, for potential applications in orthopaedics or wound healing. This includes work by Smith and co-workers, which combined a LMWG (DBS-CONHNH₂) capable of forming silver nanoparticles *in situ* from silver salts, and a PG (alginate) to attain a bead shape.³¹ These silver nanoparticle loaded beads showed good antibacterial activity against drug resistant bacteria, including both gram-positive and gram-negative examples, giving inhibition zones of 2-3 mm (Figure 4). This indicated that the beads do indeed have potential in biomedical applications.

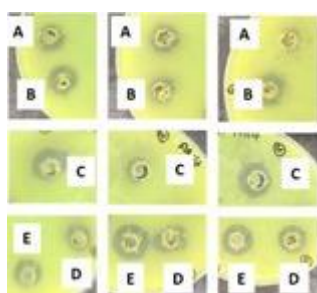
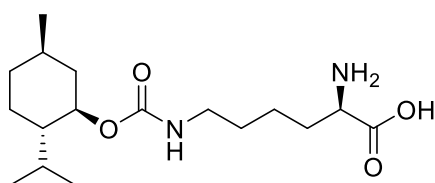


Figure 4. Disc diffusion assay from work carried out by Smith and co-workers, showing the effect of the nanoparticle loaded gel beans on the growth of drug resistant vancomycin. (A) alginate gel; (B) alginate beads; (C) hybrid gel; (D) hybrid beads; (E) DBS-CONHNH₂ gel.

In 2014, Yi and co-workers³² reported a gelator based on the natural product (-)-menthol, modified with an amino acid (Figure 5). This was capable of gelling solutions of different antibacterial agents, including zinc acetate and lincomycin. Gels formed from these solutions were shown to be more active against some bacteria than solutions of the same agents – although no reasoning was given for this effect, and the hydrogels alone showed no antibiotic activity. The gels were also thixotropic, recovering within five minutes following the application of mechanical stress, and the exact concentration of antibiotic agent could be controlled easily. This thixotropic behaviour, combined with the gelator itself being biocompatible, could lead to applications in delivery of antibiotics via injection to specific sites in the body.



6

Figure 5. The (-)-menthol derivative used to gel solutions of antibiotic agents by Yi and co-workers.

In 2016, Banerjee and co-workers³³ reported a peptide-based gelator (Figure 6), that was capable of forming gels in PBS buffer at physiological pH. The resulting gels showed activity in their own right against Gram-negative bacteria such as *E. coli* – even without the addition of any additional antibiotic agent. Although the gel does show thixotropic behaviour, and the authors suggest it would be suitable for subcutaneous injection, the time taken for the gel to recover the ability to be self-supporting was around 6 hours. This makes it likely that the gel may be better suited for the other suggested application – such as preventing the formation of biofilms on orthopaedic implants.

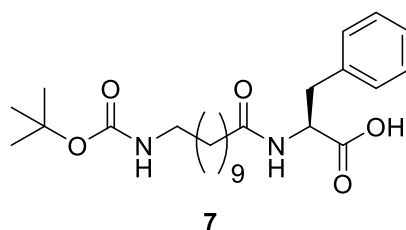


Figure 6. The gelator developed by Banerjee and co-workers, which showed antibacterial properties.

Other modified peptides, capable of forming gels, have also shown antimicrobial activity. In 2016, Laverty and co-workers reported gelators formed from NSAIDs and short peptide chains.³⁴ Three NSAIDs (ibuprofen, indomethacin, and naproxen) were investigated, each with the same short peptide consisting of two phenylalanine and two lysine residues (Figure 7). Each of these was capable of forming hydrogels.

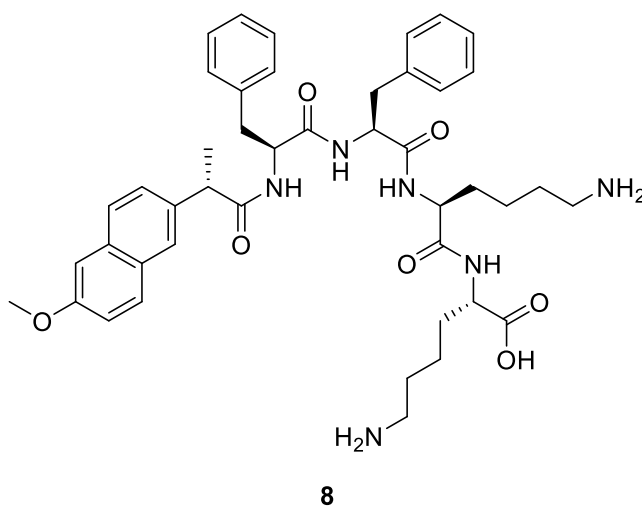


Figure 7. A modified NSAID gelator developed by Laverty and co-workers, using naproxen, two phenylalanine residues, and two lysine residues.

Following testing of the rheological properties of the hydrogels, they were investigated for antimicrobial action against four clinically relevant strains of bacteria. All three of the hydrogels developed showed some activity against both gram-positive and gram-negative strains, however, of the three, the NPX based gelator was the most promising. The suggested mechanism of action for this activity was proposed to be a combination of two factors – the hydrophobic bulk of the NPX section, and the cationic charge introduced by the lysine residues. These allow for the gelator to interact with and disrupt the bacteria cell membrane.³⁵

Interestingly, as well as the antibiotic activity observed, the NPX based gelator also maintained some anti-inflammatory activity, showing inhibition activity against cyclooxygenase (COX) enzymes, both COX-1 and COX-2. The gelator was also showed some selectivity for the COX-2 enzyme- this is desirable, as many of the gastrointestinal and renal side effects of NPX are linked to inhibition of COX-1.³⁶ These hydrogels therefore have potential to provide both antibiotic activity and analgesic effects.

In an example of the third method, Xu and co-workers³⁷ have developed an amino acid based supramolecular gel (Figure 8) that self assembles on removal of a phosphate group by a phosphatase enzyme. This can occur *in vivo* – the formation of the gel then causes the cell in which it occurs to become misshapen, resulting in bacterial cell death. In this case, the *E. coli* bacteria used were modified to overexpress this phosphatase enzyme. Without this overexpression, there was not sufficient conversion of the gelator precursor, and no gelation occurred. Although gelation was highly specific for cells that did overexpress phosphatase, this does limit applications in the real world – this type of antibiotic would only be active against bacteria that overexpress phosphatase. While this is an interesting example, it is uncommon to use this approach – likely as a result of these targeting limitations.

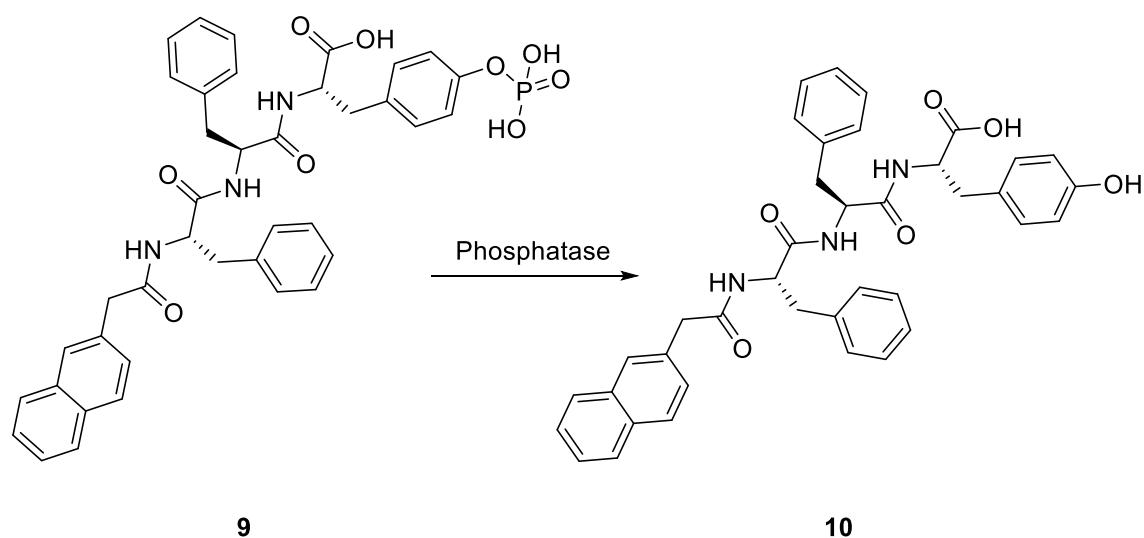


Figure 8. Dephosphorylation of compound 9 caused by phosphatase enzyme gives rise to compound 10 which self-assembles into a gel.

1.2.3 Use of Supramolecular Gels for Wound Healing

Supramolecular hydrogels are also being developed for dressings, and to aid in wound healing. Antibacterial gels can prevent the infection of wounds, helping to decrease recovery times – they also help prevent the movement of antibacterial agents into the body, reducing adverse side effects. As well as the gel providing an environment amenable to wound healing, the gelator itself can be important – in some cases the gelator has components that are important in the process of regenerating tissue.

An early example from the group of Xu used a glucosamine-based hydrogelator (Figure 9) to aid in wound healing.³⁸ Glucosamine itself is believed to play an important role in the wound healing process, helping to avoid the formation of scar tissue.³⁹ In this work, glucosamine was modified with phenylalanine and a naphthalene group, groups that are well-known to give gelation potential, in order to form two gelators with differing chirality. The hydrogel based on D-phenylalanine (**12**) was found to have slightly better biocompatibility than that prepared using L-phenylalanine (**11**). The D-phenylalanine based hydrogel was then tested for effectiveness in wound healing in mice. The application of the hydrogel led to both faster wound healing, and smaller scars than observed for the control, in which no gel was applied.

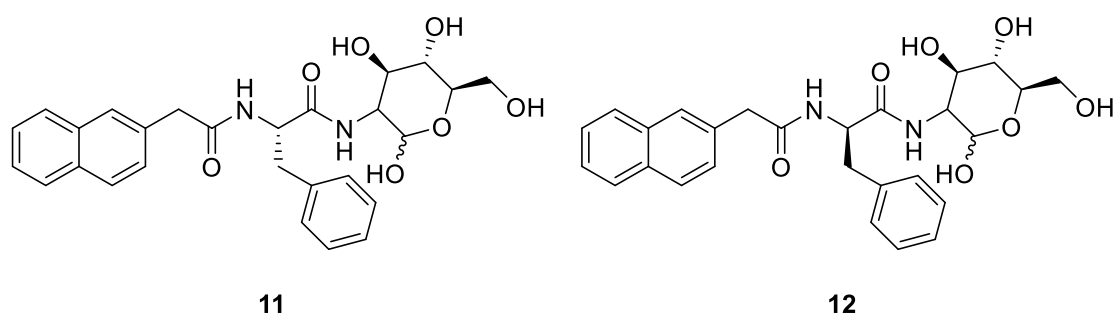


Figure 9. The glucosamine-based hydrogels developed by Xu et al. for use as aids in wound healing.

Similarly to antibacterial gels, an active component may be encapsulated within the materials that is known to aid in wound healing – this can then be released over time. Zhao and co-workers have made use of this method, developing a hydrogel based on a short peptide, that was capable of releasing NO in a controlled manner.⁴⁰ NO is produced in the body, and is known to be involved in a number of important biological pathways.⁴¹ However, delivery can be challenging – generally prodrugs are required, and these may be toxic, or metabolised before reaching the target.⁴² The group coupled a NO donor to a short peptide to form a hydrogelator, with NO being released in a highly controlled manner as a result of enzyme action – this enzyme could also be incorporated into the gel. The hydrogels gave rise to faster healing of wounds, and increased angiogenesis compared to controls.

Hydrogels can also assist in control of bleeding. Typically, polymers are used in this application, and can provide rapid haemostasis. An example of a self-assembling gel in this application was reported by Hartgerink and co-workers in 2015.⁴³ This was a peptide based hydrogel, which was capable of recovering following the application of stress, allowing it to be injected in the desired location. The hydrogel could also be loaded with batroxobin, a known anticoagulant effective even in the presence of the anticoagulant heparin.⁴⁴ However, as a small and relatively soluble molecule, it is challenging to use in controlling heavy bleeding.⁴⁵ When the hydrogel containing batroxobin was applied to a wound, bleeding was stopped rapidly, even with heparin present. Haemostasis was rapid even in comparison to commercially available treatments, indicating potential for this type of material in this area.

1.2.4 Supramolecular Gels for Cell Culture and Tissue Engineering

One of the most significant areas of recent development for LMWGs is in the field of cell culture and tissue engineering.⁴⁶ PGs such as agar have long been used to culture cells for biological

assays and other applications,⁴⁷ but interest in using LMWGs for more complex applications is growing. For example, there is a constant need for organs for transplant – and not enough donors to meet demand.⁴⁸ Furthermore, even if a donor can be found, the recipient must take medication to reduce the likelihood of organ rejection.⁴⁹ Even with this, a significant proportion of donor organs are eventually rejected.⁵⁰ An optimal solution for this problem would be to provide an organ grown from the patient’s own stem cells – but this is not straightforward. It is challenging to predict how stem cells will differentiate, and it is difficult to control - particularly to the extent that a whole complex organ could be grown. However, there are a number of approaches being investigated to improve control over cell growth. There is also great interest in the development of gels that can assist with nerve tissue growth, with applications in (e.g.) spinal cord repair.

1.2.4.1 Hydrogels for Nerve Repair

Some early work in this area was carried out by Stupp and co-workers. This group initially reported a peptide amphiphile gelator based on a five amino acid peptide (Figure 10), capable of self-assembly to form hydrogels.⁵¹ This sequence was already known to promote neurite sprouting, and to promote neurite growth,⁵² and was combined with a glutamine residue to provide a charged section, followed by alanine and glycine residues and a carbon chain, to give increasing hydrophobicity. These hydrogels were formed rapidly when a solution of gelator was mixed with neural progenitor cells (NPCs) – with the cells surviving the self-assembly process, and showed good viability. It was also found that the peptide in solution could be injected into tissue, forming hydrogels *in situ*, including in the spinal cord.

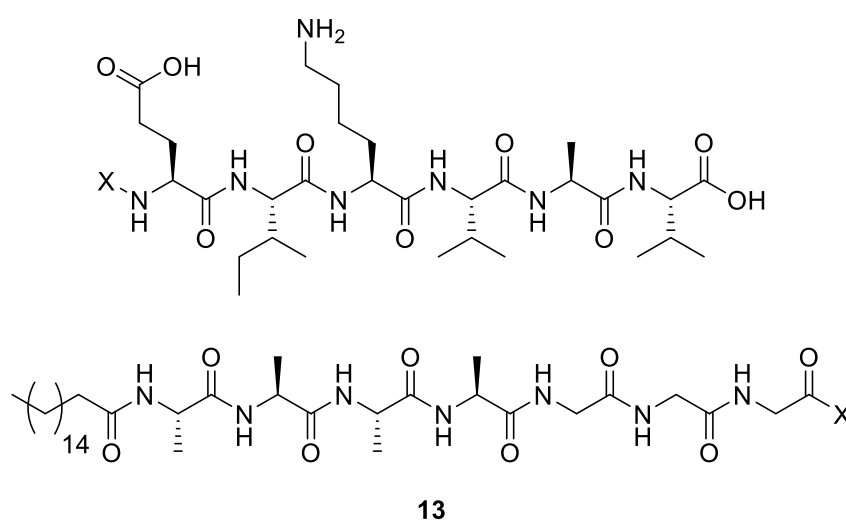
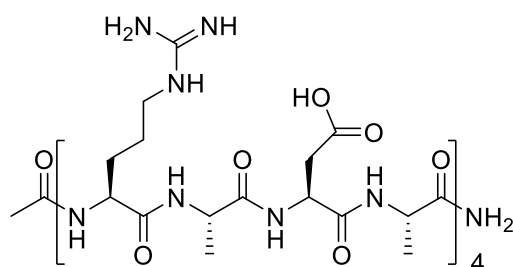


Figure 10. The peptide amphiphile gelator developed by Stupp and co-workers, based on the five peptide sequence Ile-Lys-Val-Ala-Val, that was used in repair of spinal cord injuries. X indicates where the two halves of the structure join.

This led to further work, investigating the ability of this hydrogel to promote recovery following a spinal cord injury.⁵³ The gelator was therefore injected at the site of a spinal cord injury in mice. A greater improvement was observed for this group than for any of the control groups, including that where the five amino acid peptide alone had been administered. This improvement was not observed until several weeks after the injection, but was significant. It was determined that the presence of the hydrogel helped to reduce the occurrence of increased cell size and increased cell numbers following the initial reaction to injury – the continuation of this response is believed to impact healing of spinal cord injuries. The presence of the gel also reduced the death of oligodendroglial cells – typically there is significant loss of this type of cell following injury. These factors combined helped to reduce the level of glial scarring, a factor in recovery from spinal injuries.

The ability of the gel to act as a scaffold for axons was also monitored. The material greatly increased the proportion of axons entering the injury site, and some crossed the whole of the lesion, although the paths taken were not as observed in healthy neurons. The morphologies observed were also unusual. This was observed for both motor and sensory neurons. Despite some drawbacks, this work indicates that hydrogels have the potential to act as scaffolds for tissue regeneration – even for complex nerve cells.

In other work focussing on nerve regeneration, Schneider and co-workers also developed a peptide scaffold based on alternating positive and negative amino acids.⁵⁴ This class of compounds had been shown by the same group to support cell growth in tissue culture,⁵⁵ with one in particular also able to facilitate the formation of synapses.⁵⁶ These are highly important in functioning nerves, and this therefore made this material of particular interest for nerve regeneration. This peptide, based on repeating arginine-alanine-aspartate-alanine (Figure 11), were therefore investigated for use in repair of damaged nerve cells.



14

Figure 11. The Arg-Ala-Asp-Ala repeating peptide used by Schneider and co-workers as a scaffold for regeneration of optic nerves.

The ability of the scaffold to support cell growth was tested on lesions on optical neurons. The peptide was applied as a solution, and it was observed that the presence of the scaffold gave greater improvement in tissue regeneration than for a control group. This included the growth of axons across the lesion, resulting in at least some restoration of vision in many cases. The scaffold also appeared to be biocompatible, with no inflammation observed. The breakdown of the scaffold was also observed, with most breakdown products excreted within a few weeks, and no aggregations of these observed in the brain. This suggests that scaffolds such as this could have potential in nerve regeneration.

1.2.4.2 Hydrogels in Cell Culture

In early work focussing on *in vitro* cell culture, Gough and co-workers⁵⁷ demonstrated that the composition of the gel is important for promoting cell growth. They combined Fmoc-protected di- and tri-peptides (Figure 12), with the cells being easily incorporated into the gel by triggering self-assembly of the gelators within the cell culture medium. The cells proliferated to form a 3D network, and it was also demonstrated that the presence of an aspartic acid residue was essential for proper cell adhesion in this case – indicating the importance of designing a gelator at the molecular level to achieve the desired effect.

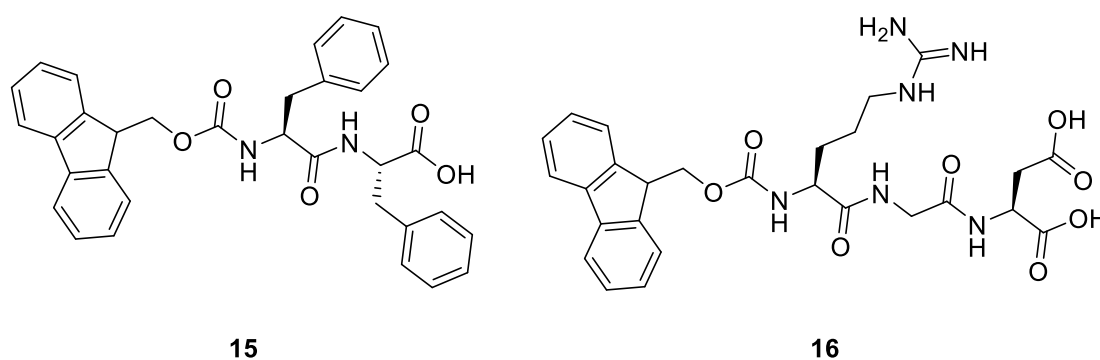
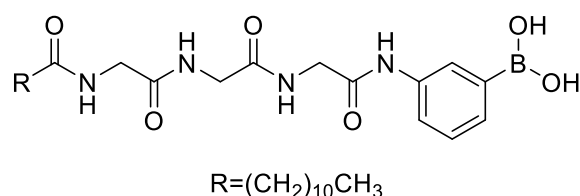


Figure 12. The peptide-based gelators used by Gough and co-workers for cell proliferation and adhesion studies.

Many studies have focussed on controlling the differentiation of stem cells. This can be achieved by modifying the stiffness of the gel on which they are grown. In general terms, a stiffer gel will lead to a harder type of tissue, such as bone, whereas a softer gel will give rise to softer tissue, such as fat or muscle.⁵⁸ In this way, the rheological (materials) performance of a gel can control the biological outcome.

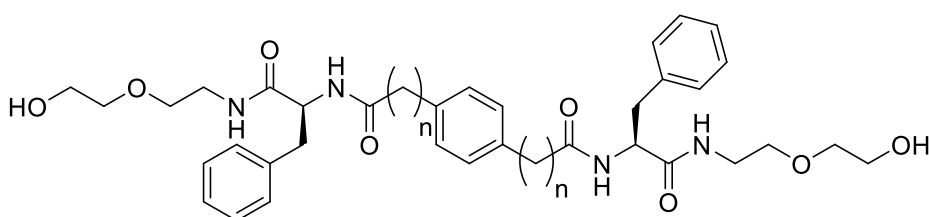
This has been demonstrated by He and co-workers,⁵⁹ who used a LMWG derived from phenylboronic acid (Figure 13) to culture mesenchymal stem cells. The stiffness of the gels was controlled by varying the concentration of gelator, and the ratio of water and PEG200 as the solvent. They found that the stiffer gels resulted in the stem cells beginning to differentiate into osteoblasts, whereas the softer gels lead to more chondrocytic differentiation. The difference in stiffness required for this difference in biological was around 10 kPa.



17

Figure 13. The gelator used by He and co-workers for the culture of mesenchymal stem cells.

In particular, LMWGs are attractive for cell culture due to effects that small modifications of the gelator can change the material properties – this is also the case with regards to cell growth. This can include changes as simple as altering the chirality of the gelator. In 2018, Feng and co-workers reported a phenylalanine derivative,⁶⁰ where the insertion of an odd or even number of methylene units impacted the chirality of the self-assembled fibres – despite no change in the chirality of the gelator itself (Figure 14). The addition of 0 or 2 units (even) gave right-handed helices, while the addition of 1 (odd) gave left-handed helices.



18

a: n=0, b: n=1, c: n=2

Figure 14. The phenylalanine based gelator used by Feng and co-workers to determine the effects of nanostructure chirality on cell behaviour.

These hydrogels were then investigated for cell culture. It was found that the material formed from gelator **18b**, made up of left-handed helices, gave an increased level of cell adhesion in comparison to the other two gelators – this in turn led to greater cell proliferation. This effect was observed with two different types of cell, despite all the gelators being derived from L-phenylalanine. This highlights the importance of having control over the structure of the

nanofibres, and the impact that simple changes can have on the nanostructure, and therefore tissue engineering applications.

1.2.5 Use of Supramolecular Hydrogels for Drug Delivery

A key area for the development of supramolecular hydrogels has been in drug delivery. Formulation is an important part of the drug development process, as the method of formulation can alter both the release profile and the way in which the drug is delivered in the body.⁶¹ These factors are very important for developing a drug prior to it entering into clinical trials. In other cases, a traditional pharmaceutical (small drug molecule) can gain enhanced activity against existing targets or additional activity against new targets by means of altering its formulation and hence its delivery mechanism. The release profile of a drug needs to be tailored to suit the required dose, as well as the way in which it is metabolised. In some cases, rapid release is required. In other situations, a gradual release of the drug over a longer period of time is required. Targeting a drug to the correct area of the body is also a key consideration – off target effects can lead to toxicity and therefore side-effects.⁶² This is a significant reason for novel therapeutics failing to pass through clinical trials.⁶³

Along with the other favourable properties that LMWGs offer for drug delivery, self-healing behaviour is a highly desirable property for certain applications.⁶⁴ This behaviour allows a material to recover following the application of increased strain or stress, such as that experienced on injection. If the recovery occurs rapidly enough following the application of the strain, a gel can be formed *in situ*, in the desired location for delivery. Supramolecular hydrogels have particular potential here as a result of the typically reversible interactions between the individual gelator molecules – these can be reformed following disruption.

1.2.5.1 Mechanisms of Release

The rate of release of a drug from a gel is dependent on the level of interaction between the API and the gel network (Figure 15),⁶⁵ and this can be altered by designing gelators to achieve the desired level of interaction. APIs can be encapsulated within the gel network, either by inclusion in the gel formation process, or by diffusion in following gel formation.⁶⁶ In some cases, there will be no interaction between the functional groups of the drug and the gel fibres, with the drug merely being held within the pores of the gel in a similar manner to the solvent. This allows for the API molecules to diffuse freely throughout the pores in the gel network. This typically leads to rapid “burst” release, with the drug leaving the gel very rapidly on administration.

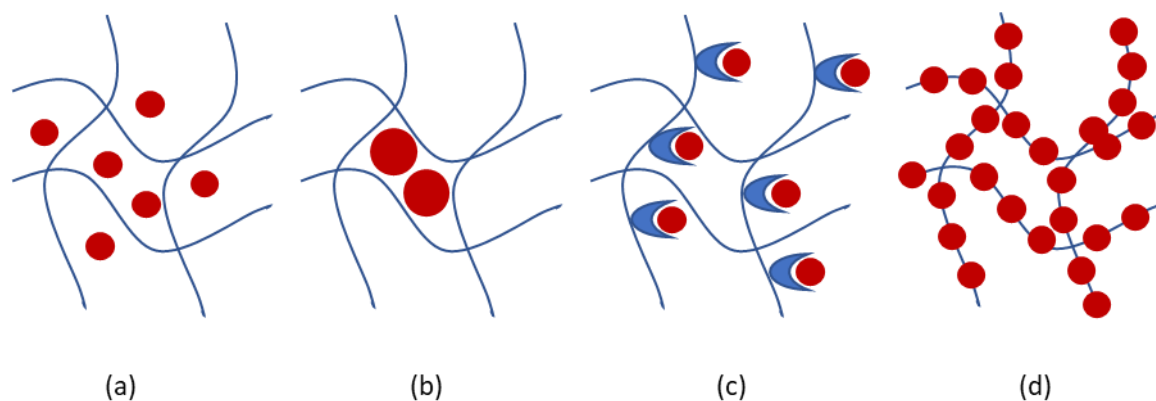


Figure 15. A schematic to demonstrate the types of interaction possible between gel nanofibres and an additive. (a) No interactions; (b) Steric interactions; (c) Non-covalent interactions; (d) Additive part of the gel network.

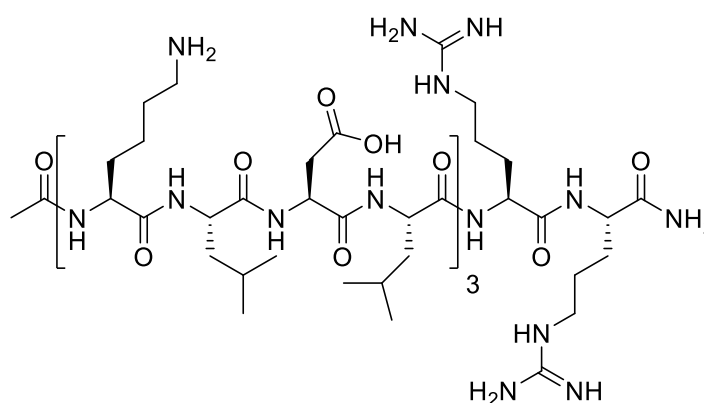
More controlled release is also possible – through interactions with the gel network. These interactions might be steric – if the drug molecule is a similar size to the pores of the gel, diffusion out of the gel might be slowed significantly. Smaller molecules will be less hindered, and therefore diffuse out of the gel faster than larger ones.

This effect was reported by Zhang and co-workers, who used a previously reported peptide based hydrogel to encapsulate a number of proteins of differing sizes, including lysozyme (the smallest) and IgG (the largest).⁶⁷ These showed significant differences in rate of release, with lysozyme release reaching a plateau after around 30 hrs. By contrast, release of IgG was still being observed after 60 hrs. The density of the network was also an important factor. On increasing gelator loading (with the loading of drug remaining the same), the network density was increased and the release of both proteins was slowed. It is possible that this simple control could lead to the ability to release two additives, at separate rates, from one gel.

However, it is difficult to predict what size pores will be formed for different gelators, and these systems are therefore challenging to develop for a specific drug. This approach has particular potential for larger biological drugs, which will be much more likely to experience steric entrapment effects.

Alternatively, there may be non-covalent interactions between the functional groups of the API, and those of the gel network. This will also slow diffusion out of the gel, and this is more likely to be predictable.⁶⁸ Liu and co-workers exploited this to achieve varying rates of release from a single hydrogel.⁶⁹ They used a gelator based on a peptide containing Lys-Leu-Asp-Leu sequences, with additional arginine residues (Figure 16). The gels also contain heparin, which interacts strongly with the arginine residues, and is effectively immobilised with the gel.⁷⁰ The two drugs,

anti-TNF- α , and hepatocyte growth factor (HGF), were encapsulated within the hydrogel. On testing the release of these drugs, it was observed that anti-TNF- α was released much more rapidly than HGF, with 70% and 30% release respectively after 120 hrs. It was suggested that this was a result of differing interactions between the additives and the network. HGF was thought to be interacting with the heparin that was in turn bound to the gel fibres – this slowed diffusion out of the gel. In contrast, anti-TNF- α was not thought to interact significantly with the gel, and therefore diffusion was much faster. This system was also demonstrated to have a positive impact on a renal injury *in vivo*. This study suggests that supramolecular hydrogels do have potential for use as dual drug delivery platforms.



19

Figure 16. The peptide used by Liu and co-workers as a dual drug delivery platform.

Another example of controlled release being obtained by interaction of the drug with the fibres was reported by Amabilino, Calpena and co-workers in 2015.⁷¹ They reported the use of a bis-imidazolium based amphiphile (**20**), capable of forming gels in water/ethanol mixtures (Figure 17). These gels were then used to encapsulate the anti-inflammatory drugs ibuprofen (**21**) and indomethacin (**22**). NMR studies indicated that all of the incorporated drug was interacting with the gel fibres. This resulted in limited release being observed *in vitro*, particularly for indomethacin. Permeation tests also indicated that the gels would make a suitable vehicle for transdermal drug delivery. This was therefore tested *in vivo*, with good anti-inflammatory effects noted after 4 hours, particularly for indomethacin.

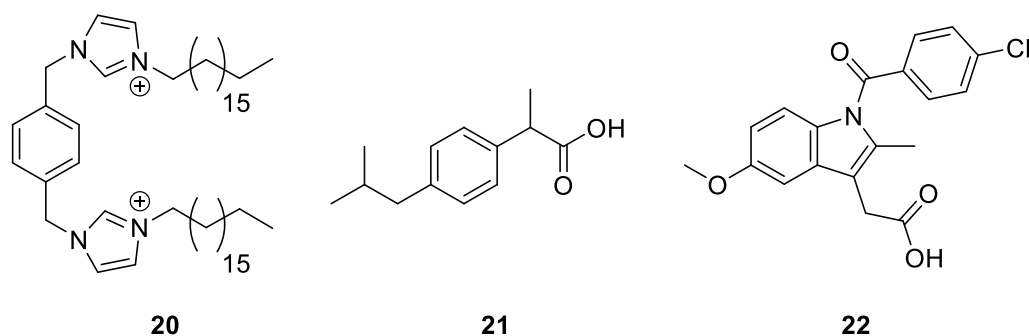


Figure 17. The bis-imidazolium based gelator used by Calpena and co-workers for encapsulation and release of ibuprofen and indomethacin.

Systems can also be designed to give faster release in some environments, and slower in others, to provide a degree of targeting – for example, different rates of release at different pH values. Drug release can also result from breakdown of the gel network, as a result of a specific stimuli, allowing the encapsulated drug to be released.⁷² Additionally, erosion of the hydrogel (more commonly reported in polymeric hydrogels) can also be a factor in the release of an active ingredient – as the gel is broken down, the additive is no longer encapsulated within that part of the gel, and is therefore released.⁷³ In most cases, it is likely that multiple factors will be impacting the rate of release – these different factors can be difficult to separate. There are a number of methods available for triggering the breakdown of supramolecular hydrogels – this is one of the factors that makes them so attractive for drug release. Often, such breakdown is triggered by enzyme action, or a change in pH, but other methods can also be used. In 2011, Hamachi and co-workers reported a protected peptide gelator (**23**) sensitive to oxidation – addition of H_2O_2 led to breakdown of the gelator, and therefore the gel (Figure 18).⁷⁴

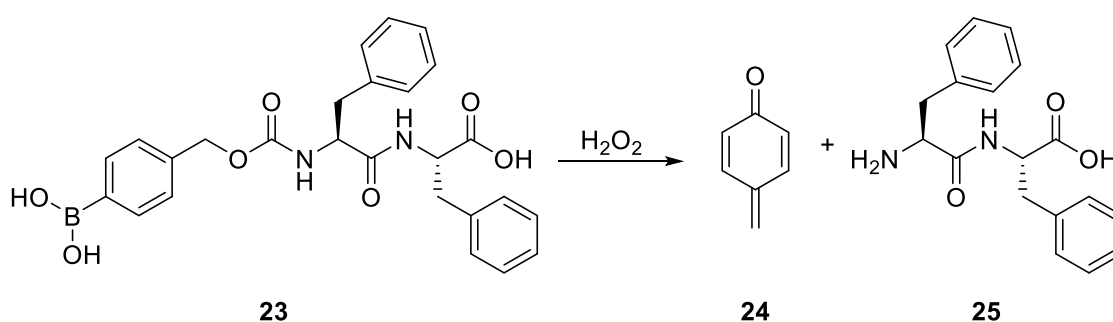
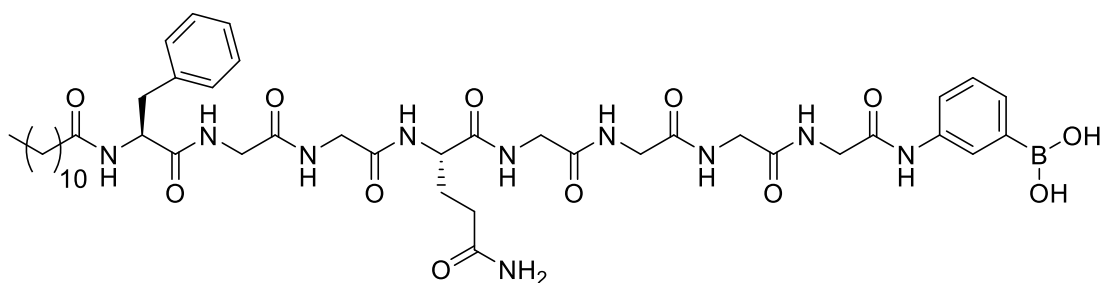


Figure 18. The gelator (left) used by Hamachi and co-workers for triggered insulin release, and its breakdown products (right) following exposure to H_2O_2 .

To introduce responsiveness to biological factors, the group encapsulated glucose oxidase within the gel. This enzyme produces H_2O_2 in the presence of D-glucose⁷⁵ – it was thought this could trigger breakdown of the hydrogel. This did indeed cause breakdown of the hydrogel, over a period of about 5 hours. The group then added insulin to the gel, along with the glucose oxidase

enzyme, and followed its release, both with and without exposure to D-glucose. When the hydrogel was not exposed to D-glucose, very little insulin (less than 10%) was released. In contrast, when D-glucose was also present, the gel broke down, and there was a corresponding release of insulin. It was suggested that this relatively simple method of triggering gel breakdown could be developed to provide a platform for insulin release in treatment of diabetes.

As well as controlling the release of a drug by controlling breakdown of the gel, the surrounding environment can impact release, without breaking down the hydrogel. An example of this was reported in 2017 by Wu and co-workers.⁷⁶ They developed a peptide-based gelator (Figure 19), capable of forming hydrogels in pH 7.4 PBS solution, and stable across a range of pH values.

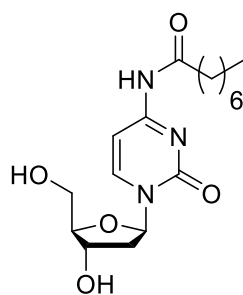


26

Figure 19. The peptide based gelator used by Wu and co-workers for encapsulation and release of doxorubicin.

The chemotherapy drug doxorubicin (DOX) was then encapsulated within the hydrogel, and release was tested at a number of pH values. Release was found to be low at a physiological pH of 7.4, and in a weakly alkaline environment (pH 8.9). There was a greater level of release obtained at acidic pH – with the greatest level of release observed at the lowest pH, 4.4. This greater release at low pH values (common in tumour microenvironments), combined with the generally very slow release (less than 10% release at any pH), led the authors to suggest that the hydrogel might be suitable for long term, slow release of DOX to treat tumours.

In 2020, Marlow and co-workers reported a study into factors impacting the rate of release of various bioactive molecules from a nucleoside based hydrogelator,⁷⁷ previously reported by the same group (Figure 20).⁷⁸



27

Figure 20. The nucleoside based gelator used by Marlow and co-workers to study the rate of release of varied bioactive molecules.

A number of proteins were chosen to be incorporated within the hydrogel – bovine serum albumin (BSA), β -lactoglobulin (β -lact), insulin and lysozyme. Of these, BSA, β -lact and insulin have varying molecular masses, but are all negatively charged under physiological conditions, whereas β -lact and lysozyme have similar molecular weights, but opposite charges. The study determined that each of the proteins interacted closely with the gel fibres, rather than being ‘free’ within the pores of the gel network. These hydrogels were also capable of protecting the incorporated proteins from enzyme action, and following injection of the hydrogel *in vivo*, no toxicity or inflammation was observed.

When release of the proteins from the hydrogel was investigated, all of the proteins had very similar release profiles, despite the differing sizes and charges. As the release rates were also similar to the erosion rate of the hydrogel, it seemed likely that this was the driving factor for release. This is at least partly a result of the significant interactions between the proteins and the gel fibres – without which there would be diffusion out of the gel. This hydrogel is a promising platform for the delivery of bioactive proteins, particularly if the rate of gel erosion could be controlled.

As well as these mechanisms of release, which typically rely on slowing diffusion for control over release rates, it is also possible to achieve triggered release from a supramolecular gel. Generally, to achieve this, the drug will be part of the gel network – and therefore cannot be released until the network is completely broken down. This breakdown can be designed to only occur in the presence of a specific stimulus, such as a particular enzyme, with the aim of targeting a specific area or pathway in the body. This is generally achieved by using a prodrug as a gelator, with the drug released as the gel is broken down. Either a known gelator can be tethered to the drug that is to be delivered,⁷⁹ or the drug can be modified to give a gelator.⁸⁰

To obtain triggered release, the drug may be incorporated within the gel structure. This requires the breakdown of the gel before any release can take place – no diffusion of the drug out of the gel takes place before this breakdown. An example of this was reported by Miravet and co-workers in 2010.⁸¹ They developed gelators based on Fmoc-L-lysine, linked to a model drug by the self-immolative linker *p*-aminobenzyloxycarbonyl (Figure 21).

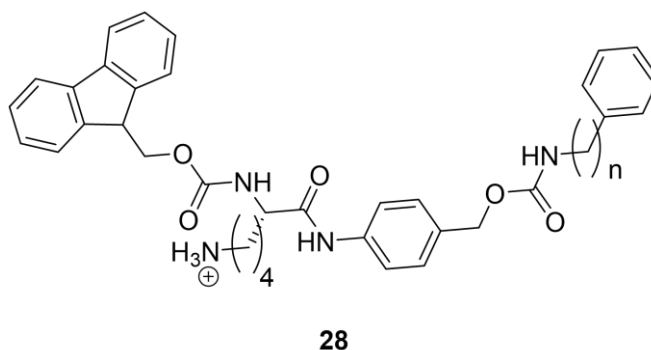


Figure 21. Model prodrug gelator developed by Miravet and co-workers for triggered drug release. $n=1$ or 2 .

These gelators were capable of forming gels in ethanol/buffer mixes, with gelation occurring on addition of buffer to a solution of the gelator in ethanol. It was then demonstrated that if the enzyme trypsin was added along with the buffer, the gel would form, before being gradually broken down by the action of the enzyme, over the course of around 30 hrs. Analysis of the resulting mixture indicated that the breakdown had occurred at the linker, leading to release of the model drug. This proof of concept work indicated that it would be possible to use such linkers for gelator prodrugs, sensitive to enzyme action, to provide triggered release.

1.2.5.2 Mechanisms of Delivery

The delivery route is also an important consideration when a drug formulation is developed. Depending on the desired route of administration, and the drug being given, different formulations will be required. Common routes of drug administration are oral or by injection.⁸² Injections may be intramuscular, intravenous and or subcutaneous. Other potential routes of administration relevant to gels include topical, transdermal, and via mucous membranes, including sublingual and nasal delivery.⁸³

Oral delivery is the most common and straightforward approach, with patients able to easily manage their own medication, and the formulations being relatively cheap to develop and manufacture. However, the drug must be protected from the acidic conditions in the stomach. This method of delivery can also be inefficient – with only a small proportion of the drug reaching the desired target. This is partly because some of the drug may never be absorbed into the

bloodstream from the small intestine. Of that which is absorbed, more will be metabolised by first pass liver metabolism prior to entry into the bloodstream – for some drugs, this can be a considerable proportion.⁸⁴

Intravenous delivery avoids these issues by delivery directly into the bloodstream. This also makes the drug available very rapidly, particularly useful in an emergency situation. However, it can be impractical to use outside of a clinical setting as intravenous injection requires a level of technical skills, and many patients would be unwilling to inject themselves in that way. Intramuscular delivery has similar issues, although sub-cutaneous injections can now be carried out using autoinjectors.

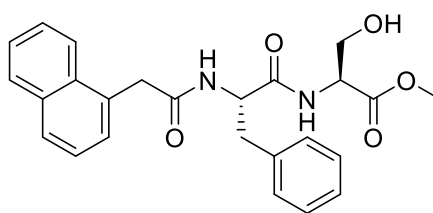
Generally, the mode of administration will often be chosen based on whether the required drug delivery is systemic or local, the time taken for the drug to be available, and whether first pass liver metabolism needs to be avoided. Systemic delivery is useful when there is no need for targeted delivery of the drug. This covers most forms of drug delivery – the drug enters the bloodstream and is transported around the whole body. Local delivery is used when the effects of a drug are only required in a very specific area, but is not always easily achievable. A good example would be drugs required to treat the lungs (e.g. asthma, cystic fibrosis etc.), which are often delivered by inhalation. The time for onset of action is also critical. Drugs delivered intravenously can be available in as little as a couple of minutes⁸⁵ – by contrast, it can take 30 minutes or more for orally delivered drugs to take effect.⁸⁶ Most other methods of delivery fall somewhere between these two.⁸⁷ Other methods allow for a slower or longer lasting release – for example, intramuscular injection can be used for slow release and depot formulations.⁸⁸

There is interest in using gels for development of new formulations across a range of delivery methods. For example, gels have been successfully used to develop topical painkillers – these are now commercially available.⁸⁹ Currently, such commercially available formulations use polymer gelators, such as carbomers or cellulose. These are present simply to provide the required thickening effect – they are not active ingredients. For topical applications, a gel has a clear advantage over a solid or a liquid formulation, providing good contact with the skin, while being viscous enough for that contact to be maintained. Gels can also be preferable over creams, as with gels there is little need for any ingredient other than the API, water or other solvents, and the gelator. This simplicity is attractive across a range of dosage forms.

It has been shown that a wide range of APIs, with a range of targets and modes of action, can be encapsulated within supramolecular hydrogels. These include painkillers, anticancer agents, antiretrovirals, antibiotics, anti-inflammatories and hormones.⁹⁰

Perhaps one of the most significant areas of development for supramolecular gels is to use them as some form of implant to act as a reservoir of drug, allowing for controlled release over an extended period of time. Here, the fact that many supramolecular gels are developed from highly biocompatible components is a significant advantage. This means that the gel containing the drug can either be injected, if it has thixotropic properties, or if this is not the case, perhaps implanted after surgery.⁹¹ The drug can then be released slowly from the gel over an extended period of time. This is attractive for two reasons – firstly, the gel will keep the drug in the desired area of the body, improving the targeting. Secondly, as the gel can be designed to be biodegradable, there is no need for additional surgery to remove the implant. A common tactic for designing novel gelators is to use molecules for which the metabolic pathway is already reasonably well-understood. This means that gelators can be chosen that will not break down to give products that have a detrimental effect. The rate of breakdown can also be considered – if the gel breaks down slowly, this can slow the rate of release of the drug. Triggered release can also be a consideration, with systems designed to not release the drug before the gel has broken down in response to a specific biological or physical trigger.

An example of using a supramolecular gel as a drug depot was reported in 2017 by He and co-workers, who used a LMWG to form a depot for cancer treatment.⁹² They used a dipeptide (Figure 22) capable of forming gels in ethanol. Although generally hydrogels are preferred for use in biomedical applications, in this case ethanol was used to provide percutaneous ethanol injection (PEI) therapy. The gel acted to keep the ethanol in close proximity to the tumour.



29

Figure 22. The dipeptide based gelator used by He and co-workers to form a drug depot for release of DOX.

Once formed, these hydrogels were injectable. This is desirable, as the gel can be formed in a very specific area, provided recovery from the higher shear strain is rapid. In this case, the gel was reformed within ten minutes following subcutaneous injection, which was fast enough for the gel to form in the desired location. As well as the effect of ethanol, additional chemotherapeutic effects were sought by encapsulating DOX within the gels. *In vivo* studies indicated that the ethanol gel loaded with DOX showed good activity against a tumour, inhibiting growth

significantly more than controls. This effect was observed for at least 30 days following the injection of three doses of the gel – indicating that slow release of the DOX was achieved.

1.3 Modification of Gelator Molecules

It is still very challenging to design molecules specifically to act as LMWGs, with most being discovered serendipitously.⁹³ This is due to the complex factors that determine whether a molecule can assemble in the manner required for gel formation. However, some progress is being made in designing gelators. Often, a gelator is developed from a molecule which is already known to self-assemble in some way – this provides a starting point for development.

1.3.1 Important Factors for Gelation

For gelation to occur, the right balance between solubility and crystallisation needs to be achieved.⁹⁴ In the case of hydrogelators, this usually requires a mix of hydrophobic and hydrophilic regions within the gelator molecule. Generally, the gelator needs to be partially soluble in water – requiring a trigger, such as heating, for complete dissolution. The gel is then formed as the gelator becomes less soluble, for example as the solvent cools down.

Generally, hydrogelators are capable of a number of different non-covalent interactions in combination. Solvophobic interactions and van der Waals interactions encourage the assembly of hydrophobic domains and drive the gelation process. Particularly important for hydrogels are hydrogen bonding interactions – both between gelator molecules, and between the gelator and the solvent.⁹⁵ These help mediate the solubility of the gelator, preventing it from simply crystallising, and can also encourage specific orientational arrangement of the gelator molecules. As a result, most hydrogelators have multiple groups that are capable of forming hydrogen bonds, as well as regions that are hydrophobic.

For gelation, it is important that the gelators assemble in a one-dimensional manner, forming nanofibres rather than crystals. If this is not the case, following the application of the gelation trigger, a precipitate will simply be formed, rather than the desired gel. This means that the shape of the gelator molecule and the orientational ability of the non-covalent interactions between gelators play a key role in controlling the assembly process to give one-dimensional order, rather than three-dimensional structures that would rather simply crystallise.

These factors therefore need to be carefully considered during gelator design. Although such design is challenging, it is highly desirable to be able to achieve this - changing the gelator molecule can lead to changes in the properties of the final material. This can allow for the

development of tuneable materials. Additionally, for the design of ‘smart materials’, it is important to consider any additional functional groups that might be able to interact with additives. Such considerations are what moves a gelator from acting merely as a thickener, to having an impact on the behaviour and interactions of the material, and endowing it with potential high-tech applications, as illustrated below.

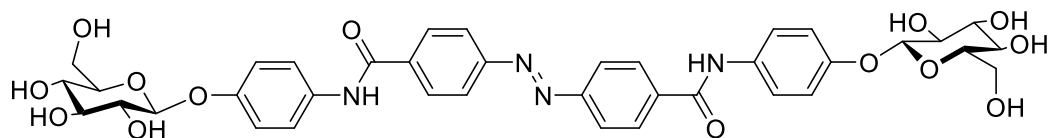
1.3.2 Common Types of Gelator Molecule

It is common for hydrogelators to be based upon natural bioavailable molecules – these often contain both hydrophilic and hydrophobic groups. It is also worth reflecting that controlled self-assembly is commonplace in nature, which might suggest that this type of building block is well-suited to the target of gelation. Modification of these molecules is also feasible using well-established synthetic methodologies, allowing for the design and tuning of gelator molecules. Natural molecules therefore provide a good starting point for the development of novel hydrogelators.

1.3.2.1 Sugars

Sugars are a common starting point for the development of hydrogelators. Sugars themselves are typically too water-soluble to act effectively as gelators – therefore they are usually modified to give them a degree of hydrophobic character. These are then capable of forming hydrogels.

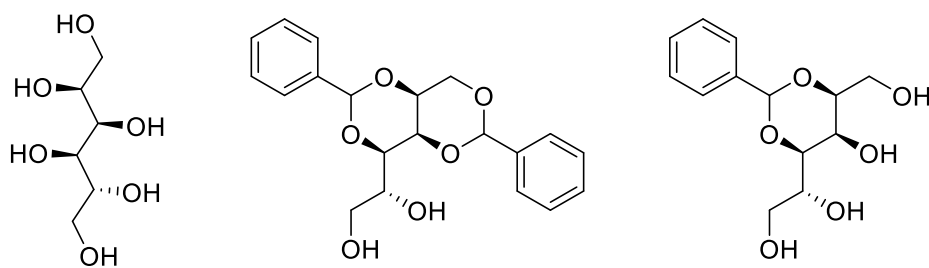
Some of the earliest sugar-based hydrogelators were reported by Shinkai and co-workers.⁹⁶ They developed a small library that combined sugar and azobenzene moieties, one of which was capable of acting as a supergelator (Figure 23). They carried out studies to determine the driving forces for gelation, which indicated that the π - π stacking resulting from the presence of the azobenzene groups was an important factor in driving gelation. There was also evidence of hydrogen-bonding interactions between the amido groups, with the sugars at each end of the gelator providing sufficient hydrophilicity for gelation to occur.



30

Figure 23. The azobenzene/sugar gelator investigated by Shinkai and co-workers.

An example of the way in which changing the structure of the gelator molecule can influence material properties can be observed with sorbitol based gelators, both the mono- and di-substituted systems are capable of forming gels (Figure 24).



31

32

33

Figure 24. The structures of *D*-sorbitol (**31**); dibenzylidene sorbitol (**32**); monobenzylidene sorbitol (**33**).

Dibenzylidene sorbitol (DBS) (**32**) itself is produced via an acetal formation, and was noted for its gelating properties as early as 1891.⁹⁷ This is a reversible process, and it is therefore likely that the process results in the formation of the thermodynamic product – this has the benzylidene group in the equatorial position. Although Brecknell *et al.* reported the stereochemistry at the acetal positions to be equatorial, there is no consensus on the stereochemistry within the literature.⁹⁸ It was mostly used to thicken organic solvents (DBS is essentially insoluble in water and therefore cannot act as a hydrogel). Simple modifications of the compound were carried out to give DBS derivatives, which in turn found significant use in the personal care industry⁹⁹ and as polymer additives.¹⁰⁰ These modifications are commonly carried out at either the free alcohol groups, or by changing the aromatic ‘wings’ (Figure 25).¹⁰¹

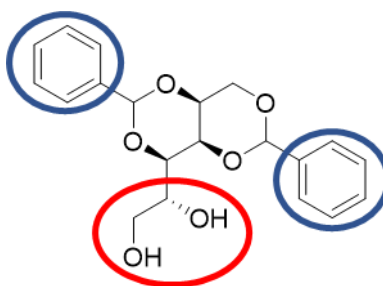


Figure 25. Common sites for modification of DBS. Blue circles: aromatic wings. Red circles: free alcohols.

However, initially these modifications, mostly carried out in industrial research, did not significantly change the solubility of the derivatives in water, with the addition of functional groups such as halogens, alkyl groups and nitro groups to the aromatic wings being targeted.¹⁰² The free alcohols can also be modified, with the primary alcohol being a more popular target due to its increased reactivity. These modifications have typically focussed on esterification of one or both of the free alcohols.^{99c} As a result of these modifications having relatively little impact on the water solubility of the molecules (indeed, if anything, they decrease it), the applications of such derivatives were still limited, particularly in biomedical settings.

While the formation of organogels can be useful, most applications of DBS derivatives in this area have continued to simply make use of the thickening ability of such molecules. This has not excluded biomedical applications, for example, a formulation of an ethanol-based DBS organogel has been applied for the topical delivery of painkillers such as tramadol.¹⁰³ DBS-based gelators have also been used in formulations of drugs that are susceptible to abuse – the addition of a DBS derivative to the formulation resulted in the separation of the API from the mix being very challenging.¹⁰⁴ While still useful, the inability of DBS to form hydrogels did limit the prospective applications of DBS derivatives in biomedical settings.

In 2013, the Smith group reported the DBS derivative DBS-CO₂H (Figure 26), which has carboxylic acid groups on the aromatic wings.¹⁰⁵ This is achieved by carrying out the acetal formation with a modified benzaldehyde, giving ester groups on the aromatic groups. The ester can then be converted by hydrolysis to give the desired carboxylic acid. The presence of these groups gave increased solubility in water, allowing for the formation of hydrogels.

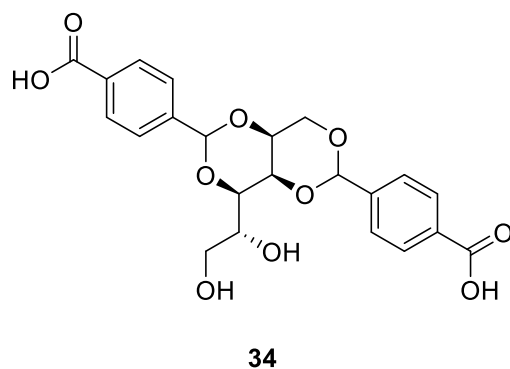


Figure 26. The structure of DBS-CO₂H.

Also in 2013, a second derivative (DBS-CONHNH₂) was reported (Figure 27).¹⁰⁶ As with the addition of carboxylic acid groups, the ester derivative is formed first. This is then converted to the acyl hydrazide by reaction with hydrazine monohydrate.

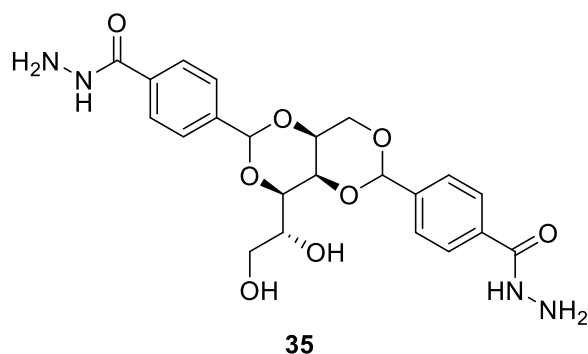


Figure 27. The structure of DBS-CONHNH₂.

Both of these are capable of forming hydrogels, and each has a different trigger. DBS-CO₂H forms gels upon a change of pH from high to low – this leads to protonation of the carboxylic acid groups, and the gel is formed as a result of the corresponding decrease in solubility.

DBS-CONHNH₂, however, is formed via a heat/cool cycle – dissolving on heating, and the gel forming once this solution has cooled. Unlike many supramolecular gels, this gelator is stable across a range of pH values (ca. 2-12), increasing the scope for potential applications.

Both of these gelators have potential for biomedical applications. DBS-CONHNH₂ is particularly of interest as a result of the interactive nature of the acyl hydrazide groups – these are capable of interacting with a number of additive functional groups, including aldehydes (via covalent reaction to form an acyl hydrazone)¹⁰⁷ and carboxylic acids (via the formation of acid-amine type interactions).¹⁰⁸ This enables this derivative to be useful in a number of different applications – especially drug delivery, with DBS-CONHNH₂ hydrogels having been shown to be capable of pH mediated release of acid-functionalised non-steroidal anti-inflammatories including naproxen and

ibuprofen.¹⁰⁹ The development of DBS derivatives that are capable of forming hydrogels should expand the range of applications that are available, particularly in biomedical areas.

Monobenzylidene sorbitol (MBS) derivatives have also been used in a number of different industrial applications, although not as widely as DBS derivatives. MBS itself was first reported in 1935,¹¹⁰ and has applications in areas such as cosmetic formulations.¹¹¹ These are more water soluble than their DBS equivalents, as a result of the larger number of free alcohol groups and smaller number of aromatic rings. Depending on the functionalisation, this opens up the possibility of them acting as hydrogelators more readily.

Some more high-tech applications of MBS derivatives have recently been reported. In one example, reported by Feng and co-workers in 2012, an MBS derivative (**36**) (Figure 28) was used to gel a KOH solution for use as an electrolyte, which showed good electrochemical stability and charge/discharge behaviour.¹¹²

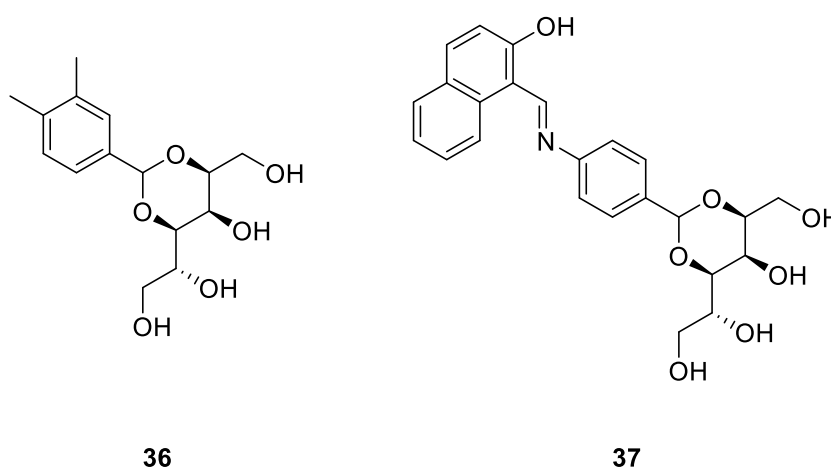


Figure 28. Left: The MBS based gelator used by Feng and co-workers as an electrolyte. Right: The MBS derivative used by Niu and co-workers.

In another example, Niu and co-workers reported an MBS derivative (**37**) (Figure 28) that formed gels in a mix of water and DMSO, which were sensitive to Cu²⁺ ions,¹¹³ with the gel network breaking down on exposure to them as a result of ligand-metal binding. It was suggested that this hydrogel would be suitable for use as a sensor for Cu²⁺ ions, with the change on exposure to the ions being visible to the naked eye. However, while there have been some preliminary investigations into MBS derivatives as hydrogels, there remains plenty of scope for further development in this area.

1.3.2.2 Amino Acids

As with sugars, amino acids are readily available molecules that typically contain multiple groups capable of hydrogen bonding, and are therefore attractive starting points for the development of hydrogelators. Additionally, many methods for the modification of amino acids are well established, and are widely used – this helps when attempting to develop a novel gelator.

Furthermore, once a gelator based on one amino acid has been developed, other amino acids can also be modified in the same way, and the changes in the properties of the resulting molecule investigated. This allows the development of a structure-activity effect understanding of this class of gelator, and furthermore, these relatively simple changes often result in gelators that have differing properties, and are therefore more suitable for different applications.

Fmoc-protected amino acids and dipeptides have been known as hydrogelators since 1995, when Janmey and co-workers reported Fmoc-Leu-Asp (**38**) (Figure 29) as being capable of forming gels in water.¹¹⁴ These hydrogels were also used for the encapsulation of antiviral drugs, and on injection of the drug loaded hydrogel, antibody production was observed in rabbits. Some years following this, Xu and co-workers reported the gelation of Fmoc-Phe (**39**), with the amino acid very slightly modified to allow for gelation to be triggered by enzyme action (Figure 29).¹¹⁵ This gelator was used as a sensor for the presence of enzymes, in this case acid phosphatase.

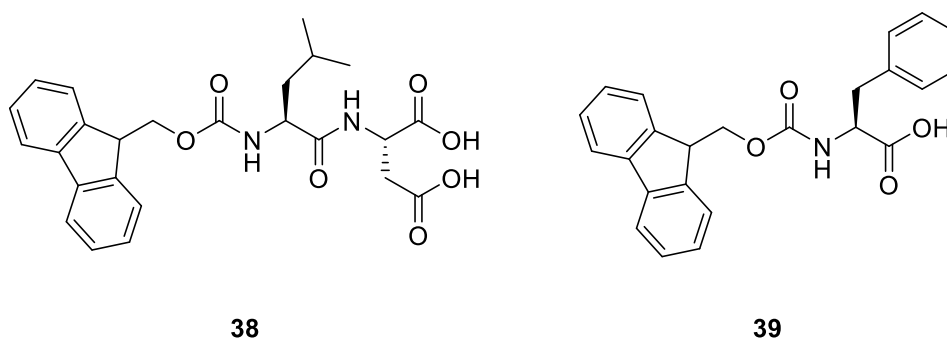


Figure 29. Early Fmoc-protected amino acid based gelators. Left: The Fmoc-Leu-Asp gelator reported by Janmey and co-workers, and used to encapsulate antiviral drugs. Right: The modified Fmoc-Phe gelator used by Xu and co-workers for detection of enzymes.

This type of gelator is promising as a result of their straightforward synthesis, good biocompatibility and simple nature. Since this time, numerous amino acid derivatives have been used in an increasingly wide range of applications.¹¹⁶ The use of Fmoc as a protecting group is especially common for this type of gelator, as a result of the π - π stacking interactions facilitating gelation, with the use of a simpler hydrophobic protecting group often not being sufficient for gelation.¹¹⁷

In 2020, Jia and co-workers reported an investigation into three amino acid based gelators.¹¹⁸ These were based on tryptophan (**40a**), methionine (**40b**) and tyrosine (**40c**), each protected with Fmoc (Figure 30). While a number of Fmoc protected amino acids have previously been reported as gelators,¹¹⁹ those described in this paper had not previously been investigated for antibacterial activity. All three were found to be capable of forming hydrogels with the material properties and antibacterial activities of the gels then investigated.

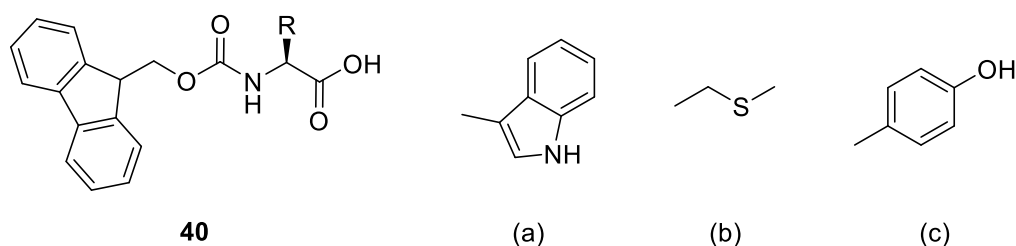


Figure 30. The gelators developed by Jia and co-workers - the general structure (**40**) and the R group present with (a) tryptophan; (b) methionine; (c) tyrosine.

It was found that changing the amino acid, alters the properties of the resulting gel. For example, each of the hydrogels had a differing stiffness – with Fmoc-Tyr being the stiffest, and Fmoc-Trp the least stiff. In an inhibition zone test, two of the hydrogels, Fmoc-Trp and Fmoc-Met, showed reasonable activity against gram positive bacteria while, Fmoc-Tyr showed no antibacterial activity against either gram positive or gram-negative bacteria. Although these gelators do have quite different structures, and therefore it is not especially surprising that the materials will have differing properties, the differences show that only relatively simple changes can be required to alter the behaviour of a gelator - simply changing an amino acid is generally a relatively straightforward procedure.

The chirality of the amino acid is also important for the material properties. Most gelators are based on L-amino acids – the naturally occurring, and therefore more widely available, form. However, the introduction of D-amino acids can lead to the resulting material having different properties. This introduction of the second enantiomer can be carried out in two ways. Firstly, the gelator can be synthesised entirely from the D- enantiomer, and this gelator used to form the gel. Alternatively, a mix of the two enantiomers can be used.

One key area in which the use of D-amino acid gelators can be particularly useful is in designing scaffolds for tissue engineering. It is known that peptides based on the non-natural enantiomer is less susceptible to being broken down,¹²⁰ and therefore a scaffold designed from D-amino acids

will be longer lasting, and may perform better than a scaffold based on L-amino acids that can break down faster as a result of the action of peptidase enzymes.

In 2013, Banerjee and co-workers reported an amino acid based gelator for the delivery of doxorubicin.¹²¹ This is an effective anti-cancer drug that is routinely administered, but has significant side effects, such as cardiotoxicity, at higher doses.¹²² Alternative, more controlled and targeted routes of delivery, rather than the usual intravenous delivery method,¹²³ are therefore of significant interest, and there are numerous examples of hydrogels (both polymeric and supramolecular) being developed to achieve this.¹²⁴ The group had already developed a gelator that was capable of encapsulating and releasing doxorubicin.¹²⁵ However, this was rapidly broken down in the presence of enzymes, which would result in rapid release of any drug. A similar gelator was therefore developed, comprised of three phenylalanine residues, Boc-protected at the N terminus. To improve the proteolytic stability of the hydrogels, D-phenylalanine was used in place of L-phenylalanine at each position, to synthesise each of the possible stereoisomers (Figure 31).

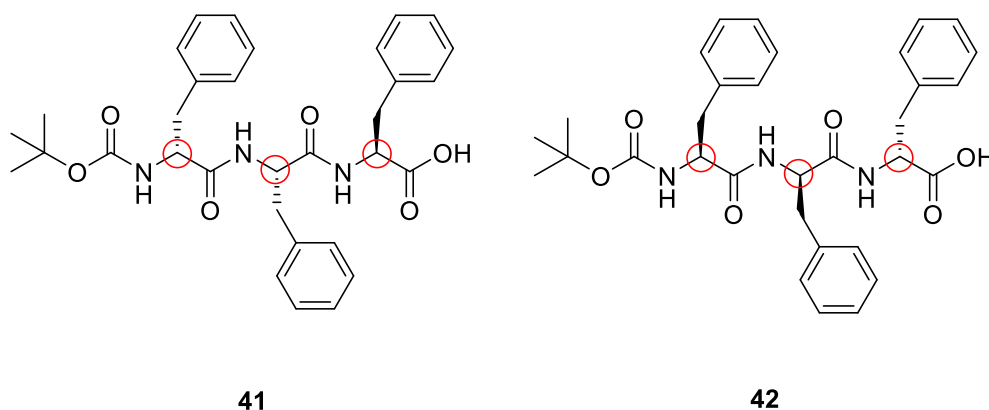


Figure 31. Two of the phenylalanine based gelators studied by Banerjee and co-workers for proteolytic stability and release of DOX. Left: amino acid sequence DLL. Right: amino acid sequence LDD. The chiral centres are shown by the red circles.

There were some immediate differences between the stereoisomers, with not all being capable of forming hydrogels. Rheological studies indicated that the position of the D-enantiomer was important in determining the stiffness of the gel. These differences are not especially surprising, as the different gelators have a diastereomeric relationship with one another and on changing the chirality, different functional groups will have a corresponding change in orientation. This leads to a change in the interactions that can take place. All of the hydrogels that were formed were capable of encapsulating doxorubicin, with each giving a similar release profile. Crucially, when the proteolytic stability of the hydrogels was investigated, those with a greater proportion of

D-phenylalanine were much more stable than their respective enantiomers, which were degraded within 24 hours. This should lead to slower drug release *in vivo*.

This is a positive development in terms of being able to control the properties of a material to fit the desired application – for example, here a different material can be obtained by simply combining different enantiomeric building blocks to give stereoisomerically well-defined products.

1.3.2.3 Nucleobases

Another class of natural molecule, nucleobases, key components of nucleotides, nucleosides and nucleic acids, are an attractive choice for supramolecular gelators. There are two categories of nucleobase – purines (including adenosine and guanine) and pyrimidines (including uracil, thymine and cytosine). Pyrimidines are based on a single ring, whereas purines have a bicyclic structure (Figure 32). Nucleosides and nucleotides also contain a ribose sugar, and it is these that typically provide a starting point for the development of hydrogelators. These molecules readily form non-covalent interactions, containing multiple sites for hydrogen bonding, and are also capable of π - π stacking, as they are aromatic. This ability to form multiple non-covalent interactions means nucleobases commonly self-assemble – the most famous result of which is DNA.¹²⁶ This type of molecule has also been known to form hydrogels for some time – with guanosine-based molecules first reported as forming hydrogels as early as 1910.¹²⁷

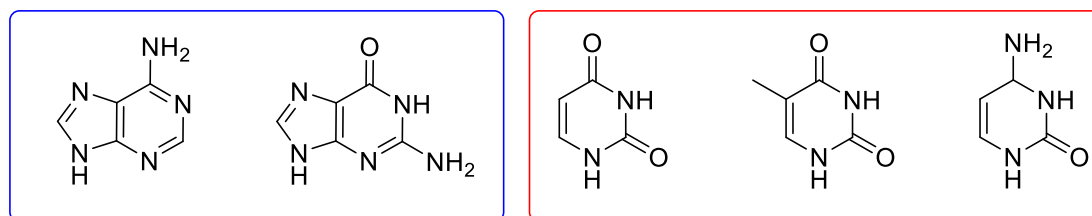
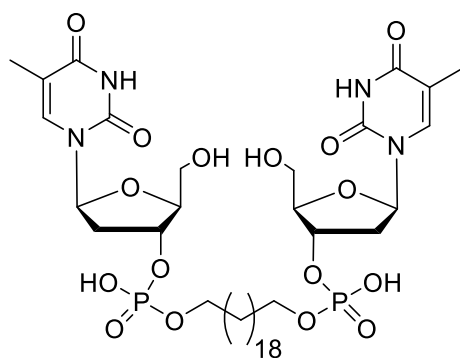


Figure 32. Left (blue box): Purines, adenosine and guanine. Right (red box): Pyrimidines, uracil, thymine and cytosine.

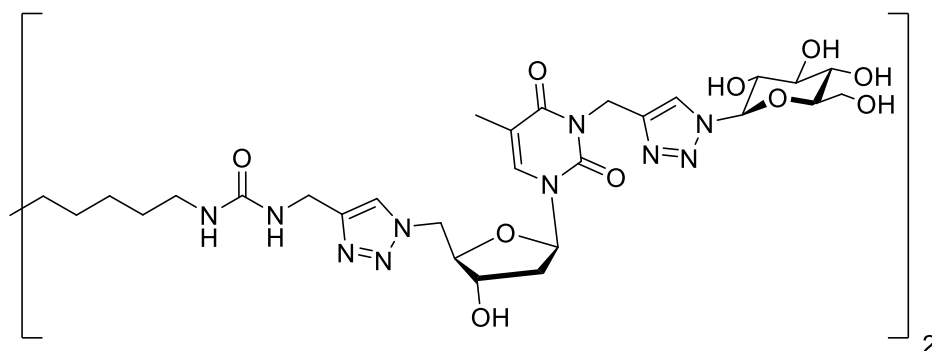
With the exception of guanosine, generally nucleosides and nucleotides require modification to increase the hydrophobicity before gelators are obtained. An early example of this was reported by Shimizu and co-workers in 2002.¹²⁸ They developed a bolaamphiphile hydrogelator composed of two phosphorylated thymidine units, linked by an alkyl chain (Figure 33). With the appropriate chain length, this could act as a hydrogel. Investigations indicated that both hydrogen bonding and π - π stacking were important for formation of the hydrogel – as would be expected for this type of hydrogel.



43

Figure 33. The thymidine-based gelator reported by Shimizu and co-workers.

Nucleotide-based gelators are also being applied in biomedical applications. In 2017, Barthélémy and co-workers reported thymine-based gelators, also containing a glucose moiety, and linked to an alkyl chain, through an amide or urea group, to form a bolaamphiphile (Figure 34).¹²⁹ In the case where the urea was used, the hydrogels could form very rapidly.

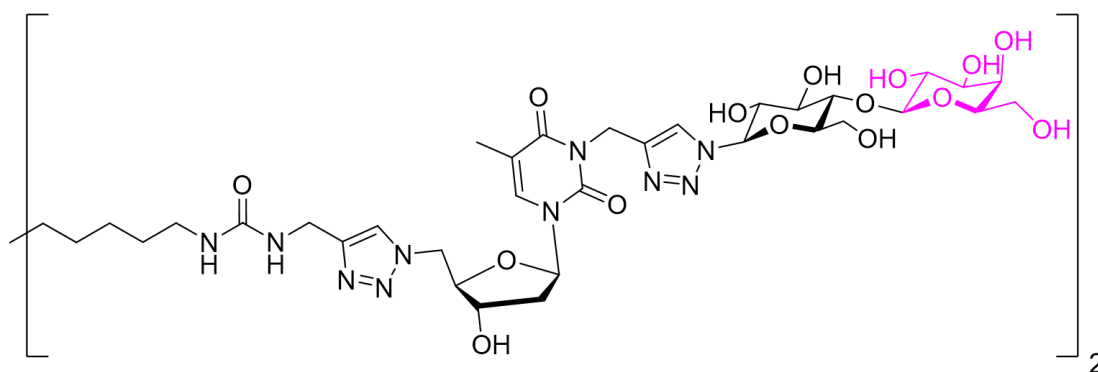


44

Figure 34. The bolaamphiphile thymine gelator developed by Barthélémy and co-workers, and tested as an injectable biomaterial.

This hydrogel was found to be thixotropic, with recovery following increased strain occurring relatively quickly, within 20 minutes. The performance of the hydrogel was therefore monitored *in vivo*, with the gel found to be stable over the course of 21 days once injected. Additionally, the gel implant resulted in only very limited inflammation. It was therefore suggested that these hydrogels might be suitable for development as drug delivery systems or tissue scaffolds.

The same group has also reported a similar gelator that is capable of forming hydrogels in the presence of the enzyme β -galactosidase (β -gal). High activities of this enzyme are associated with a number of cancers,¹³⁰ and it has therefore been used for detection of cancer cells, monitoring of drug responsiveness, and as a trigger for prodrugs.¹³¹ Sensitivity of the gelator precursor to β -gal was achieved by the addition of a lactose unit to either end of the bolaamphiphile (Figure 35).



45

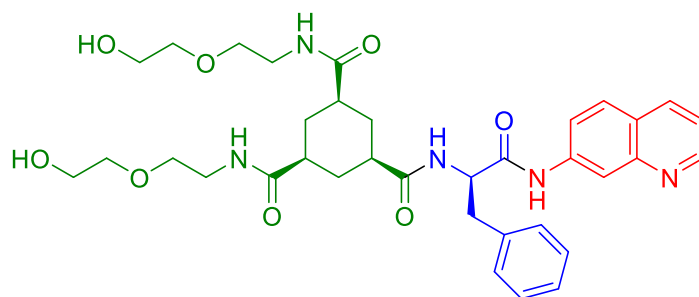
Figure 35. The β -galactosidase sensitive gelator precursor reported by Barthélémy and co-workers, with suggested applications in anti-cancer treatments. The cleavable lactose moiety is shown in purple.

On exposure to β -gal, the lactose was removed, giving the hydrogelator. This was capable of forming hydrogels in PBS buffer, with the enzyme also present. The authors suggested that, as a result of the relevance of β -gal in cancer targeting, the use of this enzyme to trigger gelation could offer an alternative therapeutic method for the treatments of relevant cancers. This example shows how known gelators can be modified with specific functions in mind.

1.3.3 Design for Drug Delivery

For drug delivery applications, developing hydrogels that allow for triggered release of a drug is attractive – this could lead to more targeted release. This approach often uses prodrugs – and these can be APIs that have been modified to give gelators. The method can mean that drug delivery can be triggered in two steps – first the bulk material must be broken down, by application of a stimulus such as pH. Following this, the gelator prodrug can then be converted into the active form of the drug, usually by enzyme action. Generally, it is hoped that the two steps will result in more targeted drug delivery.

An early example of this approach was reported by van Esch and co-workers in 2005. They used the model drug 6-aminoquinoline, which was linked to a gelling ‘scaffold’ through a linker susceptible to enzymatic cleavage (Figure 36). They showed that these modifications gave a compound that was still capable of acting as a hydrogelator – in fact, it had a minimum gelation concentration (MGC) low enough that it could be classified as a supergelator.



46

Figure 36. The gelator, modified to include a model drug, developed by van Esch and co-workers. Green: gelator scaffold, blue: cleavable linker, red: model drug.

Following this, the impact of using the molecule as a hydrogel was demonstrated. Hydrogels were prepared with the enzyme incorporated, and the release of the model drug monitored. This release was found to be very low, indicating that the assembly of the gelator into the gel fibres protects the linker from being cleaved, hence limiting release of the model drug. By contrast, when the temperature was increased (up to 45 °C), and the gel broken down, the release of the model drug was greatly increased, with the highest release at the highest temperatures. This indicates that the breakdown of the network is required before cleavage of the linker can occur.

This system shows that it is possible to develop a hydrogel system that is capable of releasing in a two-stage manner. Although this particular example would have limited potential in biomedical applications, due to the increase in temperature being required for the first stage of release, it does, however, provide a good platform for development of more relevant systems.

One area of drug delivery for which this type of hydrogel is especially attractive is in the delivery of chemotherapeutic drugs. These are typically very toxic, and commonly lead to unpleasant side effects as a result of off-target action. It is therefore especially attractive to be able to deliver these drugs only in the highly specific region of the tumour itself. Several anti-cancer drugs have therefore been modified to give gelators.^{72, 132}

In 2012, Yang and co-workers reported the development of six hydrogels, each of which was based on the anticancer drug Taxol, modified with a short peptide (Figure 37).¹³³ Taxol was linked to the peptide by an ester group. Of the six hydrogels developed, five were self-healing, and recovered following injection, with three reforming within just 5 minutes.

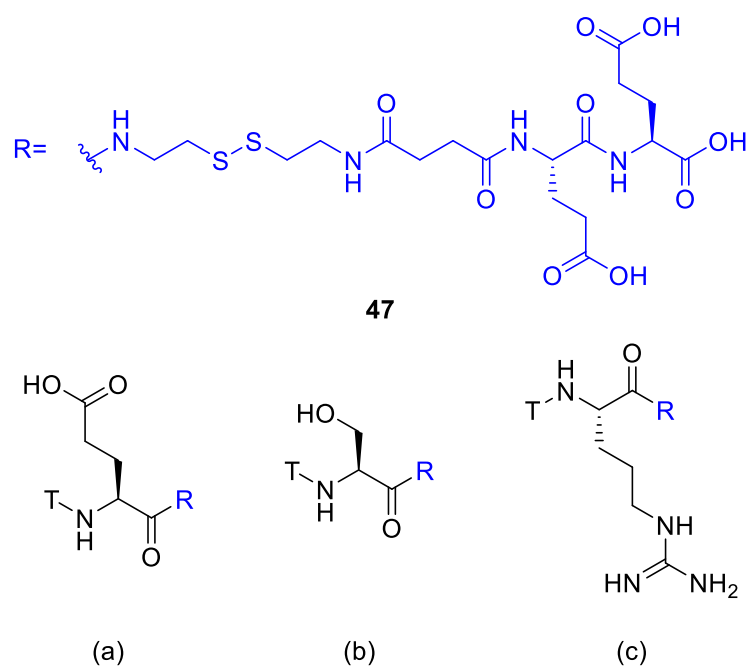


Figure 37. Three of the peptides used by Yang and co-workers to modify taxol to give self-healing hydrogelators.

Following characterisation of the hydrogels, each was tested for the release of Taxol. In the presence of buffer, and at 37 °C, the ester linking Taxol to the peptide is hydrolysed, resulting in release of the drug. Each hydrogel released Taxol at a different, constant rate, for at least the initial 12 hours. Over the first 24 hours, only a very low proportion of the total Taxol was released. However, when the gelators were tested in an IC_{50} study, very similar toxicity in comparison to Taxol alone was observed. As these hydrogels are injectable, and show predictable release of an anti-cancer drug; they may therefore be useful for targeted delivery to tumours.

This method, using a modified API as a gelator, can also be used to develop dual release systems. This was achieved in 2009 by John and co-workers.¹³⁴ They developed a number of potential gelators based on acetaminophen (paracetamol), a well-known analgesic, one of which was particularly promising due to its pH responsive nature (**48**) (Figure 38). The hydrogels formed were then capable of encapsulating a second drug, curcumin (**49**).

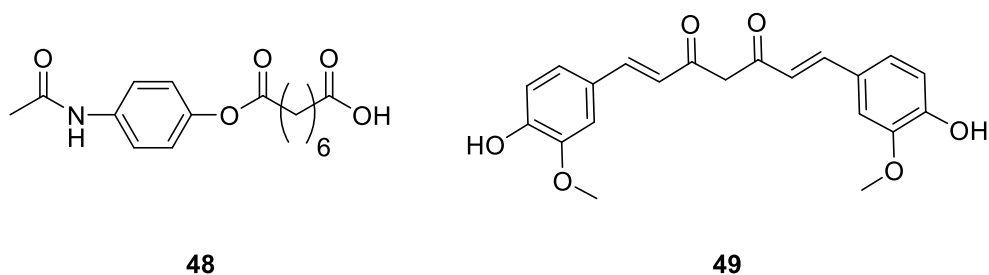


Figure 38. The acetaminophen based hydrogel developed by John and co-workers (left), and curcumin, the second drug encapsulated in the gel.

These hydrogels were found to be capable of triggered release, of both acetaminophen and curcumin. On addition of lipase, the ester bond of the gelator is hydrolysed, leading to breakdown of the gel, and release of both drugs. On addition of just water, release of neither drug was observed, indicating that the encapsulated curcumin cannot be released without breakdown of the hydrogel.

The design of a gelator can also give improved properties for certain applications. Although there has been a lot of development of various amino acid based gelators, these can be limited in some applications, as the gelators, and therefore the hydrogels themselves, are not stable to enzyme action, and can be degraded rapidly *in vivo*. To avoid this issue, as an alternative to incorporating D-amino acids as described above, hydrogels may be designed with β-amino acid residues. In 2012, Nanda and Banerjee reported two amino acid based gelators that also contained a β-alanine residue (Figure 39).¹³⁵

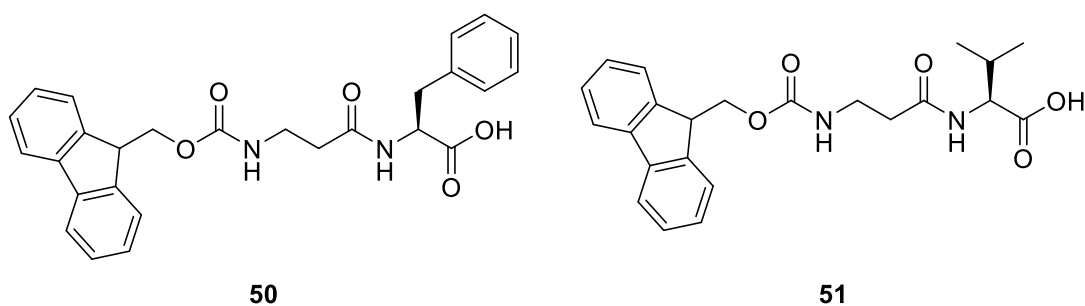


Figure 39. The amino acid based gelators developed by Nanda and Banerjee, used for slow release of bioactive molecules.

These gelators formed hydrogels via a solvent trigger, with the gelator dissolved in a small amount of DMSO, and aqueous buffer being added to trigger gel assembly. On standing, the gels were formed, with the final DMSO concentration being below 1.5% v/v, and therefore considered safe for biomedical applications.¹³⁶ Following rheological studies indicating the formation of stiff gels, the two hydrogels were tested for sustained drug release. Either vitamin B₂ (smaller) or B₁₂ (larger) was encapsulated within the hydrogels, and the release under physiological conditions

monitored. After 70 hours, around 90% of vitamin B₂ had been released, compared to around 70% of vitamin B₁₂ (although the majority of the release occurred within the first 30 hours). This was thought to be due to the larger size of vitamin B₁₂ slowing diffusion through the pores of the gel.

Additionally, the stability of the valine-based gelator towards two proteolytic enzymes was monitored – this gives an indicator of how stable the hydrogel might be *in vivo*. The gel was monitored for 50 hours, and within this timeframe, no breakdown of the gelator was observed. This suggests that, with very limited breakdown of the hydrogel, the slow release of bioactive molecules observed might still occur with the gel *in vivo*, although only one enzyme was investigated at this early stage.

1.3.1 Effects of Chirality on Self-Assembly

As previously discussed, many supramolecular gelators are chiral, as a result of being derived from natural products, and therefore have chiral centres that can be modified. Depending on the application and the type of chirality, this can impact the properties of the material.

In the case of enantiomeric gelators, which are mirror images of each other, the properties of the resulting gels will be identical, with two exceptions – response to polarised light, and interactions with other chiral objects. In some cases, the handedness of any chiral nanostructure can also change – again, this should only impact applications where other chiral objects are involved. This can be useful for selected applications, including enantioselective recognition,¹³⁷ among many other biomedically relevant applications.¹³⁸

An example highlighting the potential importance of gelator chirality in applications was reported by Koner and co-workers in 2018.¹³⁹ They developed a histidine based gelator (**52**) (Figure 40), which was found to be sensitive to the presence of amines, with different enantiomers giving a different response.

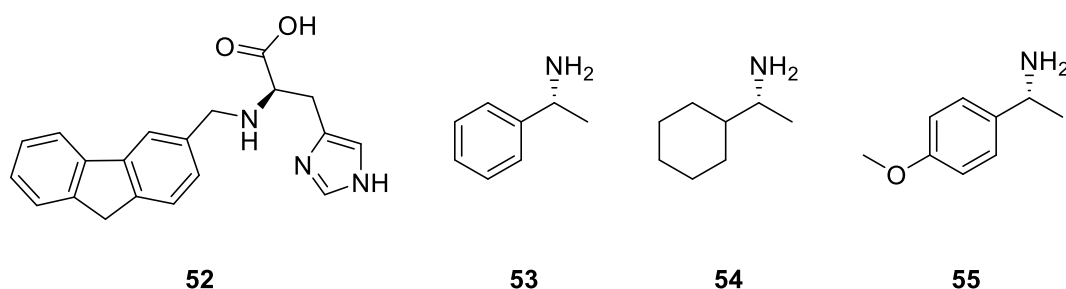


Figure 40. The histidine based gelator (*L* form shown) developed by Koner and co-workers for stereospecific detection of amines (*R* forms shown).

The group initially observed that, on mixing an aqueous solution of their gelator with (*R*)- α -methylbenzylamine (MBA) (**53**), a gel was formed – by contrast, a solution of (*S*)-MBA led only to precipitation. Circular dichroism (CD) studies indicated that although the signal from each enantiomer of MBA was reduced on addition of the gelator, this was much more significant for (*R*)-MBA, with a decrease in signal of almost 99%, compared to a 50% reduction for (*S*)-MBA. This suggested that there was greater interaction between the gelator and the *R* enantiomer than there was with the *S*.

Two other amines (**54**, **55**) were then also tested – and the same effects observed. This suggested that this gelator was capable of this type of sensing with multiple amines. This was followed by investigating the opposite gelator enantiomer – and this was found to give the opposite results – forming a hydrogel in the presence of (*S*)-MBA, and a precipitate with (*R*)-MBA. Although only a small number of amines, with relatively similar structures, were tested, consistent responses to the presence of different enantiomers were observed.

In some cases, relatively simple changes to the gelator can result in changes in the chirality of the nanostructure. Additionally, these do not always have to involve a change in the chirality of the molecule, and can just involve a small modification.

For example, in 2017, Zhao and co-workers reported a family of phenylalanine based hydrogelators, which assembled to form helical structures (Figure 41).¹⁴⁰ The chirality of the helical self-assembled nanostructures could be controlled by multiple methods.

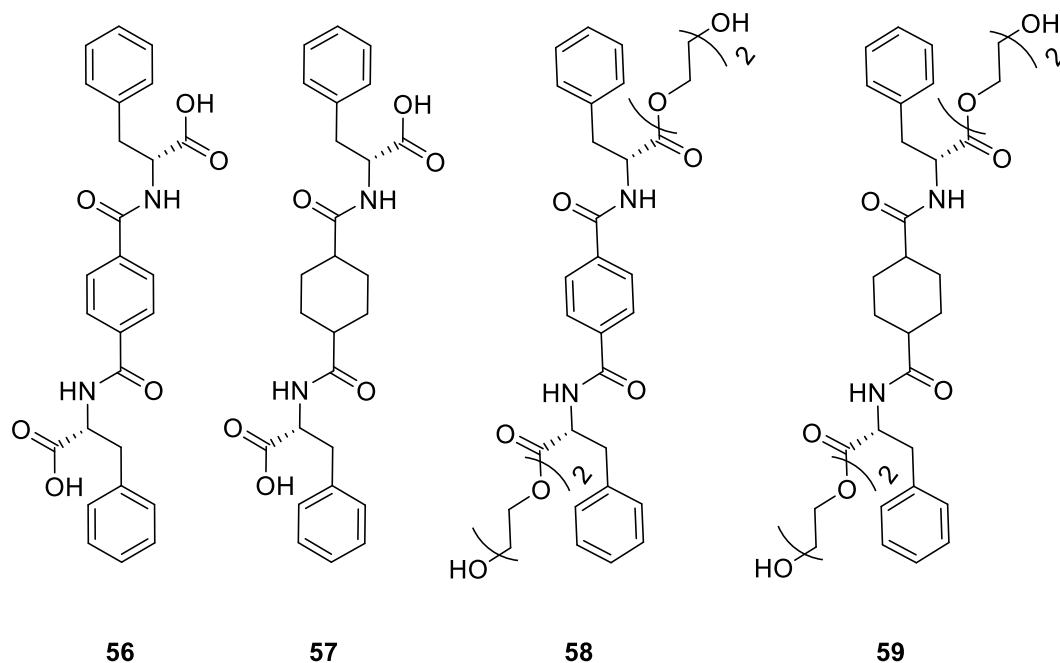


Figure 41. The *D*-phenylalanine based gelators developed by Zhao and co-workers, both with (right) and without (left) the modification with ethylene glycol groups. Each gelator was also prepared using *L*-phenylalanine.

The first of these methods was to change the chirality of the amino acid – without the ethylene glycol modification, *D*-phenylalanine-based structure **56** gives *M*-helical nanofibres, with the *L*-phenylalanine enantiomer giving *P*-helical fibres. These oppositely-handed helices were observed in SEM and TEM images of the gels formed, as well as the CD spectra indicating the formation of nanostructures with opposite chirality. This is also the case when the central connecting phenyl unit is replaced with a cyclohexane unit (**57**).

On modification of the carboxylic acid group, at the chiral centre of the molecule, with a short ethylene glycol group (**58**, **59**), it was observed in CD experiments that, for both enantiomers, the chirality of the nanostructures was inverted. This was despite there being no change in the chirality of the gelators themselves, although the modification did occur close to the chiral centre. This change occurred with either of the central connecting units used.

This work shows that relatively simple modifications to a gelator can lead to control over the chirality of the structures produced, without the need to change the chirality of the gelator. This is important for systems and applications where the chirality of the nanostructures has an impact on the performance of the material and demonstrates that multiple structural factors control the assembly mode and determine the nanoscale chirality.

As well as pairs of enantiomers, diastereomeric gelators also occur. These are not mirror images of each other, and rarely have the same physical properties. In hydrogels, this type of

stereochemistry is common when short peptide based gelators are used – these have multiple chiral centres, and therefore diastereomers can often be formed. The gels formed also rarely have identical properties – and in some cases, one diastereomer might form a gel while another does not.

An example of two diastereomeric gelators where both could form hydrogels was reported by Maity and Maitra in 2017.¹⁴¹ They combined bile acids with L- and D-phenylalanine, giving two diastereomeric hydrogelators (Figure 42). Although both of these were capable of forming hydrogels, the resulting materials had some different properties. This was especially clear in the rheological studies, with the hydrogel formed with the L-phenylalanine having a much higher G' than that formed with the D-phenylalanine. Despite these rheological differences, ZnO nanoparticles could be formed in both hydrogels.

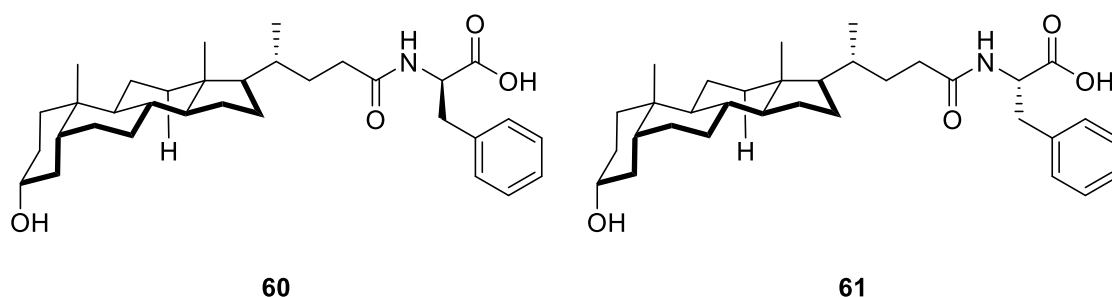


Figure 42. The phenylalanine based hydrogelators developed by Maity and Maitra, which showed different rheological properties.

1.4 Two-Component Gel Systems

Increasingly, there has been interest in developing supramolecular systems comprised of multiple components. These are of increased complexity compared to systems that use only one component. This provides greater opportunity to customise the materials that result, through changing either component, as well as being a closer mimic to natural systems, which typically comprise many different components.¹⁴²

There are a number of different types of two-component gel systems. These were classified by Buerkle and Rowan in their 2012 review,¹⁴³ and are as follows:

1. A single gelator with a non-gelling additive.
2. A combination of two individual gelators.
3. Two components that can only form gels in combination.

The first type, while containing only one component that is a gelator, will also contain one or more additives that have been added specifically to alter the material properties of the gel. The presence of this additive can result in the material being more straightforward to tune.

An example of this was reported by Barthélémy and co-workers in 2017, with the gelation properties of a nucleotide based hydrogel (Figure 43) controlled by the addition of different cations.¹⁴⁴ This gelator was paired with five different cations (Li^+ , Na^+ , K^+ , NH_4^+ , HNEt_3^+), which each gave different effects on the final material.

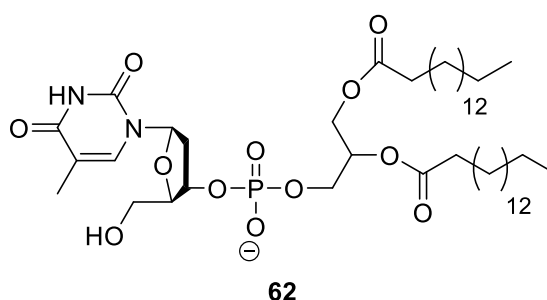


Figure 43. The nucleotide based gelator used by Barthélémy and co-workers as a hydrogel in the study.

It was observed that the different salts gave different supramolecular nanostructures, with the alkali metal salts giving tubular micelles, and forming hydrogels, while the addition of ammonium salts gave lamellar arrays – and no hydrogels. The presence of salts also impacted the rheological properties of the hydrogel – changing the overall concentration of the metal salt in the hydrogel led to changes in the G' values for each. This allows for a simple way to alter the material properties of the gelator – simply by altering the concentration of the added cation. This may in turn allow for the properties to be selected with a specific application in mind.

In 2015, Feng and co-workers reported the combination of a responsive two-component system,¹⁴⁵ comprised of one gelling phenylalanine derivative (**63**), and one non-gelling azobenzene derivative (**64**) (Figure 44), that was tested for applications in biomedical applications. When these were mixed in a 1:1 ratio, heated and allowed to cool, a hydrogel was formed.

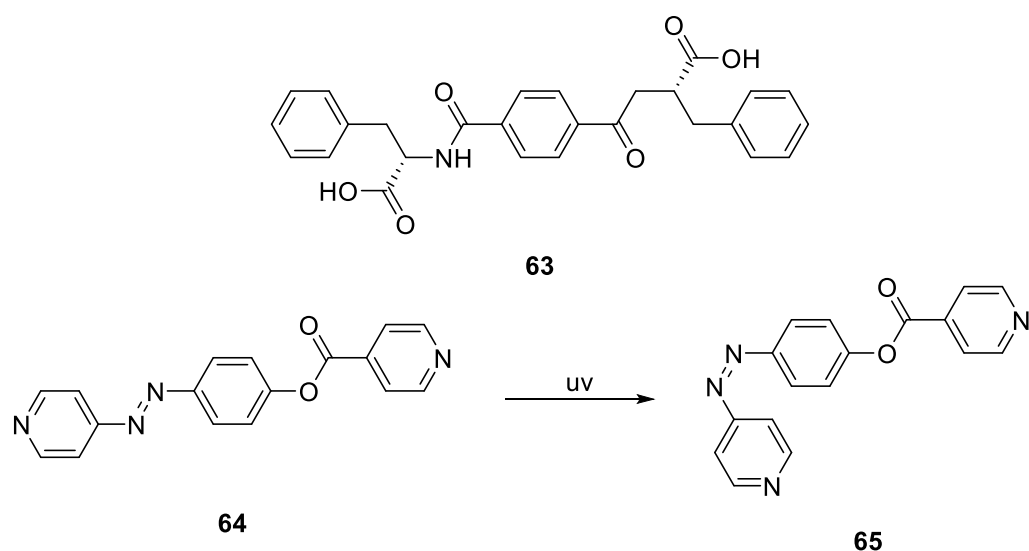


Figure 44. The two gelators used by Feng and co-workers; the phenylalanine based gelator (63), the modified azobenzene (64) and its response to UV light.

This hydrogel was found to be responsive to multiple stimuli. On heating, a solution was formed, with the gel regained on cooling. Switching the pH also controlled gelation – on an increase in pH, the gel was broken down, and reformed when pH was reduced again. The addition of α -cyclodextrin also caused the gel to be broken down, as a result of competitive interactions with the modified azobenzene. This effect could be reversed by addition of adamantane – α -CD will form preferential interactions with this over the azobenzene additive. Finally, the hydrogels were sensitive to UV light, due to the isomerisation of the azobenzene (Figure 44) from the *E* form to the *Z* form (65). This could be reversed (and the gel reformed) by exposure to another wavelength of UV light. To have a hydrogel that is responsive to such a range of stimuli is relatively unusual, especially as it could be reformed in each case.

Following this, the hydrogels were tested for the ability to encapsulate cells. It was found that cells adhered well to the hydrogels, and also proliferated well over seven days. Following this time for proliferation, the gels were broken down by exposure to UV light (this did not have any significant impact on the cells themselves), resulting in release of the cells from the hydrogels. This provides a straightforward way in which a hydrogel scaffold can be removed, without the need for enzymes or chemical methods.

The second type of multicomponent gels are materials that are formed on mixing two different gelators, each also capable of forming a gel alone. These two gelators might be self-sorted or co-assembled. Generally, multiple gelators are mixed to give materials with properties that are a mix of each individually.

An early example of this type of material was reported by Gough, Ulijn and co-workers in 2009, combining two short peptide hydrogelators (Figure 45).⁵⁷ The first of these, compound **66** formed good hydrogels under physiological conditions and was biocompatible, but only supported a very small amount of cell proliferation over seven days.¹⁴ The second, compound **67**, forms hydrogels at low pH and relatively low temperatures (ca. pH 3 and under 25 °C), but contains the tripeptide sequence Arg-Gly-Asp, which can act as a cell attachment site.¹⁴⁶ They reasoned that combining these two gelators might provide a hydrogel that was stable under physiological conditions, while giving improved cell proliferation.

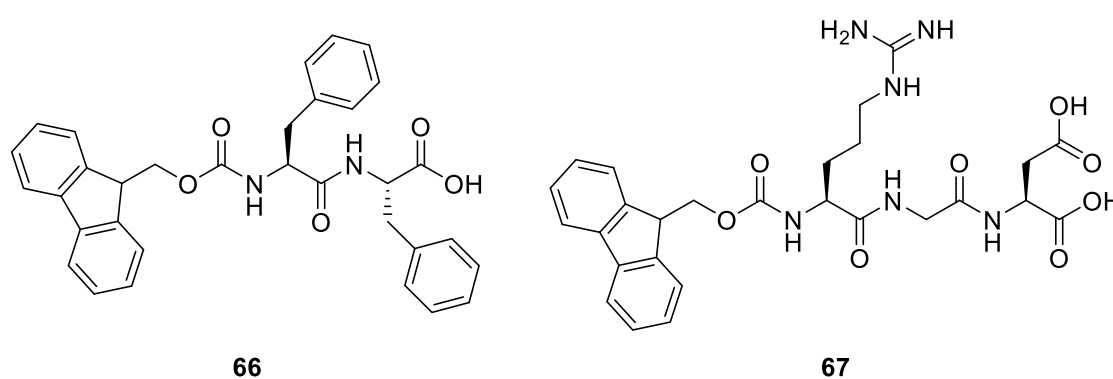


Figure 45. The Fmoc peptides used by Gough, Ulijn and co-workers to form hybrid hydrogels for cell culture.

Gels comprised of a mixture of these two gelators could be formed in cell culture media, with 10-50% of the mixture comprised of compound **67**. It was also found that varying the amount of compound **67** added could influence the material properties of the gels, with lower proportions giving stiffer gels, and higher proportions less stiff gels. This is useful as the stiffness of a hydrogel can influence stem cell differentiation. The hydrogels were then tested for cell culture, with cells encapsulated during formation of the hydrogel. Studies showed that the presence of the Arg-Gly-Asp sequence was important for cell adhesion, with the hybrid hydrogels showing good cell proliferation.

This combining of the properties of two different gelators is desirable for the development of materials with tuneable properties without the need to develop novel hydrogelators, and there has been increased interest in this area. This type of gel will therefore be discussed in more detail later in the introduction.

The third type comprises two separate components, neither of which can form gels individually – but in combinations, do form gels. In these cases, there is some interaction (or reaction) between the two components that results in the formation of the gel. This is typically reversible – meaning these gels are particularly responsive to stimuli. Common interactions include hydrogen bonding,

metal-ligand interactions, and donor-acceptor interactions.¹⁴⁷ The reversible formation of covalent bonds is also known.

This type of gel also offers opportunities for the development of interesting materials. Some may be formed simply by mixing the two components together – rather than needing a trigger such as a temperature or pH change. Additionally, modification of one or both of the components can lead to changes in properties in the material obtained. The properties might also be tuneable by varying the proportions of the two components. This allows for a system to be designed with specific material properties in mind as described in the following section.

1.4.1 Development of Two-Component Systems

Generally speaking, two-component gel systems are much rarer than single component systems. The first two component gel was reported in 1993 by Hanabusa, Shirai and co-workers.¹⁴⁸ This made use of a well-known hydrogen bonding interaction between pyrimidine (**68a** or **68b**) and barbituric acid (**69a** or **69b**) derivatives (Figure 46). Through addition of alkyl chains, the solubility of these molecules was modified, and in a 1:1 ratio, the two components were capable of forming gels in organic solvents. Investigation of the system by IR and TEM indicated that hydrogen bonding between the two components was important for the formation of the hydrogel. This illustrates one of the ways in which the components in a two-component gel system can interact.

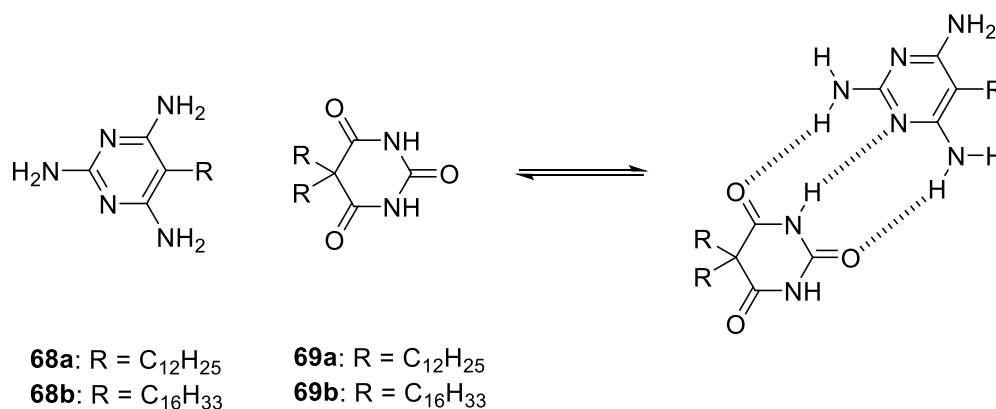


Figure 46. The two components required for gel formation in the organogel reported by Shirai and co-workers, and the reversible interactions that lead to the gel formation.

The other major type of interaction in the formation of two-component gels is the formation of new covalent bonds *in situ* (either reversibly or irreversibly), leading to the formation of a third molecule – the gelator. Once this is present, the gel is formed. An early example of this was reported by Hanabusa and co-workers in 2003.¹⁴⁹ They combined an isocyanate (**70**) and an alkylamine (**71**) – these reacted to give a urea (**72**) (Figure 47), which immediately formed

organogels in toluene. This process was reproducible over a number of organic solvents. This offers advantages for industrial applications, as there is no need to heat the gelator, simplifying the process.

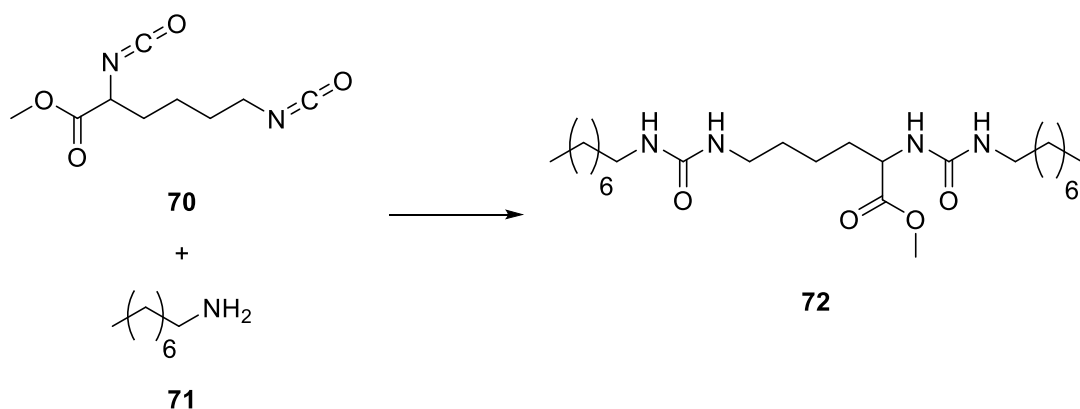


Figure 47. The gelation system developed by Hanabusa and co-workers.

In 2012, Smith and co-workers reported another example of such a system, combining lauric hydrazide (**74**) and various aldehydes (Figure 48), to form gels in DMSO.¹⁵⁰

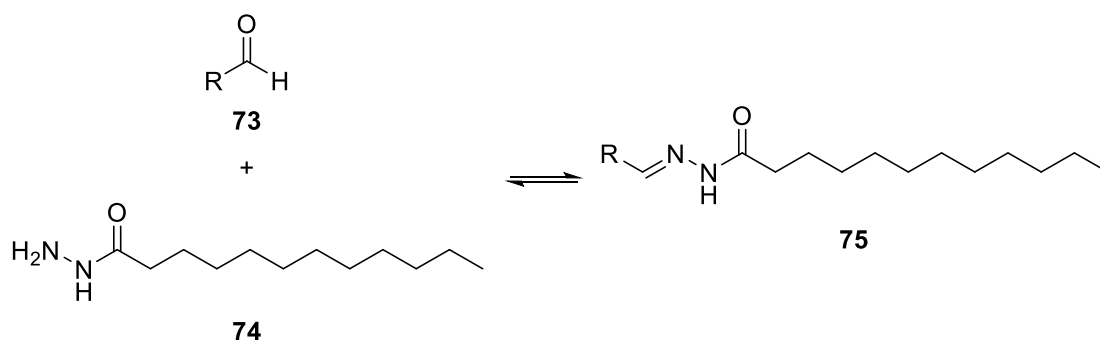


Figure 48. The scheme for the reaction between lauric hydrazide and an aldehyde, resulting in the formation of the hydrazone gelator.

Initial investigations were carried out on an equimolar mixture of lauric hydrazide and undecanal – these were combined in a 1:1 ratio, and the sample heated. On cooling, an opaque gel was formed. NMR studies indicated that formation of a hydrazone had occurred, with this being the species responsible for gelation. An aldehyde screen was then carried out, with a number of aldehydes tested with lauric hydrazide for gelation. The aromatic aldehydes tested, although they did form the equivalent hydrazone species, did not form gels. Interestingly, when a mix of undecanal and the aromatic aldehydes was used, a gel still formed, suggesting selectivity for forming the gelator molecule.

In another interesting example, van Esch and co-workers reported the formation of a hydrogel from responsive vesicles.¹⁵¹ The vesicles themselves, formed from a bisaldehyde (**76**), had already

been found to be highly responsive to external stimuli, including pH.¹⁵² In this progression of the system, the bisaldehydes were additionally combined with bisamines (**77**), leading to the reversible formation of imine bonds (Figure 49).

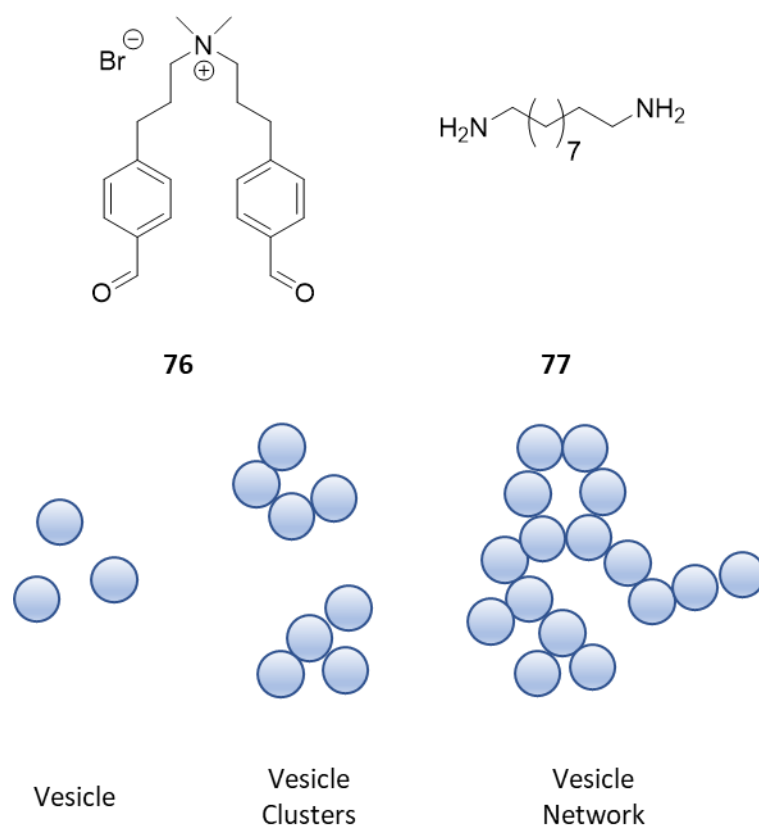


Figure 49. The bisaldehyde and a bisamine (top) used by van Esch and co-workers to form vesicles, that then assembled to form hydrogels (bottom).

For the bisamines with chain lengths of seven and nine carbons, simply mixing the components was enough for gel formation to occur. Investigation of these hydrogel materials suggested that the hydrogels were formed of a complex mixture, comprising the polymers resulting from imine bond formation, other macromolecules from this same process, and unreacted aldehyde and amine. The gels were thermally reversible, being broken down on heating, then reformed once the solution had cooled. This is a result of the reversible nature of the imine bond. Additionally, due to the pH responsive nature of the vesicles, the hydrogels themselves were also responsive to pH. On lowering of pH, a gel-sol transition occurs – this too is reversible when pH is raised again. As these hydrogels and the vesicles they are made up of are highly responsive, along with these transitions being reversible, they have potential for use in biomedical applications such as encapsulation and release of bioactive molecules.

This exploitation of dynamic covalent bonds can result in easier modifications to a gel. In 2014, Guler and co-workers reported the use of dynamic covalent linking to alter the material

properties of a peptide based hydrogel (Figure 50).¹⁵³ While this molecule was capable of forming gels, these were mechanically fairly weak. Glutaraldehyde (**79**) was added to the gels, leading to the reversible formation of an imine bond between the amine of the peptide gelator (**78**), and the aldehyde of the glutaraldehyde.

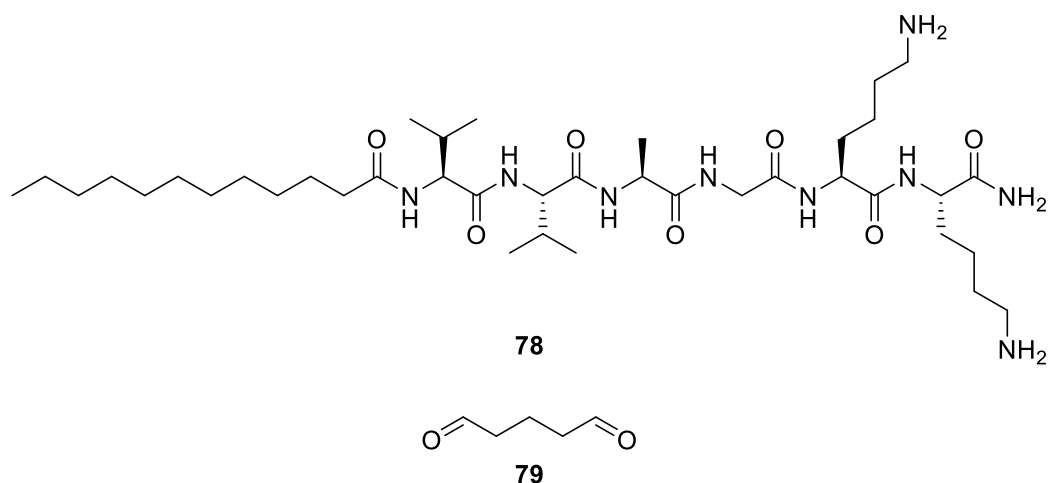


Figure 50. Top: the peptide based gelator used by Guler and co-workers. Bottom: Glutaraldehyde, used for the formation of dynamic covalent bonds.

The addition of the glutaraldehyde gave enhanced material properties, with the altered gels being both stiffer, and more resistant to strain. Additionally, the reversible nature of the imine formation meant that the gels also showed self-healing behaviour, maintained from the gels formed from the peptide alone. The addition of the aldehyde improves the characteristics of the material, with the authors suggesting that changing the concentration of glutaraldehyde added, or using different dialdehydes might give even greater scope for tuning of the material properties – although this was not investigated here. Studies found that the nature of the bond was important for gelation – when the imine was reduced to an amine, the gel collapsed, indicating disruption of the network.

1.4.2 Chirality in Two-Component Systems

As discussed previously, many hydrogelators are chiral, as they are commonly derived from natural products such as sugars and amino acids. This often results in the formation of chiral nanostructures on self-assembly. However, it can be difficult to control the chirality of these structures.

The chirality in nanofibres can be controlled by two major methods. The first of these is the ‘soldiers and sergeants’ effect, whereby an additive can control or amplify the chirality of the nanofibres. Chirality can also be controlled in a ‘majority rules’ manner. In these cases, there are

typically two enantiomers present, with the one in an excess controlling the chirality of the nanostructures. These effects are known to occur across supramolecular chemistry.¹⁵⁴

One common purpose for which non-gelling additives can be employed is in the ‘soldiers and sergeants’ scenario - to control of chirality of nanofibres. Generally, the chirality of any nanostructures formed is dependent on the chirality of the gelator, and changing this is a simple way to alter the chirality of the nanostructures.¹⁵⁵ There are relatively few reports of achiral hydrogelators – and these can still form chiral nanostructures.¹⁵⁶ However, additives can also control or amplify the chirality of the nanofibres – this additive is referred to as the ‘sergeant’. This term is also used to describe the situation where a chiral component can transfer chirality to an achiral species.

An example of this was reported by Miravet and co-workers in 2012.¹⁵⁷ They reported a bis-urea (**80**) (Figure 51) that could act as a hydrogelator in either the (*S*) or (*R*) form. As would be expected, these hydrogels showed circular dichroism signals that were of equal but opposite intensity. A second, achiral, bisurea (**81**) was also synthesised, but this was not a gelator. The effects of this on the chirality of the (*R*)-gelator were therefore investigated.

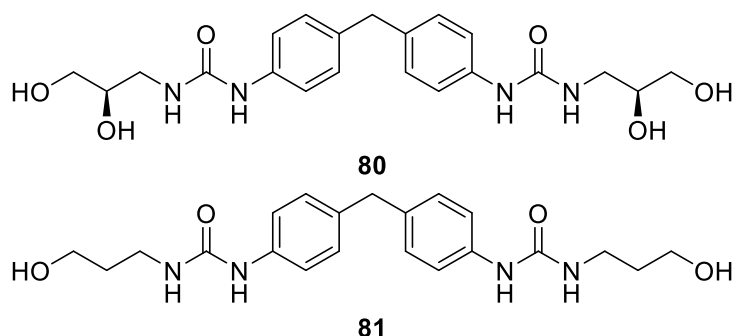


Figure 51. The bisurea based gelator (top) and non-gelling achiral additive (bottom) investigated by Miravet and co-workers. The (*R*) form of the gelator is shown, but the (*S*) form was also synthesised and investigated.

Attempts were made to form hydrogels with increasing proportions of the achiral additive – stable gels were formed with up to 0.4 equivalents of this additive. On investigation of the system by circular dichroism, it was found that a signal of greater magnitude was observed with 0.2 or 0.4 equivalents of the achiral additive. This indicates that chirality from the gelator is maintained even in the presence of achiral additives, which may even amplify this effect on the nanostructures.

Chirality of the nanostructure may also be controlled by the ‘majority rules’ effect. This occurs when whichever enantiomer is in excess dictates the chirality of the fibres. An example of this was reported by Liu and co-workers,¹⁵⁸ who developed a bolaamphiphile (**82**) (Figure 52) capable of

self-assembling to form helical nanostructures, and therefore hydrogels. As would be expected, this was the case for both the L- and the D-enantiomers, with the L-enantiomer forming left-handed helices, and the D-enantiomer right-handed helices. A racemic mixture of the two did not give any hydrogels, however, on addition of six equivalents (relative to total gelator) of melamine (**83**), hydrogels were formed. It was then found that varying the proportions of each enantiomer in the mixture could control the chirality of the nanofibres, following the pattern observed with only one enantiomer present – indicating a majority rules effect.

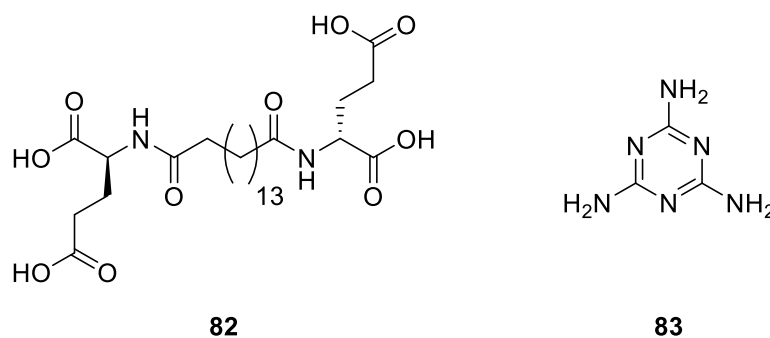


Figure 52. The bolaamphiphile gelator investigated by Liu and co-workers, and melamine, with which it can co-assemble to form hydrogels.

1.4.3 Mixtures of Enantiomers

As well as using a mix of chiral and achiral derivatives, two enantiomers of the same gelator can also be mixed. On this mixing, there are a number of possible outcomes – dependent on the difference in interactions between the enantiomers. When each enantiomer interacts more strongly with the second enantiomer, this typically leads to co-assembled fibres. When the opposite is true, and it is preferential for each enantiomer to interact with the same enantiomer, the fibres formed are more likely to be self-sorting (Figure 53).^{154c, 159} In these cases, it is possible for a mix of enantiomers to give a material with enhanced properties, in comparison to that formed from only one enantiomer.¹⁶⁰

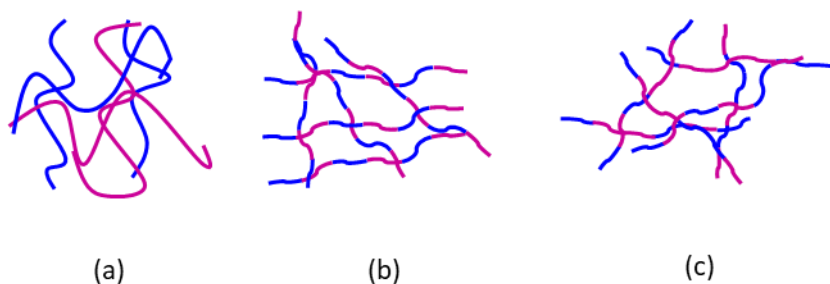


Figure 53. The different modes of self-assembly possible on mixing two enantiomers of a gelator. (a) Self-sorting, with each fibre consisting of only one enantiomer; (b) racemic co-assembly, where

each fibre contains an equal number of alternating enantiomers; (c) random co-assembly, with each fibre containing a random proportion of the two enantiomers, with no pattern.

It is also possible for the interactions between enantiomers to be disruptive – when the interactions between opposite enantiomers mean that those that are required for self-assembly are weakened, or cannot occur at all. This leads either to a gel that is significantly weaker than that formed from a single enantiomer, or the case where no gel at all is formed. Differing proportions of enantiomers can also give this effect.¹⁶¹

Which of these has occurred is generally determined using a range of techniques – starting with visually assessing whether a gel has been formed. This is generally followed by rheology and imaging, with circular dichroism also widely used when investigating gels formed from mixes of enantiomers.

In 2017, Feng and co-workers reported a case in which the combination of two enantiomers of a gelator led to the formation of a material with enhanced mechanical properties in comparison to the individual components.¹⁶² They synthesised two enantiomers of a glutamic acid based hydrogel, and found both were capable of forming hydrogels (Figure 54). They also investigated a 1:1 mixture of the two enantiomers. Not only did this mixture form good hydrogels, it also had enhanced mechanical properties in comparison to the gels formed from the individual enantiomers. This was evident in both the higher G' in the linear viscoelastic region, and in the thixotropic behaviour. All three gels formed were capable of reforming following the application of stress, but for the mixed gel, this occurred much more rapidly. This would potentially make the mixed gel more suitable for biomedical applications in which a self-healing gel is desirable.

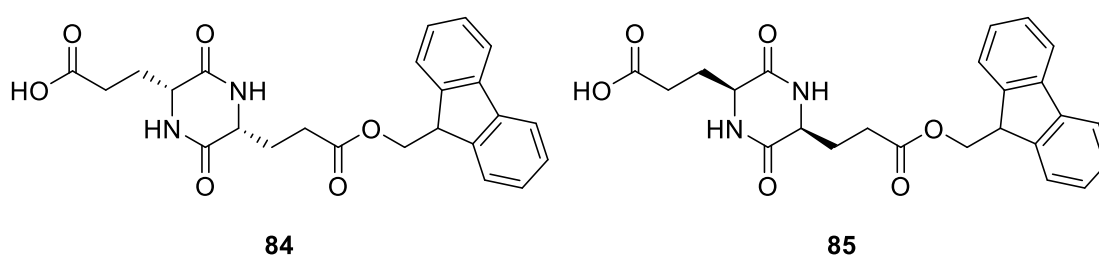


Figure 54. The two enantiomers of the glutamic acid based gelator investigated by Feng and co-workers.

In contrast, Pal and co-workers reported a hydrogel formed as a result of the interactions between histidine (**86**) and Zn^{2+} ions, under alkaline conditions (Figure 55).¹⁶³ These formed spontaneously on mixing the two components. Mixtures of D- and L-histidine were then also investigated – with the gels becoming progressively weaker as the proportion of a second enantiomer was increased. This culminated in the 50:50 mix being unable to form hydrogels at all.

It was suggested that this could be a result of the interactions responsible for gelation being stereospecific in some way.

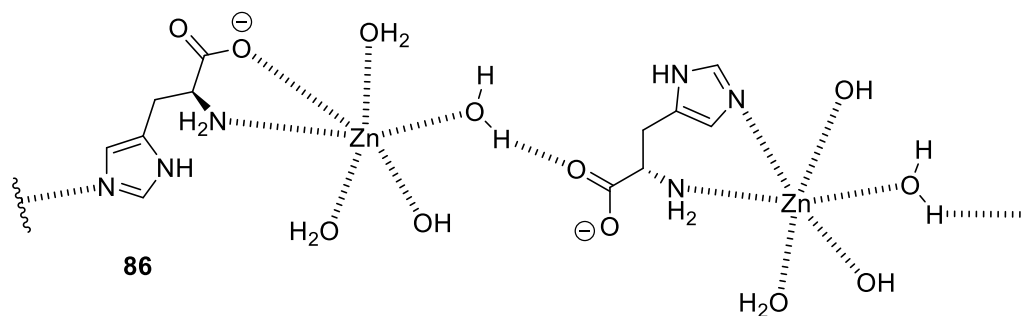


Figure 55. The proposed interactions, shown for the *L* enantiomer, for the histidine and Zn²⁺ hydrogels reported by Pal and co-workers.

1.4.4 Applications of Two-Component Gels

As a result of this ability to tune a molecule to give materials with desirable properties, there is increasing interest in using two-component gels in biomedical applications. The fact that such gels are often capable of self-healing behaviour is also attractive, as injectable hydrogels are highly desirable for biomedical applications.

In 2019, Ménard-Moyon and co-workers developed multi-component hydrogels based on protected amino acids, which also contained carbon nanotubes to aid with triggered drug release.¹⁶⁴ It was found that the combination of a modified tyrosine compound (**89**) with either Fmoc-protected tyrosine (**87**), or Fmoc-protected phenylalanine (**88**) (Figure 56), formed good hydrogels via a solvent trigger – with the gelator dissolved in DMSO, followed by the addition of water to induce gelation. The concentration of DMSO in the final gel was 2% - this concentration is low enough for use in biomedical applications.¹³⁶

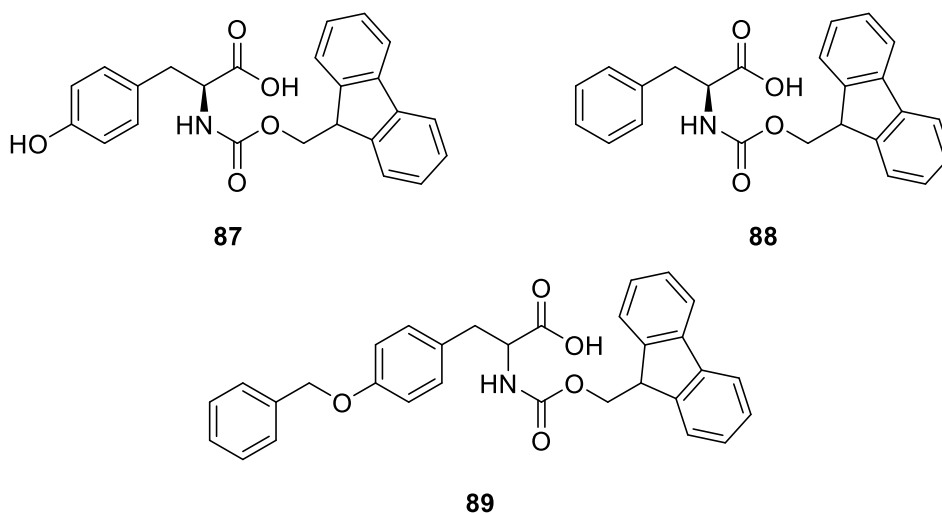


Figure 56. The amino acid based gelators used by Ménard-Moyon and co-workers. The two component gels consisted of Fmoc-Tyr(Bzl) (**89**) with either Fmoc-Tyr (**87**) or Fmoc-Phe (**88**).

Following the development of these hydrogels, oxidised carbon nanotubes were incorporated with the gels, with no impact on gelation at the chosen concentration of 0.025 wt %. When these gels were exposed to near-infrared light, the presence of the nanotubes results in heating of the gel, leading to breakdown of the tyrosine gel, and shrinkage of the phenylalanine gel. This responsiveness led to the investigation of these gels for drug delivery applications. L-Ascorbic acid was used as a model drug, and incorporated within the hydrogels. These hydrogels were then exposed to near infrared light, which led to rapid release of the model drug, with up to 80% release within ten minutes. This was in contrast to release from hydrogels prepared without carbon nanotubes, from which very little release of drug was observed – indicating that all the components are required for the hydrogel to behave in the desired manner. It was therefore suggested that these hydrogels could be used in triggered drug release. However, the heat increase of the gels as a result of exposure to UV light could also limit the applications of such materials.

The group of Dastidar have reported numerous examples of using a combination of a modified NSAID in combination with ammonium salts.¹⁶⁵ In combination, these can self-assemble to form gels in water or other biomedically relevant solvents, with anti-inflammatory effects. One such example used a gelator based on the NSAID tolfenamic acid (**91**) in combination with a primary ammonium salt (**90**) (Figure 57).¹⁶⁶ This formed hydrogels which showed good anti-inflammatory behaviour. The salts (not as a gel) also showed some anticancer properties, including inducing cell death in breast cancer cells, and reducing cell migration. It was therefore suggested that this might be useful for postoperative treatments.

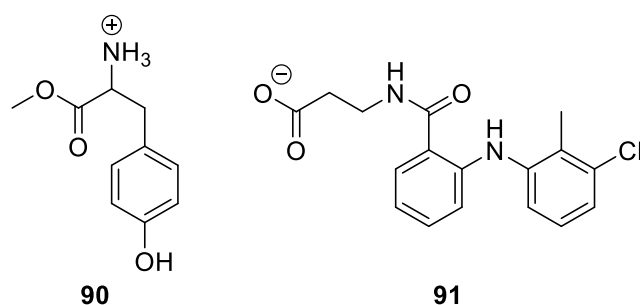


Figure 57. The NSAID and ammonium salt used by Dastidar and co-workers to form hydrogels with anti-inflammatory properties.

Ulijn and co-workers reported the use of a two-component system for tissue culture.¹⁶⁷ This combined the known hydrogelator Fmoc-Phe-Phe (**92**) with the Fmoc protected amino acid serine (**93**)– this would provide extra hydrophilic functionality within the hydrogel (Figure 58). These gels had stiffness suitable for the growth of cartilage cells, with the serine residue also able to interact with proteins. These materials were then used for the culture of pericytes. Over 35 days, an increase in cartilage biomarkers was observed – indicating that differentiation was taking place. The production of collagen is an important step in cartilage growth – in cell culture, the types of collagen produced can be unbalanced. With these hydrogels, a balance of the two main collagen types was observed – promising for the further development of these hydrogels.

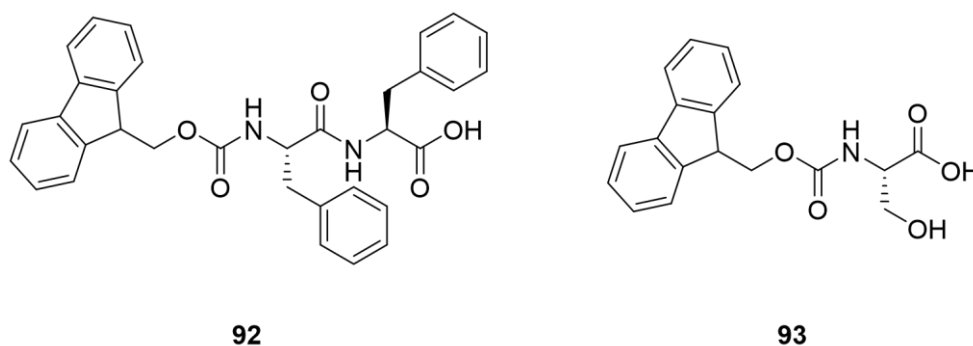


Figure 58. The two components used by Ulijn and co-workers for hydrogels for cartilage cell culture.

1.5 Hybrid Gel Systems

1.5.1 Polymer Gelators and LMWGs

A key challenge when developing supramolecular gels for practical applications is their generally low material strength. This makes them difficult to shape or manipulate, and therefore limits the scope of many applications. This barrier led to the development of hybrid gels – formed from a PG

and a LMWG. This aims to combine the mechanical strength of the more inert PG, while maintaining the responsive nature of the LMWG – achieving the “best of both worlds”.

In their 2015 review, Cornwell and Smith split the types of polymer-LMWG hydrogels into five categories,¹⁶⁸ which are as follows:

1. Polymerisation of LMWG fibres
2. Capture of LMWG network within a polymer matrix
3. Addition of non-gelling polymer to LMWG gel
4. Directed interactions between LMWG and polymer
5. Hybrid gel comprising LMWG and polymer networks

The fifth approach, the combination of two gelators, one PG and one LMWG, is a simple method for avoiding some of the drawbacks of each type of gelator, and is the approach which will be focussed on here. Polymer gelators give robust materials, but these are typically not very responsive to external stimuli once formed. In contrast, gels formed from LMWGs tend to be responsive to stimuli, but are mechanically weak, making them difficult to handle, with real-world applications therefore being limited.

In these cases, each component is also capable of forming a gel alone. Therefore, the two networks are generally self-sorting, with two separate, but intertwined, networks making up the bulk material. This class of hybrid hydrogel is especially attractive for use in biomedical applications – many polymeric hydrogelators are already widely used in applications such as cell culture, but lack the ease-of-modification or responsiveness that is desirable for further development.

The first hybrid hydrogel of this type was reported in 2009 by Yang and co-workers.¹⁶⁹ They combined agarose (**98**), a polymer gelator, with an Fmoc peptide based LMWG – H-lysine(Fmoc)-OH (**94**), and another of three Fmoc peptides (**95**, **96**, **97**) (Figure 59) – to form hydrogels with three components in total. These hybrid hydrogels showed increased mechanical strength compared to either the PG or the LMWG alone. A study using Congo Red as a model drug showed that the rate of release could be varied depending on the LMWG used – together with emission spectroscopy, this indicated that there were interactions between the LMWG fibres and the dye additive.

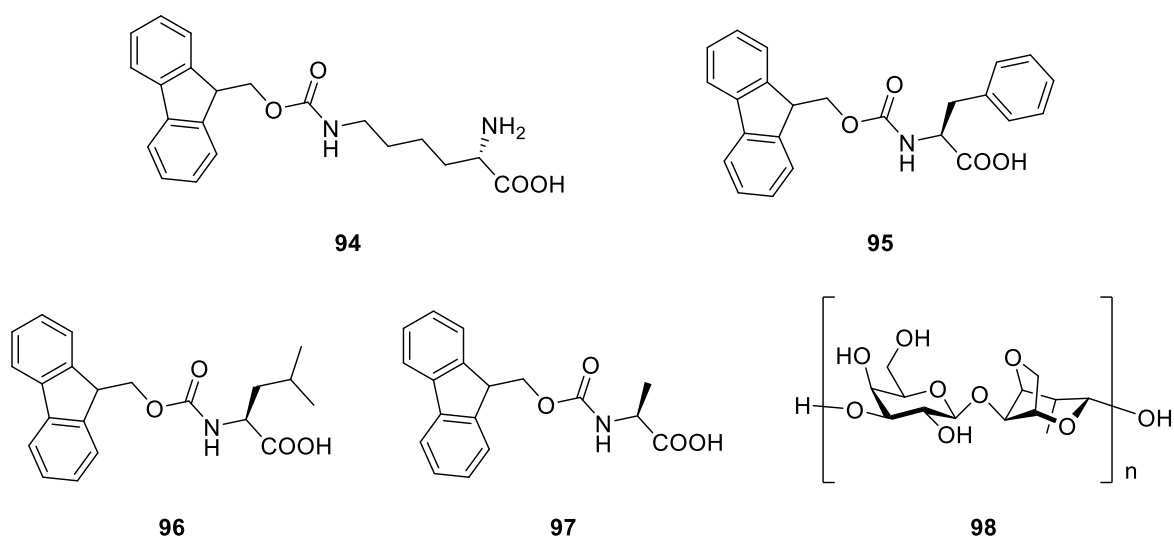


Figure 59. The gelators used by Yang et al. to develop their hybrid hydrogels.

The use of polymer gelators to improve the material characteristics of hydrogels has become increasingly popular, as a result of the relative simplicity of this method. The previously discussed DBS based hydrogelators, DBS-CO₂H and DBS-CONH₂, have both been combined with different polymer gelators as described below with the aim of improving the overall properties of the material, and consequently the range of possible applications.

DBS-CO₂H is a pH-responsive LMWG, and was combined with the PG agarose, for which gelation is triggered by heating then cooling. These two gels were chosen as a result of their different gelation triggers, which also occur at different rates – agarose forms a gel network rapidly on cooling, whereas the DBS-CO₂H network forms more slowly as pH is gradually lowered. When combined, the agarose network still forms rapidly. The formation of the DBS-CO₂H network is slowed slightly, but circular dichroism studies indicated that similar nanostructures as for the gel alone were still formed. Additionally, it was demonstrated that DBS-CO₂H maintains responsiveness to pH changes in the presence of the agarose network.¹⁰⁵

Following the characterisation of this hybrid gel, the materials were used to encapsulate and release the important anticoagulant drug heparin, which is also known to be important in cell culture.¹⁷⁰ Heparin was therefore incorporated within gels formed from both the gelators alone, and the hybrid system. Additionally, self-assembled multivalent micelles, capable of binding heparin, were incorporated. This detailed study investigated the effect of each of the four components on the others. This indicated that the DBS-CO₂H network was unaffected by agarose, modified slightly in the presence of heparin, and gel formation completely disrupted by the

micelles. However, when the micelles were bound to heparin, the gel was still formed. This demonstrated how different components can be controlled within a complex system as a result of mutual interactions between them.

The DBS-CO₂H and agarose hybrid hydrogels were capable of encapsulating and releasing heparin. This release was limited both by limited diffusion of heparin through the hydrogel network (as a result of its relatively large size) and interactions between the DBS-CO₂H gel fibres and heparin, which further slow diffusion. This is promising, as release and control of heparin is important in a number of areas. However, in this case the DBS-CO₂H hydrogels could not be used in cell culture due to the relatively low pH (5.5 and below) required. Cell culture typically takes place at higher pH values of around 7 – these hydrogels were not stable under these conditions.

This problem of instability of the hydrogel at higher pH values can be overcome by use of the second DBS derivative developed – DBS-CONH₂. Unusually for a supramolecular hydrogel, this is not pH-responsive, and is in fact stable over a wide range of pH values. This makes it very attractive for applications such as drug delivery and cell culture. However, the gels formed from the LMWG alone are mechanically very weak, and therefore challenging to handle.

As a result, DBS-CONH₂ has been combined with a number of polymer gelators with the aim of improving the overall material properties. In 2016, Okesola and co-workers reported the development of a hybrid hydrogel comprised of DBS-CONH₂ and agarose for the uptake of gold salts from aqueous solution, and subsequent spontaneous *in situ* conversion of these gold salts to nanoparticles.¹⁷¹ This effect was first demonstrated with DBS-CONH₂ alone, but these hydrogels were not robust enough to survive both the exposure to the gold solution and the following use in electrochemistry.

The agarose polymer gelator was therefore also incorporated, with both networks formed simultaneously by a heat-cool cycle. The addition of the agarose network did not impact the uptake of the gold salt, with nanoparticles formed as with DBS-CONH₂ alone. The hybrid gels with gold nanoparticles were then shown to be conductive, as well as being able to act as modified electrodes.

Following the promising results obtained for gold and silver nanoparticles with this DBS-CONH₂/agarose hybrid gel system, the formation of palladium nanoparticles was then reported by Slavík and co-workers in 2018.¹⁷² As for the previous example, the hydrogels were initially exposed to a solution of Pd salts, which are taken up by the gel, and Pd nanoparticles formed *in situ*.

Following the formation of the Pd nanoparticles, the hybrid gels were tested for catalytic action in Suzuki-Miyaura cross-coupling reactions. Initially, a range of bases and Pd loadings were screened to determine the most favourable reaction conditions (Figure 60).

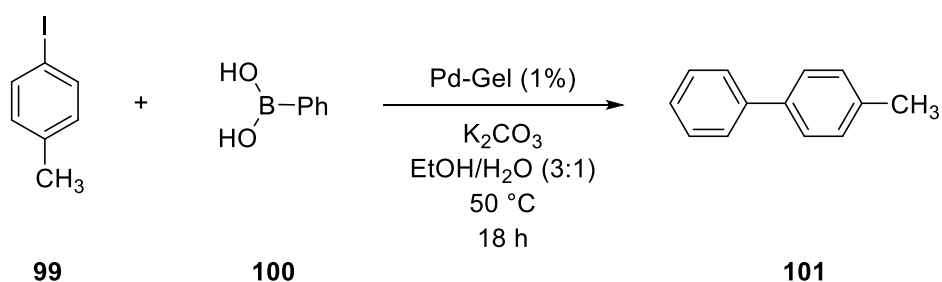


Figure 60. The reaction used by Slavík and co-workers to determine optimum conditions for the Suzuki-Miyaura cross-coupling reactions using Pd loaded hybrid gels. Shown are the optimised conditions.

A range of substrates were then screened, with aryl iodides generally giving very good yields, with both electron rich and electron poor groups present. The catalytic gels also showed good recyclability, with conversion not significantly impacted over eleven reactions with the same gel. This hydrogel therefore has good potential for use in both uptake of Pd from waste-water, and subsequent use of this Pd in cross-coupling reactions, which are highly relevant in the synthesis of pharmaceutically-active ingredients.

In addition to these applications, the DBS-CONH₂/agarose hybrid gel has also been investigated for use in cell culture.¹⁷³ In this case, heparin, and micelles to control its release, were also included, as for previously with DBS-CO₂H/agarose. Use of DBS-CONH₂ in place of DBS-CO₂H avoids the breakdown of the LMWG network under the conditions required for cell culture. It was also observed that, unlike for DBS-CO₂H, gels could be formed even on the addition of the micelles when DBS-CONH₂ was used. The hybrid gels were tested for cell culture, and good cell growth was observed. Additionally, the hydrogels were capable of releasing heparin, although the micelles could not be used to control this release, as they are cytotoxic, and leech from the gels.

As well as these DBS-CONH₂/agarose hybrid systems, capable of forming metal nanoparticles, the combination of DBS-CONH₂ with other polymer gelators has led to other potential applications, especially in the biomedical field.

In 2017, Chivers and Smith reported the combination of DBS-CONH₂ with PEGDM, a polymer gelator for which gelation is triggered by exposure to UV light in the presence of a photoinitiator.¹⁷⁴ These hybrid hydrogels were shown to be capable of encapsulating and releasing the non-steroidal anti-inflammatory drug (NSAID) naproxen, with release mediated by

pH of the receiving buffer. As the formation of the PEGDM network can be triggered by use of a photoacid, it was possible to form the polymer network in only select areas of the overall gel. This results in different areas of the gel having different mechanical strength, in the desired shape. This spatial patterning of the hydrogel is unusual for a supramolecular gel,¹⁷⁵ and allows for the hybrid gel to be formed in the desired shape – any material that is just LMWG can then easily be removed by simple washing. This leaves a shaped gel behind. In this case, a strip of gel could be formed in the centre of a tray, with pH 7 buffer on one side, and pH 4 buffer on the other (Figure 61). It was then demonstrated that there was preferential release of NPX into the pH 7 buffer.

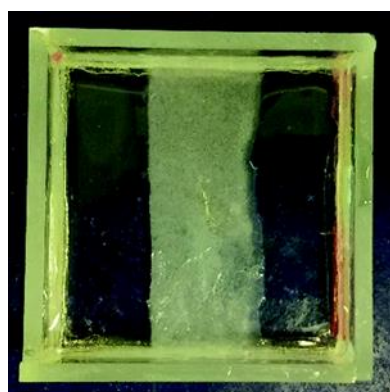


Figure 61. An image of the shaped DBS-CONHNH₂/PEGDM hydrogel, showing the strip used for pH responsive drug release. Image taken from Reference 174.

This method can also be used to form more complex shapes. In additional work, Chivers and co-workers created a hybrid gel formed in a ring (Figure 62).¹⁷⁶ These gels could be loaded with enzyme, and were then capable of acting as a simple bioreactor – only possible because of the shapes obtained.

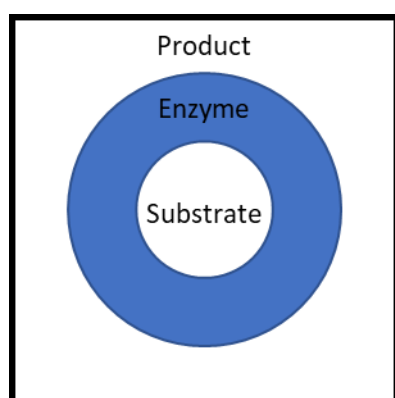


Figure 62. Schematic showing the shaped gel reactor developed by Chivers and co-workers.

1.5.2 Mixtures of LMWGs

Although there has been increasing interest in combining polymer gelators and LMWGs, there has been less exploration of combining one or more LMWGs, although this is increasingly being investigated. It is hoped that this approach will allow for the properties of the materials that are developed to be easily tuned, simply by varying the proportions of each of the gelators. This could give a very simple way of accessing materials with different properties.¹⁷⁷

When two supramolecular gelators are mixed, a number of different outcomes may occur – in analogy with the mixtures of gelator enantiomers described earlier.¹⁷⁸ In some cases, the two gelators will be entirely self-sorting, and will assemble into two separate networks, each consisting of only one gelator. There may then be interactions between the fully formed networks. This type of assembly occurs when interactions are stronger between gelators of the same type than between those of different types.¹⁷⁹

Alternatively, the gelators may co-assemble.¹⁸⁰ This occurs when the interactions between the two gelators are preferential, and leads to the formation of fibrils with the two gelators alternating. In other cases, where the strength of the interactions between the two different gelators is roughly equal to that of the interactions between two of the same gelators, random mixing can occur. This leads to the formation of fibrils that contain a mix of both gelators, but not in any fixed pattern, and the proportion of each gelator in each fibril may also vary.^{177, 181}

Of these types of self-assembly, self-sorting is the most desirable – the orthogonal networks make it easier to control the properties of the gel. There are different methods for ensuring that the two LMWGs will self-sort on assembly. These include using two gelators with different triggers for gelation, or making use of chemical differences between the two gelators to ensure they have orthogonal non-covalent interactions and hence self-assemble separately from one another.

In 2015, Adams and co-workers reported a two-component hydrogel formed from two naphthalene-functionalised dipeptides (Figure 63), both of which were capable of forming hydrogels independently.¹⁸² These dipeptides formed gels on reduction of pH – as pH is lowered, a greater proportion of a gelator is protonated, leading to a reduction in solubility and therefore gelation occurring. Each gelator had a different pK_a , and therefore protonation, and assembly into fibrils, occurs at a different pH. The slow decrease in pH was obtained by use of glucono- δ -lactone (GdL), which hydrolyses slowly in water to form gluconic acid.¹⁶

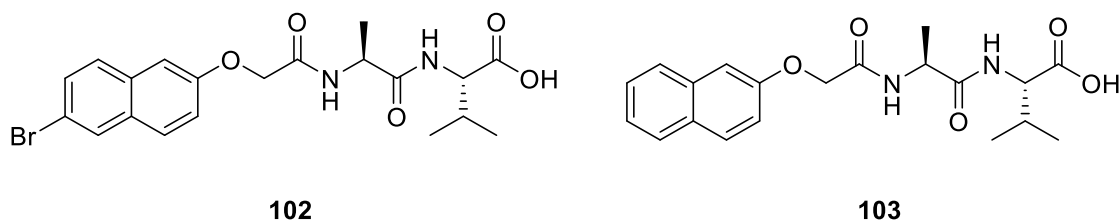


Figure 63. The dipeptide based gelators used by Adams and co-workers to form self-sorted gel networks.

The two gelators were dissolved in water at pH 10.5, and as pH was slowly lowered, the formation of the gel network was monitored by ^1H NMR spectroscopy. This indicated that gelator **102** formed a network first, as this became invisible by NMR before gelator **103**. The GdL concentration could be optimised so that all of **102** was assembled before any of **103** began to assemble, making complete self-sorting assembly highly likely. This method is attractive as it allows for good control over self-assembly. Provided the pK_a of each component is known and sufficiently different, it is possible to determine the order in which the gelators will self-assemble. It would also be possible to extend this method to work for systems containing more than two gelators, while still maintaining the control over the order of self-assembly. However, this method is limited to gelators for which gelation is triggered by pH change, and therefore any system designed by this method will be limited by the stability of the gelators at a range of pH values.

Self-sorted mixtures of gelators are also obtainable using different triggers for gelation. This allows the two different triggers to be applied sequentially, resulting in stepwise formation of each self-assembled network. In 2019, Piras and Smith reported to combination of two previously reported LMWGs, DBS- CO_2H and DBS- CONH_2 , to form a hybrid hydrogel.

As these two gelators have different triggers for gelation, with DBS- CONH_2 forming gels following a heat-cool cycle, and DBS- CO_2H on a reduction in pH, the two networks can be assembled in sequence. Equal concentrations of the two gelators were combined, with the DBS- CO_2H dissolved by increasing the pH of the solution. The mixture was then heated to dissolve the DBS- CONH_2 , and this solution transferred to a second vial containing GdL.

On cooling of the solution, the DBS- CONH_2 network forms very rapidly, with NMR indicating that around 85% is assembled within 30 minutes. The slow hydrolysis of GdL leads to slow reduction in the pH of the solution, and the resulting slow self-assembly of the DBS- CO_2H network – this process is only complete after about ten hours. The hybrid gel formed was stiffer than either of the gels formed from the individual hydrogelators. Additionally, it was possible to selectively ‘switch-off’ the DBS- CO_2H network, through an increase in pH. This caused the network

to break down. The network could then be ‘switched on’ again when the pH was lowered. Following this switching, the end material was found to have almost identical rheological properties to the material at the start. This was despite the hydrogel not being self-supporting when the DBS-CO₂H network was disrupted. Additionally, as the formation of DBS-CO₂H network is pH triggered, it was possible to pattern the hybrid gels through the use of a photoacid to trigger DBS-CO₂H gelation. The hybrid gels could then be used to generate gold nanoparticles, with smaller particles formed in areas with just DBS-CONH₂, and larger particles in the hybrid domains.

Increasingly, this type of hybrid hydrogel is being developed with specific applications in mind. In 2016, Escuder and co-workers reported the development of a hybrid hydrogel, formed from two valine based LMWGs, each with a different group for catalysis (Figure 64).¹⁸³ Each of these had previously been reported, and the catalytic activity of **105** described.¹⁸⁴ Each of these gelators is capable of acting as a catalyst in a different reaction – **105** in an aldol reaction, and **104** in an acetal deprotection.

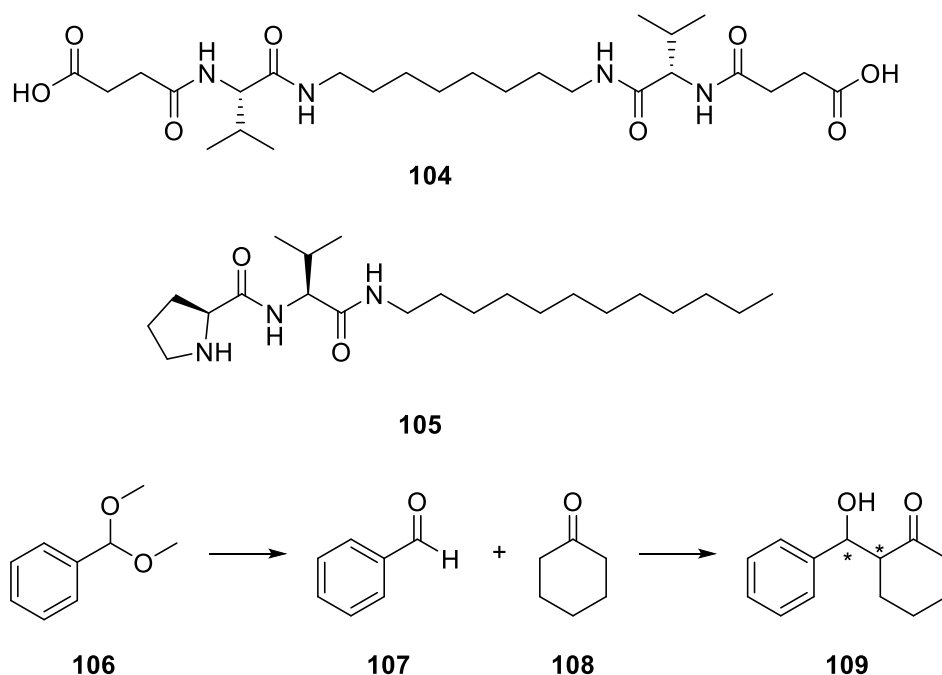


*Figure 64. The valine based gelators developed by Escuder and co-workers with **104** containing a carboxylic acid for catalysis, and **105** a proline residue. The reaction the gels catalysed is also shown.*

In this case, the two gelators were mixed with each at their MGC, to give a translucent gel. Imaging of this gel indicated that two types of fibre had been formed, suggesting that self-sorting had occurred. Further analysis, including wide angle powder X-ray diffraction (WAXD), rheology and DSC also suggested self-sorting on self-assembly. The hybrid gel system was then tested for

catalytic activity, with the acetal deprotection carried out initially. This was successful, and was therefore followed by a one pot reaction – an acetal deprotection to form one of the starting materials for a subsequent aldol condensation. This was also successful, with the aldol condensation product formed in 85% yield. This indicated that the presence of both networks did not impact the catalytic ability of the gels. When the gelators were present only in solution, no reaction took place. Additionally, when **105** was replaced with a second proline-containing gelator, more structurally similar to **104**, co-assembly of the two gelators was observed, but with no catalytic activity. This indicates that both gel assembly and the self-sorting of the gel two networks is important for achieving catalysis. This work provides a good example of how hybrid gels can provide novel materials with properties that are superior to those of the gels formed from the individual gelators. It also shows how the mode of self-assembly can be important for the final properties of the material.

As with single-component LMWG hydrogels, there is increasing interest in applying hybrid hydrogels in biomedical applications.

In 2018, Hamachi and co-workers reported a hybrid hydrogel composed of two gelators that self-sorted on assembly.¹⁸⁵ This self-sorting was achieved by combining two hydrogels with distinct structures, one peptide based (**110**), and the other lipid based (**111**) (Figure 65). Both were capable of acting as hydrogelators individually.¹⁸⁶

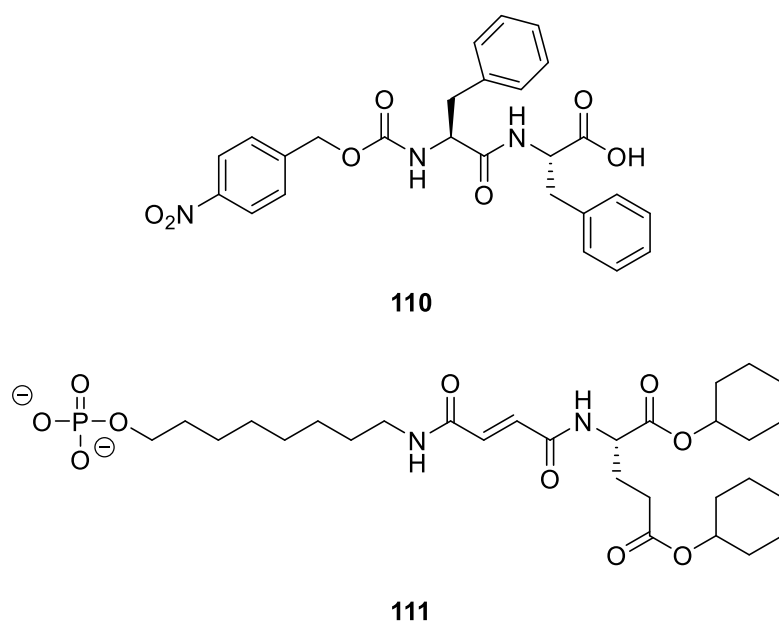


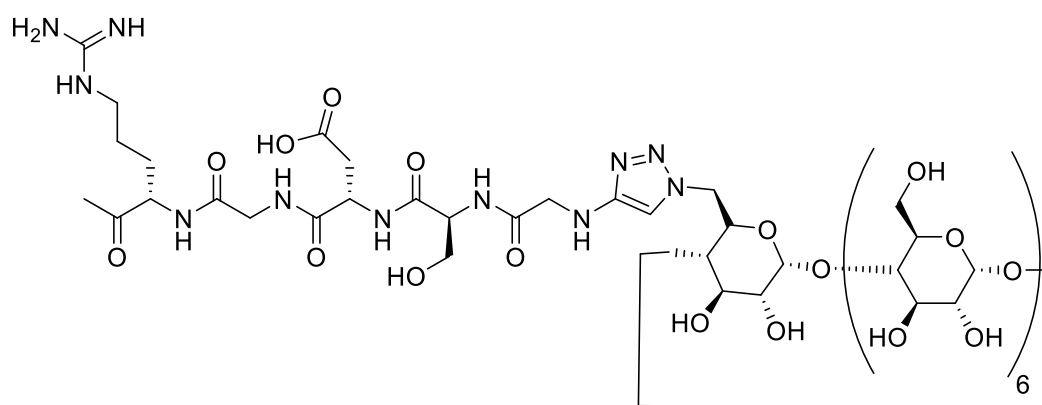
Figure 65. The gelators used by Hamachi and co-workers in a hybrid hydrogel.

When these two gelators were combined, analysis by circular dichroism and imaging indicated that the two gelators self-sorted on assembly to form two distinct networks. The two networks

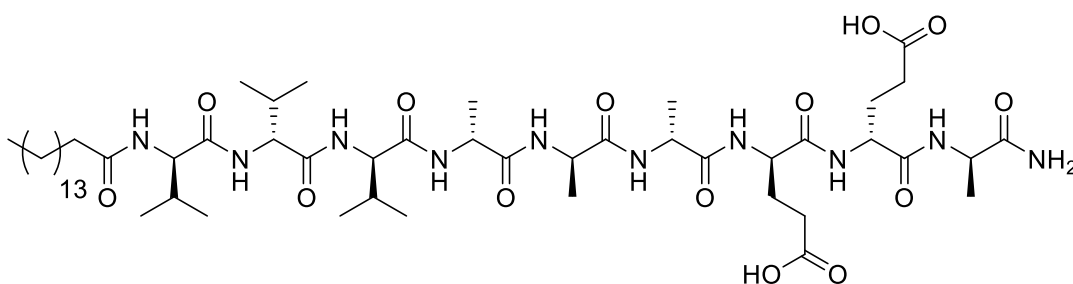
were responsive to different stimuli, the responsiveness of the hybrid gel was then investigated. For the peptide based hydrogelator, addition of $\text{Na}_2\text{S}_2\text{O}_4$ causes the gel to break down – this is a result of the reduction of the molecule, and subsequent elimination of the Npmoc moiety.⁷⁴ The lipid based hydrogel can be formed by the action of bacterial alkaline phosphatase (BAP). This removes the phosphate group by hydrolysis, leading to the molecule becoming less soluble, and transformation of the viscous liquid to a hydrogel. This occurs even in combination with the second hydrogelator.

Further investigation of the hybrid gel indicated that applying these stimuli could impact the material properties of the gel. Breakdown of the peptide network led to a weaker overall gel, eventually giving a viscous liquid, while reinforcement of the lipid network led to a gel with higher material strength. Following these observations, the hybrid gel was tested for release of selected proteins. Immunoglobulin G, myoglobin, or concanavalin were added to the gel network, and the release monitored following application of one of the previously discussed stimuli. It was observed that on addition of $\text{Na}_2\text{S}_2\text{O}_4$, release of the proteins was faster than for no stimulus, with the opposite observed on addition of BAP. This suggests that the density of the network is an important factor in the diffusion of these proteins through the gel. When one network is broken down, the network is less dense, and hence faster diffusion can occur – the opposite is true when the network is reinforced. The rate of protein release could therefore be controlled to an extent, although additional investigations would be needed to understand how different concentrations of the additives could impact the rate of release.

It is also becoming more common for more than just two gelators to be combined. In 2020, Mata and co-workers reported the use of three components to form a hybrid hydrogel (Figure 66).¹⁸⁷ This involved two peptide amphiphiles, which co-assembled to form nanofibres. Of these two, one was the main constituent of the nanofibres (**113**), and the second was modified to have a moiety capable of participating in a host-guest interaction with the third component. The third component was a shorter peptide, modified with cyclodextrin, containing an amino acid sequence known to promote cell binding (**112**). These multi-component hydrogels could be used for cell culture, with increasing proportions of the peptide **112** giving improved cell adhesion.



112



113

Figure 66. Two of the modified peptides used by Mata and co-workers in their multicomponent hydrogel. Top: the peptide containing the cell adhesion sequence, also modified with a cyclodextrin unit; Bottom: The peptide making up the majority of the nanofibres. Further modification of this gave the third component.

Therefore, while there has been increasing recent interest in developing hybrid hydrogels from multiple LMWGs, this is an area that remains underexplored, leaving much scope for further development.

1.6 Project Aims

In recent years, there has been considerable progress in the development of supramolecular hydrogels for use in biomedical applications. Increasingly, gelators are being designed with specific applications in mind, although many are still discovered by serendipity. Progress has been made in particular in the area of multi-component hydrogels, as these can offer a simple but effective way to design novel materials and to extend the scope and range of existing well-established gelation systems. Key areas of development have included the use of supramolecular hydrogels for cell culture and drug delivery.

This project will aim to develop novel hydrogel materials based on MBS and DBS derivatives. A number of methods for achieving this will be investigated – the synthesis of novel DBS and MBS derivatives, the combination of the known hydrogelator DBS-CONHNH₂ with additional gelators,

and investigation of systems formed by both the D-DBS-CONHNH₂ and L-DBS-CONHNH₂ enantiomers.

Modification of DBS has been widely reported in the literature, and many derivatives are used in commercially available products. However, these are typically organogelators, or thickeners, rather than hydrogelators. This is an area of DBS derivatives that is relatively underexplored. We will therefore synthesise DBS derivatives, with the intention that these will act as hydrogelators (Figure 67). Modifications will be chosen rationally, considering the important factors in designing a hydrogelator. MBS derivatives will also be synthesised – these have not been as investigated as much as DBS derivatives. These MBS derivatives will also be tested for the ability to act as hydrogelators.

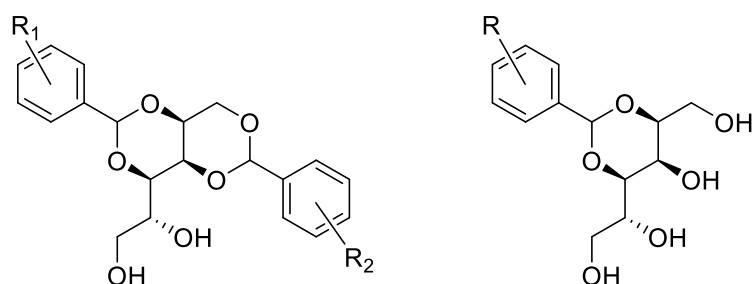


Figure 67. General structure for the DBS and MBS derivatives that will be developed. R_1 and R_2 may be the same or different.

DBS-CONHNH₂ itself has already been combined with a number of different polymeric gelators, which has improved the range of applications it can be used in. It has also been combined with the second LMWG DBS-CO₂H. In this project we will combine DBS-CONHNH₂ with a novel LMWG, to enhance the properties of the resulting gel without the need for a polymer gelator. It is hoped that the combination of two gelators will lead to a novel, tuneable, two-component hydrogel. This will also be investigated for applications in drug delivery. These will include model compounds containing carboxylic acids, and neuroactive drugs. A second gel system, based on glutamine, will also be investigated for release of neuroactive drugs. The material properties of this system will be investigated to determine the suitability for drug release applications, and the release *in vivo* investigated.

Despite DBS and derivatives being relatively widely used in industry, there is little understanding of the potential impact of the sugar chirality on the behaviour of the gelator. While the L-sorbitol based gelator is not feasible for use in large scale industrial applications due to increased cost of the starting materials, chirality is potentially still relevant in applications such as cell culture and delivery of chiral compounds – chirality is becoming an increasingly important consideration in

design of gelators for biomedical applications. L-DBS-CONHNH will therefore be synthesised, and its gelation properties compared with those of D-DBS-CONHNH₂ (Figure 68). Combinations of the two enantiomers will also be investigated, to determine the impact of combining the two on gelation. The interactions of chiral additives with the enantiopure hydrogels will be investigated – this is potentially important for biomedical applications.

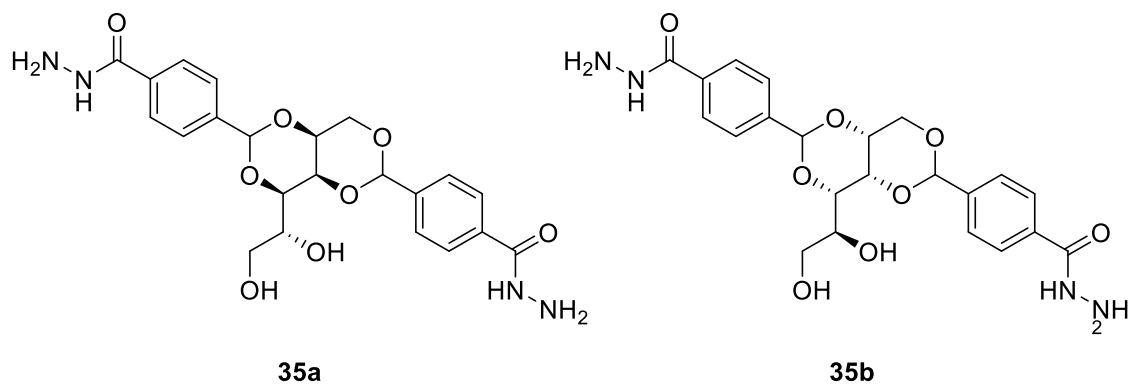


Figure 68. D-DBS-CONHNH₂ (left) and L-DBS-CONHNH₂ (right).

2. Chapter 2: Hybrid Supramolecular Hydrogels

Previously, as explained in the Introduction, DBS-CONH₂ has been used in a wide range of applications. These include drug release¹⁰⁹ and absorption of dyes¹⁰⁶ – both of which make use of the interactive nature of the acyl hydrazide groups, and their interactions with functional groups in other molecules. This drug release is also pH mediated, leading to controlled release of non-steroidal anti-inflammatory drugs (NSAIDs) including naproxen and ibuprofen. Specifically, it was argued that the carboxylic acid groups on these drugs promoted interactions with the acyl hydrazide groups, and on deprotonation to the carboxylate form, drug release was triggered. Hydrogels based on DBS-CONH₂ can also be used to sequester metal nanoparticles¹⁷¹ – these nanoparticle loaded gels can be used for catalysis¹⁷² or anti-microbial action.³¹ The versatility of the hydrogel is a result of both the interactive acyl hydrazide groups and the stability of the gels at a range of pH values – relatively unusual for supramolecular gel.

However, DBS-CONH₂ hydrogels are mechanically weak, typical for gels formed from LMWGs. This limits the potential of these gels, as they are difficult to manipulate without damage. However, combination of DBS-CONH₂ with a polymer gelator, such as agarose¹⁷² or PEGDM,¹⁷⁴ has been shown to provide additional mechanical strength, while the responsive and interactive nature of DBS-CONH₂ is maintained.

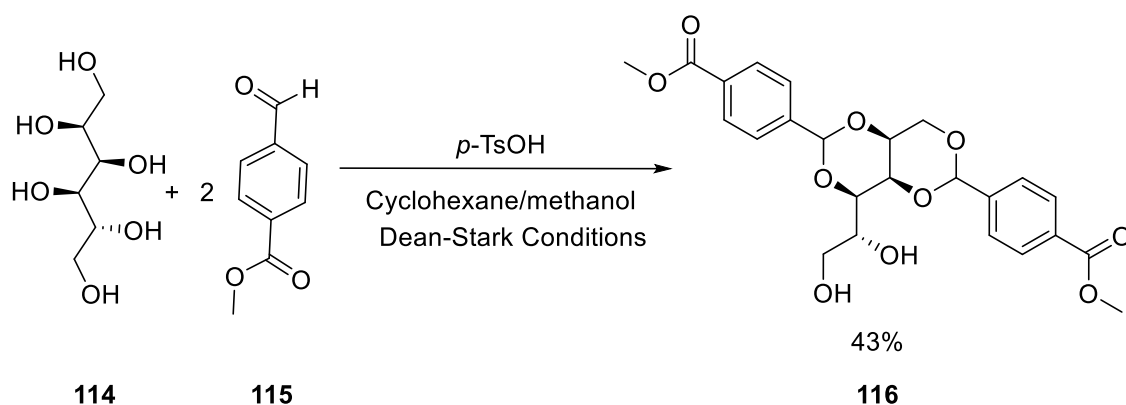
There has recently been increasing interest in combining two supramolecular gelators to form hybrid gels, with the aim being to exploit the most desirable properties of the two gelators. This avoids the use of polymer gels, which can sometimes be unresponsive and can dominate the properties of hybrid materials. The combination of two supramolecular gelators therefore has the potential to precisely and reversibly tune the properties of a hydrogel to suit the desired application.

DBS-CONH₂ was therefore combined with a novel hydrogelator, MBS-CO₂Me, which has quite different properties, to form a hybrid hydrogel. The properties of both the MBS-CO₂Me hydrogel and the novel hybrid gel were investigated, as well as initial studies into the use of these materials in drug delivery applications being performed.

2.1 Synthesis of DBS-CONH₂ and MBS-CO₂Me

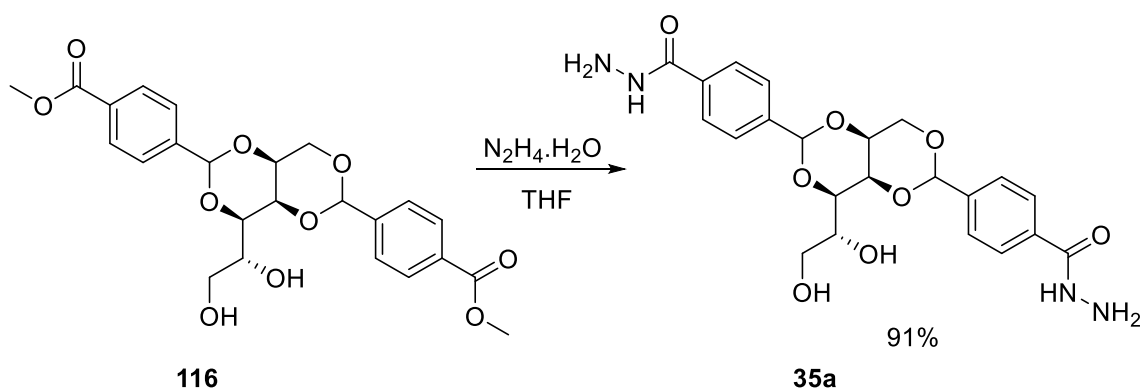
DBS-CONH₂ was synthesised in a two-step process, as previously reported.¹⁰⁶ First, D-sorbitol (**114**) is condensed with two equivalents of 4-methylcarboxybenzaldehyde (**115**), under Dean-Stark conditions, in the presence of *p*-TsOH (Scheme 2). The Dean-Stark apparatus removes the

water formed in the acetal reaction, helping to drive the equilibrium to the right. This cannot be achieved using molecular sieves or MgSO_4 , as the DBS- CO_2Me formed is insoluble, and therefore these additives would be extremely challenging to separate from the final mixture. This reaction forms DBS- CO_2Me (**116**), along with the mono- and tri- substituted derivatives. These were removed by sequential washing steps – first with hot water, to remove the more hydrophilic MBS- CO_2Me , then hot DCM to remove the more hydrophobic TBS- CO_2Me . This gave DBS- CO_2Me in a 43% yield.



Scheme 2. Synthesis of DBS- CO_2Me .

For the synthesis of DBS- CONHNH_2 , the synthesised DBS- CO_2Me was heated with $\text{NH}_2\text{NH}_2 \cdot \text{H}_2\text{O}$, converting the methyl ester to give DBS- CONHNH_2 (Scheme 3), This proceeds in excellent yield.



Scheme 3. Synthesis of DBS- CONHNH_2 .

In the process of the washing of DBS- CO_2Me , it was noted that the filtrate from the hot water wash formed a gel-like substance. This was further purified by washing with cold water, to remove unreacted D-sorbitol, and determined to be the mono-substituted product, MBS- CO_2Me (**117**), through NMR and mass spectrometry (MS) analysis. In the ^1H NMR, the acetal peak for MBS- CO_2Me is present at 5.64 ppm – distinct from the equivalent signal for DBS- CO_2Me , which occurs at 5.76 ppm. In addition, the extra alcohol protons result in larger integrations for the corresponding peaks. For ^{13}C NMR, the spectra for MBS- CO_2Me contains fewer peaks than that for

DBS-CO₂Me, although the chemical shifts are comparable to the equivalent carbons. Analysis of the product by MS also indicated the formation of a species with the expected mass for MBS-CO₂Me.

The synthesis to give MBS-CO₂Me was then optimised. Initially, the reaction using sorbitol and 4-methylcarboxybenzaldehyde in a ratio of 1:1 was tested. This led to batch-to-batch inconsistencies in the purity of the product, even after multiple washing steps. This can be most clearly observed in the ¹H NMR spectrum of the product, in the region of the acetal peak. When the product is clean, only one peak, corresponding to the acetal proton, can be observed, whereas if impure, there are multiple peaks visible, even after the purification steps (Figure 69).

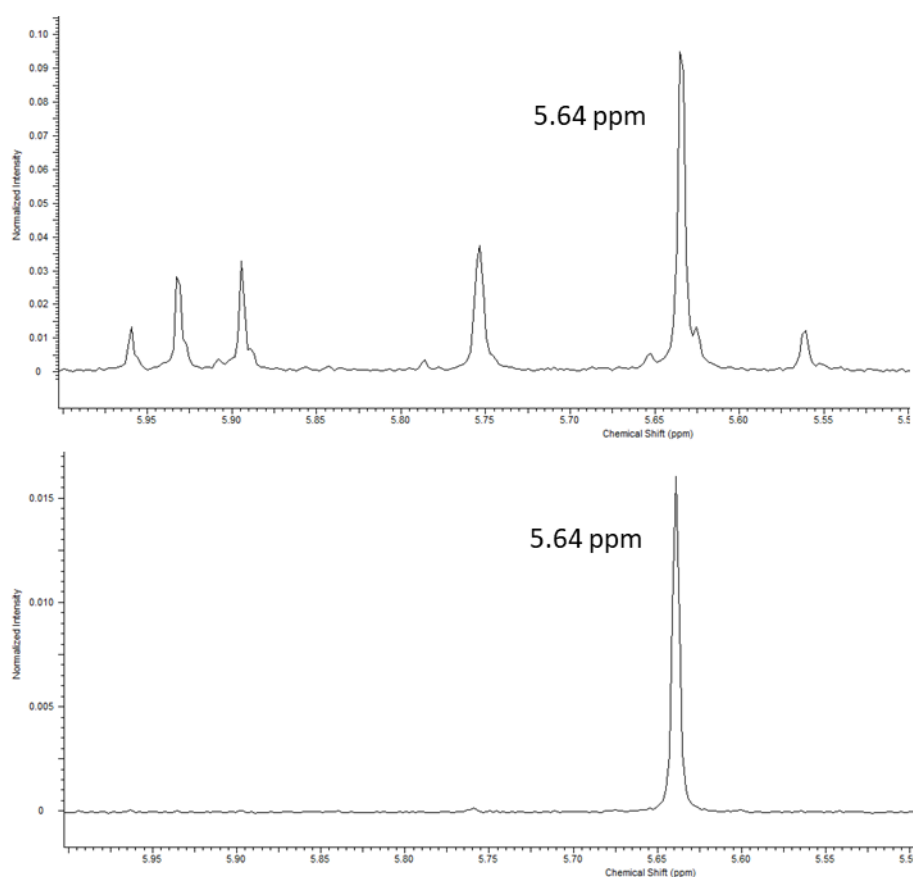


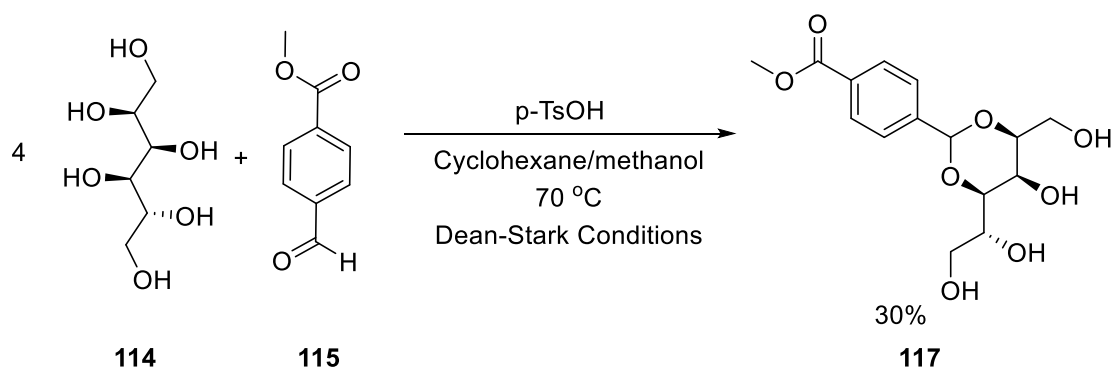
Figure 69. Top: A ¹H NMR spectrum for impure MBS-CO₂Me, highlighting the region 6.0-5.4 ppm. The peak at 5.64 ppm corresponds to the acetal proton. Bottom: A ¹H NMR spectrum for pure MBS-CO₂Me.

In an attempt to improve the consistency of the reaction, different equivalents of sorbitol were tested, whilst keeping all other reaction conditions the same (Table 1). The yield in each case is quoted with respect to the aldehyde, which is the limiting reagent.

Table 1. Optimisation of the synthesis of MBS-CO₂Me, varying the equivalents of sorbitol. The 'extra' peak integrations are for peaks in the acetal region that do not correspond to MBS-CO₂Me, that were still present after purification steps.

Ratio – Sorbitol: Aldehyde	Extra Peak Integrations	Yield / %
1:1	1.04	2
3:1	0.08	12
4:1	0.00	30
5:1	0.10	15
6:1	0.02	18
7:1	0.45	Trace
8:1	0.50	Trace

From these results, it was apparent that using four equivalents of sorbitol for every one of 4-methylcarboxybenzaldehyde gave the best conditions for synthesis of MBS-CO₂Me. This method resulted in there being no impurities remaining after washing, while maintaining a reasonable yield of 30%. Although this is a relatively low yield, the reaction can be performed on a multi-gram scale, typically yielding around 2 g of material. There was also less formation of the di- and tri-substituted products. This method was then further improved by reducing the reaction time to 1.5-2 hours, compared to the 2-3 hours for DBS-CO₂Me. This was therefore the method used for further synthesis of MBS-CO₂Me (Scheme 4).



Scheme 4. Synthesis of MBS-CO₂Me

2.2 Investigation of MBS-CO₂Me as a Hydrogel

2.2.1 Gelation and T_{gel} Testing of MBS-CO₂Me Hydrogels

Once the synthesis of MBS-CO₂Me had been optimised, its behaviour as a hydrogel was investigated - it is known in the literature that MBS derivatives can form hydrogels.^{188,189} This is in contrast to DBS-CO₂Me – which is insoluble in water, and so cannot be dissolved. The additional free alcohols of the sugar backbone make MBS-CO₂Me more water soluble – soluble enough that it can dissolve in hot water, allowing a gel to be formed. Solubility plays an important role in gelation, and this is becoming increasingly well understood.⁹⁴

As the initial gel-like substance observed in the synthesis of DBS-CO₂Me was formed on cooling an aqueous solution, it seemed reasonable that heating, followed by cooling, would be a suitable method for triggering gelation. This was indeed found to be the case.

For preparation of MBS-CO₂Me hydrogels, a known mass of gelator was added to a 7 ml sample vial, and deionised water (1 ml) added. This was sonicated for 5 minutes, resulting in a suspension, which was then heated using a heat gun until the solid was completely dissolved. On cooling overnight, a transparent gel was formed (Figure 70). Through variation of the gelator concentration, the minimum gelation concentration (MGC) was determined – a sample was considered to have formed a gel if it could be self-supporting during the tube inversion test for a time of greater than 1 minute. In this way, the MGC of MBS-CO₂Me was determined to be 0.75% wt/vol. Below this concentration, the gelator remained in solution, and hence no gels were formed. Gels could be formed up to a concentration of 1.0% wt/vol – above this concentration, although gels were formed, not all of the solid could be fully dissolved on heating, and so was not incorporated into the gel network. Although gel formation was also tested in a selection of organic solvents, the gelator was not soluble, and so no gels were formed.



Figure 70. An MBS-CO₂Me hydrogel, formed by a heat-cool cycle (at 0.85% wt/vol).

The ability of MBS-CO₂Me to form gels in buffer solutions was also investigated. Although buffers are important in many biological applications, the presence of salts, and the control over pH, can have a significant impact on hydrogel formation. The formation of MBS-CO₂Me hydrogels in buffer solution was tested using the same method as previously, with deionised water being replaced with the chosen buffer (1 ml). For details of buffer preparation, see the experimental section. Pleasingly, MBS-CO₂Me formed stable hydrogels in all the buffers tested, spanning the pH range from 5.5 to 7.5 (Table 2).

Table 2. Gelation tests for MBS-CO₂Me hydrogels in buffer solutions.

Buffer	Gel?
Tris 0.1 M	Y
Tris 0.01 M	Y
HEPES 0.01 M	Y
PBS 0.1 M	Y
PBS 0.01 M	Y
Phosphate (pH 7.5) 0.1 M	Y
Phosphate (pH 7.5) 0.01 M	Y
Phosphate Citrate (pH 6.5) 0.1 M	Y
Phosphate Citrate (pH 6.5) 0.01 M	Y
Phosphate Citrate (pH 5.5) 0.1 M	Y
Phosphate Citrate (pH 5.5) 0.01 M	Y

The thermal stability of a gel is determined by measurement of the T_{gel} – the temperature at which the transition from gel to solution occurs. This can be determined using the tabletop rheology method of tube inversion – when the material is no longer self-supporting, the T_{gel} is deemed to have been reached.

Gel samples of MBS-CO₂Me were prepared, in a range of concentrations, and placed in a thermoregulated oil bath. The temperature was slowly increased from 20 °C, at a rate of 1 °C min⁻¹. T_{gel} values, for gels prepared in water (Table 3). Gels prepared in PBS buffer and Tris buffer were also investigated – the use of buffer made no significant difference to the T_{gel} value.

Table 3. T_{gel} values for MBS-CO₂Me hydrogels at a range of gelator concentrations.

MBS-CO ₂ Me / % wt/vol	T_{gel} / °C
0.75	53 ± 0.5
0.80	54 ± 0.5
0.85	56 ± 0.5
0.90	57 ± 0.5
0.95	57 ± 0.5
1.00	59 ± 0.5

As would be expected, the concentration of gelator is increased, the T_{gel} also increases, very slightly, with the highest value just below 60 °C. This reflects the increasing network density as gelator concentration increases. It is noteworthy that MBS-CO₂Me has lower T_{gel} values than those formed by the disubstituted derivative DBS-CONH₂ ($T_{gel} = ca. 80$ °C). This is likely to be a result of the increased water solubility of MBS-CO₂Me, due to the four OH groups of the sugar backbone. This reasoning can also be applied to explain the higher MGC of MBS-CO₂Me, in comparison to DBS-CONH₂ (MGC = 0.20% wt/vol) – as the gelator is more water-soluble, a greater concentration is required for the network to assemble sufficiently.

Given that MBS-CO₂Me hydrogels are formed via a thermal trigger, it was reasoned that they might be thermally reversible. Therefore, once the gels had broken down due to the high temperature, they were left to stand overnight, to allow time for any reformation of the gel network. Over this time, the samples went from transparent solutions (possibly indicating that the majority of the gelator had been redissolved at the higher temperatures) to white, opaque gels. This was the case for all but the hydrogels at the lowest concentrations – where gels were only partially reformed. This suggests that perhaps not all of the gelator has been fully incorporated into the network – and therefore the gel cannot fully reform (Figure 71).

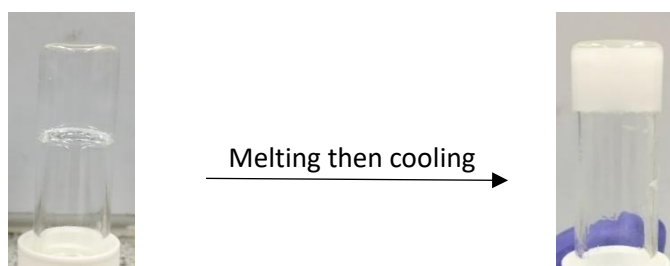


Figure 71. Change in appearance on melting, then cooling of MBS-CO₂Me hydrogels (left: gel before melting, right: gel after reforming).

Once the gels had reformed, the thermal stability of these new opaque gels was also investigated. As previously, the reformed gels were placed in a thermoregulated oil bath, the temperature gradually increased, and the stability of the gels monitored by the tube inversion method. Surprisingly, the previous melting of the gels had little impact on the thermal stability of the gels that reformed, with very little difference between the T_{gel} values for the reformed gels, and those of the original gels (Table 4).

Table 4. Comparison of T_{gel} values for initial gels, and reformed gels.

MBS-CO ₂ Me / % wt/vol	T_{gel} / °C	T_{gel} (reformed gels) / °C
0.75	53	Not fully reformed
0.80	54	Not fully reformed
0.85	56	52
0.90	57	57
0.95	57	60
1.00	59	58

These reformed gels were then once again heated beyond the T_{gel} , to give a solution, and left to cool. Once again, gels were formed – indicating that the hydrogels have good thermal reversibility. It is, however, not completely clear why the gel is transparent after the first heating cycle, but then opaque after later heating cycles. Typically, opaque gels have larger assembled structures within them,¹⁹⁰ leading to the light scattering effect. These observations may suggest that on heating, the gel fibres do not completely disassemble into free molecules, but rather disassemble into aggregates. These aggregates may then reform a gel network with a slightly different microstructure, leading to the light scattering and opacity. Adams and co-workers have been interested in related effects in pH-switchable gels.¹⁹¹ This would require further study to fully understand, but was beyond the scope of this study, as multiple thermal gel cycling has little relevance in a drug delivery setting.

2.2.2 Rheology of MBS-CO₂Me Hydrogels

Although the tube inversion test indicated that gels had been formed, this is in fact not conclusive proof that true hydrogels have been formed – as precipitate or crystals can occasionally also give a self-supporting mass. Therefore, the MBS-CO₂Me hydrogels were investigated by parallel plate rheology.

Rheology gives information on the response of a material to stress. When a stress is applied, deformation of the material will occur. There are two types of deformation – flow, and elasticity. Flow is irreversible – once the stress has been applied, and the deformation occurred, the material cannot regain its original shape. By contrast, elasticity is a reversible form of deformation, and the material will return to the original shape once the stress is removed. Flow is measured by the resistance to flow on the application of a stress, and elasticity by the measuring the deformation that occurs. Elastic materials store energy, whereas viscous material dissipate energy in the form of heat.

The rheological properties of a material are determined by the application of a sinusoidal stress. In an ideal elastic material, the resulting strain will be both proportional to and in phase with the applied stress – there is no time lag between the stress being applied and the response of the material. For an ideal viscous material, there is a delay in the response, which will be 90° out of phase.

Gels are viscoelastic materials, and therefore exhibit a mix of viscous and elastic properties. For these materials, when the stress is applied, the resulting strain will be proportional to this, but out of phase by an angle (δ) in the range 0-90°. The ratio of applied stress and observed strain gives G^* , the complex dynamic modulus. This can be separated into two components:

$$G' = G^* \cos\delta$$

$$G'' = G^* \sin\delta$$

G' is the storage modulus, representing the amount of energy that is stored by the material. G'' is the loss modulus, the amount of energy dissipated. The ratio of G'/G'' is therefore the ratio of energy stored to energy dissipated. For a viscoelastic material, more energy is stored than is dissipated – $G' > G''$. The point at which $G' = G''$ is the point at which a material is no longer viscoelastic, and instead behaves as a liquid. This measure provides a more robust check of gelation than the simple tube inversion test – for example, a viscous liquid might be self-supporting under gravity, but have $G'' > G'$.

In parallel plate rheology, oscillatory stress is applied to a sample and the response measured in terms of G' and G'' . This allows for investigation of the effects of factors such as stress amplitude, stress frequency and temperature on the material.

However, these considerations are only true within the linear viscoelastic region (LVR) – this must therefore be determined before any further studies are carried out. The LVR is considered as the region in which G' and G'' are independent of the frequency and magnitude of the stress applied.

This region can be determined by carrying out an amplitude sweep, with varying stress applied at a constant frequency. Following this, additional measurements can be carried out within these parameters.¹⁹²

As the gel samples must be transferred onto the rheometer for analysis, bottomless vials are used for sample preparation. These vials are attached to a flat glass surface, such as a petri dish. The gelator is weighed into a vial as normal, and the gelator dissolved by heating. While the solution is hot, it is transferred to the bottomless vial, and the gel allowed to form within this vial. The bottomless vial can then be removed, and the gel disc carefully transferred to the rheometer with a spatula (Figure 72). For initial studies, MBS-CO₂Me hydrogels were prepared at a concentration of 0.85% wt/vol.



Figure 72. Gel samples for rheological studies. Left: The sample once the bottomless vial has been removed. Right: a sample once it has been transferred to the rheometer.

Once the sample had been loaded, the LVR was determined through running of a strain-controlled amplitude sweep. This was performed at a frequency of 1 Hz, with the applied strain increasing from 0.05% to 100% (Figure 73). The runs were carried out in triplicate, and standard error indicated by error bars.

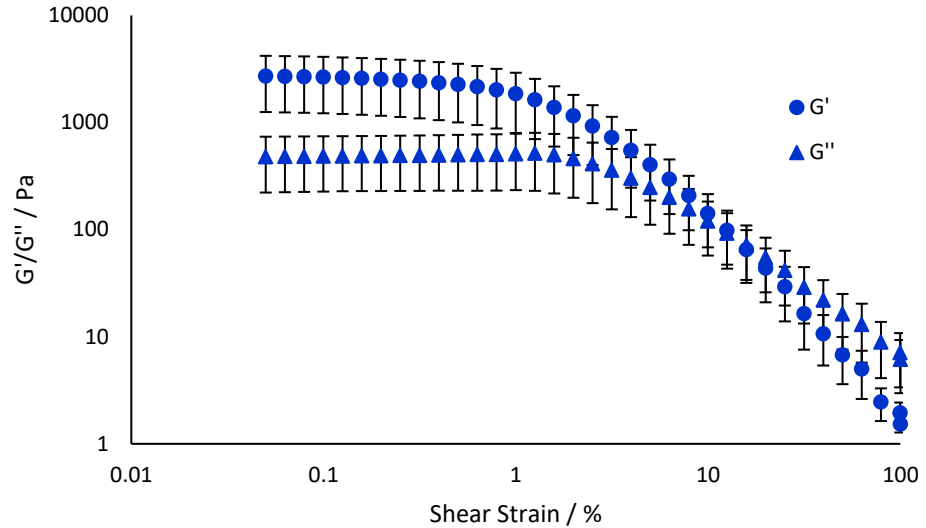


Figure 73. Amplitude sweep (0.05%-100%) for MBS-CO₂Me hydrogels at 0.85% wt/vol. Temperature 25 °C, frequency 1 Hz.

In the LVR, $G' > G''$, indicated that a gel has indeed formed, with G' having a value of around 2700 Pa – this is an indication of the stiffness of the gel. The crossover point, where $G' = G''$, occurs at around 12% - at this point the material no longer has viscoelastic properties, and is therefore no longer a gel. This value indicates the resistance of the material to shear strain.

As well as the amplitude sweep, a frequency sweep can also be carried out. Varying frequency is applied, with the strain at a constant amplitude within the LVR. If the material is a gel, G' will be independent of frequency, and therefore will remain constant despite the variations in frequency. MBS-CO₂Me hydrogels were once again investigated at a concentration of 0.85% wt/vol, with the amplitude of the strain constant at 0.158%, and the frequency varied from 0.1 Hz – 100 Hz (Figure 74).

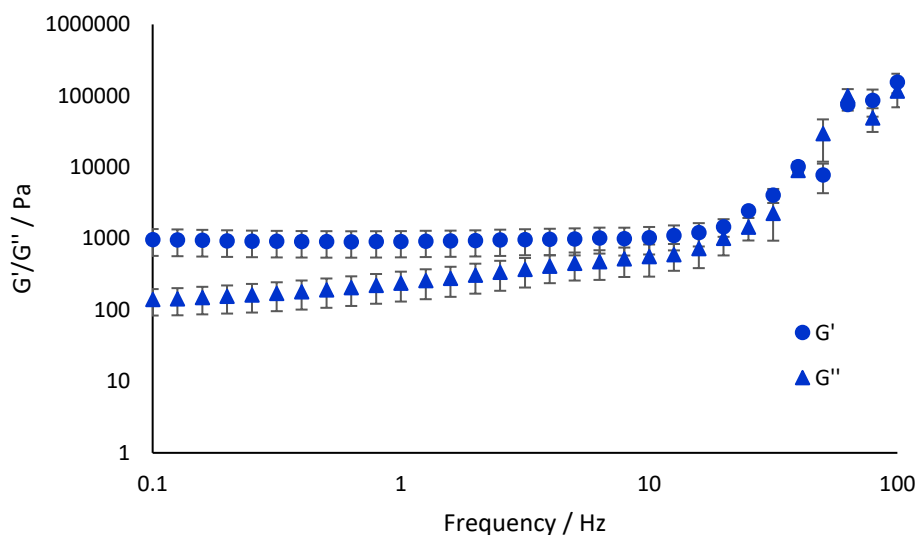


Figure 74. Frequency sweep (0.1 Hz-100 Hz) for MBS-CO₂Me hydrogels at 0.85% wt/vol. Temperature 25 °C, amplitude 0.158%.

At lower frequencies, G' is independent of the frequency, remaining constant. This is further evidence that a gel has been formed. At much higher frequencies, the gel is broken down, and this is no longer the case – the material is no longer viscoelastic.

These experiments were also carried out for the MBS-CO₂Me hydrogels that had been thermally broken down and allowed to reform, to investigate the impact of this disruption of the gel network on the physical properties of the gel.

Initially, the hydrogels were prepared as normal. These gels were then heated to above the T_{gel} value, and while the gelator was in solution, transferred to a bottomless vial, in which the gel was allowed to reform. These gel samples were then transferred to the rheometer, and amplitude and frequency sweeps carried out. For these samples, the amplitude sweep was carried out from 0.001% - 100% applied strain.

The amplitude sweep (Figure 75) indicated that, in the LVR for each gel, there was a significant increase in the G' value for the MBS-CO₂Me hydrogels, with G' being increased from 2700 Pa for the starting gel, to around 22,000 Pa for the reformed gels. However, the LVR for the reformed gels was observed at lower levels of strain. If the LVR is considered to end at the point at which G' has dropped below 5% of the initial value, MBS-CO₂Me has an LVR ending at a shear strain of around 0.25%, much higher than for the reformed gels, which have an LVR ending at a shear strain of around 0.005%. This indicates that, although the reformed gels may initially be stiffer, they begin to break down at lower levels of strain than gels that have not had the network

disrupted. This earlier breakdown is also indicated by the lower crossover point of 2% for the reformed gels, compared to 12% for the undisrupted gels.

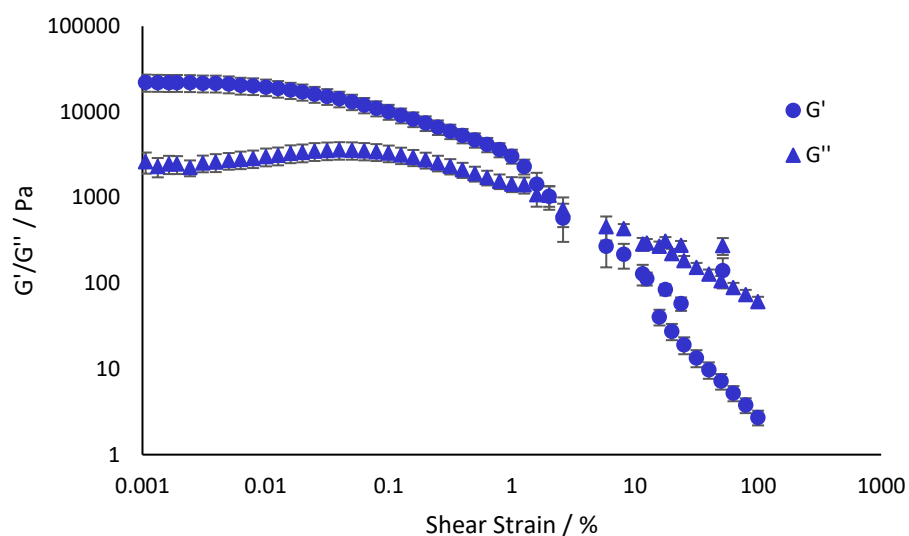


Figure 75. Amplitude sweep (0.001%-100%) for reformed MBS-CO₂Me hydrogels at 0.85% wt/vol. Temperature 25 °C, frequency 1 Hz.

The frequency sweep, (Figure 76), also indicates that gels the gels are indeed reformed – rather than the samples being self-supporting as a result of the precipitate that was visible in the reformed samples. G' was also considerably higher in the reformed gels – around 23000 Pa, further indicating that within the LVR, the reformed gels have increased stiffness. The increase in stiffness of the gels, and the greater sensitivity to shear strain is consistent with the opacity of the gels which would indicate the presence of larger more microcrystalline aggregated objects. It is often found that more crystalline aggregated gels have greater stiffness, presumably as a result of having less flexibility at the fibrillar level.¹⁹³

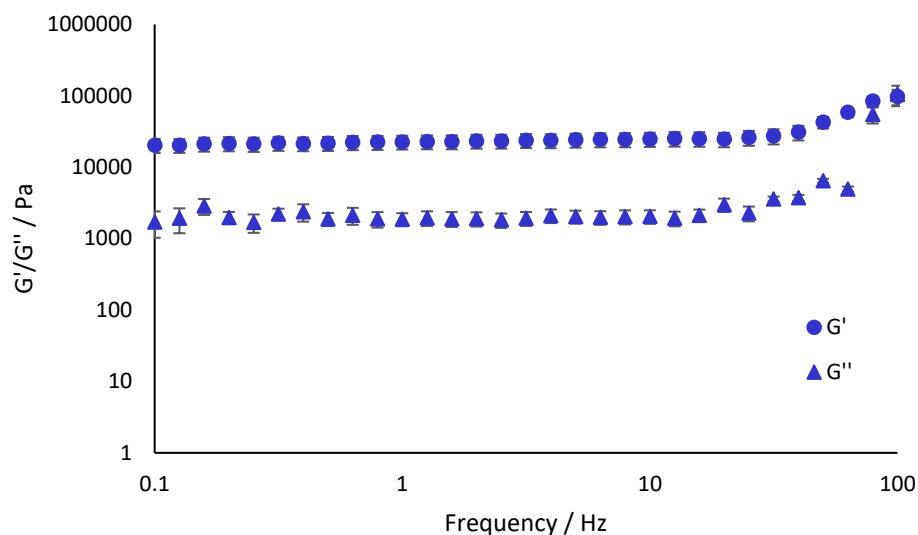


Figure 76. Frequency sweep (0.1 Hz-100 Hz) for reformed MBS-CO₂Me hydrogels at 0.85% wt/vol. Temperature 25 °C, amplitude 0.0019%.

2.2.3 Circular dichroism studies of MBS-CO₂Me

Circular dichroism (CD) is a useful tool for investigating the assembly of supramolecular nanostructures. In CD, circularly polarised light is directed through the sample, alternating between the right-handed and the left-handed. Depending on the chirality of the sample, these two forms will pass through at different speeds, with wavelength and absorbance also affected. This difference can be detected and measured, then converted to give ellipticity.¹⁹⁴ When nanostructures are present, there is greater ellipticity compared to the individual molecules in solution. This makes it possible to distinguish between a self-assembled system, and the free molecules simply being present in solution. This can be ideally monitored via a temperature change – as temperature is increased, disassembly occurs. This leads to a corresponding decrease in CD signal.

MBS-CO₂Me hydrogels were prepared at a concentration of 0.57% wt/vol, with the hot solution being transferred to a warm cuvette (pathlength = 1 mm), and the gel then allowed to form within this cuvette. Although this is below the MCG for MBS-CO₂Me, full gelation is not required to observe the assembly of the supramolecular nanostructures. At 20 °C, a CD band was visible, with a maximum absorbance at 281 nm – as the temperature was increased, this band steadily decreased in intensity, (Figure 77). This wavelength corresponds to the aromatic ring on MBS-CO₂Me, and suggests that it is being incorporated into a chiral microenvironment on self-assembly. Thus, CD provides clear evidence that self-assembly has occurred and leads to chirally-organised nanostructures. The greatest fall in ellipticity occurs between 50°C-55°C – this

corresponds with the T_{gel} values determined for MBS-CO₂Me and suggests that, as expected, significant disassembly occurs in this temperature range.

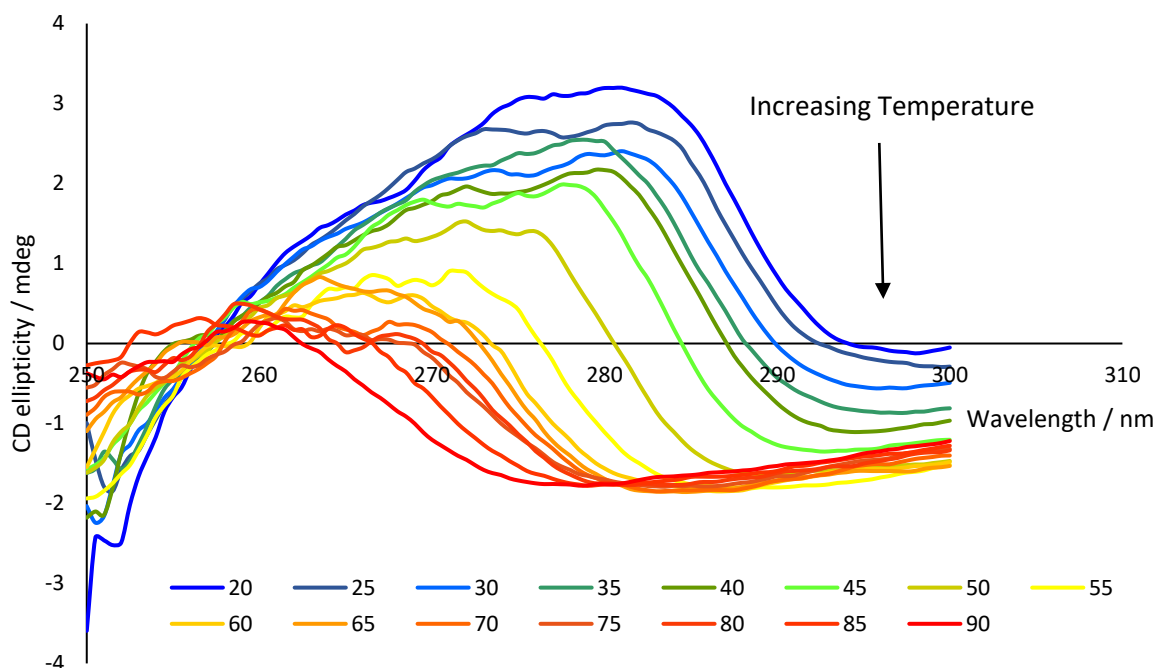


Figure 77. CD spectrum, over a range of temperatures, for MBS-CO₂Me.

It is worth noting that when recording CD spectra, the total absorbance must be carefully considered – too high an absorbance will lead to an unreliable reading. This is a result of too little light reaching the detector. This can be monitored by the recording of the high tension (HT) voltage – any reading over 600 volts indicates that the measurement is not reliable. For these MBS-CO₂Me samples, there were no readings over 600 V, and therefore no points needed to be excluded from the analysis.

2.2.4 Imaging of MBS-CO₂Me

Electron microscopy can be a useful tool to gain insight into the structure of a supramolecular gel – the most common methods are scanning electron microscopy (SEM) and transmission electron microscopy (TEM). These methods can be used to visualise the network that is present upon gelation.

For imaging, MBS-CO₂Me hydrogels were prepared at a concentration of 0.9% wt/vol. To prepare the samples for TEM, a small portion of the gel was transferred by drop-casting to a heat-treated copper TEM grip. Excess material was removed using a filter paper, and the sample left to air-dry for 20 minutes. A uranyl acetate stain was used for contrast. For preparation of SEM samples, a small portion of the gel was transferred to a copper support, then freeze-dried by plunging into

liquid nitrogen. The samples were then lyophilised for twelve hours, before any excess material was removed. The dried sample was then sputter coated with a thin layer of gold/palladium, to prevent sample charging, placed on a metal SEM stub, and imaging carried out.

However, a number of factors must be taken into consideration when interpreting the images obtained – mostly relating to the preparation of samples for microscopy. For electron microscopy to be carried out, a sample must be dried. This means that, rather than the hydrated sample, a xerogel is in fact being observed. This drying step can have profound effects on the structures of the gel.¹⁹⁵ For example, the loss of solvent, and therefore volume, can lead to aggregation of the nanofibres. This effect can be minimised by freeze-drying the sample, limiting the thermal energy available for network reorganisation, and ensuring that the drying is rapid. However, this method can result in the formation of ice crystals, which can lead to additional distortion of the sample. Where the facilities are available, CryoEM is an excellent method for imaging gels, as the imaging is carried out on a hydrated sample, and the freezing is achieved very rapidly, preventing the formation of larger ice crystals.¹⁹⁶ Use of more than one technique can also help to identify if artefacts are indeed being observed. Additionally, with the high magnification obtained with SEM and TEM, only a very small portion of any sample can be imaged – this may then not be representative of the overall sample. It is important to ensure that representative images are displayed.

Despite these limitations, imaging is still a valuable tool for analysis of gels. The network can be observed, with individual fibres often visible. It can also be useful for multicomponent gels,¹⁷⁷ where the fibres of the different components may be distinct. It can also be useful for comparisons between samples of related gelators, which have been prepared in the same way.

Imaging of MBS-CO₂Me hydrogels indicated that a network had indeed formed, with the fibrous network structure clearly visible. In the TEM image (Figure 78), the helical nature of the fibres can be clearly seen. In the SEM image, the helices are harder to see, but some can nonetheless be observed in the top right-hand corner of the image. The TEM image in particular shows fibres that are relatively homogeneous, with each of the fibres having a diameter of around 8 nm. The SEM image shows the 3D nature of the network.

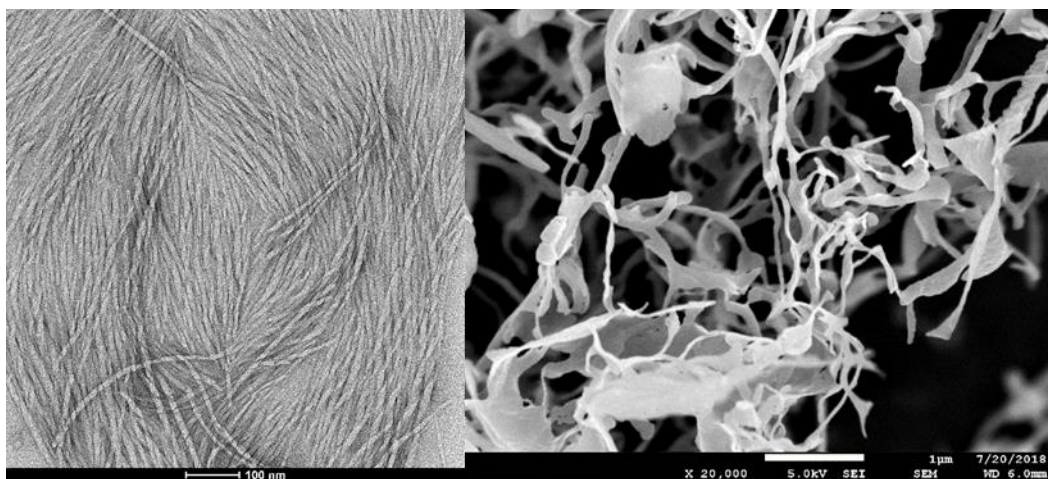


Figure 78. Left: TEM image of the MBS-CO₂Me hydrogel, scale bar 100 nm. Right: SEM image of an MBS-CO₂Me hydrogel, scale bar 1 μm.

Imaging was also carried out for the reformed MBS-CO₂Me hydrogels. These were prepared as normal at a concentration of 0.90% wt/vol. These hydrogels were then heated until solution, and allowed to cool. On cooling, a white, opaque gel was formed. The gels were prepared for imaging as previously.

The resulting images indicated that the network had indeed been reformed, with the TEM image (Figure 79) showing similar helical fibres to those observed for the gels before heating. The fibres have also maintained the fairly homogenous nature previously noted. However, the SEM image shows fibres that are quite distinct from those of the untreated gel – they appear much smoother. This indicates that, although the network is reformed, there are some morphological changes.

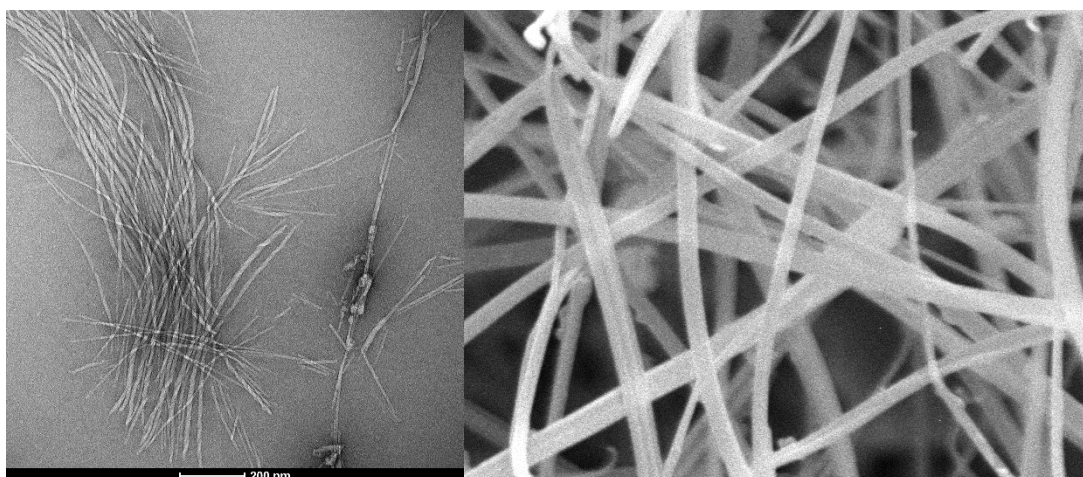


Figure 79. Imaging for the thermally reformed MBS-CO₂Me hydrogels. Left: TEM image, scale bar 200 nm. Right: SEM image, magnification x20,000.

2.2.5 Release From MBS-CO₂Me Hydrogels

Once the MBS-CO₂Me hydrogels had been characterised as described above, their ability to encapsulate and release active pharmaceutical ingredients (APIs) was investigated.

Initially, the stability of the MBS-CO₂Me hydrogels with respect to buffer was investigated – this is an important factor in the rate of release. MBS-CO₂Me hydrogels (1 ml) were prepared at a concentration of 0.85% wt/vol, and 6 ml of buffer placed on top. These were then placed in a 37 °C incubator, and the stability of the gels monitored visually.

Following the addition of the buffer, breakdown of the hydrogels was very rapid, and after two hours, very little gel was still intact (Figure 80). This was reasoned to be due to the relatively high water solubility of the MBS-CO₂Me gelator, as a result of the four alcohol groups – this is believed to be the same reason for the fairly high concentrations required for gelation. Although this rapid breakdown means that any drug incorporated into the gel will likely be released quickly, this can be useful for certain modes of delivery where rapid release of a drug is desirable, such as transdermal delivery.

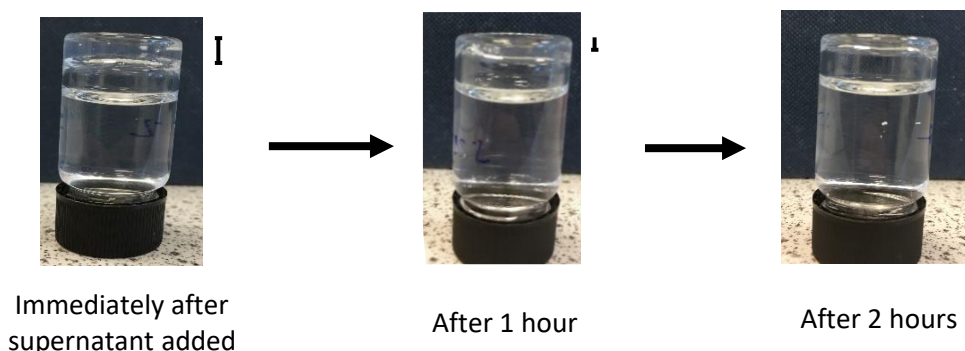
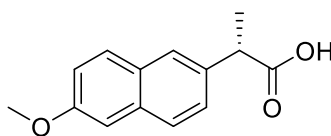


Figure 80. Breakdown of MBS-CO₂Me hydrogels on addition of aqueous media, over two hours.

Previously, naproxen (NPX) (**118**) has been incorporated into DBS-CONHNH₂, and pH-mediated release demonstrated. We wanted to investigate if a similar effect might be observed with the MBS-CO₂Me hydrogels. NPX (Figure 81) is a nonsteroidal anti-inflammatory (NSAID) which gives effective pain relief – however, it is known to give side effects in the upper gastrointestinal tract, including stomach ulcers, with long term use.¹⁹⁷ It is therefore desirable to minimise release in a low pH environment such as the stomach, and give maximum release in higher pH environments, such as the intestine.



118

Figure 81. The structure of naproxen.

MBS-CO₂Me hydrogels with a gelator concentration 0.85% wt/vol and NPX (1 mg) were prepared as described previously, with NPX being added at the same time as the gelator as a mixture of solids. The drug and gelator were therefore present in a 1:6 ratio – this is a lower proportion of API than is ideal, but these hydrogels contain a relatively high loading of gelator, and the incorporation of NPX is limited by its solubility in water. This would also allow for more direct comparison between release from these MBS-CO₂Me hydrogels, and the previously investigated DBS-CONH₂ hydrogels, as this proportion of NPX keeps the total amount loaded into the hydrogel constant. Following the heat cool cycle, translucent hydrogels were formed.

For the release of NPX from the MBS-CO₂Me hydrogels, 6 ml of pH 7 buffer was placed on top of each gel, and the samples placed in an incubator at 37 °C. At each timepoint, aliquots of 2 ml were removed from the gel, and the release of NPX into the buffer quantified by UV-vis, with absorbance being recorded at 329 nm. All drug release studies were carried out in triplicate, and standard error indicated by error bars. The aliquot was then returned to the gel. Although MBS-CO₂Me has significant absorbance in the region of 285 nm, there was enough difference between the two maximum absorbances to allow for accurate quantification of NPX release.

The release of NPX was rapid, with the majority of the drug (ca. 80%) being released within the first two hours (Figure 82). This is as expected – with release being primarily mediated by the erosion of the gel, with this mechanism dominating over diffusion of NPX out of the gel. This is a

significant limitation in achieving controlled slow drug release. However, the rapid release may still be useful, in an application where it is desirable to have drug delivered very rapidly.

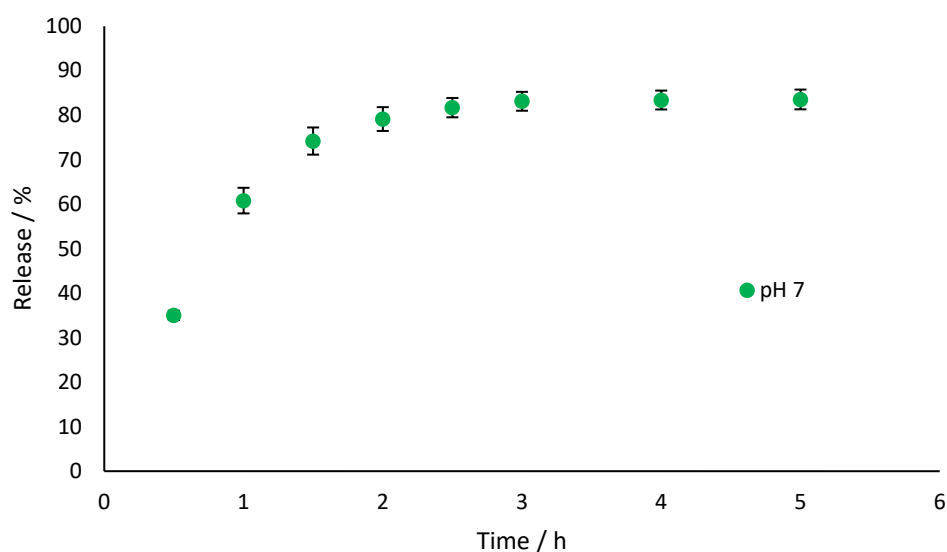


Figure 82. Release of NPX from MBS-CO₂Me hydrogels (1 ml) into pH 7 buffer (6 ml), at 37 °C.

2.3 Development of Hybrid Hydrogels

MBS-CO₂Me has good material strength (see above), however, its potential applications in drug delivery are significantly limited due to the instability of the hydrogels with respect to aqueous media. This is a contrast with DBS-CONHNH₂, which is stable in the presence of aqueous media at a range of pH values, but has poor mechanical strength, making it difficult to handle. The two gelators also give hydrogels with quite different thermal stabilities. The two gelators were therefore combined – hoping that a hybrid material with a desirable mix of properties would be formed. In principle, we reasoned it should be possible to precisely tune the performance of such materials by tuning the ratio of the two different self-assembling components.

2.3.1 Gelation and T_{gel} Testing of Hybrid Hydrogels

Although both MBS-CO₂Me and DBS-CONHNH₂ hydrogels are formed by a heat-cool cycle, the MGCs for each are quite different – 0.20% wt/vol for DBS-CONHNH₂, and 0.75% wt/vol for MBS-CO₂Me. A known mass of each of the two gelators was weighed into a vial. Deionised water was then added, and the suspension sonicated. This was then heated until all of the solid was dissolved, and on cooling, a translucent gel was formed (Table 5).

Table 5. Selected concentrations of DBS-CONH₂ and MBS-CO₂Me tested for gelation in the hybrid hydrogel.

DBS-CONH ₂ / % wt/vol	MBS-CO ₂ Me / % wt/vol	Sonication time / mins	Gel?
0.10	0.33	5	PG
0.28	0.35	5	PG
0.10	0.80	10	G
0.20	0.10	10	G
0.20	0.35	10	G
0.24	0.10	10	G
0.28	0.70	10	G
0.28	0.80	10	G
0.28	0.90	10	G

The total MGC of the hybrid gel was found to be 0.30% wt/vol (DBS-CONH₂ at 0.2% wt/vol and MBS-CO₂Me at 0.10% wt/vol). The hybrid gels could also form with each gelator below their individual MGC (DBS-CONH₂ at 0.16% wt/vol and MBS-CO₂Me at 0.20% wt/vol). In addition, 10 minutes of sonication, before the heat-cool cycle, was found to improve gel formation.

As the two gelators have quite different T_{gel} values, with MBS-CO₂Me hydrogels *ca.* 55 °C, and DBS-CONH₂ hydrogels *ca.* 80 °C, the effects of varying the concentration of each gelator on the thermal stability of the hydrogels was investigated. It was reasoned that those hydrogels with a greater concentration of MBS-CO₂Me would have lower T_{gel} values, with the opposite being true for those gels with a greater concentration of DBS-CONH₂.

Hydrogels with varying proportions of the two gelators (by mass) were prepared, with the total concentration of gelator kept constant at 0.48% wt/vol, and the T_{gel} values for these determined by the tube inversion method (Table 6). For hydrogels, measurements are carried out to 100 °C – above this point, it is not possible to determine whether breakdown of the gel is due to disassociation of the network, or disruption as a result of the solvent boiling.

Table 6. T_{gel} values for hybrid hydrogels, with varying concentrations of the two gelators. For all the gels, total gelator concentration is 0.48% wt/vol. Note: at 65% MBS-CO₂Me, no gel was formed.

% MBS-CO ₂ Me	T_{gel} / °C
26	100+
29	100+
35	100+
40	96
45	81
51	69
56	64
61	51
70	33
75	26

By varying the concentrations of the two gelators, it was possible to access T_{gel} values from 26 °C to 100+ °C demonstrating that materials outcomes can be tuned in these hybrid gels simply by programming the input parameter of gelator loading.

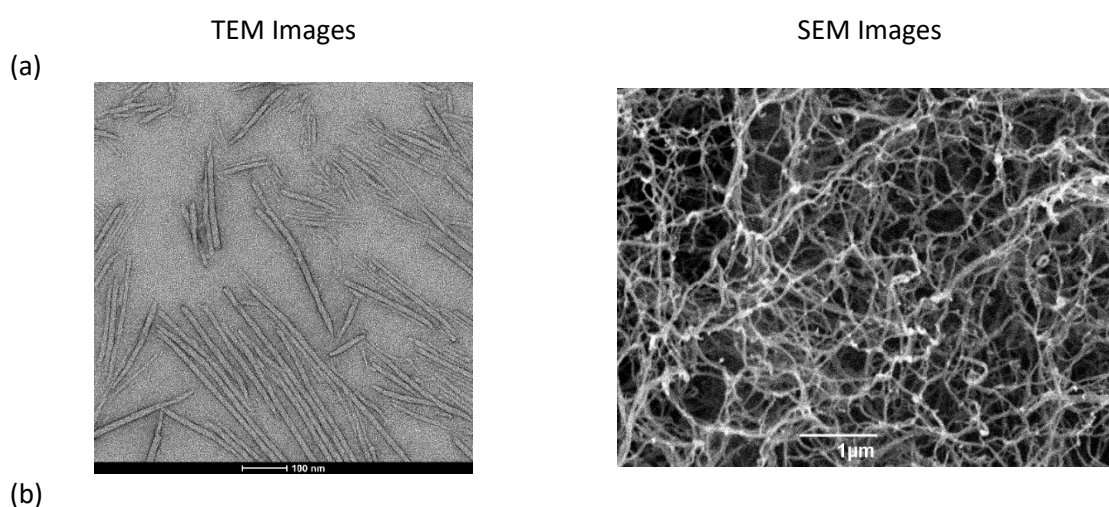
As was expected, the hydrogels with a lower proportion of DBS-CONH₂ gave lower T_{gel} values, with the T_{gel} value increasing in line with DBS-CONH₂ concentration. Further tests in which the total gelator loading was also changed were then carried out (Table 7). – These studies indicated that as well as the T_{gel} being influenced by the proportion of each gelator, the total amount of gelator was also important. As would be expected, a greater total gelator concentration led to higher T_{gel} values.

Table 7. Selected T_{gel} values for hybrid hydrogels, with varying total concentrations, and varying proportions of the two gelators.

% DBS-CONHNH ₂	% MBS-CO ₂ Me	Total Gelator / % wt/vol	T_{gel} / °C
44	56	0.36	49
39	61	0.63	51
69	31	0.35	53
58	42	0.48	63
45	55	0.53	79
80	20	0.51	100+
50	50	0.6	100+

2.3.2 Imaging of Hybrid Hydrogels

The hybrid hydrogels were then investigated by both SEM and TEM. Hybrid hydrogels with varying concentrations of the two gelators were prepared, and prepared for imaging using the same method as described previously. As the nanofibres of the two individual gelators are similar in morphology, it is not possible to distinguish two separate networks (Figure 83). However, the self-assembly process clearly still occurs for the mixed system, with the type of assembly also maintained. The TEM images show relatively homogenous, helical fibres, with the diameter of the fibres varying slightly across the samples. The samples with the lowest total gelator loading had the lowest fibre diameters of around 14 nm, with those samples with the highest fibre loading having the thickest fibres, at around 26 nm.



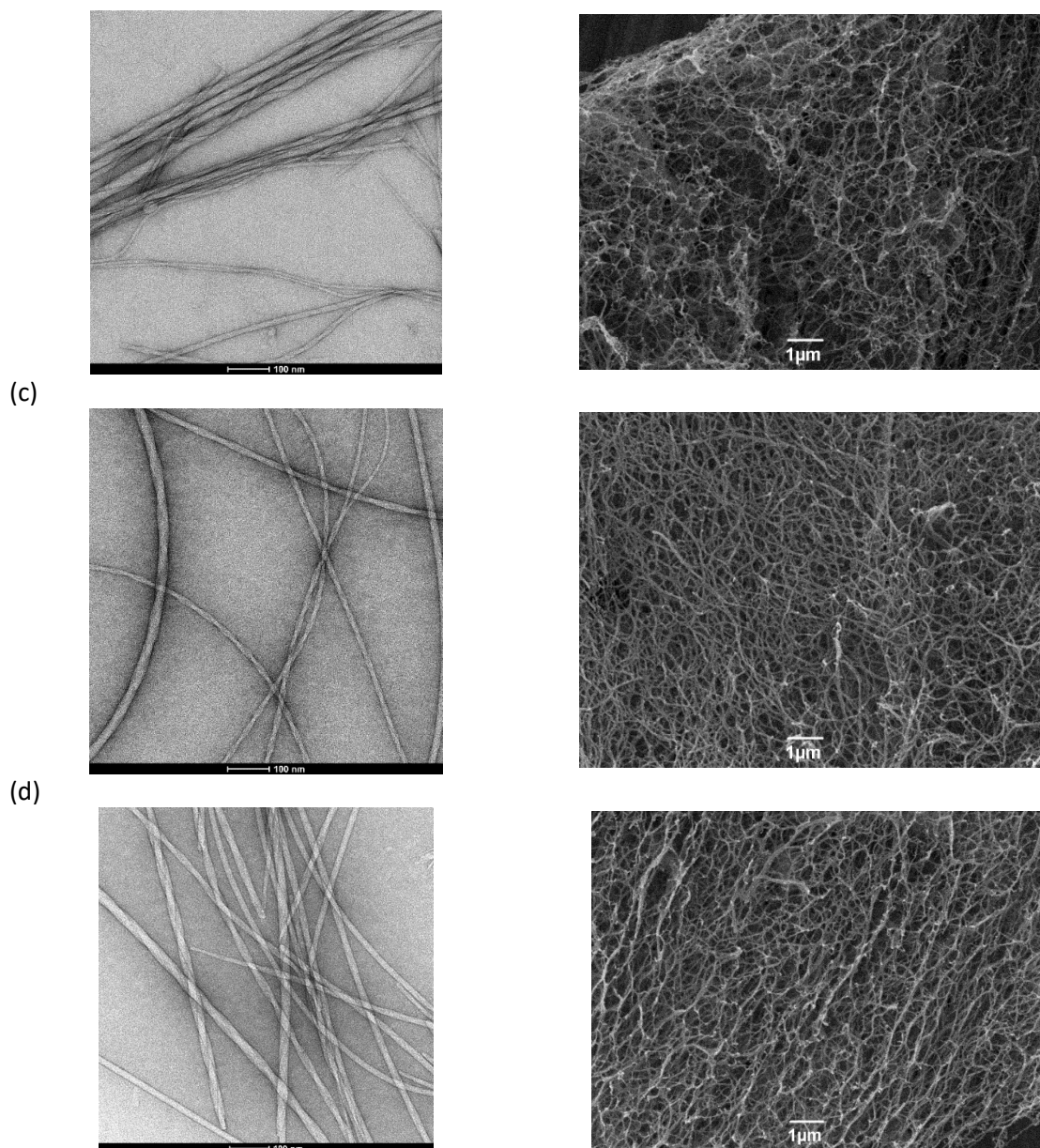


Figure 83. TEM (left) and SEM (right) images of DBS-CONH₂ and MBS-CO₂Me hybrid hydrogels (a) 0.20% wt/vol and 0.10% wt/vol respectively, (b) 0.20% wt/vol and 0.80% wt/vol respectively, (c) 0.28% wt/vol and 0.10% wt/vol respectively, (d) 0.28% wt/vol and 0.80% wt/vol respectively. Scale bar for TEM 100 nm, for SEM 1 μm.

2.3.3 Rheology of Hybrid Gels

The material properties of the hybrid hydrogels were then investigated by rheology. Samples for rheology were prepared in the same manner as previously, with two gelators weighed into a vial together, then heated to dissolve. While the solution was hot, it was transferred to a bottomless vial attached to a plate, and the gel formed in this vial. The vial can then be removed, and the gel disc transferred to the rheometer for analysis.

Initially, the hybrid hydrogels were compared to the gels formed by the two gelators individually. DBS-CONH₂ hydrogels have a G' value of around 1200 Pa in the LVER, with the more robust MBS-CO₂Me hydrogels having a higher G' of around 2800 Pa. It was therefore hoped that the stiffer MBS-CO₂Me would reinforce the weaker DBS-CONH₂. The two hydrogels have very similar resistance to strain, indicated by the similar crossover points of around 10%.

Rheology was carried out on hybrid hydrogels with varying concentrations of MBS-CO₂Me ('high': 0.80% wt/vol, 'low': 0.10% wt/vol) and DBS-CONH₂ ('high': 0.28% wt/vol, 'low': 0.24% wt/vol). As previously, the first test to be run was the amplitude sweep, with the frequency kept constant at 1 Hz, while the strain varied from 0.05%-100%. This allows for determination of the LVR, as well as giving information on the material properties of the gel including stiffness and resistance to strain.

Pleasingly, the hybrid hydrogels with a high proportion of MBS-CO₂Me were indeed stiffer than either of the two individual hydrogels, with G' values of over 6000 Pa (Figure 84). This is a considerable increase in stiffness, and indicates that, at this concentration, the MBS-CO₂Me is indeed acting to reinforce the overall network. The total gelator concentration is also greater, and this likely also contributes to the increased gel stiffness. This increased stiffness does come at the cost of reduced resistance to strain – with both these hybrid gels having a crossover point of *ca.* 3%. This is lower than either of the two individual gelators. Particularly for the gel with the greatest overall loading, there was considerable variability between the individual samples. This is believed to be due to the reduced resistance to strain causing some of the gel discs to fracture, leading to variability in stiffness.

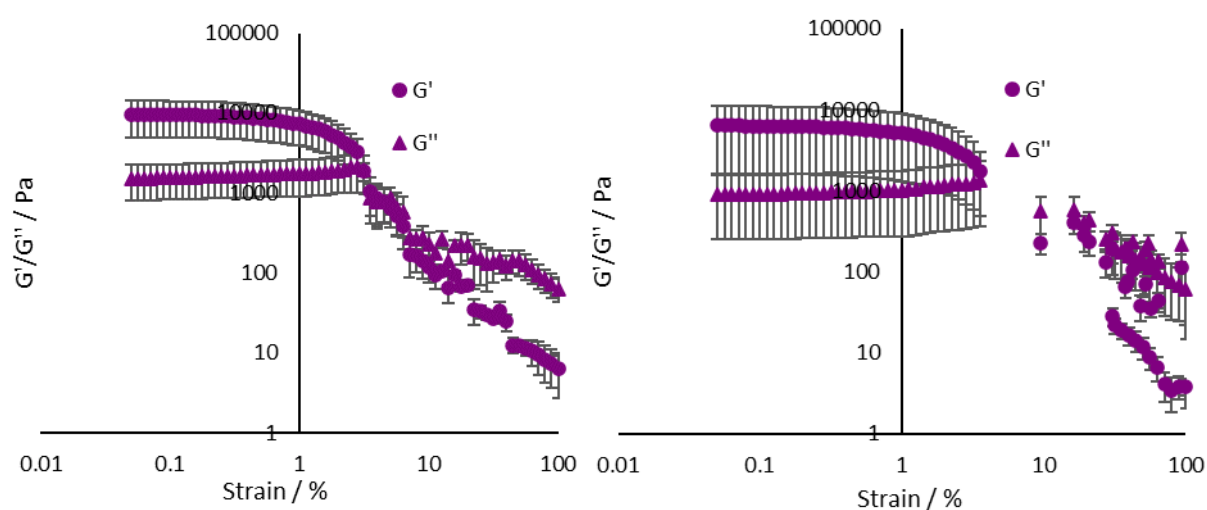


Figure 84. Amplitude sweep (0.05%-100%) for hybrid hydrogels. Left: 'high' MBS-CO₂Me, 'low' DBS-CONH₂. Right: 'high' MBS-CO₂Me, 'high' DBS-CONH₂. Temperature 25 °C, Frequency 1 Hz.

However, in contrast to this increased stiffness, the hybrid gels with the lower concentrations of MBS-CO₂Me had lower stiffness than the hydrogels formed by the gelators alone, with G' values of under 400 Pa (Figure 85). In this case, the loading of MBS-CO₂Me is below the MGC for that gelator, at only 0.10% wt/vol. It is therefore possible that the MBS-CO₂Me is not assembling fully, and so instead of reinforcing the DBS-CONH₂ network, may actually disrupt this network, resulting in the decrease in stiffness.

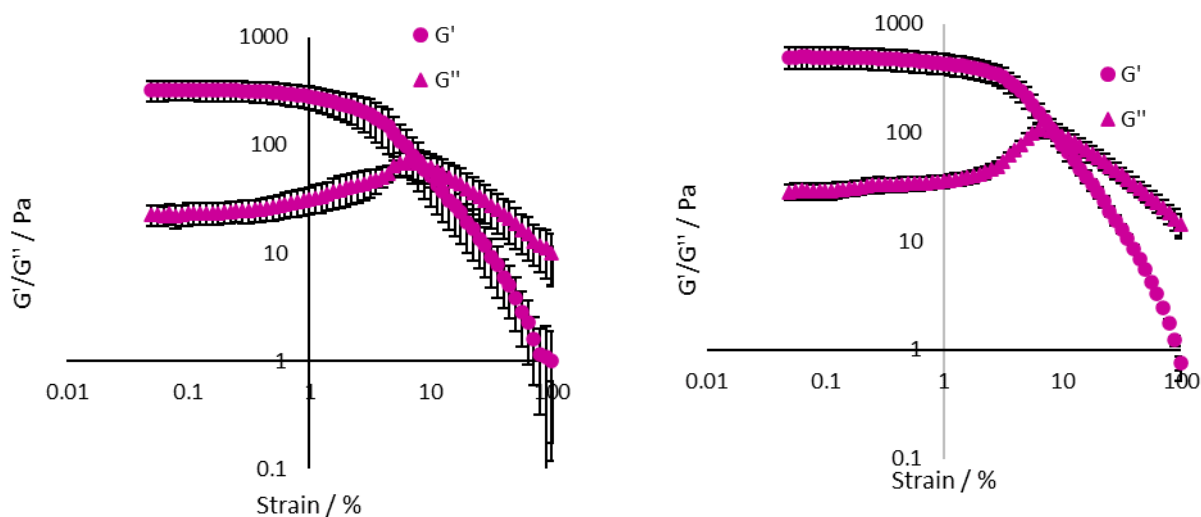


Figure 85. Amplitude sweep (0.05%-100%) for hybrid hydrogels. Left: 'low' MBS-CO₂Me, 'low' DBS-CONH₂. Right: 'low' MBS-CO₂Me, 'high' DBS-CONH₂. Temperature 25 °C, Frequency 1 Hz.

It is therefore possible to tune the material properties of the hybrid hydrogels, by varying the concentration of the two gelators, principally MBS-CO₂Me. This can provide a material that is stiffer than the individual hydrogels, or one that is less stiff than either (Figure 86). This approach could allow for the tuning of the material so the desired rheological properties can be obtained, depending on the targeted application.

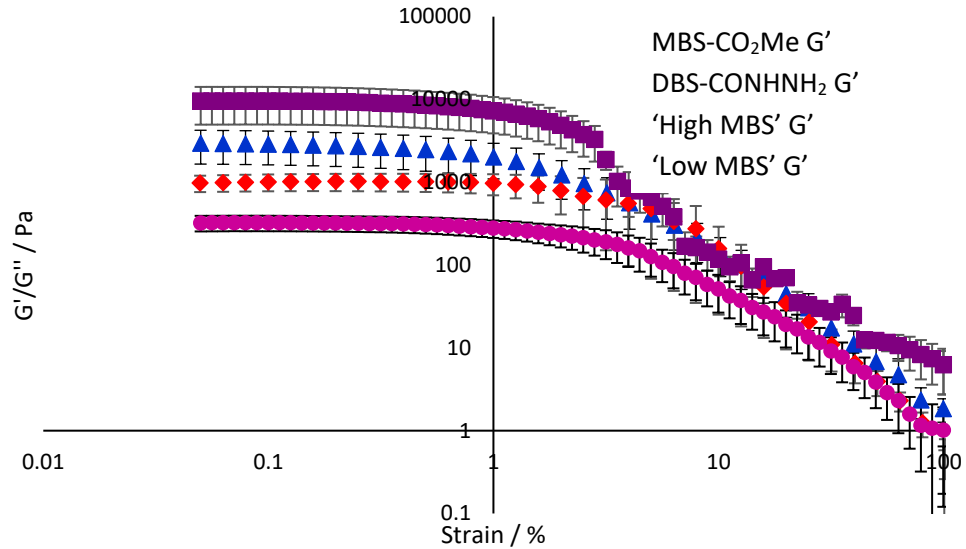


Figure 86. Amplitude sweeps (0.05%-100%) for MBS-CO₂Me hydrogel, DBS-CONH₂ hydrogels, hybrid hydrogels with 'low' MBS-CO₂Me (0.10% wt/vol), 'low' DBS-CONH₂ (0.24% wt/vol), and 'high' MBS-CO₂Me (0.80% wt/vol), 'low' DBS-CONH₂ (0.24% wt/vol). Temperature 25 °C, frequency 1 Hz.

Although it was clear that the mechanical properties of the hybrid hydrogels could be controlled by varying the two components, initially, both the proportions of the two gelators, and the total gelator loading were changed. These results did indicate that with a greater proportion of MBS-CO₂Me, which alone forms stiffer gels, the hybrid hydrogels were stiffer. However, increasing the proportion of MBS-CO₂Me also resulted in a greater total loading of gelator. Therefore, further rheological studies were carried out, with total gelator loading (by mass) kept constant, and only the proportions of the two gelators changed.

Hybrid hydrogels were therefore prepared, with a total concentration of 0.48% wt/vol. These were made up of either 3.0% DBS-CONH₂ and 3.4% MBS-CO₂Me, or 2.4% DBS-CONH₂ and 2.4% MBS-CO₂Me. The gels were prepared as for previous rheology samples. Again, an amplitude sweep was carried out initially (Figure 87), with strain varied from 0.01%-100%, and frequency kept constant at 1 Hz. This allowed the LVR to be determined, and a frequency sweep was then carried out, at a strain within this region.

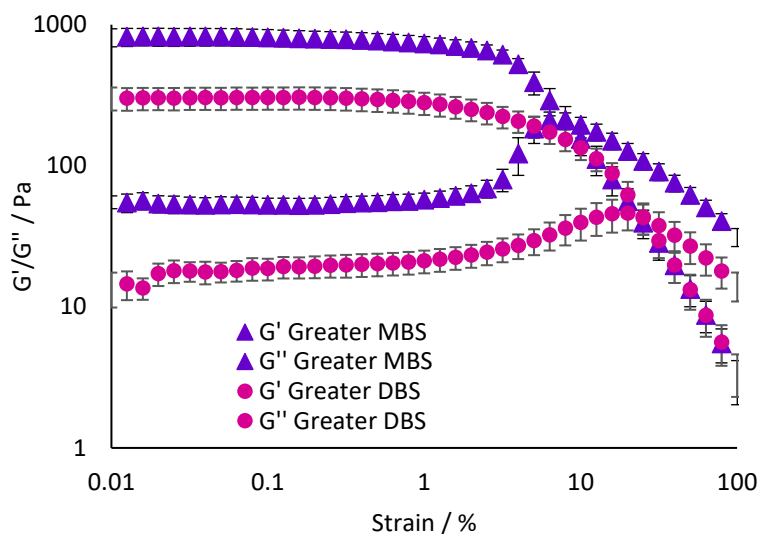


Figure 87. Amplitude sweep (0.01%-100%) for MBS CO₂Me and DBS CONH₂ hybrid hydrogels, with a total gelator loading of 0.48% wt/vol, in different proportions of the two gelators. Temperature 25 °C, frequency 1 Hz.

Despite the total loading of gelator being the same for both the hydrogels, as hoped, the hydrogels with the higher proportion of MBS-CO₂Me were stiffer than those with the higher proportion of DBS-CONH₂. The higher proportion of MBS-CO₂Me gave a G' in the LVR of around 820 Pa. This is greater than the G' of around 300 Pa for the hydrogels with the greater proportion of DBS-CONH₂. This indicates that the simply varying the proportions of the two gelators can give control of the mechanical properties, as well as changes in the total loading.

2.3.4 NMR Studies for Hybrid Hydrogels

The immobilisation of the gelators within the hybrid gel was then investigated via NMR studies. These initially aimed to understand the level of assembly of MBS-CO₂Me within the hybrid gel when concentrations of this gelator were below the MGC (0.75% wt/vol).

Hybrid hydrogels (0.10% wt/vol MBS-CO₂Me and 0.28% wt/vol DBS-CONH₂) were prepared in an NMR tube, using a 50:50 mix of D₂O and H₂O. Interestingly, the solubility of MBS-CO₂Me was considerably reduced when using D₂O alone. Although replacing H₂O with D₂O has been shown to impact the solubility of a range of molecules, including cyclodextrins,¹⁹⁸ lysozymes,¹⁹⁹ amino acids,²⁰⁰ and carbohydrates,²⁰¹ the reasons behind this are not yet fully understood.²⁰² These gels were prepared as normal, with the addition of DMSO (2 μl) as an internal standard, until the heat-cool cycle. At this point, the hot solution was transferred to a warm NMR tube, and then allowed to cool *in situ*, forming the gel.

The amount of 'free' gelator can then be determined by standard ^1H NMR, as any that is incorporated into the solid-like network will not be visible in the NMR spectrum, due to broadening of the peaks. Any gelator is not incorporated into the self-assembled network and is instead 'mobile' in the liquid-like phase, however, will be visible, and the concentration can be determined by comparison to the internal standard.²⁰³

These studies indicate that, on average, 64% of MBS-CO₂Me is not incorporated within the network at this concentration, although there is significant variation of 11% across the samples. This suggests that, although some MBS-CO₂Me is assembling, perhaps along with the DBS-CONH₂ that is also present, this is not occurring reliably, and so this assembly will not routinely contribute to the overall hybrid gel.

On increasing the concentration of MBS-CO₂Me to 0.28% wt/vol and 0.48% wt/vol, there was a decrease in the proportion of 'free' MBS-CO₂Me, to 48% \pm 14 and 15% \pm 4 respectively. This indicates that as the concentration of MBS-CO₂Me is increased, a greater degree of self-assembly into the solid-like phase can occur. At the slightly lower concentration of 0.28% wt/vol, there is again quite significant variation in the proportion of assembled MBS-CO₂Me – with the concentration being below the MGC for this gelator, it possible that assembly into supramolecular structures may occur differently from sample to sample, dependent on factors such as nucleation events.

The effect of temperature on the disassembly of the network was then investigated in order to gain insight into whether in the fully-formed hybrid hydrogels, the two gel networks were independently self-sorted, or whether the two gelators were incorporated into mixed fibres. Hybrid hydrogels (0.80% wt/vol MBS-CO₂Me, 0.22% wt/vol DBS-CONH₂) were prepared as previously. At these concentrations, neither gelator is visible in the spectrum at room temperature, indicating that all of the gelator has assembled into the solid-like network. As the temperature is increased, MBS-CO₂Me signals become visible at 40 °C, and by 65 °C, around 90% is free (Figure 88). This is in agreement with the T_{gel} of MBS-CO₂Me, and results from the relatively high solubility of this gelator. In contrast, the first signal corresponding to free DBS-CONH₂ only appears at 55 °C, with 90% being mobile at 85 °C. This reflects the higher T_{gel} value of this LMWG. Although the first of the DBS-CONH₂ begins to disassemble at 55 °C, before the MBS-CO₂Me is completely disassembled, the overall disassembly occurs in a largely sequential manner, indicating that there is good degree of self-sorting of the two networks, with each gel network having its own clear thermal sensitivity retained within the hybrid gel.

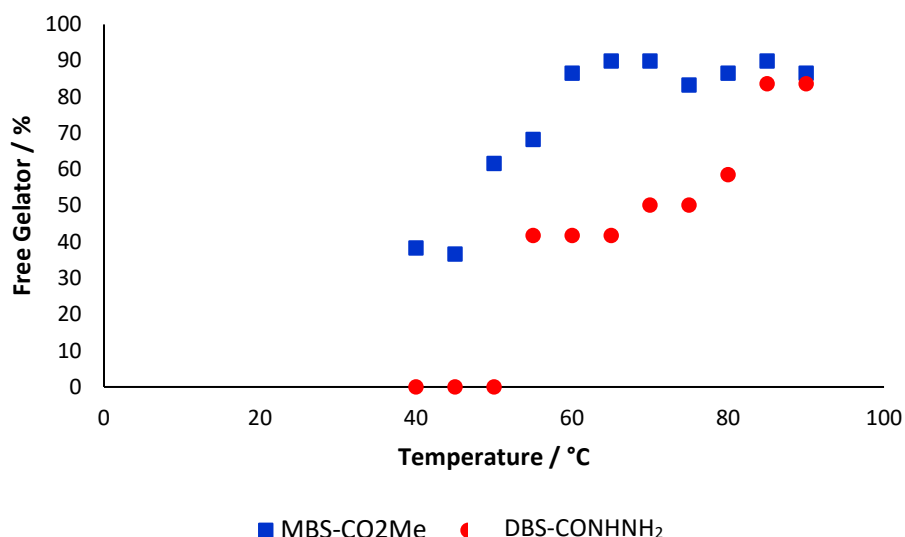


Figure 88. The breakdown of the hybrid hydrogel with increasing temperature, monitored by ¹H NMR spectroscopy.

2.3.5 Drug Release from Hybrid Hydrogels

2.3.5.1 Naproxen

Given that DBS-CONH₂ can give pH-mediated release of naproxen,¹⁰⁹ as a result of the interactions between the functional groups of the gelator and the drug, studies were carried out to determine whether this ability had been maintained in the presence of MBS-CO₂Me.

Hybrid hydrogels containing NPX were prepared by addition of the three solids (the two gelators and the drug) to a vial, with deionised water (1 ml) added, followed by 10 minutes sonication. The resulting suspension was then heated until the solid was dissolved. On cooling, a white, opaque gel was formed.

To monitor release of NPX, buffers of different pH values were added to the gels, and amount of NPX released quantified by monitoring the UV-vis absorbance at 329 nm. Pleasingly, the hybrid hydrogels showed pH mediated release of NPX (Figure 89), indicating that the responsive nature of the DBS-CONH₂ network had been maintained. At pH 7, there is rapid initial release of NPX, with over 65% released with the first three hours, and maximum release of 90% after seven hours. In contrast, at pH 5.5, there is much slower release – after three hours, only around 30% has been released, and total release is under 50% even in seven hours.

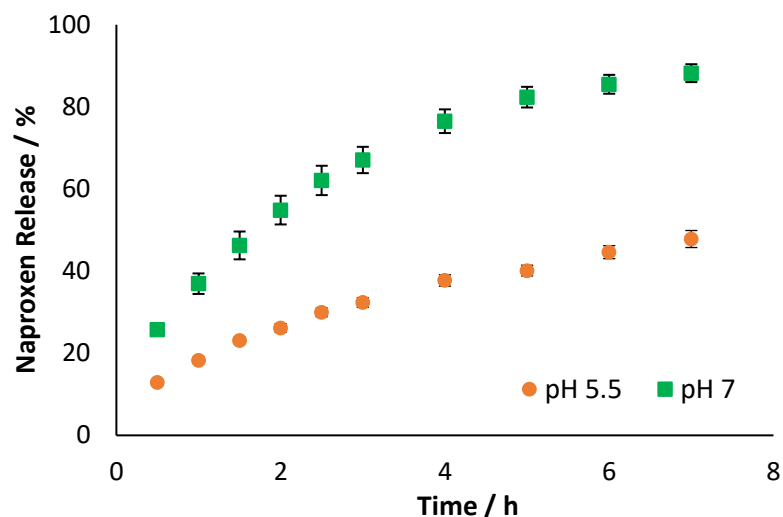


Figure 89. Release of NPX from DBS-CONHNH₂ and MBS-CO₂Me hybrid hydrogels (1 ml), into pH 7 buffer (6 ml) or pH 5.5 buffer (6 ml), at 37 °C.

This difference in release at the two different pH values is a result of the interactions between the acyl hydrazide groups of the gelator, and the carboxylic acid groups of NPX – these occur when NPX is protonated (Figure 90). At a lower pH, NPX, which has a pK_a of 4.15,²⁰⁴ is protonated to a greater degree, and hence there is increased interaction between drug and gelator. This in turn leads to lower release. NPX is also less soluble at lower pH values, and this is also likely to contribute to lower release at pH 5. The release from the hybrid hydrogel is very similar to that previously observed with DBS-CONHNH₂ alone, and is clearly distinct from the rapid, erosion driven release from MBS-CO₂Me hydrogels. It is therefore clear that DBS-CONHNH₂ can exert control over drug release in the hybrid hydrogel.

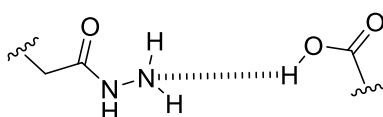


Figure 90. The hydrogen bonding interaction between the hydrazide groups of the gelator and the carboxylic acid group of NPX.

2.3.5.2 Atorvastatin

Although it is useful to be able to release NSAIDs such as NPX in a pH mediated manner, the required oral dose for a therapeutic effect of such a drug is typically at least 250 mg – this is much more than could be practically incorporated in dispersed form in a 1 ml gel, and far exceeds the molar equivalence of any low-molecular-weight gelator. Given drug-gelator interactions help to mediate the release, this is a significant limitation. Therefore, having demonstrated proof of principle with naproxen, we moved on to investigate another more potent class of drug for their potential to be incorporated within the gels.

Statins are prescribed to lower cholesterol, and are among the most commonly prescribed classes of drugs in the UK.²⁰⁵ Typically, initial doses are 5-10 mg – much more relevant for gel delivery on this scale. Furthermore, as daily drugs that are taken for extended periods of time, potentially for life, controlled delivery of this class of pharmaceutical is of high potential value.²⁰⁶ A number of statins contain a carboxylic acid functional groups – these in particular have the potential to directly interact with the hydrazide groups of the gelator, as is the case with naproxen, opening the possibility of controlled release. In the longer term, subcutaneous injection of gel depot formulations containing statin drugs could potentially be an effective way of moving away from daily tablet dosing.²⁰⁷

Atorvastatin (**119**) (Figure 91), was selected for incorporation into the hybrid hydrogels. Atorvastatin is a commonly prescribed statin, administered as the calcium salt. Due to poor water solubility and extensive first pass metabolism, the bioavailability is low, at around 14%. Despite this, the typical therapeutic range for treatment with atorvastatin is 10-80 mg.²⁰⁸

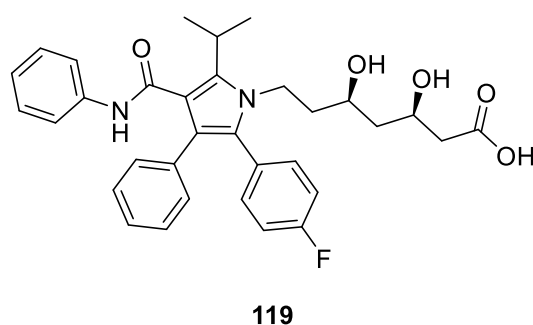


Figure 91. The structure of atorvastatin, a commonly prescribed statin.

Initially, the incorporation of atorvastatin within the hybrid hydrogels was investigated. The atorvastatin was added as a solid, along with the two gelators (MBS-CO₂Me at 0.80% wt/vol, DBS-CONHNH₂ at 0.30% wt/vol). To improve the solubility of atorvastatin, 10% DMSO in water was used as a co-solvent – despite this, only 0.4 mg of statin could be added and fully dissolved. These samples were then prepared as previously – 10 minutes sonication, followed by a heat/cool cycle. On cooling, translucent gels were formed. The requirement for full dissolution of statin within the gel may not ultimately be important. However, for these preliminary studies, we wanted to ensure we were working with homogeneous materials.

The release of atorvastatin from the hybrid gels was then investigated. Buffer was placed on top of the prepared gels, and the release of the drug followed by monitoring the UV-vis signal at 253 nm. However, due to the low solubility of atorvastatin, along with the low concentrations actually present, it proved very challenging to quantify the release into the buffer – with very low

UV absorbances that varied considerably. This therefore resulted in very poor release profiles (Figure 92).

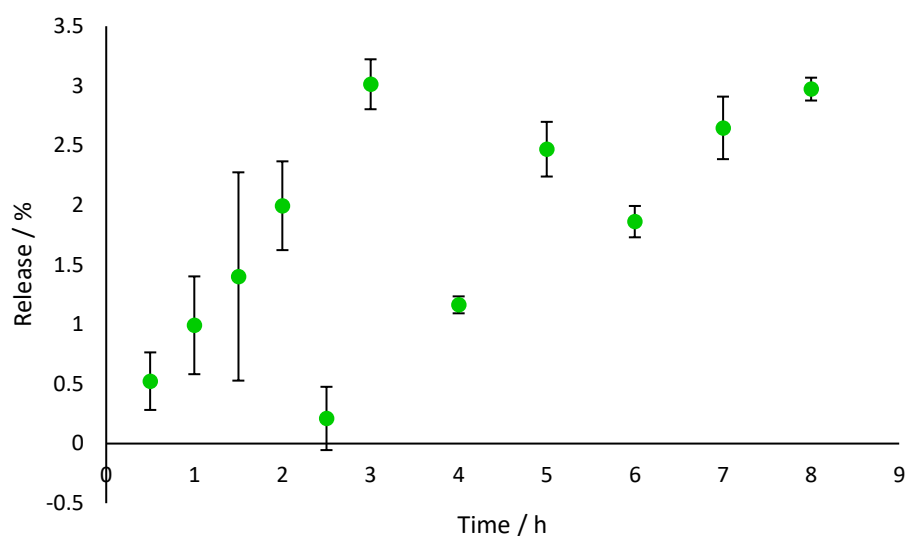


Figure 92. Release of atorvastatin from hybrid hydrogels (1 ml), into pH 7 buffer (6 ml) at 37 °C, quantified by UV-vis.

It was therefore decided to use an alternative method for quantification of atorvastatin release – HPLC. This is a commonly used method for quantification of statins. Initially, an HPLC method was developed to ensure separation of atorvastatin and the other components that might be present in the samples – MBS-CO₂Me and DBS-CONH₂. This was achieved by dissolving, as much as possible, the components in methanol (in which atorvastatin is freely soluble, but the two gelators are not). This was followed by filtration, to remove any undissolved solid. The three components were prepared separately, along with a mixed sample. It was determined that the solvent system 45% acetonitrile, 55% pH 4 buffer (0.01 M), with a C18 column, gave separation of the three components (Figure 93).

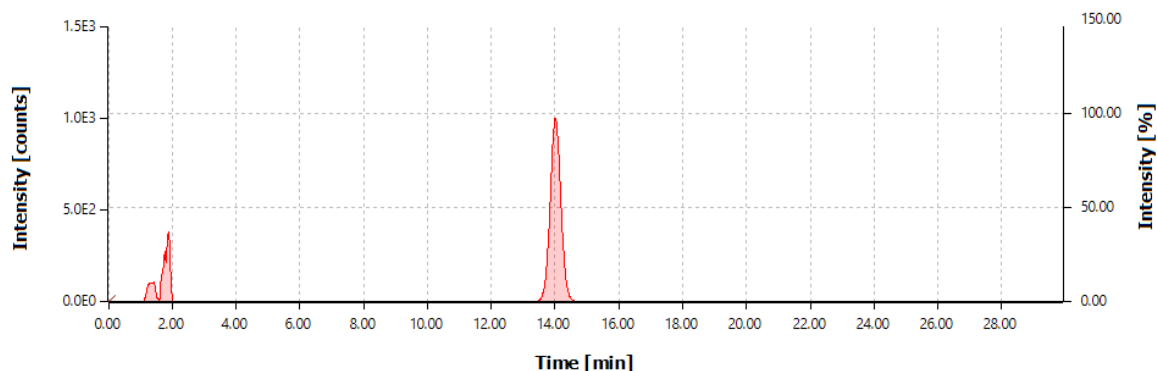


Figure 93. HPLC trace for a mixed sample of atorvastatin, DBS-CONH₂, and MBS-CO₂Me. The two gelators appear before 2 minutes, the atorvastatin at 14 minutes.

This HPLC approach allowed a calibration curve to be prepared for atorvastatin, by preparation of samples of known amounts of atorvastatin, dissolved in methanol. These were then run using the above method, and the peak areas measured. This could then be used to quantify the release of atorvastatin from the gels.

The release of atorvastatin into pH 7 buffer was then investigated. Hybrid gels (MBS-CO₂Me at 0.80% wt/vol, DBS-CONH₂ at 0.28% wt/vol) were prepared, with atorvastatin (5 mg) also added as a solid. These samples were then sonicated for 10 minutes, followed by a heat-cool cycle. On heating in this case, not all of the atorvastatin was dissolved, but homogeneous opaque, white gels were still successfully formed. This was confirmed by parallel plate rheology (Figure 94), with a G' value in the LVR at around 11200 Pa. This is slightly higher than for the hybrid gels without atorvastatin, however, the hydrogels containing 5 mg of atorvastatin do also have a slightly higher loading of gelator.

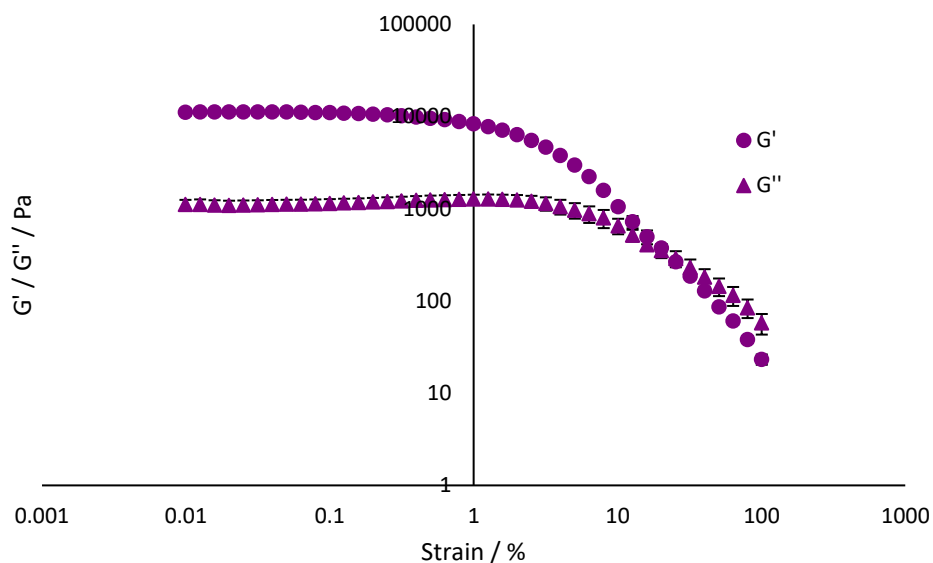


Figure 94. Amplitude sweep (0.01%-100%) for hybrid hydrogels containing 5 mg of atorvastatin. Temperature 25 °C, frequency 1 Hz.

The release was then investigated. On top of each gel was placed pH 7 phosphate buffer (6 ml), and the samples stored in an incubator at 37 °C. At each timepoint (hourly for the first 8 h, every 24 h thereafter), 1 ml of buffer was removed from the gel. This was then replaced with fresh buffer. The removed aliquot was dried, and the residue re-dissolved in methanol. This was then filtered to give the sample for HPLC. The release was followed for 240 hours.

Over the first eight hours, around 40% release was obtained, with 75% release reached after 240 hours (Figure 95). While it is possible that there are some interactions between the drug and the gelators, it seems likely that the slow release here is predominantly limited by the low water solubility of atorvastatin. The replacement of the buffer allows for a concentration gradient to be

maintained. This seems especially likely after the first 24 hours, where the longer intervals allow for the buffer to become completely saturated.

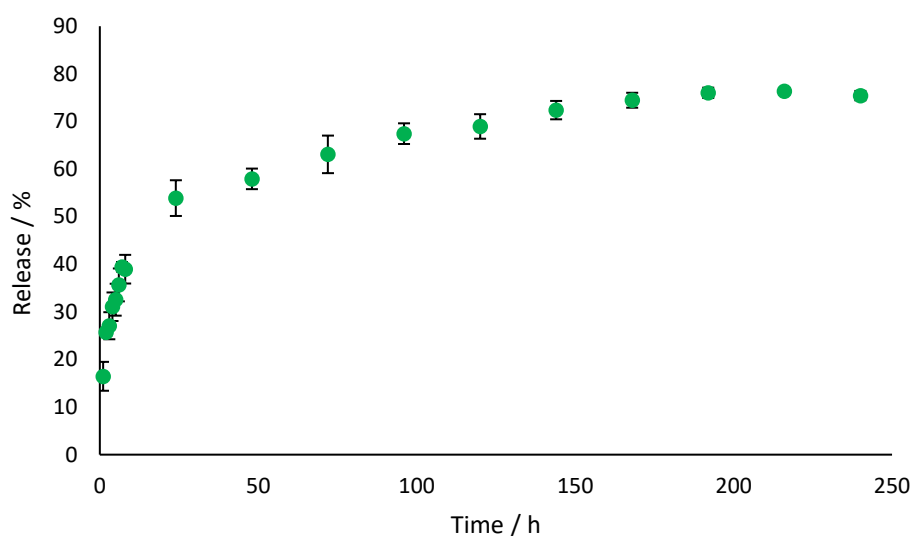


Figure 95. Release of atorvastatin from hybrid hydrogels (1 ml), into pH 7 buffer (6 ml, 1 ml replaced at each timepoint) at 37 °C, over 240 hours, quantified by HPLC.

In a biological system, due to the constant maintenance of such concentration gradients, release would likely be faster than demonstrated here. Additional work with this drug could focus on changes in release rate with the buffer replaced more regularly, as this may give faster release, as well as greater total release. The rate of release could also be investigated at a greater range of pH values.

2.4 Conclusions

Initially, a novel hydrogelator, MBS-CO₂Me, was developed, and the material properties of the resulting hydrogels investigated. The hydrogel was also investigated for the encapsulation and release of naproxen, and gave rapid, burst release.

As the properties of MBS-CO₂Me hydrogels, including mechanical strength and thermal stability, were quite distinct from those of the previously investigated DBS-CONH₂, the two gelators were combined to form a two-component supramolecular hydrogel. The resulting hybrid hydrogels had properties that could be tuned, by varying the proportions of the two gelators – with those with more MBS-CO₂Me giving hydrogels with improved mechanical strength, while those with more DBS-CONH₂ had greater thermal stability.

The hybrid gels also retained the ability of DBS-CONH₂ to interact with additives, and demonstrated pH responsive release of NPX, similar to that observed with DBS-CONH₂ alone.

Additionally, the hybrid gels could be used to encapsulate the statin atorvastatin, and demonstrated release of this over an extended length of time.

Further work in this area would focus on tuning the hybrid gels to give different release profiles, potentially enabling application in a range of drug delivery settings, including the investigation of additional statins. The two component gels could also be investigated for use in wider applications of biomedical science, such as tissue engineering. The release of statins from other types of gel, that may be suitable for use in different routes of administration, could also be investigated.

3. Chapter 3 – Development of Gel Beads for Statin Release

It has become increasingly common to combine LMWGs with PGs.¹⁶⁸ This approach is intended to combine the most desirable features of the two types of gelator – usually the responsiveness of the LMWG, and the mechanical strength of the PG. These combinations typically give materials that are more suitable for real-life applications.

Although DBS-CONHNH₂ has properties that give it potential for a number of applications, the gels that it forms have relatively low mechanical strength. This makes their general handling very challenging, and thus limits practical applications. Therefore, in recent years DBS-CONHNH₂ has been combined with a number of polymer gelators. Initially, studies focussed on poly(ethyleneglycol dimethacrylate) (PEGDM) (**120**) and agarose (**98**) (Figure 96). These two polymers have differing triggers for gelation – PEGDM being photoinitiated in the presence of a radical initiator, and agarose being triggered by heating and cooling.

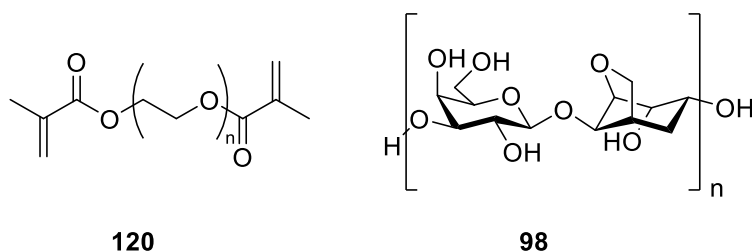


Figure 96. The structures of the polymer gelators, PEGDM (left) and agarose (right) that have previously been combined with DBS-CONHNH₂.

On combination of the LMWG and the PG, it is important that the desirable properties of the LMWG are maintained. This was the case for DBS-CONHNH₂ and PEGDM, with pH-mediated release of NPX being achieved both with and without PEGDM present.¹⁷⁴ The presence of PEGDM also allows for photopatterning of the gel into desired shapes – this has allowed development of shaped ‘gel reactors’, which in combination with enzymes, can be used in catalysis.¹⁷⁶ Similarly, on combination with agarose, DBS-CONHNH₂ was still capable of forming metal nanoparticles, which then allows the catalysis of cross-coupling reactions.¹⁷² Additionally, combining DBS-CONHNH₂ and agarose to form a hybrid hydrogel in which the complementary properties of the two gelators combined was shown to improve cell growth during cell culture compared to the PG alone, with the DBS-CONHNH₂ acting to provide more effective cell adhesion points within the hybrid gel.¹⁷³

More recently, DBS-CONH₂ has also been combined with the PG alginate (**121**) (Figure 97). This is a natural biopolymer, and forms hydrogels as a result of ionic crosslinks formed when it is exposed to calcium ions. As alginate is bioderived (from brown algae), biocompatible and biodegradable,²⁰⁹ it is an attractive option for combination with LMWGs to form hybrid systems.

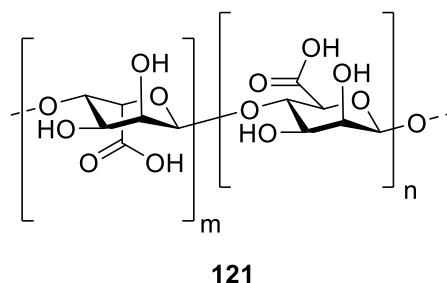


Figure 97. Alginate, a natural biopolymer that can be combined with DBS-CONH₂.

Another interesting feature of calcium alginate hydrogels is the rapid gelation that occurs on addition of the alginate solution to calcium chloride solution. As gelation occurs so rapidly, if the alginate is added dropwise, gel beads can be formed.²¹⁰ This is well known within the food industry,²¹¹ as well as in the pharmaceutical industry.²¹² Additionally, beads with a 'core-shell' structure can be prepared, with a second component forming the inner 'core' and being surrounded by a 'shell' of the calcium alginate gel. In such cases, the core component is generally a second polymer.²¹³

Recently, in work carried out by Dr Carmen Piras, our research group reported the development of gel beads formed from alginate, with a core of self-assembled DBS-CONH₂.²¹⁴ These beads had diameters of 3.0-3.6 mm. The size of the beads could also be controlled by varying the volume used for their formation – with beads as small as 0.75 mm obtained. In this case, the purpose of the calcium alginate is to act as a template mould, to control the assembly of the LMWG into beads – this is not possible with the LMWG alone, as the materials do not have the required mechanical strength to form discrete self-supporting spheres. As a result of the different gelation triggers for alginate and DBS-CONH₂, it was also possible to control the spatial organisation of the networks, through changing the points at which stimuli were applied. In this way, both interpenetrating and core-shell arrangements of the two gel networks within the beads could be achieved (Figure 98).

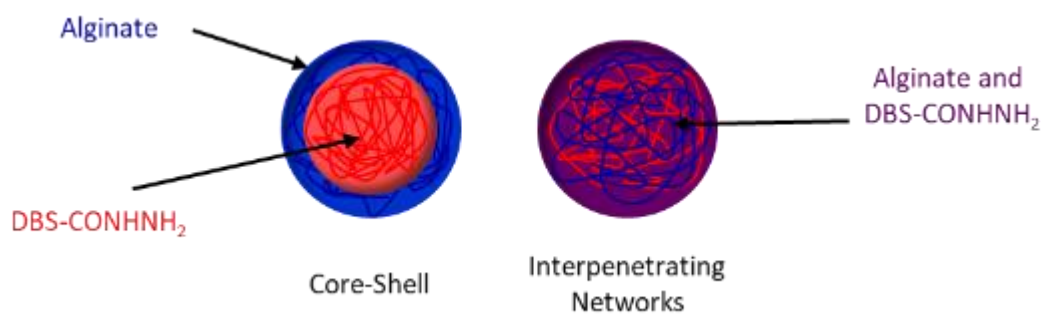


Figure 98. A representation of the two types of network that can be formed in the alginate/DBS-CONH₂ hybrid beads, depending on the order in which the stimuli for gel formation are applied.

Following the initial development of the gel beads, they were tested to confirm that the desirable properties of DBS-CONH₂ had been maintained in the presence of alginate. The formation of palladium nanoparticles, previously demonstrated for DBS-CONH₂ hydrogels, was therefore investigated with the newly developed beads. It was found that, on addition of PdCl₂ solution, the hybrid alginate and DBS-CONH₂ hydrogels were indeed capable of forming Pd nanoparticles *in situ*. The beads were then used to catalyse a Suzuki-Miyaura cross-coupling reaction, and demonstrated good catalytic ability. The hybrid gel beads have now also been used for the *in situ* formation of silver nanoparticles – these beads demonstrated antimicrobial activity against drug resistant bacteria.³¹

Following development of these relatively large hybrid gel beads, attention was turned to reducing their size. Recently, both nanobeads and microbeads have been of increasing interest in biomedical applications.²¹⁵ This is a result of their having the general properties of hydrogels – high water content and generally good biocompatibility, combined with a high surface area, as a result of the small size. This leads to fast responses to environmental conditions, as well as diffusion being able to take place rapidly.²¹⁶ They are therefore valuable as carriers for a range of biologically-relevant molecules. Hybrid gel beads of DBS-CONH₂ and alginate, with a diameter of ca. 800 nm were therefore developed using a suspension approach in the presence of a stabilising surfactant.²¹⁷

Having determined that the microbeads were stable in solution over a period of many months, as well as on injection through a syringe needle, the microbeads were then tested for biomedical applications. They were successfully loaded with heparin, an anti-coagulant that is also used in cell culture, as it is capable of improving cell proliferation and growth.²¹⁸ The release of heparin from the microbeads was demonstrated first by simply monitoring the release into buffer. This indicated that around 41% of the heparin was released from the microbeads. This was followed

by investigating the effects of this release of heparin on the proliferation of cells. This found that the presence of heparin led to greater levels of cell proliferation than occurred with no heparin present.

Following on from earlier work in this thesis working with statin drugs, we reasoned that gel beads may be an appropriate platform for encapsulation and delivery of such drugs. We therefore targeted a range of self-assembled gel beads in order to determine their relative abilities to achieve controlled release of statins.

This was undertaken as collaborative work. Dr Carmen Piras developed and characterised the novel gel beads, and prepared all the gel samples used. The drug release studies were carried out by myself. For the purposes of this initial study, we targeted the formation of the larger millimetre-sized hybrid gel beads because of their ease of handling and study.

3.1 Development of DBS-CONHNH₂ and Alginate Gel Beads

As mentioned previously, hybrid gel beads composed of the LMWG DBS-CONHNH₂, and the PG alginate have been developed by Dr Carmen Piras. Through changing the order in which the gelation stimuli are applied, it is possible to control the structure of the beads – forming either an interpenetrating network, or a core-shell structure.

Initially, gels were formed in vials, to demonstrate control over forming the two separate networks and to gain a detailed understanding of the orthogonal assembly of the two networks. In the first method, a suspension of DBS-CONHNH₂ (0.3 wt/vol), in alginate solution (0.5% wt/vol), was heated, dissolving all of the LMWG. On cooling, the DBS-CONHNH₂ network is formed. A solution of CaCl₂ was then added, and allowed to diffuse into the gel. This triggers the formation of the second gel network, as the alginate is crosslinked.

Following this, hybrid gel beads with a core-shell structure were fabricated. This was achieved by heating a suspension of DBS-CONHNH₂ (0.3% wt/vol), with alginate (0.5% wt/vol), until all of the LMWG was dissolved. At this point, instead of simply allowing the solution to cool, the hot solution was added dropwise to CaCl₂ solution. This leads to the alginate being crosslinked immediately. Simultaneously there is rapid cooling of the solution, and hence formation of the DBS-CONHNH₂ network. This leads to the formation of the core-shell beads, with DBS-CONHNH₂ forming the core, and calcium alginate the outer core (Figure 99).

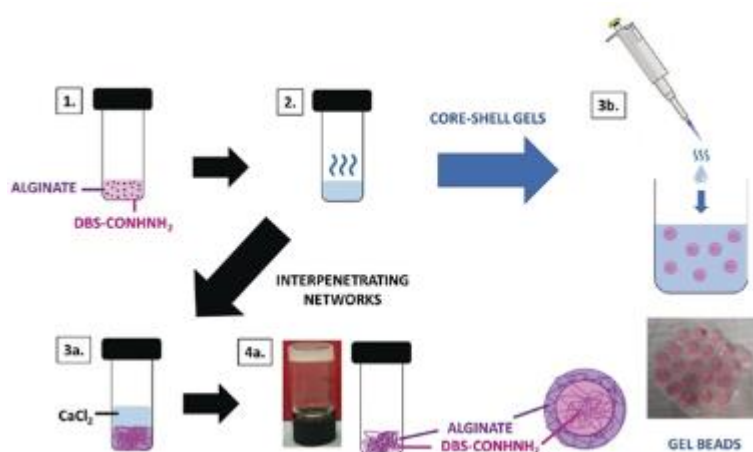


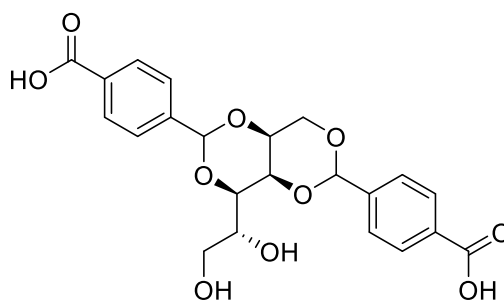
Figure 99. Preparation of the hybrid alginate/DBS-CONH₂ hydrogels in vials, and the hybrid core-shell beads. Reproduced from reference 214.

The structure of the beads was confirmed by optical microscopy, with the cross section clearly showing the difference between the inner and outer sections of the beads. This also showed a clear difference in comparison with beads formed of only alginate – these did not show the same core-shell structure.²¹⁴

It was also important to understand what proportion of gelator was incorporated within the beads, and therefore ¹H NMR studies were carried out to determine how much LMWG was within the beads. The hybrid beads were prepared, and dried. The DBS-CONH₂ was then dissolved in DMSO-*d*₆ (this does not dissolve the alginate), and the concentration of gelator determined by use of acetonitrile as an internal standard. These studies indicated that the majority of DBS-CONH₂ was incorporated within the gel beads during gel bead synthesis, with over 90% being incorporated. This indicates that this alginate approach is indeed an efficient way of capturing and stabilising self-assembled DBS-CONH₂ gel beads.

3.2 Development of DBS-CO₂H and Alginate Gel Beads

As well as DBS-CONH₂, a second DBS based gelator, DBS-CO₂H (**34**) (Figure 100), has also been used in a number of applications within the group, including in combination with polymer gelators.²¹⁹ For DBS-CO₂H, gelation is triggered by lowering the pH to below the pK_a value of the carboxylic acid groups (ca. 5.4) – this leads to protonation of the carboxylic acid groups, and consequently the solubility of the gelator is reduced and a gel is formed. This mode of gelation is distinct from those of both DBS-CONH₂ and alginate.



34

Figure 100. The structure of DBS-CO₂H.

Following the development of the DBS-CONHNH₂ and alginate beads, efforts were then made to fabricate similar beads, but with the LMWG in this case being DBS-CO₂H. Gel beads based on DBS-CO₂H have not previously been reported in the literature. In addition to demonstrating the general applicability of our alginate gel bead formulation method, these materials are of particular interest due to the pH responsive nature of the DBS-CO₂H network, which is stable below a pH of around 5.5, but breaks down in more basic conditions. This is especially interesting for drug release applications in which this pH value is of key importance. For example, the stomach is more acidic than the pK_a value of DBS-CO₂H, whereas the intestine is less acidic. Meanwhile, skin has a very similar pH value to the pK_a of the gelator. It is therefore clear that the responsiveness of DBS-CO₂H occurs at a physiologically-interesting and potentially useful pH value.

In work carried out by Dr Carmen Piras, alginate and DBS-CO₂H hybrid gel beads were therefore developed. To achieve this, the different rates in formation of the networks was exploited, as alginate forms gels very rapidly on addition of Ca²⁺ ions, while DBS-CO₂H forms more slowly, as a result of decreasing pH. To form the beads, DBS-CO₂H (0.3% wt/vol) and alginate (0.5% wt/vol) were combined in aqueous solution. This mixture was added dropwise to an acidified (using HCl, 0.1 M) CaCl₂ solution, and the alginate network formed immediately, giving small, transparent gel beads. Over time, the beads gradually became more translucent, a visual indication of the formation of the DBS-CO₂H network being formed as the pH was lowered. The gel beads formed were 2.8-3.3 mm in diameter which reflected the droplet size being added to the CaCl₂/HCl solution.

In this case, the formation of the two hybrid gel networks is reliant on the presence of both H⁺ and Ca²⁺ ions. It seemed likely that the beads would form with interpenetrating networks, rather than the core-shell structure observed in the combination of DBS-CONHNH₂ and alginate. Indeed, a uniform structure was observed by optical microscopy, with the beads again cut in half, before

being embedded in resin and dyed with toluidine blue. This showed a consistent structure across the whole cross section of the gel bead (Figure 101). SEM imaging of the cross section further indicated that the network extended across the whole bead, with both gelators being in their assembled state. Importantly, there was no evidence of any solid-like, non-self-assembled material present within the gel, which agrees with the hypothesis that assembly is being controlled by the presence of the H^+ and Ca^{2+} triggers.

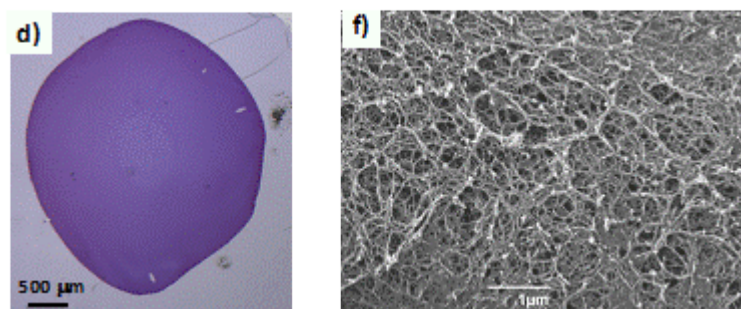


Figure 101. Optical microscopy (left) and SEM (right) images for cross sections of DBS-CO₂H/alginate beads.

Following the imaging that indicated that the two gelators had both assembled to form networks, the self-assembly of DBS-CO₂H was further investigated by an NMR experiment. DBS-CO₂H and alginate beads were formed, using D₂O instead of H₂O, and were added to an NMR tube, also containing D₂O and an acetonitrile internal standard. Any of the individual gelator components that were not assembled into 'solid-like' nanofibres could therefore be quantified. This study indicated that, for both DBS-CO₂H and alginate, all of the gelator was assembled in the beads.

This was followed by determination of how much DBS-CO₂H was incorporated into the gel beads. The hybrid beads were prepared in water, then dried, and DMSO-*d*₆ added. This dissolves the DBS-CO₂H, but not the alginate. Acetonitrile was added as an internal standard, and the concentration of DBS-CO₂H could thus be determined. This indicated that around 94% of the LMWG was incorporated within the gel beads during their preparation.

3.3 Development of DBS-CONHNH₂, DBS-CO₂H and Alginate Gel Beads

Following the successful development of both these types of hybrid gel bead, three-component beads, containing DBS-CONHNH₂, DBS-CO₂H and alginate were developed by Dr. Carmen Piras. Previously, the two LMWGs have been combined, with spatial control over different domains being achieved either by photopatterning²²⁰ or diffusion.²²¹ As these two gelators have differing properties, and the beads formed by each with alginate also differ, it was considered that combining the three gelators would lead to beads with interesting properties.

To fabricate the three-component beads, the methods used for the two types of two component bead were combined. DBS-CO₂H (0.3% wt/vol) was dissolved in a basic, aqueous solution, along with DBS-CONH₂ (0.3% wt/vol) and sodium alginate (0.5% wt/vol). This suspension was then sonicated, to ensure all of the solid was dispersed, followed by heating to dissolve all of the DBS-CONH₂. While still hot, drops of the solution were added to acidified CaCl₂ solution. As soon as the hot gelator solution was added to the CaCl₂ solution, small gel beads were formed. The beads had a diameter of 3.0-3.5 mm, reflecting the droplet size added into the CaCl₂ solution. Similarly to the DBS-CONH₂ and alginate beads, these three-component beads have a core-shell structure. In this case, we suggest that the core is primarily DBS-CONH₂ and DBS-CO₂H, and the shell is mainly alginate and DBS-CO₂H. Optical microscopy was carried out, with beads embedded in resin, then stained with toluidine blue. This clearly showed the core-shell structure of the beads (Figure 102). SEM imaging also indicated that the gelators within the beads were assembled into a sample spanning nanofibrillar network, and there was no evidence of solid-like non-assembled material, indicating that the nanoscale assembly process was well controlled during the synthesis.

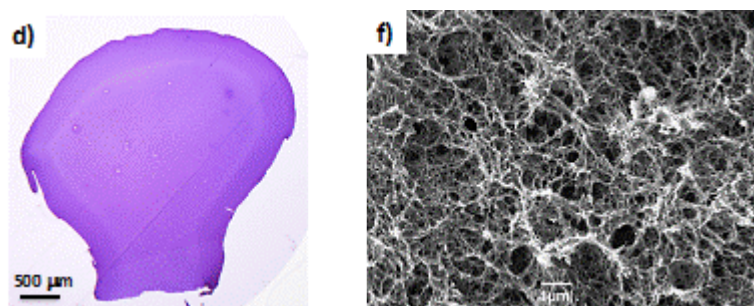


Figure 102. Optical microscopy (left) and SEM (right) images for cross sections of the 3-component gel beads.

The self-assembly of the beads was further investigated by ¹H NMR, to determine what proportion of the gelator was assembled within the beads. The three-component beads were therefore prepared, using D₂O in place of H₂O. They were then added to an NMR tube, which also contained D₂O, along with acetonitrile as an internal standard. No signals from any of the three gelators were observed in the ¹H NMR spectrum, indicating that all three gelators were indeed in their assembled state within the beads.

The incorporation of the DBS gelators into the beads was also investigated. The three-component beads were prepared, then dried. DMSO-*d*₆ was then added – this will dissolve the DBS gelators, but not the alginate. An acetonitrile standard was also added, to allow the amount of gelator to

be determined. This test determined that for each LMWG, over 90% of the gelator was successfully incorporated into the beads during the fabrication process.

3.4 Properties of the Types of Bead

3.4.1 Rheology For the Different Materials

To compare the mechanical properties of the types of gel, hybrid gels were prepared in vials, so that parallel plate rheology carried out. This was done for DBS-CONH₂/DBS-CO₂H gels, DBS-CONH₂/alginate gels, DBS-CO₂H/alginate gels, and the three-component gels (Table 8).

For each two-component gel, the hybrid material was stiffer than either of the two components individually, with the presence of the second network providing reinforcement for the first.

DBS-CO₂H and alginate gels have a G' of around 5300 Pa – considerably greater than for either component alone (DBS-CO₂H, 360 Pa; calcium alginate, 1420 Pa). Similarly, DBS-CONH₂ and alginate gels have a G' of around 8300 Pa, indicating greatly improved mechanical strength (DBS-CONH₂ alone has a G' of 800 Pa). In the case of these gels, it is important to note that there is not a core-shell structure present, as the gels have been prepared in vials, rather than as beads, and therefore the core-shell structure cannot form. The samples can therefore be considered as sample spanning, fully interpenetrated multi-component networks.

A key comparison was between DBS-CO₂H/DBS-CONH₂ hybrid gels, and the three-component gels. The DBS-CO₂H/DBS-CONH₂ hydrogels are stiffer than either of their two components individually, with a G' of around 5410 Pa. On addition of alginate, there is once again a significant increase in G' , to around 19000 Pa. It should be noted that, again, these beads do not have a core-shell structure, but extended interpenetrating network structures, as they are prepared in vials.

Table 8. G' values for gels formed from DBS-CONH₂, DBS-CO₂H and alginate.

Gel	Loading LMWG / % wt/vol	Loading Alginate / % wt/vol	G' / Pa
DBS-CONH₂	0.4	-	800
DBS-CO₂H	0.4	-	360
Alginate	-	0.6	1420
DBS-CONH₂/DBS-CO₂H	0.3	-	5410
DBS-CONH₂/Alginate	0.3	0.5	8300
DBS-CO₂H/Alginate	0.3	0.5	5300
Three Component	0.3	0.5	19000

This indicates that for this family of gels, the presence of multiple gel networks increases the stiffness of the overall material. Furthermore, it is evident that the presence of calcium alginate significantly enhances gel stiffness, underpinning its key role as a robust polymer gelator in allowing the gel beads to have well-defined self-supporting structures. This is as expected – it is well known that the presence of a PG along with a LMWG gives a gel that is stiffer.¹⁶⁸ It is also notable that the three-component gel is stiffer than any of the two component hybrids, demonstrating (as in Chapter 2), that two different LMWGs can form multi-component networks with enhanced rheological properties.

3.4.2 pH Responsiveness of Gel Beads

The impact of changing the pH on the proportion of DBS-CO₂H within the gel bead network was also investigated. This is important for the potential drug delivery applications. To determine the effect of pH, two-component DBS-CO₂H/alginate gel beads were prepared in D₂O, and transferred to an NMR tube, to which was also added further D₂O, a small amount of NaOD, and an acetonitrile internal standard. This was then left overnight, before a ¹H NMR spectrum was recorded. The amount of DBS-CO₂H that has disassembled and was no longer part of the gel network could then be determined. It was found that around 48% of the DBS-CO₂H present in the beads was freely mobile within the solution following standing overnight. This is perhaps less than would be expected – it is possible that the remaining DBS-CO₂H is interacting with the calcium alginate network in some way, preventing full mobility, and therefore not appearing in the ¹H NMR spectrum. It is, for example, plausible that when deprotonated, the carboxylate-functionalised DBS can bind to the Ca²⁺ ions within the calcium alginate, hence remaining somewhat immobilised by the presence of the PG network. However, these beads are nonetheless clearly pH responsive, making them potentially interesting for drug delivery.

It was also important to understand if, in the presence of two additional gelators (DBS-CONH₂ and alginate) in the three-component system, the pH responsiveness of DBS-CO₂H was also maintained in the same way as for the DBS-CO₂H/alginate beads as described above and the same method was used here.

In this case, around 61% of DBS-CO₂H became mobile on deprotonation, along with around 19% of DBS-CONH₂. We suggest that some DBS-CONH₂ is mobilised as a result of the disruption of interactions between the two LMWGs as the DBS-CO₂H network is disassembled – it is known that there are some interactions between the networks formed by the two gelators.²²⁰ Clearly,

however, these three-component beads retain the fundamental pH responsiveness programmed into them by the presence of DBS-CO₂H.

3.5 Release of Rosuvastatin from Hybrid Beads

The pH-responsive nature of these gel beads makes them interesting vehicles for potential drug delivery applications. It was therefore decided to investigate the release of an API, rosuvastatin (**122**) (Figure 103). As discussed in Chapter 2, statins are medications that lower cholesterol – for this reason, they are widely prescribed to reduce the likelihood of cardiovascular events such as strokes or heart attacks.²²² Attractively for gel delivery, statins are typically therapeutically active in relatively low doses, in the region of 5-40 mg – such doses can feasibly be easily incorporated into a relatively small volume of gel carrier.²²³ Rosuvastatin is typically administered as a daily, oral tablet, with the majority of the drug being absorbed in the intestine.²²⁴

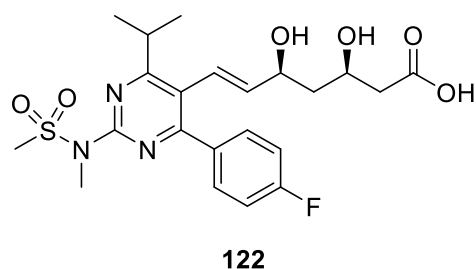


Figure 103. The structure of rosuvastatin, the API incorporated within the gel beads.

Therefore, these novel multicomponent beads were tested for incorporation and release of the statin drug rosuvastatin calcium. This was carried out for all of the previously described hybrid beads, as well as for beads based on calcium alginate alone. The different types of multicomponent gel were also prepared in vials and compared to the individual LMWGs, as well as the two combined. Additionally, two different release media were chosen for these studies, neutral Tris-HCl (pH 7.4, Tris-HCl 10 mM, NaCl 150 mM) and mildly acidic sodium acetate (pH 4.0, 0.1 M) – this was to determine the effect of changing pH on any interactions between the drug and the gel network, and the impact of this on the release of the drug. Release of rosuvastatin was monitored by UV-vis spectroscopy, with rosuvastatin having a maximum absorbance at 251 nm. For each experiment, control gels containing no rosuvastatin were also monitored, to ensure the observed signals were a result of the drug being released, rather than the gelator. All gel beads used in the study were prepared as described previously.

3.5.1 Incorporation of Rosuvastatin

The first step was to ensure that the gel beads were capable of encapsulating rosuvastatin. An aqueous solution of rosuvastatin calcium (0.11 mM) was prepared, and each sample stood overnight in this solution (4 ml), to allow for diffusion of the drug into the gel. The drug solution was then removed, and the amount of rosuvastatin remaining quantified by UV-vis. This allowed the amount of rosuvastatin that was incorporated into the gels to be determined. This was typically around 0.22 μmol per gel sample. It is worth noting that for the studies reported here, we preferred to use systems in which the rosuvastatin was fully soluble to facilitate release studies using buffer solutions and effective spectroscopy. This means the absolute concentrations are relatively low, and below the therapeutic value. However, we anticipate that further development would involve optimising the incorporation of higher loadings of insoluble drug into these gel carriers (see future work).

3.5.2 Release from Gel Beads

Once the beads had been loaded with rosuvastatin, the release of the drug was determined. The release buffer (6 ml) was added to the samples, which were then incubated at 37 °C. At each timepoint, an aliquot (2 ml) was removed from the sample, and release of rosuvastatin determined by UV-vis spectroscopy. The aliquot was then returned to the sample. This was carried out in triplicate, and standard error indicated by error bars. This was carried out using both Tris-HCl (pH 7.4, Figure 104) and sodium acetate (pH 4.0, Figure 105) as release buffers, with the control samples monitored in the same way in each case.

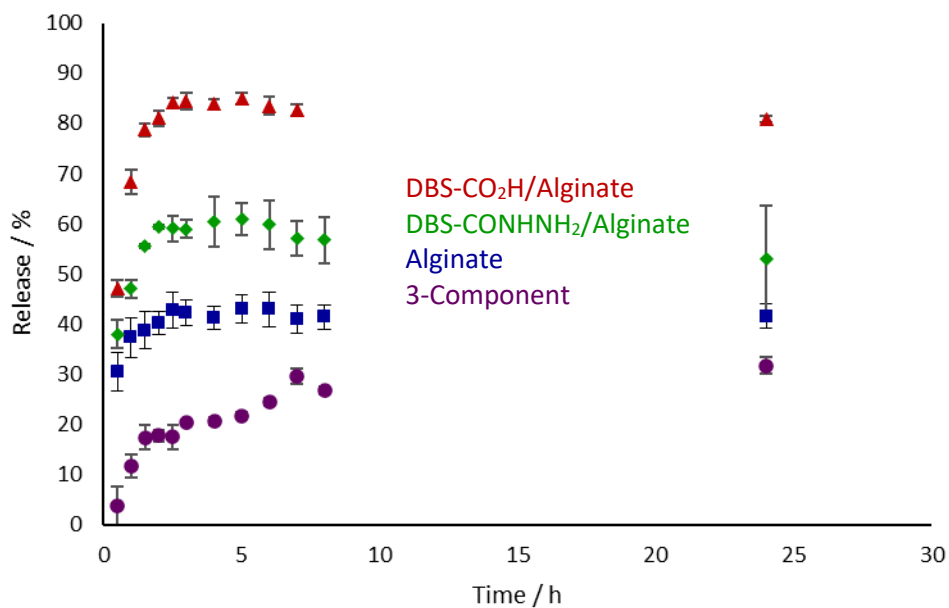


Figure 104. Release of rosvastatin from gel beads (total 1 ml), into Tris HCl pH 7.4 buffer (6 ml) at 37 °C, over 24 hours.

When using Tris-HCl (pH 7.4) as the release buffer, the most rapid release occurred for DBS-CO₂H/alginate beads, with 85% release having occurred within about 2 hours. Similarly, for both DBS-CONHNH₂/alginate beads, and alginate beads alone, most release occurred within the first two hours. However, total release was lower, reaching about 60% for the DBS-CONHNH₂/alginate beads, and around 40% for the alginate beads. The three-component system showed much slower release, with the maximum only reached after 24 hours, and with the amount released being relatively low at only about 30%.

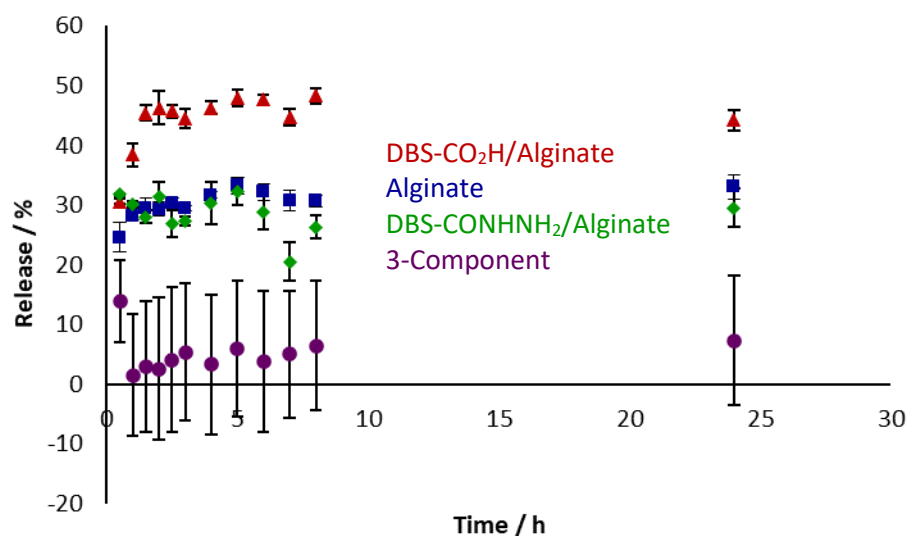


Figure 105. Release of rosvastatin from gel beads (total 1 ml) into pH 4.0 sodium acetate buffer (6 ml) at 37 °C.

Changing the release medium to sodium acetate buffer (pH 4.0), and thereby reducing the pH, had a significant effect on the release of rosvastatin. For all the types of bead, release was reduced considerably. For the DBS-CO₂H/alginate beads, release was reduced to around 45%. The DBS-CONHNH₂/alginate beads also saw a significant decrease in release, to about 30%. However, the alginate beads showed a similar level of rosvastatin release to pH 7.4. The three-component beads gave very slow and low amounts of release, with only 7% of rosvastatin released after 24 hours.

These release profiles are a result of a number of different factors. A key consideration is that rosvastatin is a weak acid, with a pKa of 4.6.²²⁵ Therefore at pH 7.4, more than 99% of the drug is in the ionised form, which has greater solubility in water than the non-ionised form at pH 4, where the drug is mostly protonated, and therefore less soluble. This accounts for the overall lower release from the beads at pH 4.0, compared to at pH 7.4.

Another secondary factor controlling and modifying drug release are the potential interactions between rosvastatin and the gel network – where these interactions are present, release will be lower. It is interesting that the calcium alginate gels alone limit the release of rosvastatin, suggesting there are interactions between the drug and the network – this is most likely between the carboxylic acid of the rosvastatin, and the calcium ions that form part of the PG network. These interactions would be expected to persist even when the pH is 7.4, and this is indeed

observed for release from calcium alginate gels, where changing pH appears to have little impact on drug release.

When DBS-CO₂H is also present, however, the release of rosuvastatin is increased. This is especially noticeable at pH 7.4. We suggest that at this higher pH value, the DBS-CO₂H network itself begins to deprotonate and disassemble (see NMR studies in Section 3.4.2). It is therefore possible that some of the deprotonated gelator interacts with the alginate network (indeed, this possibility was identified in our NMR studies (Section 3.4.2). This will compete with the interactions of rosuvastatin with the calcium alginate network, and therefore enable more drug release can occur. This effect therefore indicates that the DBS-CO₂H/alginate beads are capable of pH-triggered release as a result of competitive interactions between the different components present.

It has been demonstrated previously that DBS-CONH₂ is capable of pH-mediated release of the anti-inflammatory drug naproxen as a result of acid-base interactions between the drug and the acylhydrazide functional group of DBS-CONH₂. Similarly here, for DBS-CONH₂/alginate gel beads, lower release is observed at lower pH values – with the overall release doubling from 30% at pH 4.0 to 60% at pH 7.4. We suggest that, as for naproxen, this is due to the increase in pH effectively ‘switching off’ the acid-base interaction between rosuvastatin and the DBS-CONH₂ network, due to deprotonation of rosuvastatin.

Intriguingly, we found there was a significant difference between the release from gels formed in vials compared with the gels in the form of beads (Figure 106). For the DBS-CONH₂ combination, we observed greater release from the beads at a higher pH value – possibly due to the increased surface area, or perhaps a result of the greater interpenetration of the calcium alginate network, which may interact with the deprotonated rosuvastatin, limiting release from the gels in vials. This effect is reversed at the lower pH value, possibly as a result of the core-shell nature of the beads – possibly because under these conditions, the relatively tightly packed alginate shell limits release from the beads.

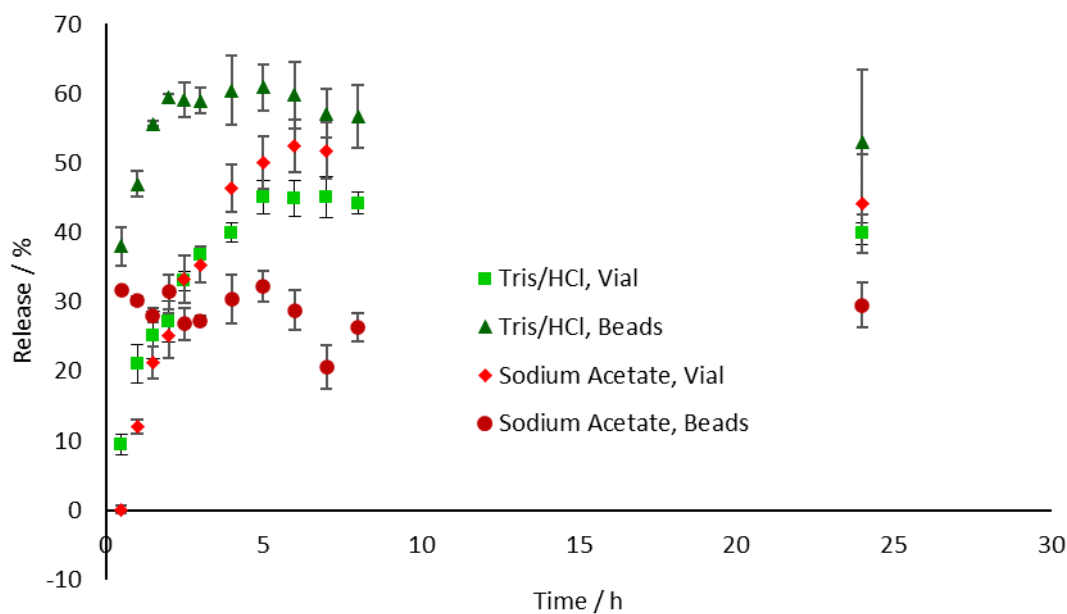


Figure 106. Release of rosvastatin from DBS-CONHNH₂/alginate gels, prepared either as beads (total 1 ml) or in vials (1 ml), into either Tris/HCl or sodium acetate buffers (6 ml) at 37 °C.

For DBS-CO₂H/alginate hybrids, this difference in release for the beads and the gels prepared in vials was much less pronounced (Figure 107). This suggests that the core-shell nature of the DBS-CONHNH₂/alginate beads is in some way influencing release of the drug – as the equivalent gels in vials do not have this core shell structure. This is also the case for the DBS-CO₂H/alginate gels, with neither the beads nor the gels prepared in vials having a core shell structure. However, it is hard to fully understand these effects in detail.

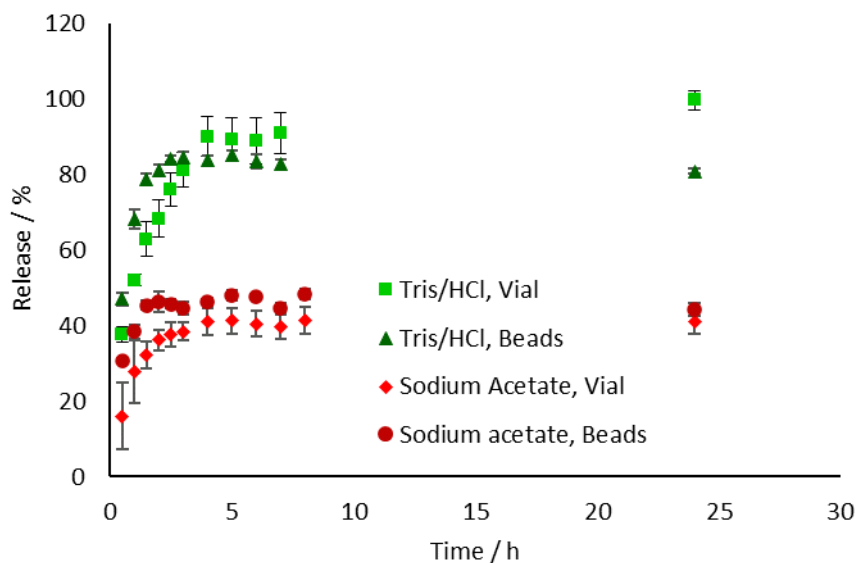


Figure 107. Release of rosuvastatin from DBS-CO₂H/alginate gels, prepared either as beads (total 1 ml) or in vials (1 ml), into either Tris/HCl, or sodium acetate buffer (6 ml) at 37 °C.

The three-component system shows the lowest release at both pH 7.4 and pH 4.0, with release being especially limited and slow at pH 4.0, with only 7% of the drug being released in 24 hours. This is thought to be predominantly due to the interactions between the drug and the DBS-CONHNH₂ network. Furthermore, as these three-component beads are formed in the presence of HCl (unlike the DBS-CONHNH₂/alginate beads), this may contribute to a lower pH within the beads themselves. This would ensure that more of the rosuvastatin is deprotonated, increasing the potential for these drug-network interactions. Additionally, the presence of the three gelators leads to a network that is more densely packed – this further limits release. Release is also low from the three-component system at pH 7.4 – this is thought to be partly due to the tightly packed network, but also that interactions between DBS-CONHNH₂ and DBS-CO₂H may limit the interactions of deprotonated DBS-CO₂H with the calcium alginate network, and hence allow for interactions between rosuvastatin and the calcium alginate network to be retained even when the DBS-CO₂H network is disassembled.

In summary, pH mediates the release of rosuvastatin from these gel beads partly as a result of the pKa value of the drug itself, with greater drug release at higher pH values. However, the precise composition of the multi-component gel system plays a key role in mediating this effect as a result of interactions between different components within the beads. Indeed, in the case of calcium alginate alone, pH only has a very small effect on drug release, whereas in the presence of the low molecular weight gelators, drug release can be effectively doubled. For the three-

component gels in particular, there is some potential for the use of these systems as slow release statin delivery systems, and this should be further explored in future.

3.6 Conclusions and Future Work

By creating DBS-CO₂H/alginate beads, it has been demonstrated that the Smith group's alginate gel bead methodology can be extended to pH-triggered hydrogels as well as heat-cool systems. Given the prevalence of pH-triggered LMWGs in the literature, this is an important breakthrough, which illustrates that the alginate gel bead stabilisation method is a potentially widely applicable fabrication technique, applicable across a range of different hydrogelators.

These pH-responsive gel beads, formed from multiple components, are capable of encapsulating and releasing the drug rosuvastatin, commonly prescribed to lower cholesterol. Importantly, the precise composition of the bead plays a key role in modulating the extent of drug release and the impact of pH on this process.

The polymer component of the gel gives increased mechanical strength, as well as allowing the material to be shaped into beads. The LMWGs that are also part of the beads are responsive, with DBS-CO₂H disassembling at higher pH values, and DBS-CONH₂ giving direct interactions between the gel network and the drug additive, especially at lower pH values.

It was found that these beads released rosuvastatin in a pH-dependent manner, with release typically being much reduced at the lower pH of 4.0. This was observed across all the types of bead and results from the protonation of the drug limiting its release under these conditions. Generally, the presence of DBS-CO₂H enhanced delivery, especially at pH 7.4, when this network is disassembled. It is argued that in the carboxylate form, this disassembled gelator prevents interaction of the drug with other components of the gel bead, such as calcium ions, by a competitive binding mechanism. In contrast, DBS-CONH₂ decreases drug delivery, an effect which is particularly noticeable at pH 4.0, where it can interact with rosuvastatin as a result of forming an acid-base interaction under these conditions, as well as in the three-component system, which gave slow and limited drug release.

This range of drug release, both in terms of rate and the overall amount released, allows for tuning of the rosuvastatin delivery by modifying gel bead composition. This gives potential for use in a range of settings, with the type of bead varied depending on the rate of release required. As previously discussed, statins are widely-used to lower cholesterol – for this application, slow release, providing a steady supply of drug, would be desirable. Increasingly, statins are also being shown to have a positive effect on bone growth.²²⁶ For example, statins have also been shown to

improve outcomes for periodontitis – in these cases, rapid, localised release is desired – some of these formulations could also be useful in this regard.²²⁷

Further work in this area will investigate fabrication of injectable microgels with smaller gel bead diameters (ca. 1 μm), and the application of these for statin delivery. It is suggested that injectable microgels capable of slow statin release may be particularly suitable for long-term treatment of patients with this type of medication, which is often prescribed for a period of very many years. Injectable slow release formulations have been demonstrated to be of significant clinical value in the field of contraception, and it is suggested that long-term cholesterol management could be dealt with in a similar way. They may also be useful in bone-healing applications as a result of the potential for the microgel to retain the drug in a well-defined local area after injection.

Future work would also focus on incorporating different drugs into this gel bead system. For example, there are a wide range of statin drugs that could be studied, as well as extending the application of this gel system to other drugs and disease targets.

4. Chapter 4 – Synthesis of Novel Sorbitol Derivatives

1,3;2,4-Dibenzylidene sorbitol (DBS) (**32**) has been known and exploited for its thickening properties for over 100 years – with the first report as early as 1891.⁹⁷ As DBS and its derivatives were increasingly investigated, 2,4-monobenzylidene sorbitol (MBS) (**33**) was also discovered (Figure 108).

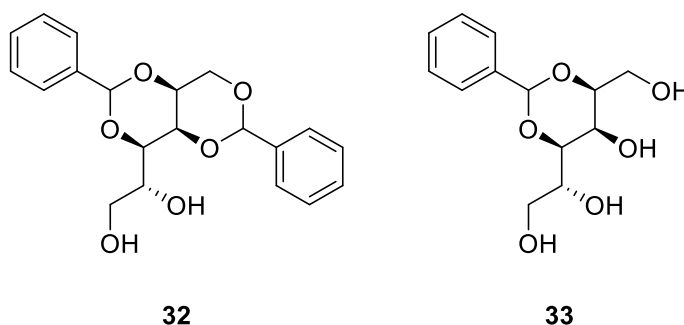


Figure 108. The structures of dibenzylidene sorbitol and monobenzylidene sorbitol.

Currently, DBS derivatives are widely used in a range of commercial applications for their thickening properties, mostly based on their ability to form organogels. These applications tend to make use of the physical effects of including DBS in a formulation – rather than any chemical effects - particularly in the personal care industry, in products including deodorant sticks²²⁸ and lipsticks.^{99b} DBS derivatives are also capable of thickening oil-in-water emulsions, and so have found use in a variety of products such as suncreams²²⁹ and make-up.²³⁰ DBS has also been widely used as an additive in polymers, as a clarifying²³¹ or nucleation agent.²³² In this latter case, the self-assembly of DBS into nanostructures within the molten polymer phase helps to control the polymer crystallisation event, leading to polymers with greater transparency.

There has been increasing interest in modifying DBS to give derivatives with desirable properties. These modifications typically focus on two main parts of the molecule – the aromatic ‘wings’, and the free alcohol groups of the sugar backbone (Figure 109). A common technique for modification of the ‘wing’ is to simply replace benzaldehyde with an alternative aldehyde – this then forms the novel derivative by the same condensation reaction. Common groups used for functionalisation include alkyl chains²³³ and halogens.²³⁴

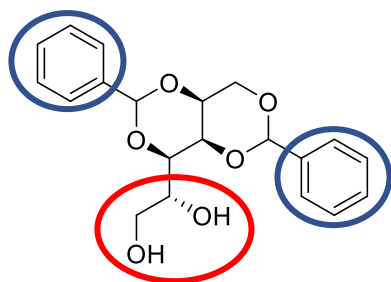
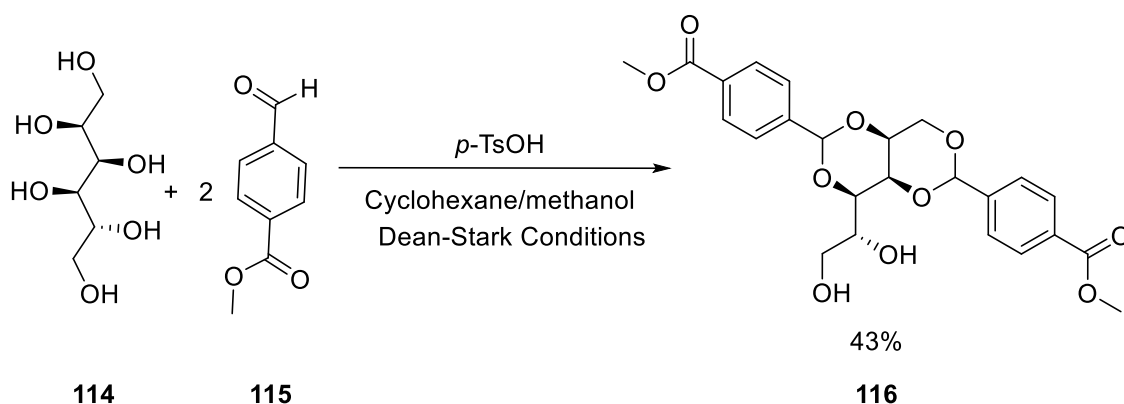


Figure 109. DBS, with the key sites for modification marked. Blue circles - aromatic 'wings'. Red circle - free alcohols.

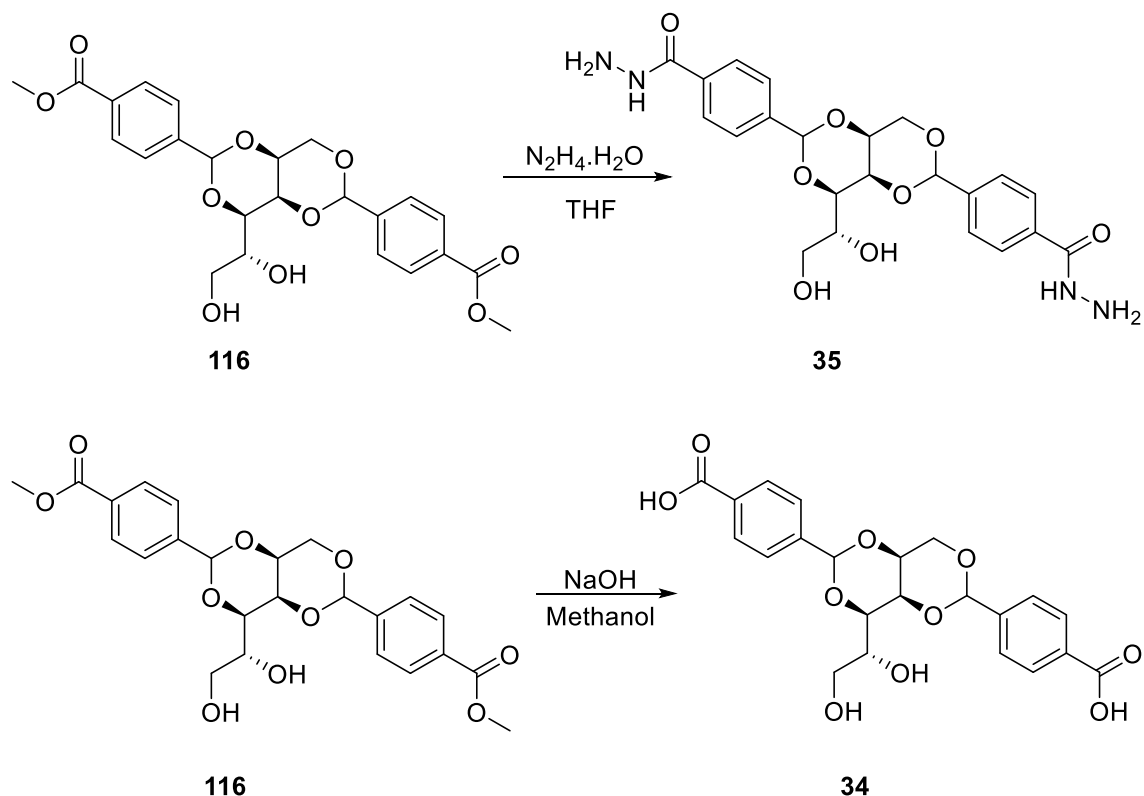
As described in the introduction, DBS and its derivative are also beginning to be exploited for more 'high-tech' applications. These have been limited as a result of DBS forming gels only in organic solvents.

For DBS derivatives to be capable of forming hydrogels, the hydrophilicity of the molecules needs to be slightly increased - achieved with modification of the 'wings' of the DBS molecule. Smith and co-workers were the first to achieve this by a simple two step synthesis. Initially, benzaldehyde was replaced with 4-methylcarboxybenzaldehyde and the condensation reaction carried out. The DBS-CO₂Me can then be isolated (Scheme 5).



Scheme 5. The synthesis of DBS-CO₂Me.

Once DBS-CO₂Me has been separated from the mono and tri substituted derivatives that are also formed, the ester groups can be easily converted to give either an acyl hydrazide¹⁰⁶ or a carboxylic acid (Scheme 6).¹⁰⁵ These two derivatives are capable of forming hydrogels – each with a different trigger for gelation. DBS-CONHNH₂ hydrogels are formed following a heat cool cycle, and DBS-CO₂H following a decrease in pH. This method of pH-triggered gelation is common for supramolecular gels.¹⁶



Scheme 6. The conversion of DBS-CO₂Me (**116**) to give DBS-CONHNH₂ (**35**) or DBS-CO₂H (**34**).

In addition to having different triggers for gelation, these gels also have different properties. DBS-CONHNH₂ hydrogels have good stability across a range of pH values – additionally, the hydrazide groups are capable of interacting with chemical additives, including aldehydes¹⁰⁷ and carboxylic acids.¹⁷⁴ These hydrogels can also achieve *in situ* formation of metal nanoparticles, including silver³¹ and gold.¹⁷¹ This gives this class of hydrogels potential in applications including drug delivery,¹⁰⁹ pollutant removal¹⁰⁶ and catalysis.¹⁷²

DBS-CO₂H hydrogels are formed by a pH change – as a result, the gels formed are not stable at higher pH values. However, this method of formation allows for the gel to be patterned, using a photo-acid to decrease the pH.²²⁰ This allows for good spatial control of the formation of the network, and therefore some of the material properties.

Although having access to these two gelators with their differing properties is useful, the only way to combine the effects is to mix the two gelators to give a hybrid material. An attractive alternative method for achieving a mix of properties could be to synthesise a 'non-symmetric' DBS derivative, containing both a hydrazide group and an acid group. Combining the two functionalities may allow the development of a gelator with properties intermediate between the two individual gelators. This would increase the flexibility of the DBS based system, potentially opening up new applications for this class of gelator. Investigations have therefore been made

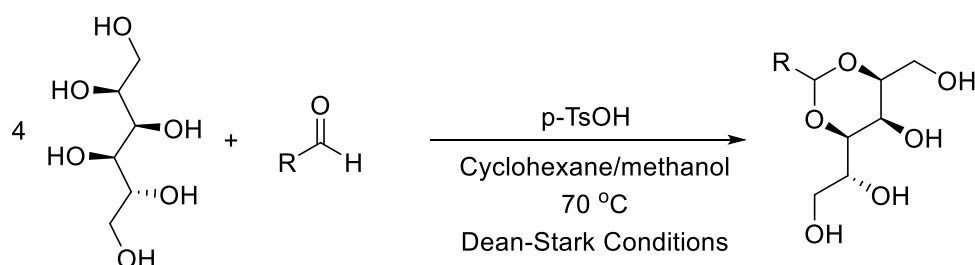
into the synthesis of non-symmetric DBS derivatives, primarily based upon DBS-CONHNH₂ and DBS-CO₂H.

Given our interest in extending the range of DBS hydrogels, we also noted that generally, there has been much less investigation of MBS derivatives in comparison to DBS derivatives. Although MBS itself does have potential applications in cosmetics,²³⁵ derivatives of MBS have not been widely reported. However, there is great potential for this type of system to form hydrogels – indeed this has been previously reported.^{188, 189} Encouraged by this, along with the successful synthesis of MBS-CO₂Me described in Chapter 2, and its useful behaviour as a hydrogelator, a number of additional MBS derivatives were also targeted, and their gelation ability investigated.

4.1 Synthesis of MBS Derivatives

4.1.1 General Procedure

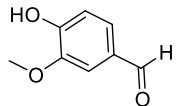
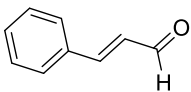
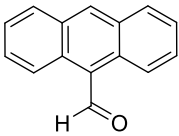
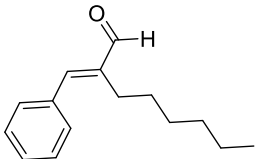
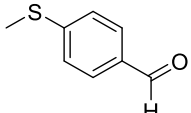
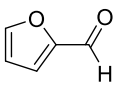
Initially, the synthesis of a variety of MBS derivatives was attempted. A range of aldehydes with different functionalities were selected. The conditions for the reaction were chosen based on the previous synthesis of MBS-CO₂Me. Therefore, for each derivative, the same general procedure was followed, with 4 equivalents of D-sorbitol being condensed with the chosen aldehyde, under Dean-Stark conditions, and using *p*-TsOH as the acid catalyst (Scheme 7).



Scheme 7. General scheme for the synthesis of MBS derivatives.

Following analysis of the crude product, the purification steps were then varied for each aldehyde. The results of the aldehyde screening, along with the isolated yields for each reaction, are shown in Table 9.

Table 9. Aldehydes investigated for formation of MBS derivatives, using the standard Dean-Stark conditions. Yield quoted is relative to the aldehyde. Trace indicates a small amount of product could be observed in ^1H NMR, but not isolated.

Aldehyde	Yield
	47%
	32%
	Trace
	Trace
	52%
	Trace

Of the aldehydes investigated, vanillin, cinnamaldehyde and 4-methylthiobenzaldehyde gave successful reactions, and the final MBS derivatives could be separated from the reaction mixture in pure form. Typically, this required only the removal of any remaining aldehyde, and the excess sorbitol. Unlike for the synthesis of MBS-CO₂Me, there was not significant formation of di or tri substituted derivatives. Purification was achieved by washing first with methanol, to remove the aldehyde, then with water to remove excess sorbitol. In the case of these three aldehydes, this left the desired product as a white solid.

In the ^1H NMR spectra for MBS derivatives, a distinctive peak, representing the acetal proton, was present at around 5.5 ppm. This was the case for all the derivatives successfully synthesised. This is combined with the loss of any aldehyde peak in the reaction mixture. Each derivative also showed peaks in the aromatic region, typically shifted in comparison to those observed for the starting aldehyde.

In the case of 9-anthracenecarboxaldehyde, although ^1H NMR and mass spectrometry (MS) of the crude product indicated that a reaction had taken place, and a small amount of MBS-Anthra had been formed, purification proved extremely challenging. Numerous washing steps were attempted – however, these did not prove to be successful in isolating the desired product. The crude product was therefore analysed by TLC, to allow for column chromatography to be carried out. Although not every component of the crude product could be dissolved in any one of the solvents tested, a distinct spot, not resulting from aldehyde and sorbitol, was observed when the product was dissolved in ethyl acetate. Ethyl acetate also gave suitable separation when used as the mobile phase, and column chromatography was therefore attempted. However, although separation was achieved, each fraction only contained a very small amount of material, and when the fractions were analysed by ^1H NMR and MS, there was no product present. It was concluded that only a trace of the desired product had been formed, visible in initial analysis, but very difficult to isolate. Due to the difficulties isolating the desired product, this synthesis was not pursued any further.

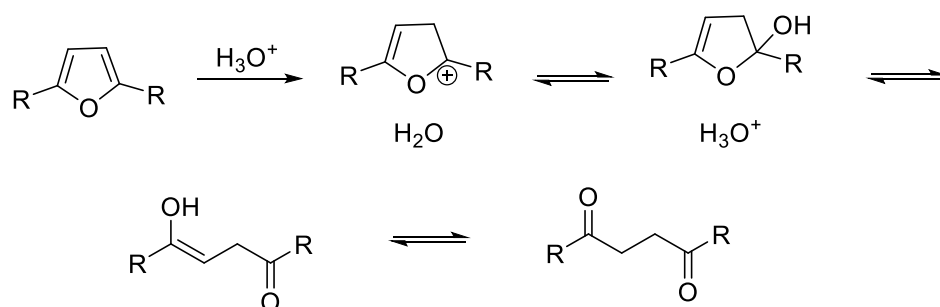
Similarly, for MBS-Hexcin, ^1H NMR of the crude product indicated that an acetal had been formed, with MS also indicating that the desired product had been formed. Again, numerous washing steps were attempted, and although excess sorbitol was removed, the remaining products could not be separated. Column chromatography of the crude product was therefore attempted, but although separation was achieved, none of the isolated fractions contained any MBS-Hexcin. Similarly as for MBS-Anthra, it is believed that only a very small amount of MBS-Hexcin is ever formed, and therefore this compound was also not investigated any further.

4.1.2 Synthesis of MBS-Fur

In the case of furfural, ^1H NMR spectroscopy of the crude product indicated that, although the desired acetal may have been formed, this was present only in very small quantities, with the majority of the material being unreacted aldehyde and sorbitol. The crude product was therefore washed with methanol then water, to remove these impurities. This left a black solid that was highly insoluble, and therefore could not easily be analysed. It is known that furfural may polymerise in the presence of acid. The polymer of furfural formed in acid is a black, insoluble resin – like that observed in this reaction.²³⁶

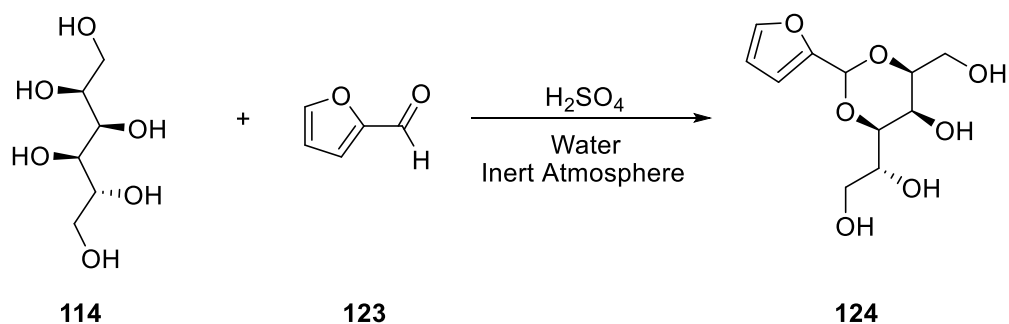
There are two main methods proposed for the polymerisation of furfural – depending on whether the reaction takes place in aqueous or anhydrous conditions. In aqueous conditions, an acid is also required, while in anhydrous conditions, either an acid or a base can act as a catalyst. In

anhydrous conditions, temperatures of at least 100 °C are also required.²³⁷ While the reaction for the formation of MBS derivatives is carried out under Dean-Stark conditions, to minimise the amount of water in the reaction, it is feasible that there is enough water present for the polymerisation to take place – the temperature of 70 °C is too low for the anhydrous method. The polymerisation under these conditions is a hydrolytic ring opening – to generate open-chain aliphatic products (Scheme 8).



Scheme 8. Ring opening polymerisation of furfural.

Therefore, alternative methods for the synthesis of MBS-Fur (**124**) were sought. A method for the synthesis of MBS-Fur described in the literature is carried out under an inert atmosphere, and at room temperature, to minimise the formation of the polymer resin (Scheme 9),²³⁸ and therefore this method was attempted.



Scheme 9. Synthesis of MBS-Fur (124).

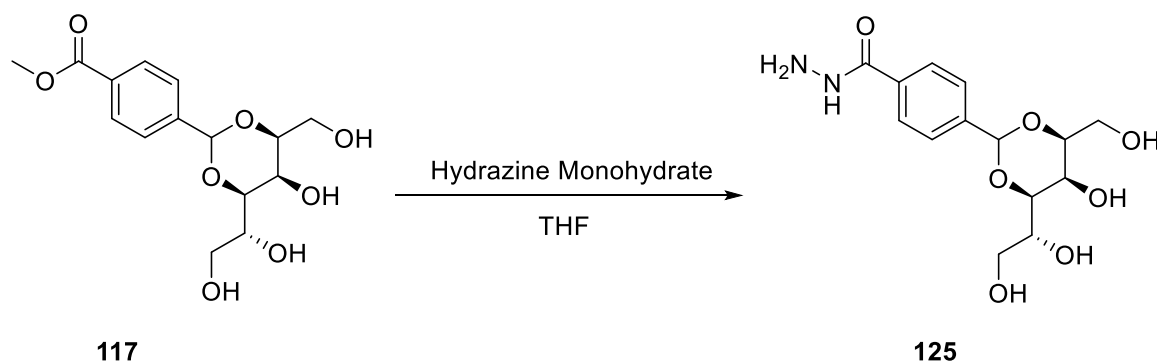
Initially, H₂SO₄ and water were added to a flask, which was then purged with nitrogen. Sorbitol was then dissolved in the minimum amount of water, and added to the acid, then furfural added slowly. The reaction was then allowed to proceed, at room temperature, overnight. 2-Propanol was added, and the reaction mixture filtered. However, unlike described in the literature, at this point no solid was present. The solvent was therefore removed from the reaction mixture to give a dark brown solid. At this stage, ¹H NMR showed a peak in the acetal region, suggesting that some MBS-Fur had been formed. A large amount of sorbitol was also present, and this was removed by washing with cold water, leaving a black solid. This solid was then washed with

ammonia in acetone, with only some of the solid dissolving. The solid was therefore washed with copious amounts of acetone, to leave a dark brown solid. ¹H NMR of the solid indicated that this was the desired product, although isolated only in a very low yield of 0.5%. As well as the dark brown solid, there was also an insoluble black solid present – this could not be analysed, as it was not soluble in even DMSO. It was considered that this solid was likely to be polymerised furfural, and it was therefore removed by filtration. As only a very small amount of the desired product could be isolated, this was not considered practical for further investigation.

4.1.3 Synthesis of MBS-CONHNH₂

MBS-CONHNH₂ (**125**) has previously been reported,¹⁸⁸ and the disubstituted molecule, DBS-CONHNH₂ has previously been used in numerous high-tech applications.²³⁹ The synthesis of this molecule, from MBS-CO₂Me, was therefore attempted.

First, MBS-CO₂Me was synthesised according to the previously described procedure. This was then converted to MBS-CONHNH₂ (Scheme 10) by a method similar to that used to convert DBS-CO₂Me to DBS-CONHNH₂. MBS-CO₂Me was suspended in THF, and then an excess of hydrazine monohydrate slowly added. This mixture was heated to reflux, and the reaction allowed to continue overnight. On cooling, a white solid was formed, which was removed by filtration, then washed with small amount of water to give the product as a white solid.



Scheme 10. Synthesis of MBS-CONHNH₂.

This reaction proved to be capricious, and some attempts failed to produce any product. However, on occasion, yields of up to 18% could be obtained. Additionally, attempts were made to replicate the previously reported procedure, which used methanol in the place of THF, which were also unsuccessful.

4.2 Gelation Screening of MBS Derivatives

The MBS derivatives were then screened for gelation ability, first focussing on MBS-Van and MBS-Cin, both of which could be reproducibly synthesised in good yield and purity. A known mass of each derivative was weighed into a sample vial, and 0.5 ml of deionised water added. The solid was then dissolved by heating. After cooling, gelation was checked by the tube inversion method. Some samples were also sonicated before heating, to aid with dissolution, but this did not appear to have any impact on the gelation event. For each derivative, a range of concentrations was investigated (Table 10).

Table 10. Screening for gelation of MBS-Van and MBS-Cin. All used 0.5 ml of water. S=solution, V=viscous liquid, C=crystals.

Concentration / % wt/vol	Gelator	
	MBS-Van	MBS-Cin
0.1	S	V
0.2	S	V
0.3	S	V
0.4	S	V
0.5	S	C
0.6	S	C
0.7	S	-
0.8	S	C
0.9	S	-
1.0	S	C

At all concentrations, MBS-Van was too soluble to form hydrogels – once dissolved, it remained in solution. The more hydrophobic MBS-Cin, although it did not remain in solution at concentrations above 0.5% wt/vol, formed small, needle like crystals on cooling. At lower concentrations, a slightly viscous liquid was formed, but this did still flow easily when the tube inversion test was performed.

Further investigations were then carried out, with either water/DMSO or water/ethanol as the solvent mix – at appropriate concentrations, such mixes can be relevant in pharmaceutical applications.²⁴⁰ Water and PEG 200 (common in cosmetic formulations)²⁴¹ mixes were also investigated. A known mass of each gelator was weighed into a sample vial, and 1 ml of the relevant solvent system added. The solid was dissolved by heating, and, on cooling, gelation

investigated by the tube inversion test. The concentrations used, and selected results of the screen, are shown in Table 11.

Table 11. Gelation screening for MBS-Van and MBS-Cin, in water/DMSO and water/ethanol mixes. S=solution, C=crystals. All samples were at 0.3% wt/vol.

Solvent mix	Gelator	
	MBS-Van	MBS-Cin
1% DMSO	S	C
2% DMSO	S	C
3% DMSO	S	C
4% DMSO	S	C
5% DMSO	S	C
10% Ethanol	S	S
20% Ethanol	S	S
30% Ethanol	S	S
40% Ethanol	S	S
50% Ethanol	S	S
60% Ethanol	S	S
70% Ethanol	S	S
80% Ethanol	S	S
90% Ethanol	S	S
100% Ethanol	S	C
5% PEG 200	S	S

As previously, no gels were formed. Furthermore, when samples at the higher gelator concentrations (0.6% wt/vol for MBS-Cin, 0.7% wt/vol for MBS-Van) were used, still no gels were formed, in any solvent mix. It was reasoned that the additional alcohol group of MBS-Van increases its hydrophilicity, leading to this compound being too water soluble to form gels. Although MBS-Cin is less water soluble, the appropriate balance between solubility and crystallisation cannot be achieved, with crystals forming in place of a gel in the presence of DMSO, whereas with ethanol or PEG200 as a co-solvent, this system is also too soluble for gelation to occur.

These two molecules were also tested with a range of organic solvents. Samples were prepared as previously by addition of one of the compounds (0.5% wt/vol) to a sample vial, and the relevant

solvent (0.5 ml) added. This was then heated carefully until the solid was dissolved, or the solvent was boiling. On cooling, the tube inversion test was used to check for gelation (Table 12).

Table 12. Solvent screen for MBS-Cin and MBS-Van. All samples at 1% wt/vol.

Solvent	Gelator	
	MBS-Van	MBS-Cin
Acetone	I	I
Methanol	P	P
Toluene	I	I
Ethyl Acetate	I	I
Chloroform	I	I
2-Propanol	I	S
DMSO	S	S
Cyclohexane	I	I
Diethyl ether	I	I
Acetonitrile	I/G	P

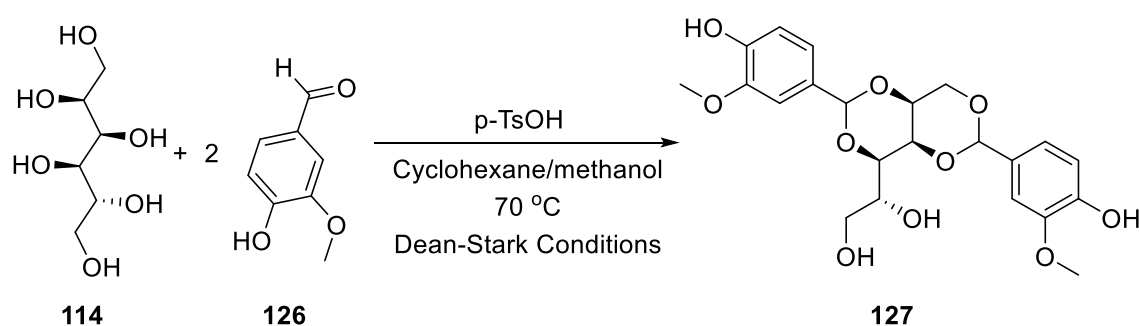
Once again, there was little success with gelation with these two compounds, with both being insoluble in the majority of the solvents investigated. Although MBS-Van did form an apparent gel in acetonitrile, this was not reliably reproducible, and as a result was not investigated further.

Following investigation of MBS-Van and MBS-Cin for gelation, MBS-Fur and MBS-CONHNH₂ were also investigated for the ability to form hydrogels. In the case of MBS-Fur, the brown solid could not be dissolved in water at any concentration, and therefore no gels were formed. Despite literature reports of MBS-CONHNH₂ being capable of forming hydrogels, despite attempting to form hydrogels at numerous concentrations, and with mixes of solvents, no hydrogels could be formed reproducibly.

4.2.1 Attempted Synthesis of DBS-Van

In all of the aqueous solvent systems tested, MBS-Van was too soluble to form hydrogels, remaining in solution once dissolved by heating. It was reasoned that, if the mono-substituted version was too water soluble for gelation to occur, the di-substituted version, which would be more hydrophobic, would be a promising candidate for a hydrogelator. This is similar to the contrast between DBS-CO₂Me and MBS-CO₂Me – however, in this case, DBS-CO₂Me is too insoluble to form hydrogels, while the more hydrophilic MBS-CO₂Me is an effective gelator.

Efforts were therefore made to synthesise DBS-Van (**127**). Two main methods were investigated. The first followed the same method used for the synthesis of DBS-CO₂Me – condensation of two equivalents of aldehyde with sorbitol, with *p*-TsOH as a catalyst, under Dean-Stark conditions (Scheme 11).

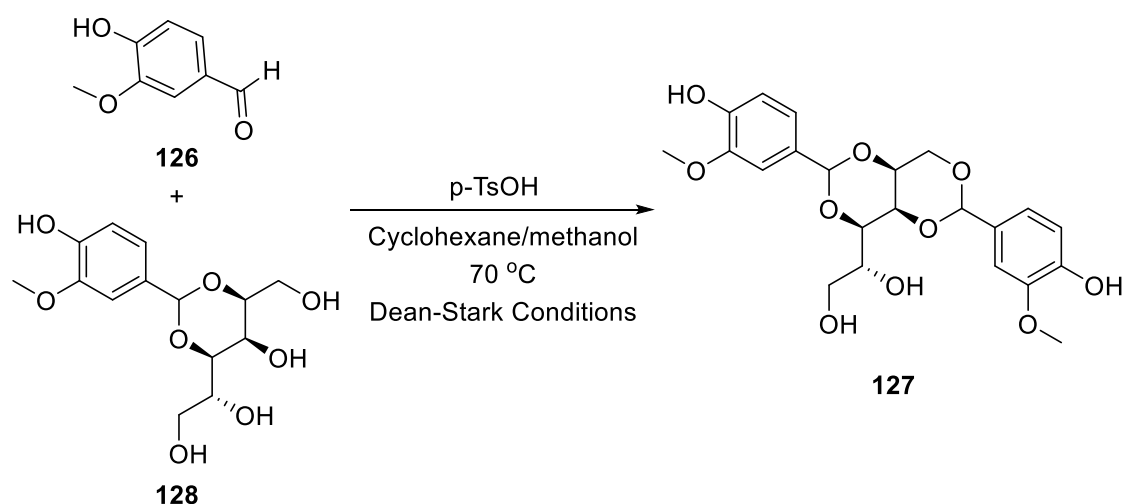


Scheme 11. The first proposed method for the synthesis of DBS-Van.

This reaction was allowed to proceed for 2 hours. After this time, a white and green solid had formed, which, on drying, underwent a colour change to blue-grey. When ¹H NMR was carried out for the crude product, peaks were present in the acetal region of the spectrum, indicating that some reaction had occurred. Additionally, MS indicated that a species with the expected mass for DBS-Van had been formed, along with MBS-Van.

Attempts were therefore made to purify the desired compound. However, this proved challenging, and no DBS-Van could be isolated – it is thought this is due to only a very small amount of DBS-Van being formed in the reaction. There may also be issues with the solubility of the product that impacted the purification steps.

A second method was therefore attempted for the synthesis of DBS-Van (**127**). First, MBS-Van (**128**) was synthesised by the method described previously. A second substitution was then attempted, again under Dean-Stark conditions (Scheme 12).



Scheme 12. The second proposed method for synthesis of DBS-Van.

After the reaction had proceeded for 2 hours, a white solid was suspended in a colourless solution. This solid was removed by filtration, and analysed by ^1H NMR and MS. Separately, the solvent was removed from the colourless solution *in vacuo*, to give a green oil. This oil was also analysed by ^1H NMR and MS.

This analysis indicated that the oil did not contain any of the desired DBS-Van. However, MS of the crude solid indicated that some DBS-Van was present, along with MBS-Van. Unfortunately, ^1H NMR showed that very little DBS-Van had been formed, with the majority of the material being MBS-Van. Although some attempts were made to separate out the desired product, these were not successful. As before, it was reasoned that only a very small amount of DBS-Van is formed, making isolation very challenging.

Before further investigations into this could be carried out, work from Amabilino and co-workers was published, in which some of the same compounds were synthesised, characterised and tested for gelation.²⁴² Amabilino and co-workers had interest in this class of materials as potential 'green gelators' given that they are synthesised from compounds extracted from renewable resource. Similarly to the work presented here, both MBS-Van and MBS-Cin were synthesised, and tested for gelation. As in our own work, neither were found to form hydrogels. Additionally, however, MBS-*i*Pr (Figure 110) was synthesised from 4-isopropylbenzaldehyde (cuminaldehyde, a component of essential oils found in cumin), and this system was found to form hydrogels. It is worth reflecting that the solubility of the aromatic substituent in cuminaldehyde is intermediate between cinnamaldehyde and vanillin, and would indicate that the precise tuning of solubility parameters is an essential feature in gelator discovery.

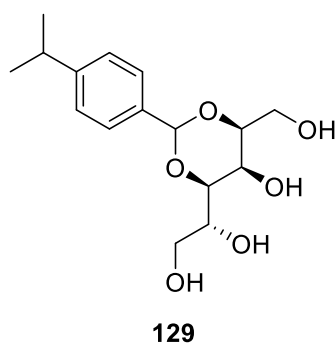


Figure 110. Structure of MBS-iPr.

As well as these investigations, Amabilino and co-workers reported attempts to synthesise DBS-Van – with similar problems being experienced as in our work. As a result of this published work, and the lack of success with our own efforts, this line of study was discontinued. It was, nonetheless, pleasing to see good agreement with work that had been going on elsewhere, giving us confidence in the methods we had been using.

4.3 Gelation Studies for MBS-SMe

We then moved on to investigate the gelation of MBS-SMe (Figure 111). The disubstituted version, DBS-SMe, had been previously investigated in our group by Nicole Whitelaw, and showed very interesting gelation properties, acting as a supregelator in alcohol/water mixtures at exceptionally low loadings (much lower than related DBS derivatives) with the resulting gels having good thermal stability, with the gels formed at these low concentrations not breaking down until relatively high temperatures are reached.²⁴³

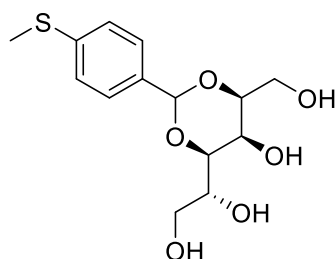


Figure 111. Structure of MBS-SMe.

For each sample, a known mass of MBS-SMe was added to a sample vial, and deionised water (0.5 ml) added. This was then heated until the solid was dissolved, and the resulting solution left to cool. Once cooled, gelation was tested, initially using the tube inversion method. A range of concentrations were investigated (Table 13).

Table 13. Gelation screening for MBS-SMe. Each sample used 0.5 ml water. Results: P=precipitate, I=insoluble, C=crystals, G=gel, WG=weak gel.

Concentration / wt/vol	Result
0.03	P
0.1	I/C
0.2	I/WG
0.3	I/G
0.4	I/G
0.5	I/G
0.6	I/G

At all but the lowest concentrations, MBS-SMe was partially insoluble on heating, with not all of the solid being dissolved. Despite this, at concentrations of 0.2% wt/vol and above, MBS-SMe did form an apparent cloudy hydrogel, (Figure 112), although at 0.2% wt/vol, this was very weak and collapsed readily. This novel hydrogel was therefore further investigated.



Figure 112. Apparent hydrogel formed by MBS-SMe, following a heat/cool cycle (0.3% wt/vol).

4.3.1 T_{gel} Studies for MBS-SMe

The thermal stability of the hydrogels was investigated. Samples were prepared by addition of a known mass of MBS-SMe to a sample vial, along with deionised water (0.5 ml). The samples were heated until the water was boiling, then left to cool. On cooling, opaque gels were formed. These were heated in an oil bath, at a rate of 1 °C a minute, and the T_{gel} determined by the tube inversion test (Table 14).

Table 14. T_{gel} values for MBS-SMe hydrogels, formed at a range of concentrations.

Concentration / % wt/vol	T_{gel} / °C
0.30	23
0.40	23
0.50	41
0.60	25

Between 0.30% wt/vol and 0.50% wt/vol, there was an increase in the T_{gel} from 23 °C to 41 °C – increases such as this are typically observed with increasing concentration. The decrease in T_{gel} at 0.6% wt/vol may be a result of some MBS-SMe not being fully dissolved – as concentration increases, this problem will become more significant. This insoluble material is not incorporated into the network, and indeed can disrupt it, hence weakening the overall hydrogel network, and reducing the T_{gel} .

Although the tube inversion test is a useful quick indicator for whether gelation has occurred, this alone is not sufficient to prove that a gel has formed; a highly viscous liquid may also be self-supporting, as can networks of crystals. Further tests must therefore be carried out to confirm that gelation has taken place.

4.3.2 Rheology of MBS-SMe

To confirm if a gel had indeed been formed, parallel plate rheology was carried out. Samples were prepared at a concentration of 0.4% wt/vol. The gelator was added to a mass spec vial, along with 0.5 ml of water. This was then heated until the solvent was boiling. On cooling, a white gel was formed. The gel was then transferred to the rheometer, using a spatula. Although attempts were made to form the MBS-SMe hydrogels in bottomless vials, these were not successful.

Initially, an amplitude sweep was run, with strain 0.001-100%, allowing the linear viscoelastic region (LVR) to be determined (Figure 113). The LVR occurs at a strain of under 0.01%, with the G' in this region around 400 Pa. This indicates that the MBS-SMe hydrogels only behave in a viscoelastic manner at very low strain.

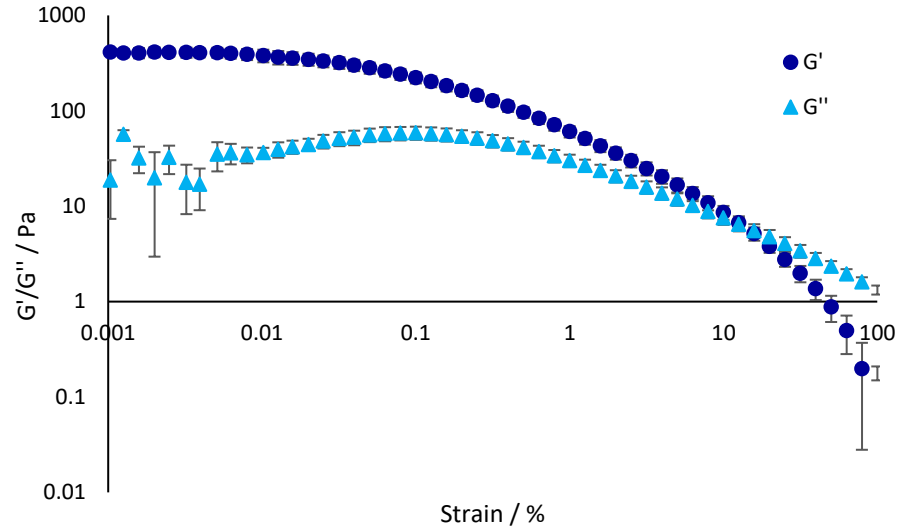


Figure 113. Amplitude sweep (0.001%-100%) for MBS-SMe hydrogels (0.40% wt/vol). Temperature 25 °C, frequency 1 Hz.

Additionally, a frequency sweep was performed, with the amplitude kept constant at 0.01%, and frequency varied from 0.1-100 Hz, was carried out (Figure 114). Samples were prepared as previously. For viscoelastic materials such as hydrogels, G' should be independent of frequency. For this material, G' is constant up to around 7 Hz, indicating that a gel is indeed present at lower frequencies. However, 7 Hz is a relatively low frequency for gel breakdown to be observed, which would agree with the view from amplitude sweep rheology that these gels are not particularly stable.

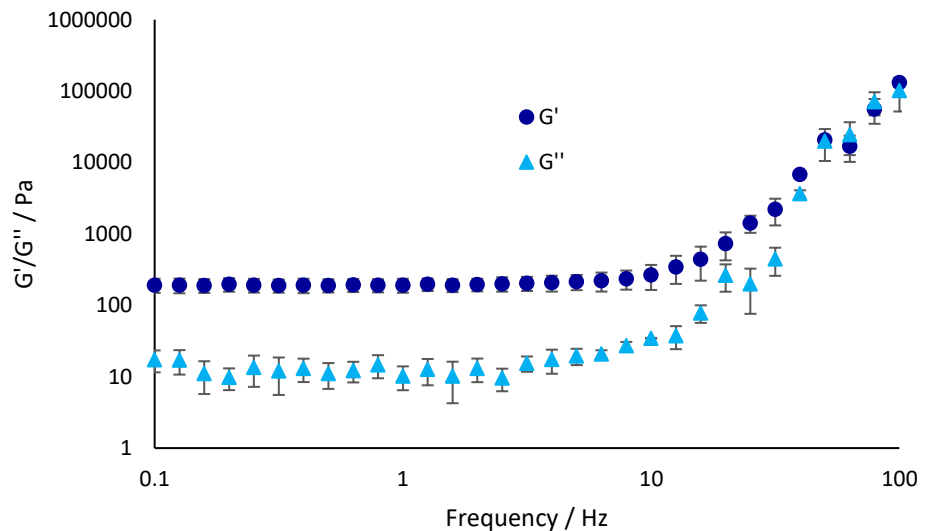


Figure 114. Frequency sweep (0.1 Hz-100 Hz) for MBS-SMe hydrogels (0.40% wt/vol). Temperature 25 °C, frequency 1 Hz.

In summary, therefore, rheological studies therefore indicated that a gel has indeed been formed by MBS-SMe, although it is mechanically fairly weak, probably as a result of the fact it likely contains some undissolved material that disrupts the overall network assembly and integrity.

4.3.3 Imaging of MBS-SMe

To further investigate the formation of the gel network, imaging was carried out, using both SEM and TEM. Samples were prepared at 0.40% wt/vol, and prepared for imaging as previously discussed. Although there are limitations when considering dried samples that have been imaged, as discussed in Chapter 2, they can still provide some useful insights into the nature of the material. Interestingly, the images obtained for the MBS-SMe hydrogels, (Figure 115), show both relatively rigid microcrystals, and a more flexible nanoscale network more typical of a gel. This suggests that the material has a mix of microcrystalline and gel-like character.

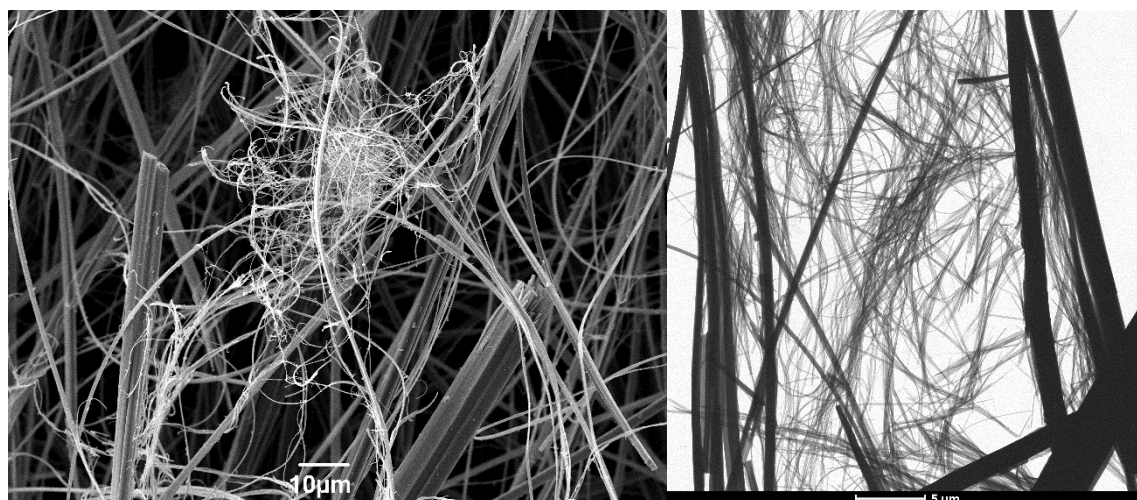


Figure 115. Images of the hydrogels formed by MBS-SMe (0.40% wt/vol). Left: SEM, scale bar 10 μm . Right: TEM, scale bar 5 μm .

Combined with the rheology, these results indicate that MBS-SMe is capable of forming hydrogels, although they do also have some microcrystalline character. The presence of some crystals is consistent with the weakening of the overall gel network, resulting in the reduced stiffness and generally low mechanical strength of these materials.

4.4 Synthesis of Non-symmetric DBS Derivatives

The initial target for the synthesis of this type of DBS derivative was DBS-CO₂H/CONH₂ (**130**) (Figure 116). As previously discussed, it is desirable to have a derivative that contains two separate functionalities, which can respond to different stimuli, and have different levels of

interaction with the environment, as this may increase the potential applications for any material formed.

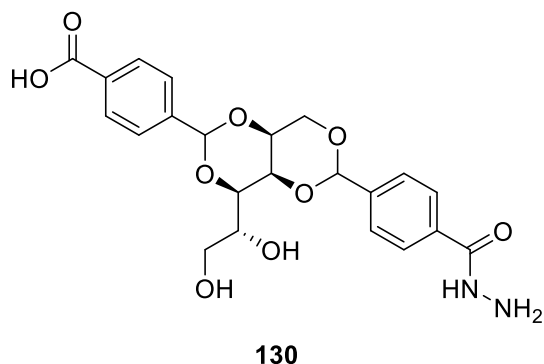


Figure 116. The structure of DBS-CO₂H/CONHNH₂.

A number of different methods were investigated for the synthesis of DBS-CO₂H/CONHNH₂. The first of these focussed on first synthesising the non-symmetric DBS-CO₂H/CO₂Me (**131**) (Figure 117), to then be converted into the desired product. For this initial step, two synthetic routes were explored.

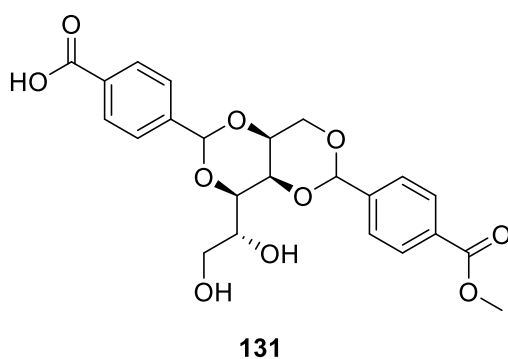
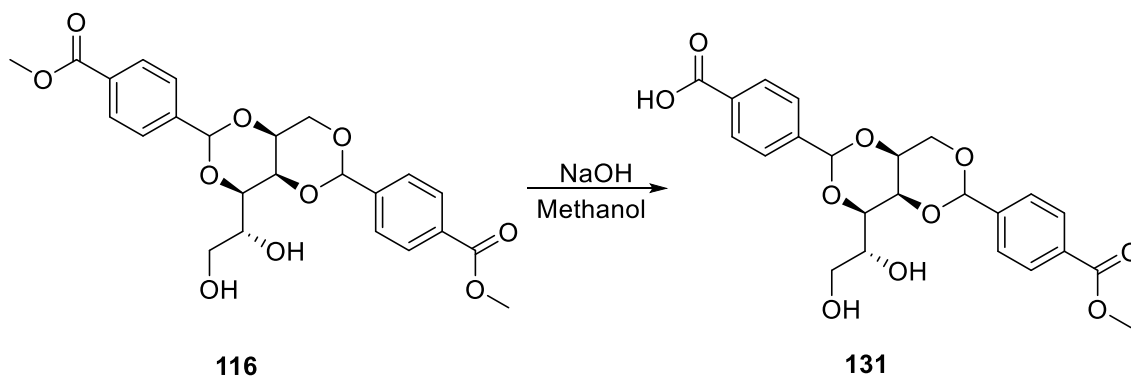


Figure 117. The structure of DBS-CO₂H/CO₂Me.

The first method is similar to that for conversion of DBS-CO₂Me to DBS-CO₂H, with NaOH being used to hydrolyse the ester (Scheme 13). However, rather than using an excess of NaOH, only one equivalent was used, with the aim that only one of the two ester groups would be converted. Although this would be unlikely to be selective, as the two wings on 1,3:2,4-dibenzylidene-sorbitol are not actually equivalent to one another, and it would be theoretically possible to hydrolyse the ester group on either wing, it was nonetheless reasoned that this may be a suitable starting point to determine the feasibility of the reaction.



Scheme 13. The synthesis of DBS-CO₂H/CO₂Me from DBS-CO₂Me. Although only one product is shown in the scheme, it is possible that hydrolysis could occur at either ester group.

This reaction was therefore attempted, with DBS-CO₂Me suspended in methanol, with one equivalent of NaOH, heated to reflux and left overnight. On cooling, a white solid precipitated. This was filtered and analysed by ¹H NMR and MS. Unfortunately, MS indicated that none of the desired product had been formed. The solvent was also removed from the filtrate *in vacuo*, and the resulting white solid also analysed. In this case, MS showed that although a mix of DBS-CO₂H and DBS-CO₂Me was present, there was no evidence of the mixed compound being present (Figure 118). Similarly, ¹H NMR showed resonances that could be attributed to either of these two compounds, and although it is possible any NMR peaks corresponding to DBS-CO₂H/CO₂Me could have been overlapping with these, it is more likely, when combined with the lack of evidence of formation in MS analysis, that none, or only very little, of the desired product had been formed.

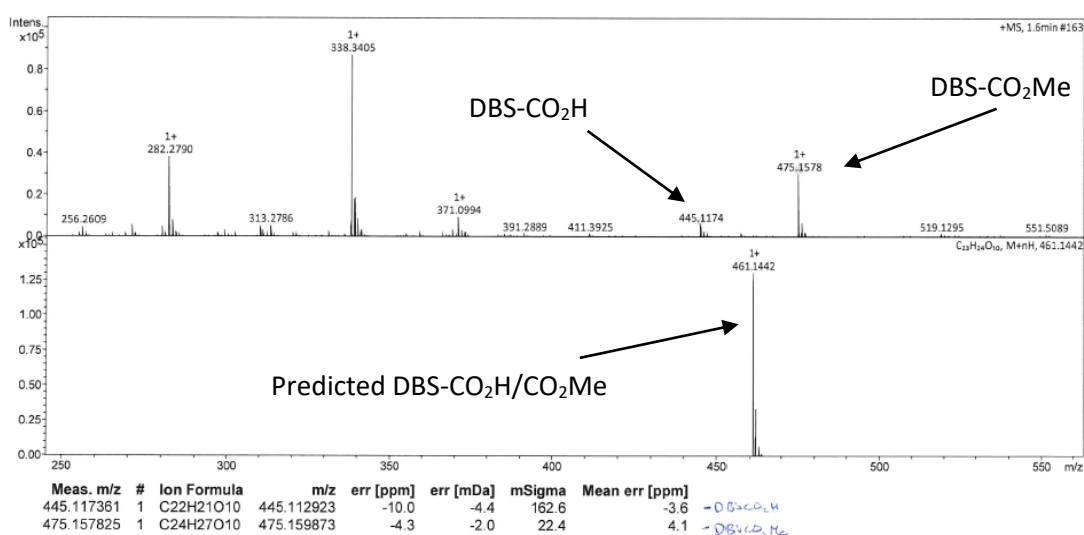
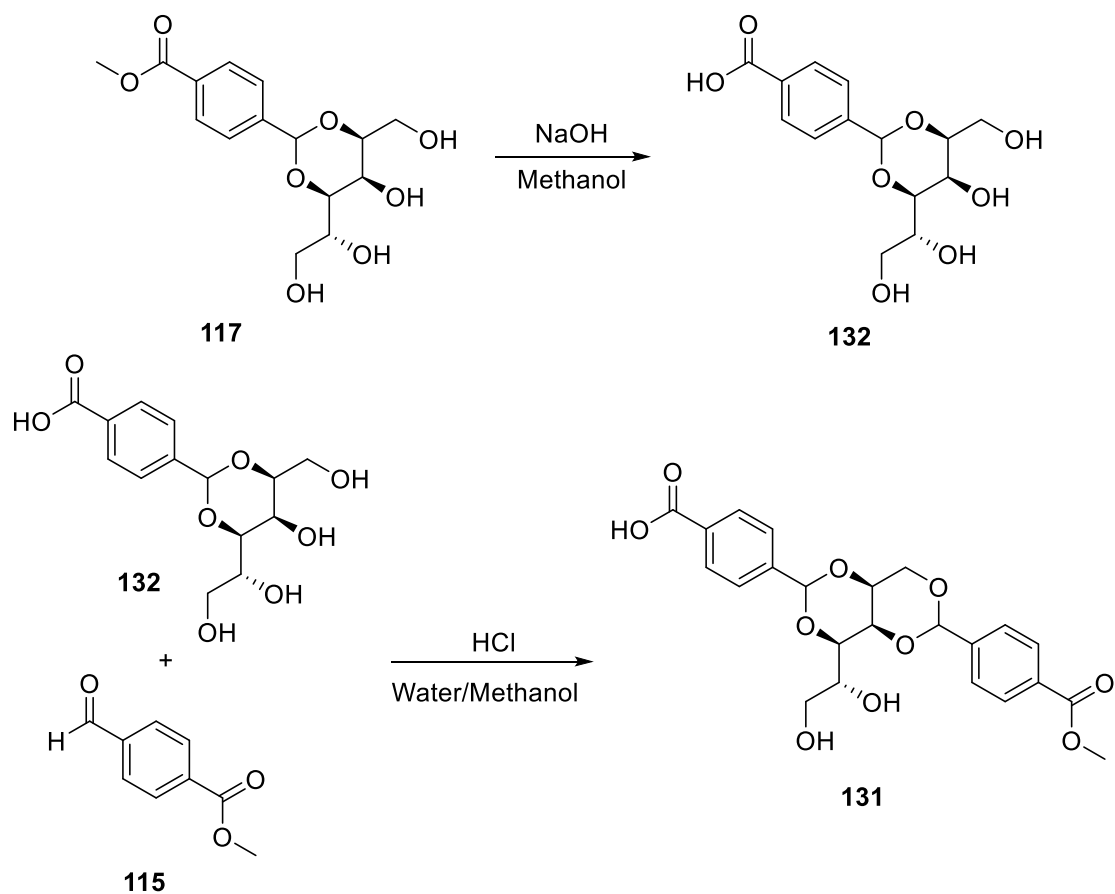


Figure 118. Mass spectrum for the attempted synthesis of DBS-CO₂H/CO₂Me. The bottom half shows the predicted output, the top half the experimental spectrum.

A second route, a two-step process, was therefore investigated. First, MBS-CO₂Me (**117**) would be converted to the carboxylic acid equivalent, MBS-CO₂H (**132**). This would then be further reacted

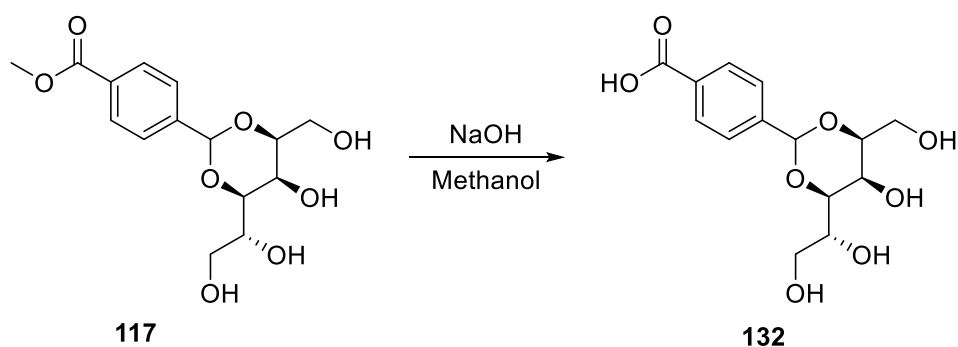
with 4-methylcarboxybenzaldehyde (**115**) to give the desired DBS-CO₂H/CO₂Me (**131**) (Scheme 14).



Scheme 14. The proposed two-step route for the synthesis of DBS-CO₂H/CO₂Me.

4.4.1 Synthesis of MBS-CO₂H

The synthesis of MBS-CO₂H was therefore carried out. Initially, MBS-CO₂Me (**117**) was prepared and isolated as described in Chapter 2. The second step (Scheme 15), was to convert the ester group to a carboxylic acid, by hydrolysis with NaOH.

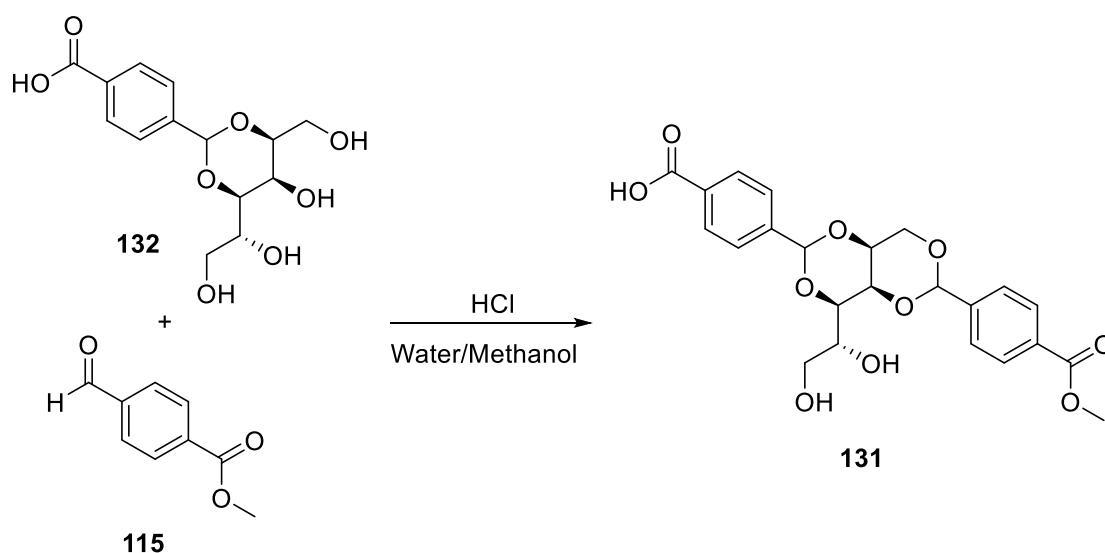


Scheme 15. The conversion of MBS-CO₂Me to give MBS-CO₂H.

Based on the method for the conversion of DBS-CO₂Me to DBS-CO₂H,¹⁰⁵ MBS-CO₂Me was suspended in methanol, and an excess of NaOH added. This was heated, and the reaction left to proceed overnight. Once the colourless solution had been allowed to cool, the solvent was removed *in vacuo*, to give a colourless oil. This was redissolved in water, and acidified using NaHSO₄. The solvent was again removed *in vacuo*, and the resulting white solid washed with a small amount of water. On analysis by ¹H NMR and MS, it was evident that the reaction had been successful, and MBS-CO₂H had indeed been formed in a 44% yield. This was indicated by the loss of the ester peak in the ¹H NMR spectrum, as well as the presence of a species at 314 in the mass spectrum. This compound was also investigated for gelation ability, with both a heat/cool cycle and a decrease in pH used as a trigger – however, only solutions were obtained.

4.4.2 Further Reaction of MBS-CO₂H

Once MBS-CO₂H (**132**) had been isolated, the next step of the reaction was to carry out a second acetal formation. It was hoped that this step (Scheme 16) would give the desired DBS-CO₂H/CO₂Me. Unlike for previous reactions, this was not performed under Dean-Stark conditions, but used alternative, milder, reaction conditions, modified from a known literature method for the synthesis of mono-benzylidene sorbitol (MBS).²⁴⁴ This was in an attempt to minimise the reverse reaction, and therefore reduce the level of mixing of the aldehydes.



Scheme 16. Synthesis of DBS-CO₂H/CO₂Me from MBS-CO₂H.

Therefore, 4-methylcarboxybenzaldehyde was dissolved in methanol, while MBS-CO₂H was suspended in water. These were combined, and the resulting suspension cooled to 0 °C, before

the addition of HCl as a catalyst. The reaction was allowed to warm to room temperature, and monitored by TLC.

After 24 hours, there was no change in the TLC, and therefore the reaction was heated to reflux. After 3 hours of heating, TLC indicated that some reaction had taken place, and the reaction was stopped. On cooling, a white precipitate was formed, and this was removed by filtration. This was analysed by ^1H NMR and MS. The ^1H NMR showed that a reasonable amount of aldehyde was still present, and other peaks overlapped with the expected for both DBS-CO₂H and DBS-CO₂Me. However, MS showed that some of the desired product had indeed been formed, with some MBS-CO₂H also still being present. It was therefore reasoned that, as the formation of an acetal is a reversible reaction, a mix of products had been formed.

Efforts were therefore made to isolate the desired DBS-CO₂H/CO₂Me. Initially the remaining aldehyde was removed, by washing with methanol. However, due to the remaining product being very insoluble, further purification proved very challenging.

4.4.3 Purification of DBS-CO₂H/CO₂Me

Due to the lack of solubility of the product, options for purification were limited. Therefore, HPLC was investigated, to both confirm the nature of the mixture, and to attempt to separate the components.

For this purpose, a number of different compounds were investigated, for comparison to the reaction mixture. These included MBS-CO₂H, DBS-CO₂H, DBS-CO₂Me, and the product itself. As the solubility of these compounds is generally poor, they were dissolved in DMSO, with a water/methanol mix as the solvent system. A number of different mobile phase compositions were used, but no good separation of the reaction mixture was achieved.

Therefore, further investigations into the makeup of the product were carried out, with LC-MS being used to determine what species might be making up the single peak visible in the HPLC trace. This again used a water/methanol mix as the solvent system, with the proportion of methanol was increased from 55% to 65% over the course of the run. Mass detection was set for 461, the mass of DBS-CO₂H/CO₂Me, and 474, the mass of DBS-CO₂Me (Figure 119).

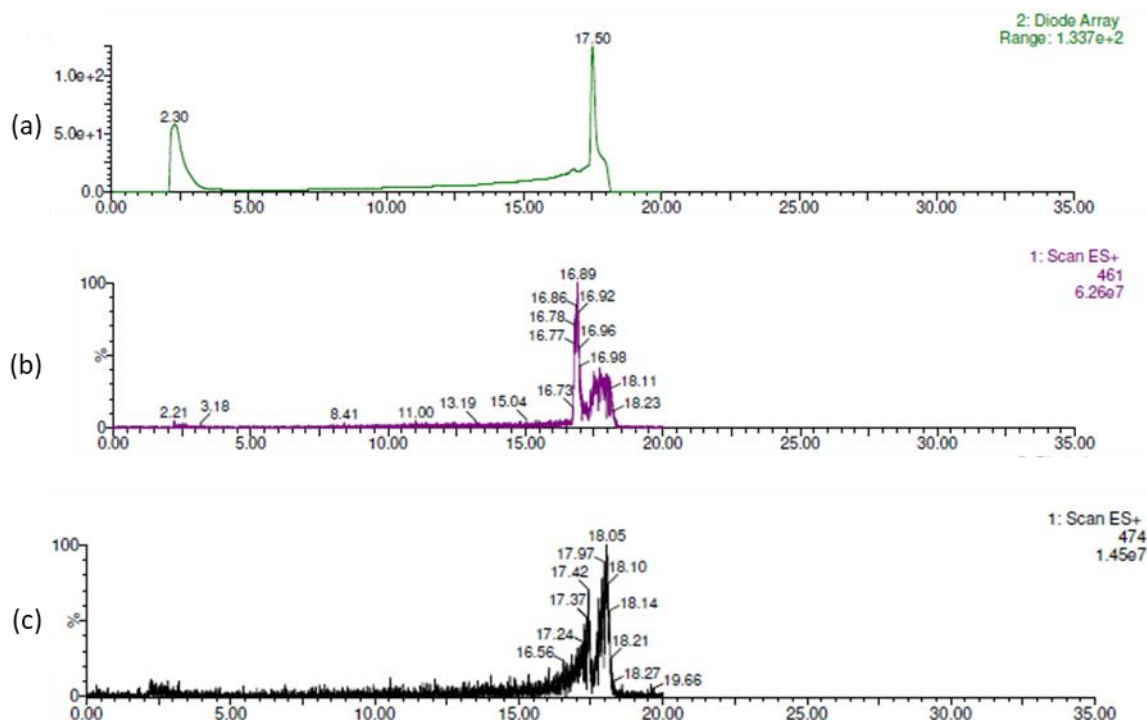


Figure 119. (a) HPLC trace for the product of the DBS-CO₂H/CO₂Me reaction; (b) LC-MS trace of the reaction mixture, scanning at a mass of 461; (c) LC-MS trace for the reaction mixture, scanning at a mass of 474.

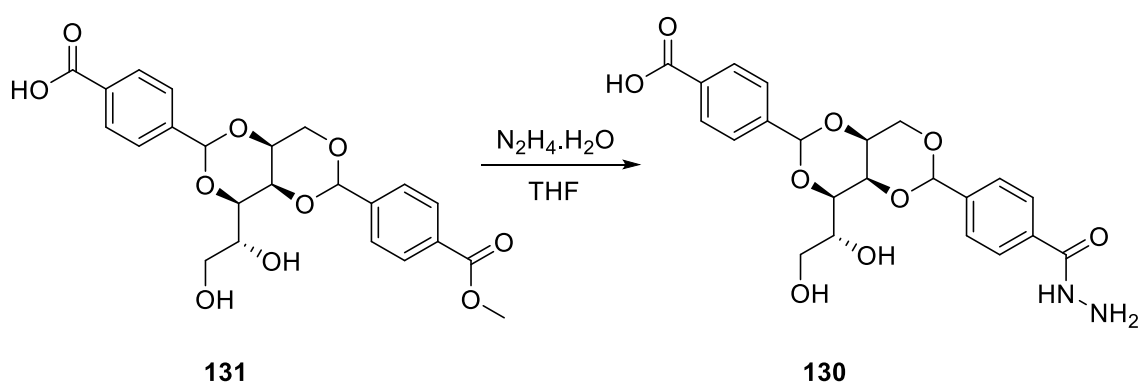
The LC-MS showed that the single peak visible in the HPLC trace contained both DBS-CO₂Me and DBS-CO₂H/CO₂Me. Although only one peak was visible, the mass scans indicated that there might be very slight separation of the two compounds, with DBS-CO₂H/CO₂Me eluting just slightly earlier than DBS-CO₂Me, as would indeed be expected in reverse phase HPLC, given its slightly higher polarity.

It was therefore attempted to separate these two components by prep HPLC, in the hope that even if some fractions were mixed, some pure DBS-CO₂H/CO₂Me might be obtained. Prep HPLC was carried out using the same solvent system as previously, with the prep column used an equivalent to the HPLC column used previously.

Fractions were collected if they contained any species with a mass of 461. These fractions were then concentrated, and reanalysed by LC-MS. However, none of the collected fraction showed any peaks, in the LC trace or the MS. As a result, attempts to purify the compound at this stage were halted.

4.4.4 Synthesis of DBS-CO₂H/CONHNH₂

Although pure DBS-CO₂H/CO₂Me (**131**) could not be obtained, it was decided to proceed to the next stage of the reaction with the mix of products, in the hope that, if a further reaction took place, the purification might be simplified. Therefore, the mix from the DBS-CO₂H/CO₂Me reaction was reacted with hydrazine monohydrate (Scheme 17).

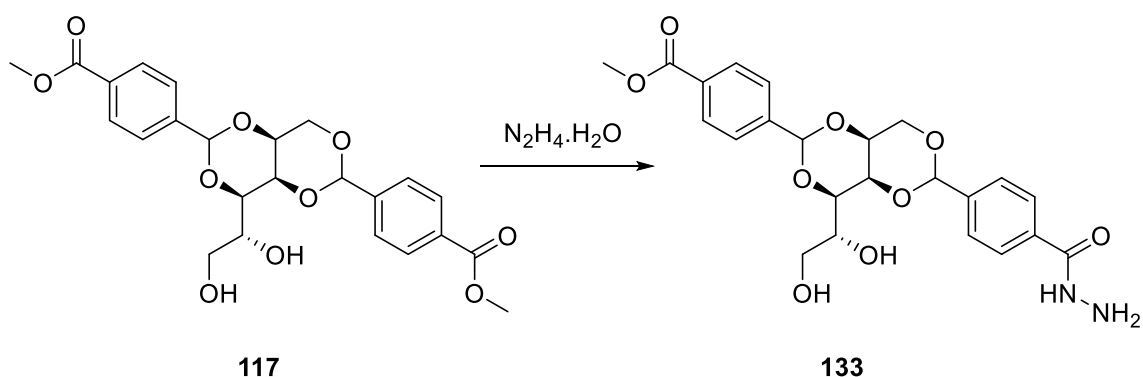


Scheme 17. The synthesis of DBS-CO₂H/CONHNH₂ from DBS-CO₂H/CO₂Me.

Initially, DBS-CO₂H/CO₂Me was suspended in THF, before an excess of N₂H₄·H₂O was added. This was then heated to reflux, and monitored by TLC. This reaction was carried out multiple times, with varying equivalents of hydrazine monohydrate and reaction times. In no case was any product formed, evidenced by TLC, which showed no additional spots, and ¹H NMR and MS, both of which showed no peaks that could be attributed to the desired product. Only starting material could be recovered.

4.4.5 Synthesis of DBS-CO₂Me/CONHNH₂

As an alternative to the problematic synthesis of DBS-CO₂H/CO₂Me, initial direct conversion of one of the esters in DBS-CO₂Me to a hydrazide was also investigated (Scheme 18). It was reasoned that this alternative route might give a product that was easier to separate, and therefore the reaction was attempted. Once again, we note that if successful, this approach would be expected to yield a mixture of different products as a result of the non-equivalence of the aromatic wings. Nonetheless, in gel formation, a mixture of this type could still be of very significant value.



Scheme 18. Synthesis of DBS-CO₂Me/CONHNH₂ from DBS-CO₂Me.

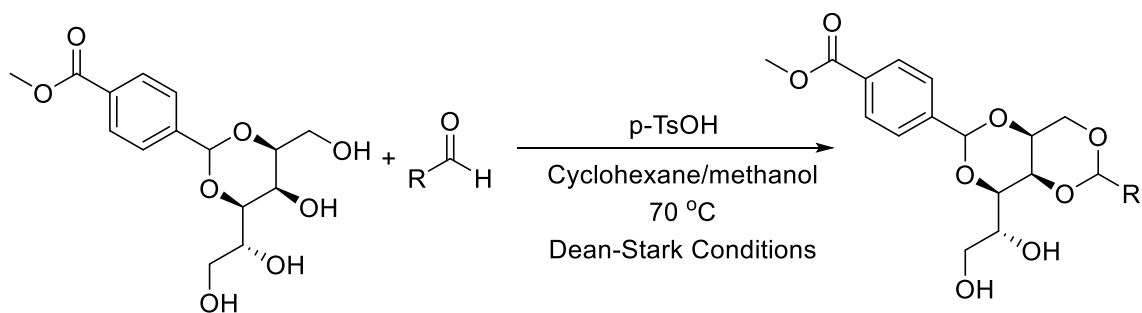
Therefore, DBS-CO₂Me (**117**) was suspended in THF, with one equivalent of N₂H₄·H₂O. This mixture was heated to reflux, and allowed to proceed overnight. When the reaction was analysed by TLC, ¹H NMR, and MS, there was no indication that any reaction had taken place. This was indicated by there being no additional spots in the TLC, no characteristic hydrazide peak in the ¹H NMR, and no species of the expected mass in MS.

This was not an especially surprising result. The conversion of DBS-CO₂Me to DBS-CONHNH₂ requires a significant excess of N₂H₄·H₂O.¹⁰⁶ As no reaction observed at all, and increasing the amount of hydrazine would likely just result in conversion of both esters, this method was not pursued any further.

As a result of the lack of success with this reaction, following the issues with the synthesis of DBS-CO₂Me/CO₂H, particularly with regards to purification, this line of research was not continued any further, and instead, alternative non-symmetric derivatives were investigated.

4.5 Conversion of MBS Derivatives

Following the difficulties of first synthesising a non-symmetric derivative, then converting the desired groups in the desired manner, a different method was investigated. This centred on the use of MBS derivatives, for which a reliable synthetic procedure had been developed, as starting materials. These were then simply reacted with a different aldehyde, in an effort to synthesise a simple non-symmetric DBS derivative. A general scheme for this reaction, with MBS-CO₂Me as the starting MBS derivative, is shown in Scheme 19.



Scheme 19. General scheme for the reaction of MBS-CO₂Me with a further aldehyde, for the formation of a non-symmetric DBS derivative.

Although in Scheme 19, the second substitution is only shown to occur at the 1,3 position, as the formation of an acetal is a reversible procedure, it is possible that there will be scrambling of the aldehydes, with the starting MBS derivative being broken down, and either aldehyde then being available to react in the more favourable 2,4 position. Additionally, it is then possible for either aldehyde to react in the second position. This results in there being a number of possible products theoretically being formed – these are indicated in Figure 120, with MBS-CO₂Me again used as the example starting material. However, such derivatives have previously been synthesised,²⁴⁵ and so this route was still considered to be worth pursuing.

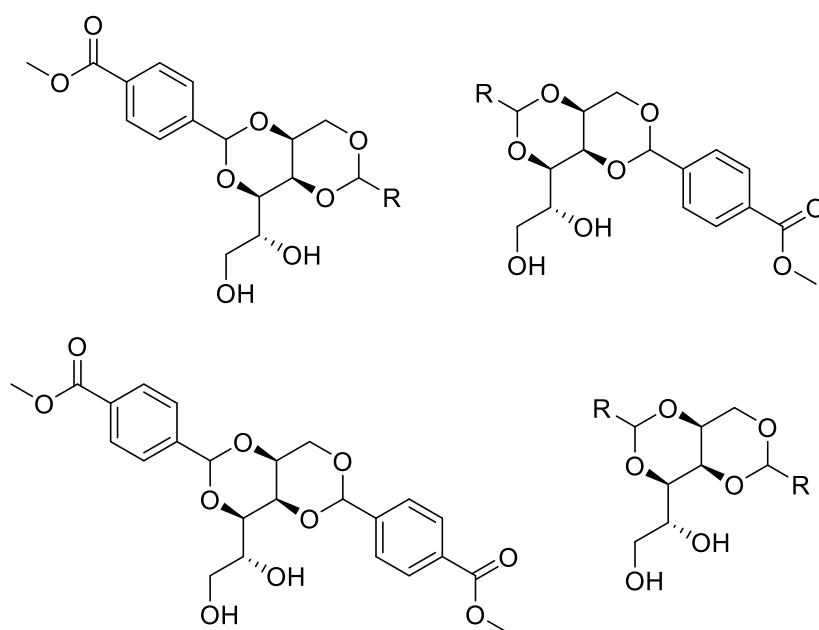
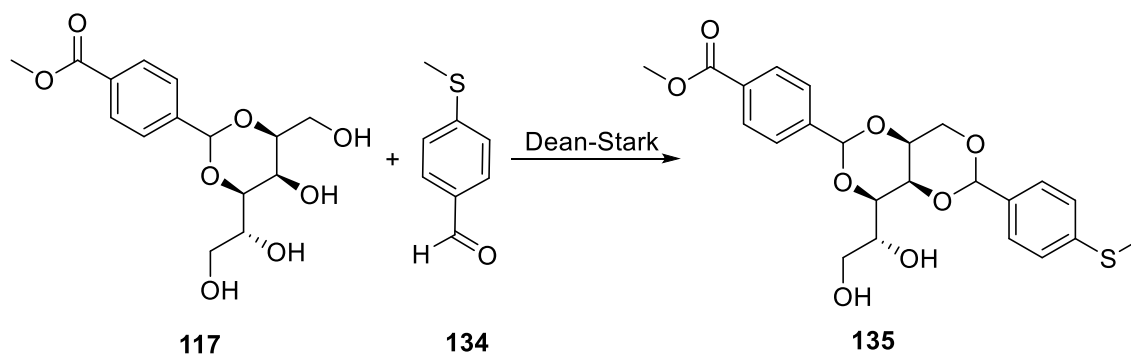


Figure 120. The DBS derivatives that may be formed with MBS-CO₂Me and a second aldehyde.

4.5.1 Synthesis of MBS-CO₂Me/SMe

The first aldehyde to be investigated was 4-(methylthio)benzaldehyde (**134**). This was chosen as previously both DBS-SMe and MBS-SMe had been synthesised successfully. Additionally,

MBS-SMe is capable of forming hydrogels, while DBS-SMe forms gels in various solvents, and shows interesting gelation characteristics. To try and minimise the level of mixing of the two aldehydes, the reaction was carried out under Dean-Stark conditions, which remove water, and should therefore reduce the likelihood of the reverse reaction occurring (Scheme 20).



Scheme 20. The reaction of MBS-CO₂Me with 4-(methylthio)benzaldehyde to form a DBS derivative.

The same general method was followed as the synthesis of a standard MBS or DBS derivative under Dean-Stark conditions, but with MBS-CO₂Me (**117**) used as the starting material in place of D-sorbitol. This was suspended in a cyclohexane/methanol mix and heated to 50 °C, before 4-(methylthio)benzaldehyde and *p*-TsOH, dissolved in methanol, were added dropwise. The reaction was then heated to 70 °C, and allowed to proceed for 1.5 hours, with more solvent added as necessary. After this time, an oily, green solid had formed. This was removed by filtration, and washed sequentially with methanol, hot water, DCM and ethyl acetate. However, the solid was found to be highly insoluble.

Analysis by ¹H NMR and MS indicated that the solid was likely to contain a mix of DBS-CO₂Me, DBS-SMe, and the desired DBS-CO₂Me/SMe (**135**). However, as the resulting solid had very poor solubility, the multiple components could not be separated by washing, and the solid could not be columned.

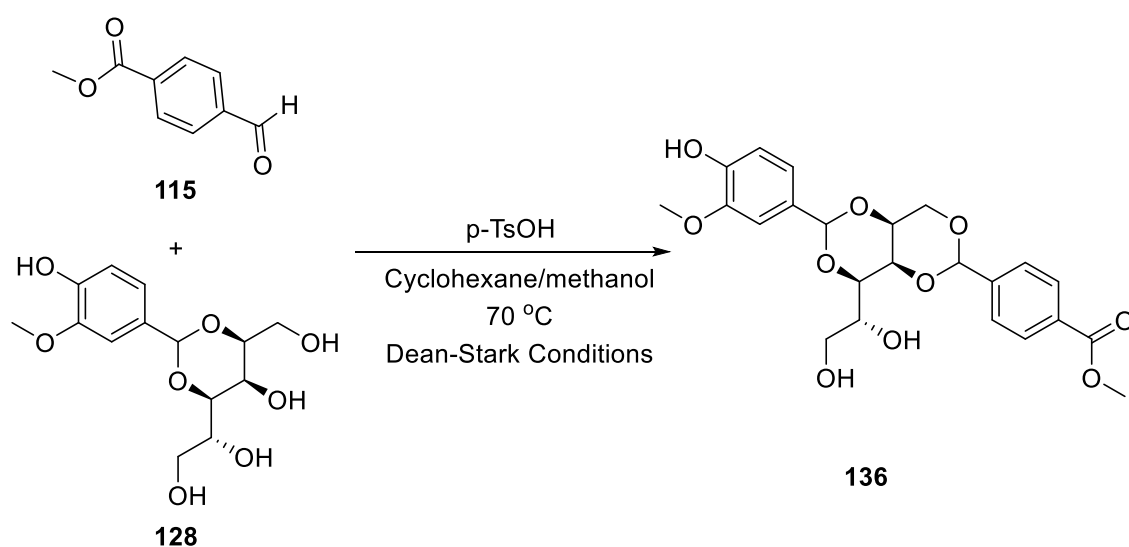
However, such non-symmetric derivatives have nonetheless previously been reported to be synthesised in a similar way for industrial applications.²⁴⁶ These are typically synthesised by simply mixing two different aldehydes and a sugar – with no significant attempts made to gain any selectivity. The resulting product mixtures are then tested for gelation, rather than the separated products.

It was therefore decided to test the mixture obtained from the reaction for gelation, despite the lack of success with separation. Initially a concentration of 0.1% wt/vol was used, with the solid added to a vial along with deionised water (0.5 ml). It was then attempted to dissolve the solid, by

both heating, and sonication followed by heating. In neither case was the solid dissolved, and no gels were formed.

4.5.2 Synthesis of DBS-Van/CO₂Me

Following attempts to synthesis DBS-CO₂Me/SMe, an alternative MBS derivative was investigated for use as the starting material – MBS-Van (**128**), as this could be obtained in good purity, and reasonable yield. In previous studies, MBS-Van was consistently too soluble to form gels, so it was thought that by performing an additional substitution, a more hydrophobic derivative, that could be capable of gelation, might be formed. Additionally, formation of a second acetal in the 1,3 position of the sugar has been shown to be highly unfavourable for vanillin – it was reasoned that this might reduce the number of possible products formed. Given that the formation of DBS-CO₂Me is well established, 4-methylcarboxybenzaldehyde (**115**) was chosen as the second aldehyde (Scheme 21).



Scheme 21. The synthesis of DBS-Van/CO₂Me. Although only one product is shown in the scheme, a number of different substitutions might be possible.

The same general method was followed as for the synthesis of DBS-CO₂Me, with MBS-Van suspended in a cyclohexane/methanol mix in place of D-sorbitol. This was heated to 50 °C, under Dean-Stark conditions, before the aldehyde and *p*-TsOH catalyst, dissolved in methanol, were added dropwise, and the temperature increased to 70 °C. The reaction was then allowed to continue for around 2 hours.

After this time, a white solid had been formed. This was removed by filtration, and MS carried out on this crude product. This indicated that there was some DBS-Van/CO₂Me (**136**) present. It was therefore attempted to isolate the product. However, the solid was very insoluble – with very

little being dissolved in any of the solvents investigated, including DMSO. This led to issues with both the purification, and the characterisation of the product. Although some attempts were made towards the purification, these were not successful, and no product could be isolated.

As a result of the lack of success with these reactions, particularly with regards to purification, this line of research was discontinued – as the desired products were formed with only very limited success, were extremely challenging to isolate, and did not form gels in the mixtures obtained.

4.6 Improved ^1H NMR Assignment of Protons in the Sugar Backbone

One issue faced previously had been incomplete or inaccurate assignment of the ^1H NMR spectra of DBS derivatives. As a final part of this synthetic work, we therefore resolved to fully assign the ^1H NMR spectrum of DBS- CO_2Me . This was achieved at high resolution using a 500 MHz spectrometer. Initially, the peaks corresponding to the alcohol protons were identified. This was achieved using the HMBC spectrum, showing 1J C-H coupling. The signals at 4.91 ppm and 4.46 ppm, each corresponding to one proton, were the only signals that did not couple directly to any carbon peak. This, combined with the splitting patterns of a doublet, and a doublet of doublets (appearing as an apparent triplet) respectively, indicated that these were indeed the OH protons in positions 14 and 15 respectively. Attempts were made to confirm this by a D_2O shake. However, due to the insolubility of DBS- CO_2Me in water, when D_2O was added to a sample dissolved in $\text{DMSO}-d_6$, a partial gel was formed, and there was substantial precipitation. A D_2O shake was therefore carried out with a sample of MBS- CO_2Me , and the corresponding peaks were no longer visible in the spectrum. The protons of the sugar backbone have been labelled for easier identification (Figure 121).

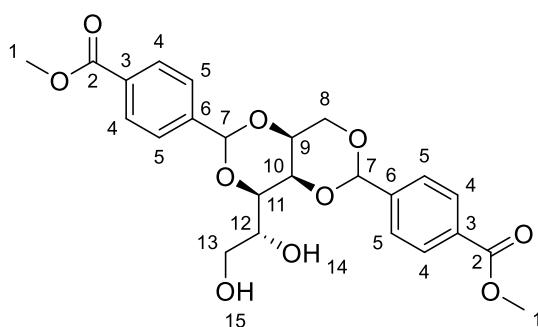


Figure 121. DBS- CO_2Me , with labels for NMR assignment.

Once the OH signals had been unambiguously identified, this in turn allowed identification of the corresponding carbon peaks, through the HSQC spectrum. This led to the identification of H_{12} , at 3.79 ppm and H_{13} , at 3.62 and 3.47 ppm (Figure 122). As the resolution of these peaks was good, the coupling constants could be determined, providing further evidence for these assignments.

A combination of the HSQC and COSY spectra then allowed for identification of H₁₁, and H₁₀, at 3.90 and 4.01-4.00 ppm respectively, and the corresponding carbons. However, precise assignment of H₈ and H₉ was not possible, as these signals form an overlapping multiplet at 4.26-4.18 ppm. The individual signals could not be identified even with the use of the 2D spectra.

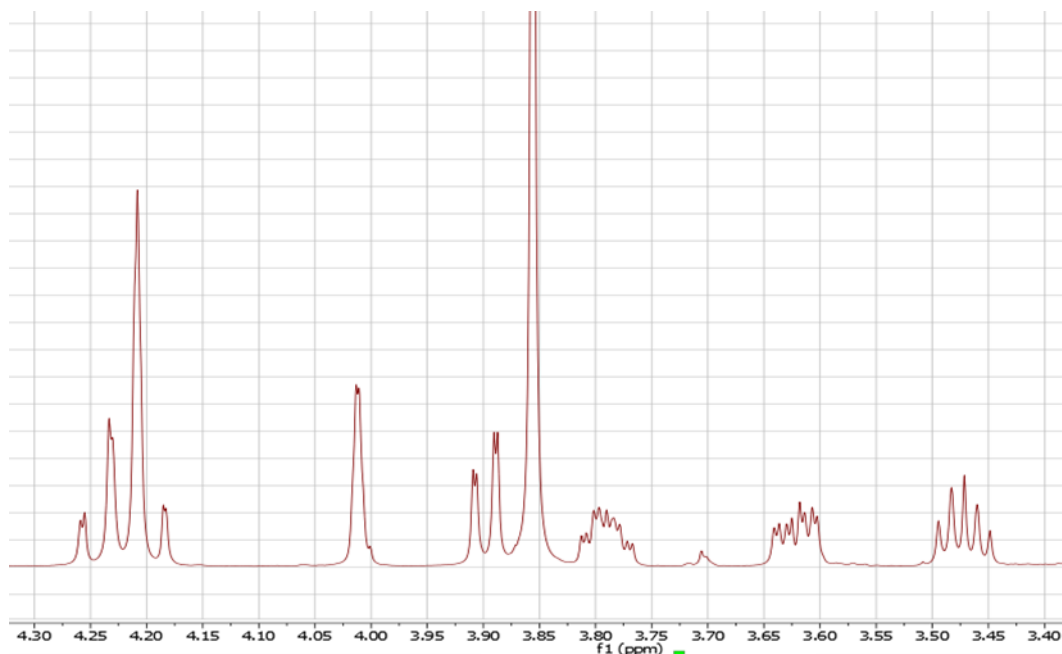


Figure 122. The sugar region of the ¹H NMR for DBS-CO₂Me.

In the aromatic region, improved resolution has led to the signal (corresponding to aromatic H₄) at 8.00-7.97 ppm appearing as a complex multiplet (Figure 123). Such multiplets are relatively common for para-substituted aromatics, and occur when the chemical shifts of two separate protons, that are coupled, are not significantly larger than the coupling values. This leads to second order effects in the coupled system. Additionally, the two aromatic rings of DBS-CO₂Me are very slightly different, further complicating the aromatic region of the spectrum. A second multiplet at 7.63-7.59 ppm is also present. This can be attributed to aromatic H₅, as the COSY spectrum indicates some coupling of these protons to the acetal proton.

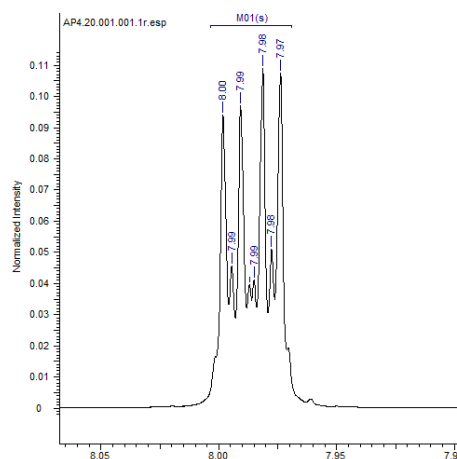


Figure 123. The complex multiplet at 8.00-7.97 ppm in the 500 MHz ^1H NMR spectrum for DBS- CO_2Me .

4.7 Conclusions and Future Work

The synthesis of a range of different MBS and DBS derivatives has been investigated, with varying levels of success in terms of both synthesis and gel formation.

A number of MBS derivatives were successfully synthesised, and if produced in a reasonable yield, these could generally be successfully isolated, and tested for gelation. MBS-Van and MBS-Cin are notable in having been fully produced from renewable resources, however, neither formed gels in any of the solvent conditions investigated. This was in-line with results from Amabilino and co-workers that were published after our work on these was complete. Although most of the isolated derivatives did not form hydrogels, MBS-SMe did form weak hydrogels. However, the gels that were formed were opaque in appearance, and detailed characterisation indicated the presence of microcrystals as well as a nanofibrillar network. Those derivatives that were only formed in very small amounts proved very challenging to isolate, often as a result of solubility limitations and these could not be obtained in great enough amounts to allow for gelation screening.

The synthesis of non-symmetric DBS derivatives was also attempted – and although some were formed in small amounts, these proved highly difficult to isolate, with the selectivity of the reactions also being very difficult to control. This made this line of research very challenging, and eventually, it was decided not to pursue it any further.

Although much of the research carried out here was ultimately not successful, there are still some useful conclusions to be drawn. In industry, DBS itself is widely used, but there is relatively little use of its derivatives, or MBS and its derivatives. While DBS is currently used mostly simply for the thickening or gelation properties, increasingly, there is interest in use of the derivatives for more high-tech applications, in a wider range of applications.

Interestingly, it is quite common in the patent literature to do things such as treat sorbitol with two different aldehydes and simply use the resulting product on the assumption that it is the product with one of each aldehydes attached.²⁴⁷ Our studies here would suggest that such assumptions are unlikely to be correct, and that such reports should therefore be treated with significant caution.

To help expand the application of sorbitol-based thickeners, a greater understanding of what functionalities may, or may not, be introduced into DBS based molecules is of considerable value. It is also important that, as DBS derivatives are desired to be used on a large scale, that any synthesis and purification is straightforward, with the desired product being obtained in a reasonable yield. In the longer term, this can help target the design of such molecules for selected applications.

5. Chapter 5 – Chirality of DBS-CONHNH₂

Many hydrogelators are based on molecules that occur naturally, such as amino acids²⁴⁸ or sugars,^{101, 249} which contain chiral centres. As a result, when these molecules are modified to give the gelator, this will also contain chiral centres.

Generally, the physical properties of gel-phase materials formed from two enantiomers will be the same, as the enantiomers have identical chemical properties. There are two key areas in which differences can be observed if there is chirality on the nanoscale – the morphology of the fibres, and the response to polarised light. This makes imaging and CD important techniques for monitoring the transfer of chirality from individual molecules to the nanoscale.²⁵⁰

As well as comparing the two enantiomers separately, the two may be combined, and the effects this has on self-assembly investigated. When two enantiomers are mixed in equal quantities, there are a number of possible outcomes. In many cases, the interactions between the two gelators are disruptive, giving a weaker gel, or no gelation at all.²⁵¹ In rarer cases, the interactions between the two enantiomers may be stronger, and this will result in the formation of a stronger gel.^{155b, 252}

In cases where self-assembly, and gelation, still occur, the two enantiomers may be interacting in a number of ways (Figure 124). There may be self-sorting, where the enantiomers form separate fibrils and fibres. These can then interact to form the overall gel. The gelators may also form a true racemate, or a pseudo racemate. In a true racemate, the gelators are arranged in a regular, alternating pattern, whereas in a pseudo racemate, the gelators are mixed, but randomly rather than in a repeating manner.¹⁵⁹

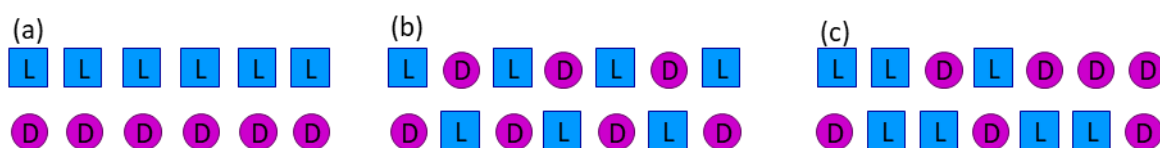


Figure 124. Different modes of assembly for a mix of two different enantiomers. (a) self-sorting; (b) true racemate; (c) pseudo racemate.

There has recently been increasing interest in chirality in gels, as there is some evidence that this can have an impact in their applications - as the different enantiomers can give different nanoscale morphologies, this can impact the properties of the bulk material. This is particularly true for interactions with other chiral compounds or nanostructures. This is especially relevant in biomedical applications, as most involve some form of chiral molecule. Hydrogels, and the

impacts of chirality, are therefore being investigated in a number of areas, including cell culture,^{60, 253} drug delivery,²⁵⁴ cancer therapy,²⁵⁵ and bio-imaging.²⁵⁶

In the case of cell culture, it has been shown that cell culture can be controlled by use of one gel enantiomer over another. Feng and co-workers have shown that cell adhesion can be controlled by changing the gelator enantiomer used – with left-handed nanofibres giving increased adhesion and proliferation, with the opposite effect observed with right-handed nanofibres. Some differences in cell differentiation were also observed between the two gel enantiomers – indicating that there is the possibility of controlling cell growth through the use of different enantiomers.

While the exact reason for the difference in cell behaviour was unclear, it was likely a result of either the difference in the helical nanofibres, or a chiral interaction between the cells and the gel fibres at a molecular level, an example of the use of different enantiomers in drug delivery, reported by Xu and co-workers has made use of the difference susceptibility of peptide based enantiomers to enzyme activity. The presence of the unnatural D-enantiomer in the peptide gelator results in increased stability to proteolytic enzymes – this effect is well known.²⁵⁷ As the gels do not break down as rapidly, release of active additives (in this case, isotopes for imaging) is slowed.

As discussed in previous chapters, derivatives of DBS are increasingly being developed for more high-tech applications. All of the studies thus far have made use of DBS derivatives synthesised from D-sorbitol – this is the naturally occurring sugar, and so is cheaper and more widely available. Indeed, DBS used in an industrial setting is derived from D-sorbitol. Obviously, for industrial use, where it is required to synthesise the molecules on a very large scale, it is clearly important to consider the cost of the starting materials.

However, there has been some interest in how a change in chirality affects DBS and its ability to form gels. The behaviour of D-DBS has been compared to a racemic mixture of D- and L-DBS, with the mixture found to be incapable of forming gels. However, L-DBS alone was not investigated. This makes it harder to properly understand the differences between the two enantiomers, compared to using the two individually.²⁵⁸

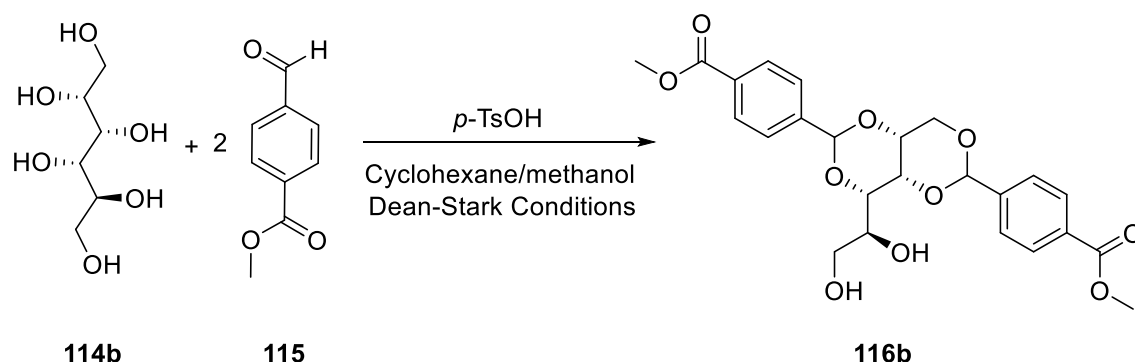
The DBS derivative DBS-CONHNH₂, which is capable of forming hydrogels, and has been investigated for a number of high-tech applications in our laboratory, is generally formed from D-sorbitol. However, in high-tech applications, bulk quantities of gelator are not necessarily required, and gelators based on L-sorbitol may potentially offer some advantages with regard to

stability against biodegradation, perhaps limiting interactions with biosystems. It was therefore decided to synthesise L-DBS-CONHNH₂, and confirm the two enantiomers have the same behaviour, with the exception of interactions with chiral additives or polarised light. Mixtures of D- and L-DBS-CONHNH₂ would also be investigated. Following the initial gelation studies, the two gelators would be used in some of their previously developed applications, including release of active molecules and cell culture, and any differences in behaviour between the two enantiomers identified.

5.1 L-DBS-CONHNH₂

5.1.1 Synthesis of L-DBS-CONHNH₂

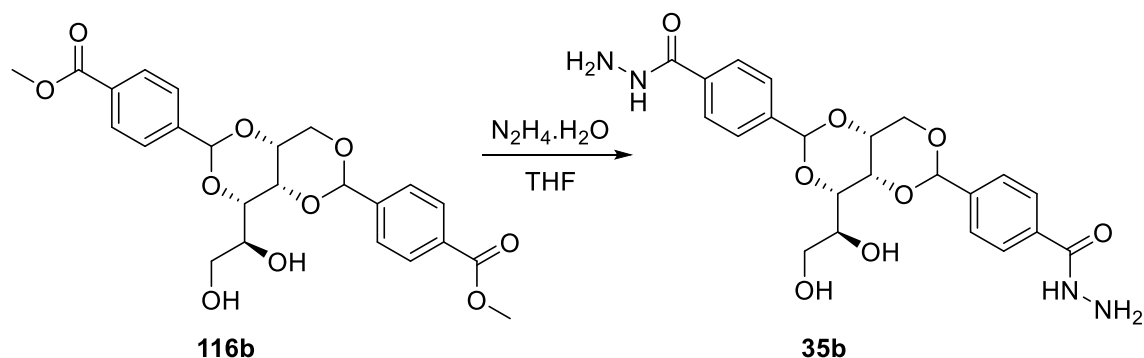
First, L-DBS-CO₂Me (**116b**) was synthesised. This was achieved following the same method as is used for the synthesis of D-DBS-CO₂Me (**116**) (see Chapter 2). To synthesise the L enantiomer, the D-sorbitol (**114**) normally used in the first step of the reaction was simply replaced with L-sorbitol (**114b**) (Scheme 22).



Scheme 22. Synthesis of L-DBS-CO₂Me.

L-Sorbitol was suspended in cyclohexane/methanol, and heated to 50 °C under Dean-Stark conditions. At the same time, 4-methylcarboxybenzaldehyde was dissolved in methanol with *p*-TsOH. This solution was then added to the sorbitol suspension, before the temperature was increased to 70 °C. The reaction was then allowed to continue for two hours, and a white solid obtained. This was washed first with cold methanol, to remove any unreacted aldehyde and the acid catalyst. This was followed by washes with boiling water, to remove any MBS-CO₂Me that had been formed, then boiling DCM, to remove any TBS-CO₂Me. The remaining white solid was analysed by ¹H NMR and MS, and confirmed to be L-DBS-CO₂Me, obtained in a yield of 57%.

The second step of the reaction is conversion of ester to hydrazide (Scheme 23). This was achieved by reaction with N₂H₄·H₂O.



Scheme 23. Synthesis of L-DBS-CONHNH₂.

L-DBS-CO₂Me (**116b**) was suspended in THF, before hydrazine monohydrate was added slowly. This was then heated to reflux, and left overnight. This gave a white solid, which was removed by filtration, and washed with water. This was analysed by ¹H NMR, and the presence of the characteristic hydrazide peak indicated that L-DBS-CONHNH₂ (**35b**) had indeed been formed, in an excellent yield of 90%. The characterisation of L-DBS-CONHNH₂ was in full agreement with that previously reported for D-DBS-CONHNH₂, with the exception of the [α]_D measurement, which was equal and opposite as would be expected.

5.1.2 Gelation Testing of L-DBS-CONHNH₂

Once L-DBS-CONHNH₂ had been formed, it was then tested for gelation ability. As this enantiomer has the same physicochemical properties as the more commonly used D-DBS-CONHNH₂ (except for its handedness) it would be expected that it should form hydrogels in exactly the same manner. Screening was therefore carried out to confirm this.

To test for gelation, a known mass of L-DBS-CONHNH₂ was added to a sample vial, and 0.5 ml of deionised water added. This was then sonicated for 15 minutes to form a suspension, before the solid was dissolved by heating. The resulting solution was then left to cool, before gelation was tested by tube inversion (Table 15).

Table 15. Gelation screen for L-DBS-CONH₂.

Concentration / % wt/vol	L-DBS-CONH ₂	D-DBS-CONH ₂
0.16	S	S
0.20	G	G
0.25	G	G
0.28	G	G
0.30	G	G
0.37	G	G

As expected, the two enantiomers showed the same ability to form hydrogels, with the same minimum gelation concentration of 0.20% wt/vol. Following these initial tests, the thermal stability of the gels was investigated. It is known that D-DBS-CONH₂ hydrogels are stable to high temperatures, with most concentrations having a T_{gel} value over 100 °C.

Hydrogels of L-DBS-CONH₂ were therefore prepared as previously, at the same range of concentrations. Once the gels had formed, the thermal stability was tested. The hydrogels were placed in a thermoregulated oil bath, and the temperature increased at a rate of 1 °C min⁻¹. The gels were monitored by the tube inversion test. The temperature at which a gel was no longer self-supporting under gravity was recorded as the T_{gel} . These could then be compared with the values for D-DBS-CONH₂ (Table 16).

Table 16. Thermal stability of L-DBS-CONH₂ and D-DBS-CONH₂. Note: T_{gel} values are only monitored up to 100 °C for hydrogels - above this, it would not be possible to determine if the loss of the gel is due to the breakdown of the network or the evaporation of the solvent.

L-DBS-CONH ₂ / % wt/vol	T_{gel} / °C	D-DBS-CONH ₂ / % wt/vol	T_{gel} / °C
0.20	72	0.20	66
0.25	97	0.25	96
0.28	100+	0.28	99
0.30	100+	0.30	100+
0.37	100+	0.37	100+

At the same concentrations, the T_{gel} values for the gels formed by each enantiomer are very similar, with the biggest differences observed at the minimum gelation concentration. As is common, the T_{gel} values increase with increasing gelator concentration, up to 100 °C.

5.2 Comparison of the Two Enantiomers

5.2.1 Rheology of D-DBS-CONH₂ and L-DBS-CONH₂

As discussed in previous chapters, the best method for gaining insight into the mechanical properties of a soft material is to carry out rheology. The hydrogels formed by the two enantiomers were therefore investigated by parallel plate rheology.

For rheology, samples were prepared at a concentration of 0.28% wt/vol, for both the D- and the L- enantiomers. These gelators were weighed into vials, sonicated for 15 minutes to give a suspension, and the solids then dissolved by heating. While the solutions were hot, they were transferred to a bottomless vial attached to a petri dish. Once the solutions had cooled, and a translucent gel had formed, for both the enantiomers, the bottomless vial could be removed and the gel disc transferred to the rheometer for analysis.

The first rheology experiment carried out was the amplitude sweep – this allows for the LVR for the hydrogel to be determined, and also gives information on the stiffness and resistance to strain of the gel. For each enantiomer, this was carried out with a strain of 0.05-100%, with frequency kept constant at 1 Hz (Figure 125).

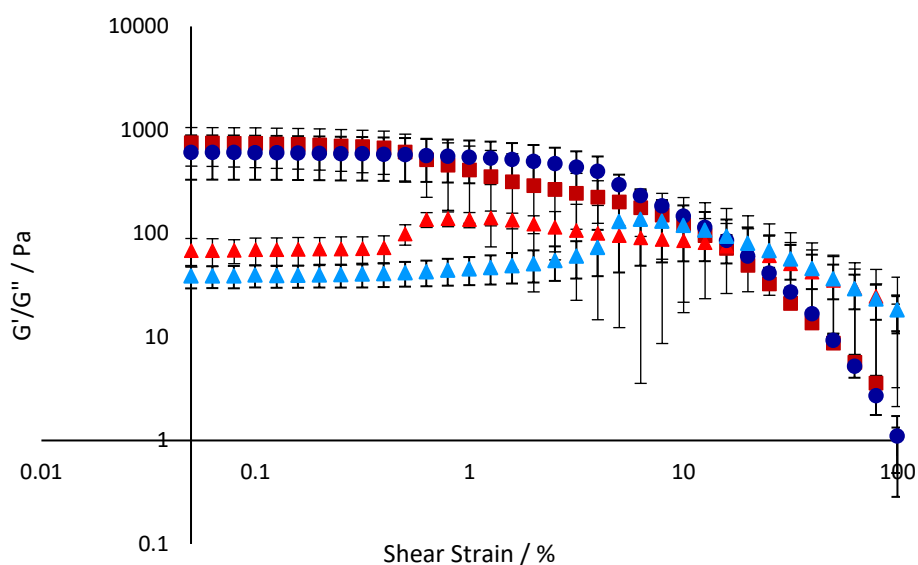


Figure 125. Amplitude sweep (0.05%-100%) for D-DBS-CONH₂ and L-DBS-CONH₂ hydrogels, gelator concentration 0.28% wt/vol. Dark blue circles: D-DBS-CONH₂ G', Light blue diamonds: D-DBS-CONH₂ G'', Dark red squares: L-DBS-CONH₂ G', Light red triangles: L-DBS-CONH₂ G''. Temperature 25 °C, frequency 1 Hz.

As would be expected, the values of G' in the LVR are very similar for the two enantiomers, indicating that the hydrogels formed have similar stiffness. The two gels also have a very similar

crossover point at around 8% strain, showing very similar resistance to strain. The two materials formed by the two enantiomers are therefore mechanically very similar.

As well as the amplitude sweep, a frequency sweep was also carried out. When a material is viscoelastic, the G' value will be independent of frequency. The frequency sweep for the two hydrogels was carried out with frequency varied from 0.1-100 Hz, with the strain kept constant at 0.02% (Figure 126).

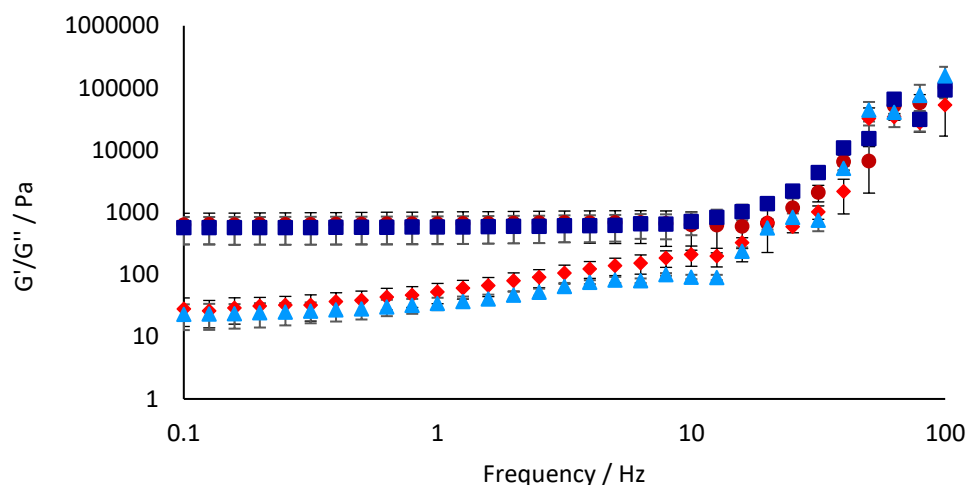


Figure 126. Frequency sweep (0.1 Hz-100 Hz) for D-DBS-CONH₂ and L-DBS-CONH₂ hydrogels, gelator loading 0.28% wt/vol. Dark red circles: D-DBS-CONH₂ G', Light red diamonds: D-DBS-CONH₂ G'', Dark blue squares: L-DBS-CONH₂ G', Light blue triangles: L-DBS-CONH₂ G''. Temperature 25 °C, amplitude 0.1%.

As with the amplitude sweep, the two hydrogels showed very similar values of G' – as expected, this remains constant, despite increasing frequency, to around 10 Hz. However, the G'' value starts increasing from about 1 Hz. Once a frequency of 10 Hz is reached, the gels are hardening and then breaking down, and therefore no longer behave in a viscoelastic manner. This breakdown occurs at a very similar frequency for both enantiomers of the gelator.

5.2.2 Imaging of D-DBS-CONH₂ and L-DBS-CONH₂

To compare the morphologies of the nanofibres formed by the two gelators, both TEM and SEM imaging were carried out. For this, L-DBS-CONH₂ samples were prepared at a concentration of 0.28% wt/vol. These gels were then prepared for imaging as described in previous chapters, and the resulting images could be compared with those already obtained for D-DBS-CONH₂ (Figure 127).¹⁷³ As previously discussed, there are considerations to take into account when imaging gels, primarily due to the drying process. However, imaging is still a valuable method for understanding

self-assembly, particularly if comparing two chemically-related samples that have been prepared in exactly the same way.

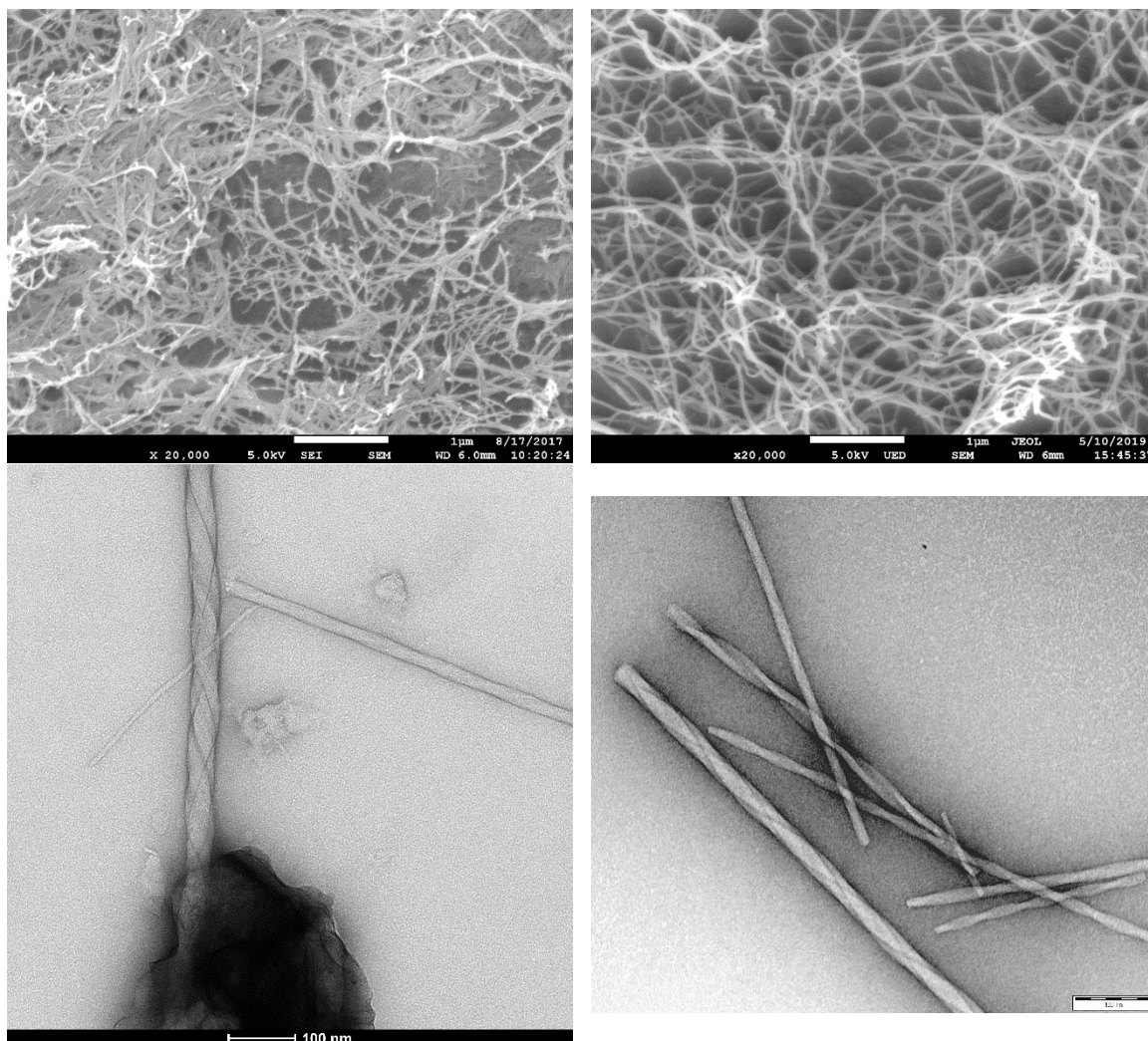


Figure 127. Imaging of *L*-DBS-CONHNH₂ (0.28% wt/vol) and *D*-DBS-CONHNH₂ (0.4% wt/vol) hydrogels. Top: SEM images, magnification $\times 20,000$, (left: *L*-DBS-CONHNH₂, right: *D*-DBS-CONHNH₂). Bottom: TEM images, scale bar 100 nm, (left: *L*-DBS-CONHNH₂, right: *D*-DBS-CONHNH₂).

In both cases, the SEM images show that a network of fibres has indeed been formed. These images also indicate that the network is quite highly branched, with fibres of a similar size (ca. 30 nm in diameter) being formed from the two enantiomers. In the TEM images, it is possible to observe the helical nature of the fibres formed, although any change in the handedness of the fibres cannot easily be determined. From the images obtained, the two enantiomers do appear to give very similar morphologies of nanofibre – suggesting that the self-assembly process does not change significantly on changing the enantiomer. This is as expected – the only change would be in the handedness of the fibre. In this case, evidence for this is inconclusive, as the pitch of the helix is wide, and there appear to be left and right handed helical grooves equally spaced on the nanofibers in both cases, making it difficult to determine which way the helix is twisting.

5.2.3 Circular Dichroism Studies for D-DBS-CONHNH₂ and L-DBS-CONHNH₂

5.2.3.1 Introduction to Circular Dichroism

As discussed in Chapter 2, circular dichroism (CD) is a useful tool for observing the self-assembly of nanoscale structures, due to changes in the magnitude of the observed signal when nanostructures are present. Circularly polarised light is directed through the sample, alternating between right-handed and left-handed. Any sample with no chirality will not give a signal in the CD spectrum, whereas a chiral molecule will show a signal in the same region as its UV absorbance. However, molecules that are not self-assembled generally give only a low intensity signal. If the individual molecules assemble to form a chiral nanostructure, the CD signal becomes much stronger. It is therefore possible to both observe the formation or breakdown of nanofibres, and to determine if any chirality in an individual gelator has been translated to the nanoscale.¹⁹²

The two forms of polarised light are affected differently depending on the chirality of the sample. Each will pass through the sample at a different speed, with the absorbance and wavelength also affected. These differences can be measured, and converted to give ellipticity. When nanostructures have been formed, the ellipticity will generally be of a greater magnitude. When two samples are formed from two enantiomers, the ellipticity is expected to be of equal, but opposite, magnitude. This makes this technique particularly valuable for observing the behaviour of two different gelator enantiomers. Variable temperature CD is especially useful – at low temperature, the nanostructure is present, and the ellipticity is large. As temperature is increased, the structures begin to disassemble, and rather than the supramolecular structure, there are individual molecules in solution. This should correspond with a decrease in ellipticity and helps confirm that the CD signal is indeed associated with the self-assembled state.

5.2.3.2 CD Studies of D-DBS-CONHNH₂ and L-DBS-CONHNH₂

The two enantiomers were therefore investigated by CD spectroscopy. Samples were prepared at a concentration of 0.10% wt/vol – although this is below the minimum gelation concentration for DBS-CONHNH₂, samples prepared at a higher loading were found to be too concentrated to give useful spectra. For CD, a transparent sample is required – for DBS-CONHNH₂, this means a lower concentration is required. The loading chosen is only just below the minimum gelation concentration, and as such, there is still sufficient gelator for nanostructures to form. As normal, the samples were prepared by first sonicating for 15 minutes, then heating to dissolve the solid. While this solution was hot, it was transferred to a warmed CD cuvette, in which self-assembly could occur. This process was carried out for both enantiomers.

The samples were then analysed by variable temperature CD. The first measurements were taken at 20 °C, with the following measurements taken at 5 °C intervals, up to a temperature of 90 °C. Both enantiomers showed a CD band with a maximum absorbance at around 272 nm (Figure 128). This wavelength is consistent with the organisation of the aromatic wings of DBS-CONH₂ into a local chiral environment on self-assembly. As expected, at lower temperatures, this band had a greater magnitude of ellipticity, indicating that self-assembling nanostructures are indeed present. On heating, the CD band slowly decreased in intensity and shifted to slightly lower wavelengths. The biggest change in ellipticity, indicating disassembly of the supramolecular structures, occurred between 75 °C and 85 °C – in line with the T_{gel} value observed for DBS-CONH₂ hydrogels. Importantly, the CD spectra observed for D-DBS-CONH₂ and L-DBS-CONH₂ were equal and opposite in ellipticity, reflecting the enantiomeric relationship of the self-assembled nanostructures formed in each case.

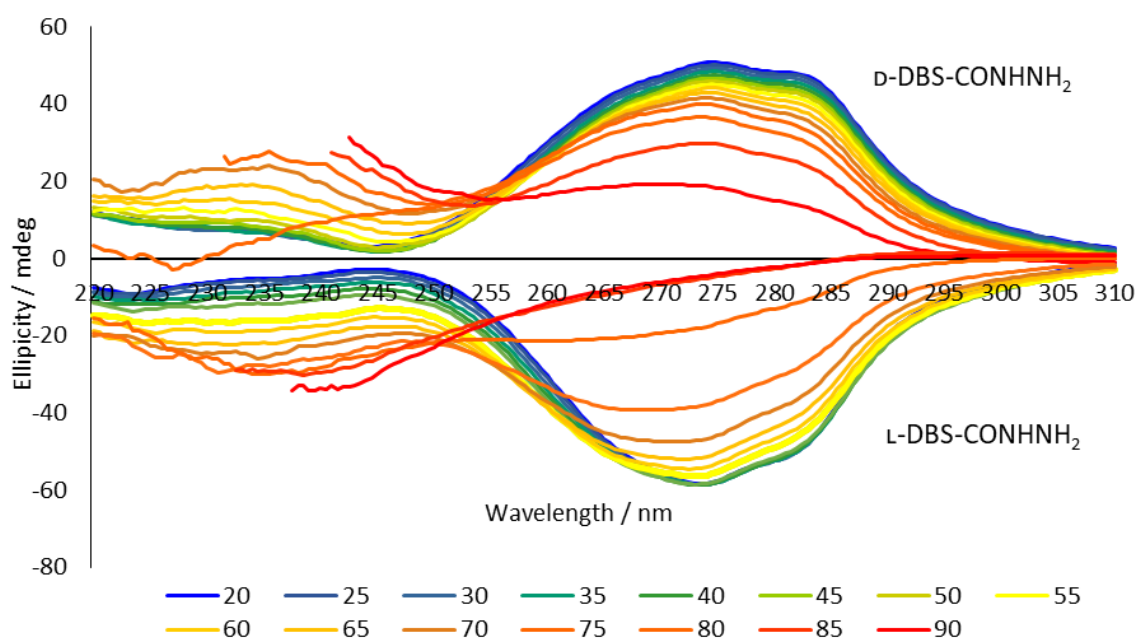


Figure 128. The CD spectra for D-DBS-CONH₂ and L-DBS-CONH₂. The highest temperatures are in red, and the lowest in blue.

When recording CD spectra, it is important to consider the absorbance of the sample – if this is too high, too little light will reach the detector, and reliable spectra will not be obtained. This is known as oversaturation. The level of light reaching the detector can be monitored by observing the high tension (HT) voltage, as this is roughly proportional to absorbance. As a result, HT is typically measured alongside the ellipticity. If the HT value rises about 600 V, this is an indication that the absorbance is too high for reliable readings to be obtained. In this case, only a small portion of the measurements were over 600 V – the corresponding ellipticity values have been

removed from the analysis. All the affected points were at wavelengths of less than 250 nm, and therefore the overall analysis was not impacted.

5.3 Mixtures of D-DBS-CONHNH₂ and L-DBS-CONHNH₂

As would be expected, the two enantiomers of DBS-CONHNH₂ both formed gels, which had comparable physical properties such as T_{gel} values and mechanical strengths as described above. The key difference was observed in CD analysis, with the hydrogels formed by each enantiomer having an equal and opposite impact on circularly polarised light.

Following comparison of the hydrogels formed from the two gelators, the impact of mixing the two enantiomeric gelators on the properties of the gels was investigated. As discussed earlier, when two enantiomers of a gelator are mixed, the resulting interactions may be destructive, resulting in either a weaker gel being formed, or gelation not occurring at all. Alternatively, the interactions between the two different enantiomers may be stronger, resulting in a stronger gel than with a single enantiomer. Indeed for the parent compound DBS it has been reported that mixing enantiomers disrupts the gel forming ability, with no gel state being observed.¹⁶ We therefore wanted to determine the impact of mixing the two enantiomers on the resulting hydrogels – if indeed gels were formed.

5.3.1 Gelation Studies and Thermal Stability

Different ratios of the two enantiomers, D-DBS-CONHNH₂ and L-DBS-CONHNH₂, were investigated. These samples were prepared by addition of a known mass of each of the two gelators to a vial, followed by sonication, then heating until all of the solid was dissolved. Once the sample had cooled, gelation was tested by the tube inversion test (Table 17). The total concentration of gelator was kept constant at 0.28% wt/vol.

Table 17. Gelation screen for mixtures of D-DBS-CONHNH₂ and L-DBS-CONHNH₂. The percentage of each gelator shown is the proportion of the total gelator, at a loading of 0.28% wt/vol. G=Gel.

D-DBS-CONHNH ₂ / %	L-DBS-CONHNH ₂ / %	Gel?
90	10	G
80	20	G
70	30	G
60	40	G
50	50	G
40	60	G
30	70	G
20	80	G
10	90	G

In contrast to the previous reports for unmodified DBS,¹⁶ at all proportions of the two gelators, a gel was still formed. These gels were somewhat less reproducible than those formed from the individual enantiomers, suggesting that the gels may be weaker (see below). This indicated that mixing the two enantiomers might lead to disruptive interactions, although not to such a level as to prevent a gel from forming.

These mixed enantiomer gels were therefore further investigated, with the thermal stability initially being explored. The hydrogels were prepared as previously, with the total gelator loading kept at 0.28% wt/vol. These gels were then heated, in a thermoregulated oil bath, at a rate of 1 °C min⁻¹, and the temperature at which they broke down was monitored by the tube inversion test (Table 18).

Table 18. T_{gel} values for D-DBS-CONHNH₂ and L-DBS-CONHNH₂ hydrogels. Total gelator loading 0.28% wt/vol.

L-DBS-CONHNH ₂ / %	T_{gel} / °C
0	82
10	50
20	35
30	43
40	31
50	47
60	52
70	38
80	34
90	48
100	78

For all of the mixtures, the T_{gel} value was significantly lower than that observed for the hydrogels formed from a single enantiomer (ca. 80 °C at this concentration). This indicates that the mixture of the two enantiomers results in interactions that are weaker, and therefore an overall network that is also weaker. This results in the lower thermal stability of the mixed enantiomer gels (Figure 129). However, there was no evidence of very significant differences depending on the specific ratio of the two enantiomers. This might suggest that even a small amount of the ‘wrong’ enantiomer disturbs the assembly process and that a new gel structure therefore results.

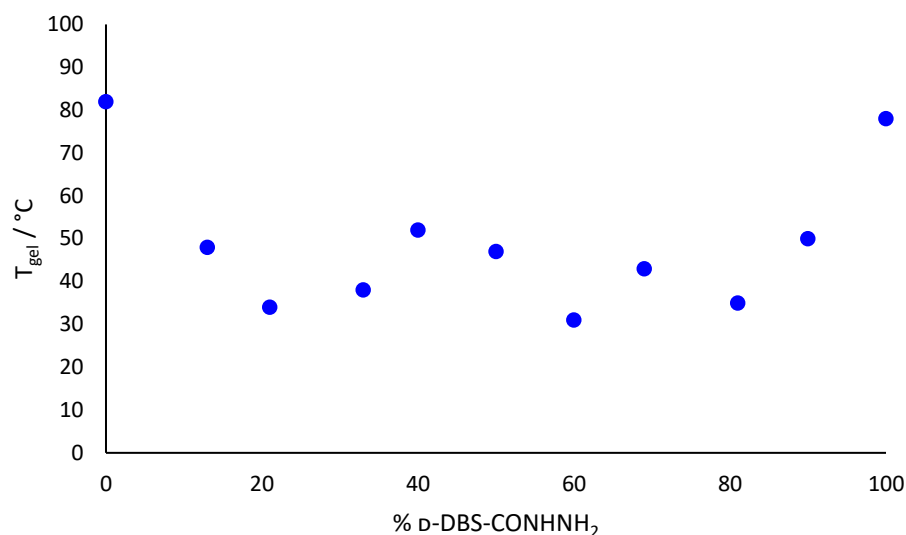


Figure 129. T_{gel} values for D-DBS-CONH₂ and L-DBS-CONH₂ hydrogels, and the hydrogels formed from mixtures of the two enantiomers.

To further investigate the impact of mixing the two enantiomers, an NMR study was carried out, to determine if the mixing was resulting in less gelator being incorporated into the gel network. When NMR is carried out on a gel, any gelator that is incorporated into the gel network will not appear in the spectra, as a result of long relaxation times, and subsequent broadening of the signals. It is therefore possible, by addition of an internal standard, to quantify any gelator that is in solution, rather than incorporated into the network.²⁰³

Two different samples were prepared, using D₂O in place of H₂O, and with a DMSO internal standard (2 μ l). One contained just L-DBS-CONH₂, and the second a 50:50 mixture of L-DBS-CONH₂ and D-DBS-CONH₂. The samples were prepared as normal, until the heat/cool cycle. At this point, while the solution was still hot, and the gelator still dissolved, it was transferred to an NMR tube, and the gel formed within the NMR tube.

In both cases, very little ‘free’ gelator was visible in the spectra (Figure 130). For the L-DBS-CONH₂ hydrogel, only 1.5% of the total gelator in the sample was visible in the ¹H NMR spectrum, with the vast majority being incorporated into the network. For the racemic gel, this rose to 3.6% ‘free’ gelator – a small increase compared to the single enantiomer, but the majority of the gelator has still assembled into a network. This indicates that, even though the overall network is weaker, the two enantiomers still assemble into some sort of ‘solid-like’ network even when mixed.

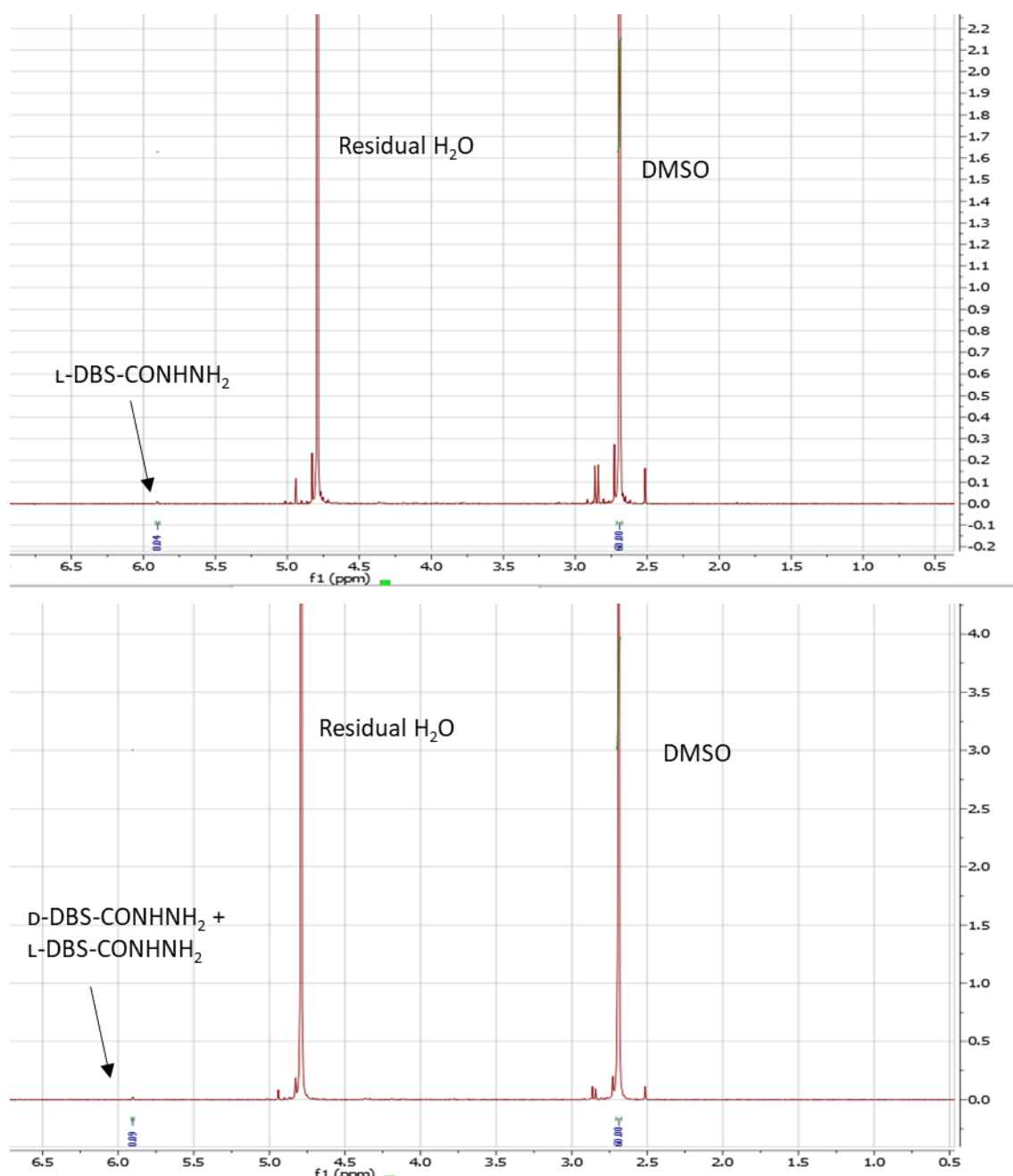


Figure 130. ^1H NMR spectra for L-DBS-CONH $_2$ (top) and D-DBS-CONH $_2$ and L-DBS-CONH $_2$ (bottom) hydrogels. Total loading for both hydrogels is 0.24% wt/vol.

5.3.2 Rheology of D-DBS-CONH $_2$ and L-DBS-CONH $_2$ Hydrogels

Following the initial gelation studies, rheology was carried out for a selection of mixed D-DBS-CONH $_2$ and L-DBS-CONH $_2$ hydrogels. This was to both confirm that hydrogels had indeed been formed (although the tube inversion test is a useful indicator of gelation, alone it is not enough to prove gelation), and further investigate the impact of mixing the two enantiomers on the mechanical properties of the hydrogels.

These studies looked at hydrogels with three different proportions of gelator – 50:50 D-DBS-CONH₂: L-DBS-CONH₂, 25:75 D-DBS-CONH₂: L-DBS-CONH₂, and 75:25 D-DBS-CONH₂: L-DBS-CONH₂. These could then also be compared to hydrogels formed from each of the two enantiomers individually.

Initially, samples were prepared for rheology as previously – formed in a bottomless vial attached to a petri dish, and transferred to a rheometer. Although gels were formed, they were mechanically very weak, and very difficult to transfer to the rheometer without breaking. An alternative method for preparing these samples for rheology was therefore developed. The normal procedure for preparing these gels was followed, up to the heat/cool cycle. At this point, the hot solution was transferred to a bottomless vial that had been placed on the bottom plate of the rheometer – the plate was also heated to 40 °C. This was then left for the solution to cool, and the plate then cooled to 18 °C. This method resulted in gel discs being successfully formed on the rheometer, allowing analysis to be carried out.

Initially, an amplitude sweep was carried out. This varies the strain applied to the material, while keeping the frequency constant. This allows the LVR to be determined, and also gives information regarding the mechanical properties of the gel. For each of the hydrogels, an amplitude sweep was carried out with the amplitude varied 0.01-100%.

The amplitude sweep for the 50:50 mix of enantiomers (Figure 131) indicated a G' value of around 230 Pa – considerably lower than the value of around 600 Pa for L-DBS-CONH₂. This is further evidence for the interactions between the two enantiomers being disruptive, as the hydrogels formed have much lower stiffness. The interactions are not, however, sufficiently disrupted to prevent the formation of a gel - as evidenced by the clear LVR, the materials formed from the racemic mixture do behave viscoelastically. The crossover point of around 10% strain is also fairly comparable to that of the gels formed from a single enantiomer – ca. 12%. This indicates that, despite the racemic gels being less stiff, the resistance to strain of the material is less affected.

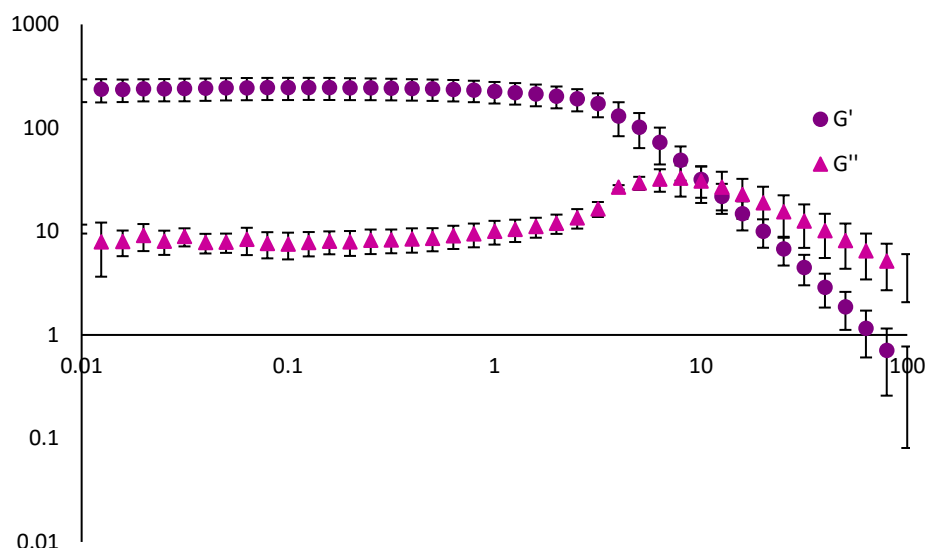


Figure 131. Amplitude sweep (0.01%-100%) for racemic DBS-CONHNH₂ hydrogels. Total gelator loading 0.28% wt/vol. Temperature 25 °C, frequency 1 Hz.

The two 25:75 mixes also showed significant drops in the value of G' in the LVR, indicating that a smaller amount of the 'wrong' enantiomer also induces the formation of less stiff hydrogels (Table 19). The variation in G' and yield stress for these mixes indicates the unpredictable nature of these hydrogels, which could be a result of the variable level of self-assembly when both enantiomers are present.

Table 19. G' values for mixes of *D*-DBS-CONHNH₂ and *L*-DBS-CONHNH₂ hydrogels (total concentration 0.28% wt/vol).

Ratio <i>D</i> -DBS-CONHNH ₂ : <i>L</i> -DBS-CONHNH ₂	G' / Pa	Yield Stress / %
100:0	740 ± 300	15
75:25	420 ± 70	25
50:50	240 ± 60	10
25:75	240 ± 50	79
0:100	610 ± 280	15

As well as the amplitude sweep, a frequency sweep was also carried out. If a material is viscoelastic, the G' value will be independent of frequency. This is therefore a valuable method for determining if a material is viscoelastic. For the racemic gels, a frequency sweep was carried out with the frequency varied 0.1-100 Hz, and the strain kept constant at 0.063%.

At lower frequencies (<10 Hz), the G' value for the racemic gels was independent of frequency (Figure 132), offering further confirmation that a viscoelastic material, a gel, has been formed. As observed with the amplitude sweep, the G' value, of around 280 Pa, is lower than that observed for the hydrogels formed from just one enantiomer, which had a G' value of around 580 Pa. This again shows the reduced mechanical strength of the mixture compared to the single enantiomer gels. It is perhaps interesting to reflect that although the difference in G' is only ca. a factor of two, the gels have very different physical handling characteristics – those made from a single enantiomer can be transferred onto the rheometer plate by hand, whereas those made from mixtures of enantiomers cannot, and have to be made *in situ* as described above.

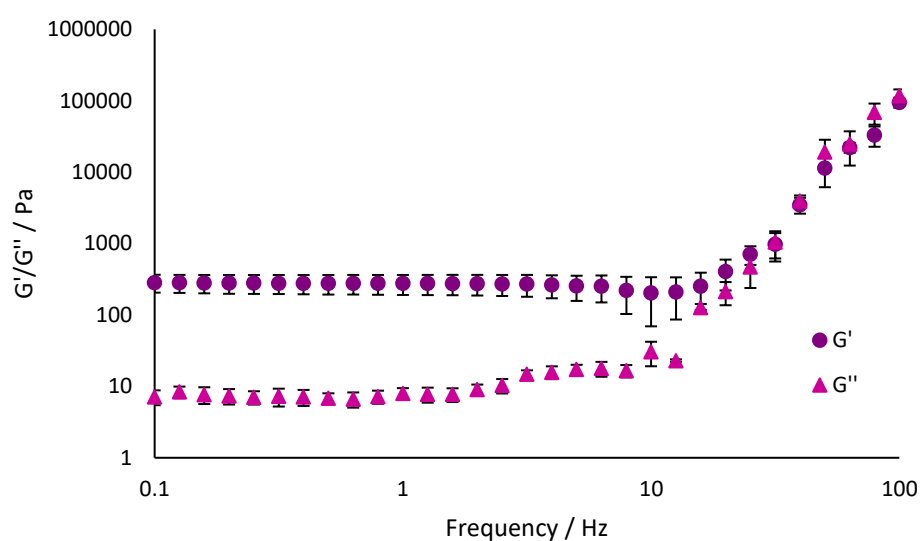


Figure 132. Frequency sweep (0.1 Hz-100 Hz) for racemic DBS-CONH₂ hydrogels. Total gelator loading 0.28% wt/vol. Temperature 25 °C, amplitude 0.05%.

5.3.3 Imaging of the Mixed Hydrogels

To determine whether there were any significant changes to the network with the mixed system, imaging was carried out for the gels based on a 50:50 mixture of enantiomers. These mixed gels were prepared as previously discussed, with the samples then prepared for imaging as described previously. Both SEM and TEM images were obtained. Although sample preparation can impact the structures observed in electron microscopy, such images can still give insight into the nature of the networks formed, particularly for comparative studies where the samples are prepared using the same method.

The SEM images of the racemic mixture (Figure 133), shown with images of L-DBS-CONH₂ for comparison, indicate that it is still self-assembling to form a sample spanning network. Indeed, the images show a branched network similar to that obtained with L-DBS-CONH₂ alone. The

TEM images, however, are quite different – with the fibres appearing either narrower, and/or larger but significantly more fragmented in the mixture than in the single enantiomer gel. This lack of homogeneity may be a factor in the reduced thermal stability and mechanical strength of the racemic hydrogels. This suggests that the 50:50 mixture of enantiomers has a different self-assembly mode, which is less well-defined, resulting from the disruptive nature of the interactions between the two enantiomers.

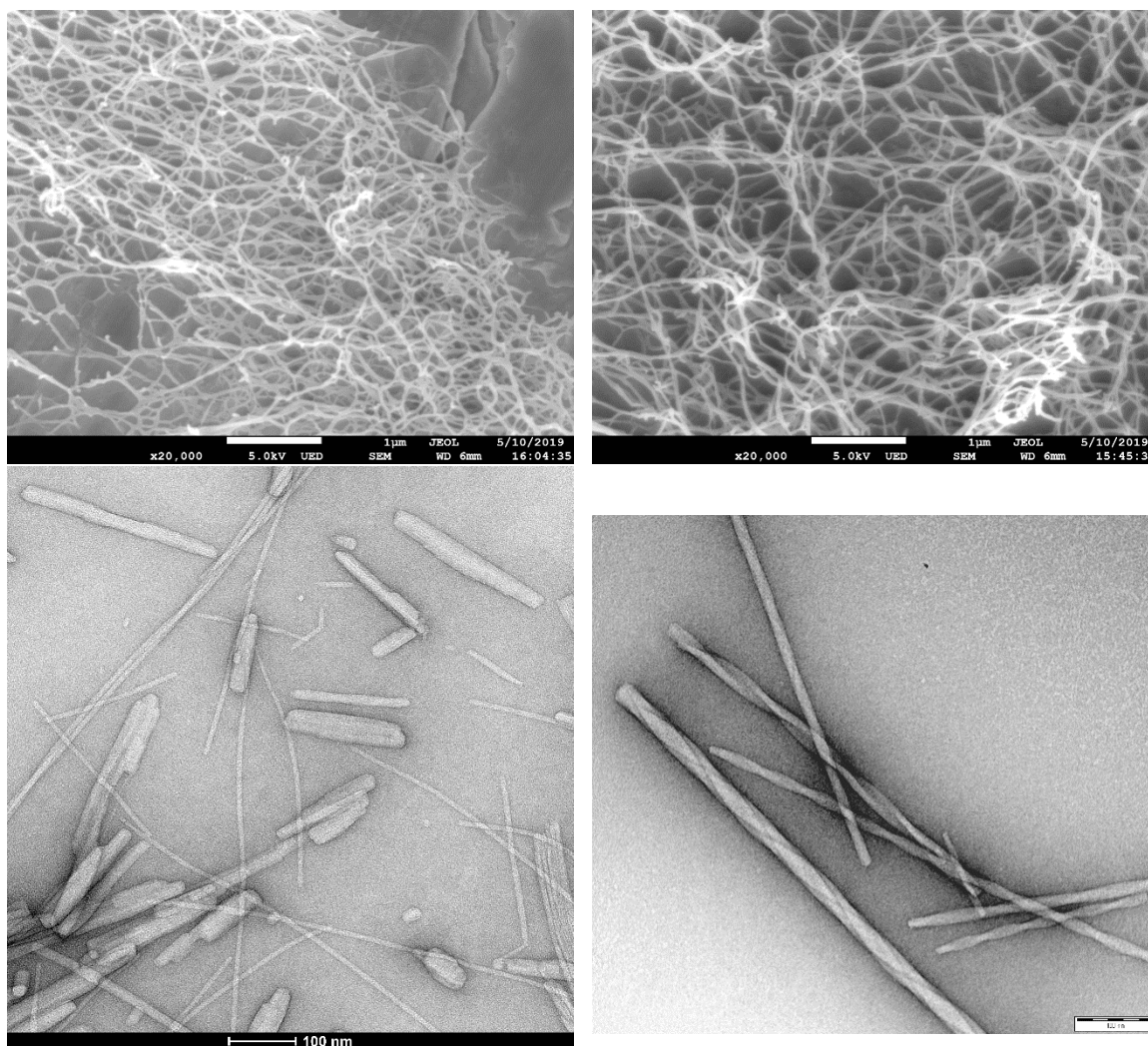


Figure 133. SEM (x20,000) (top) and TEM images (scale bar 100 nm) (bottom) for racemic hydrogels (left) and L-DBS-CONH₂ hydrogels (right). Total gelator loading for both samples - 0.28% wt/vol.

5.3.4 Circular Dichroism for Mixed Samples

As previously discussed, CD is a very useful tool for investigating the way in which the chirality of an individual molecule impacts the chirality of a nanostructure formed by self-assembly. For mixtures of two gelator enantiomers, CD can offer useful information on how self-assembly occurs, particularly whether one enantiomer dominates the chirality of the nanostructures.

Mixtures of the two enantiomers were therefore investigated by CD, using a total gelator loading of 0.1% wt/vol – as previously, this is below the minimum gelation concentration, but sufficient for the formation of self-assembled nanostructures. Samples were prepared as previously, with the hot solution being transferred to a warm CD cuvette, and then allowed to cool.

These samples were then analysed by CD. Measurements were carried out at 20 °C, to ensure nanostructures would be present, and the ellipticity observed at the previously determined maximum of 272 nm. The ellipticity of the mixtures could then also be compared with that of gels formed from just one enantiomer (Figure 134).

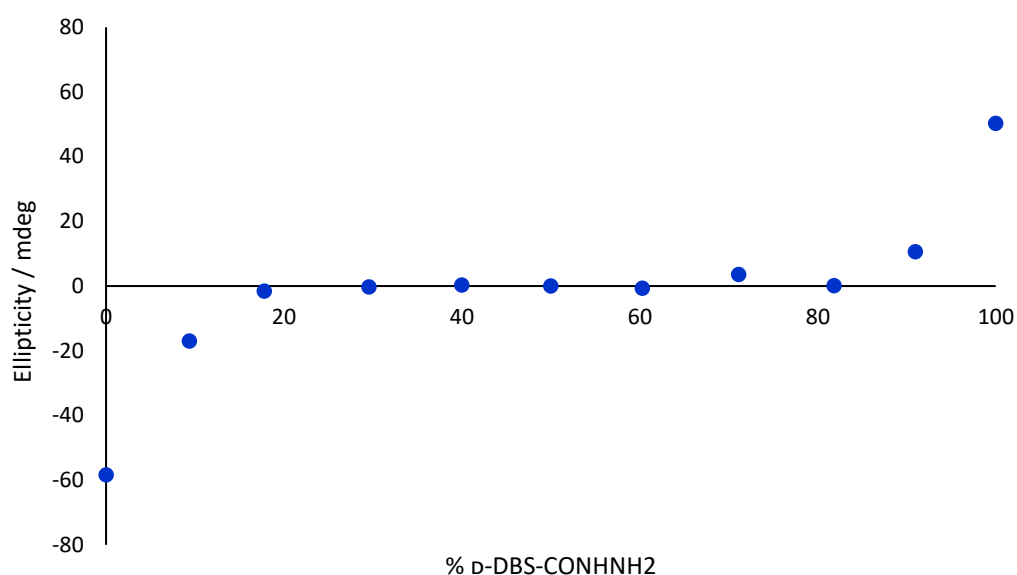


Figure 134. Ellipticity, measured at 272 nm, for mixed D-DBS-CONH₂ and L-DBS-CONH₂ hydrogels, total gelator loading 0.1% wt/vol.

On addition of even a small proportion of a second enantiomer to the gelator mixture, the chirality of the nanostructures was almost completely lost. At a 90:10 ratio of one enantiomer to the other, there was an ellipticity of around ± 20 mdeg, this is a considerable drop from the ellipticity, of around ± 60 mdeg, observed in the hydrogels formed from one of the two enantiomers. Once 20% of the mixture is the opposite enantiomer, the overall ellipticity of the supramolecular nanostructures is completely lost. This indicates that the interactions between the two enantiomers result in supramolecular nanostructures that are not chiral – even when only a relatively small proportion of the total gelator is the ‘wrong’ enantiomer. This is in-line with the observation that even a small amount of the opposite enantiomer leads to a significant decrease in the thermal stability of the gel. It is also in support of the view that significantly different nanostructures are observed for the racemic system by TEM. Clearly, therefore, this is somewhat similar to native DBS, in which mixing enantiomers has a disruptive effect on assembly, however,

in this case, the gel-forming properties are not completely lost, and hence a gel weakening effect is observed rather than a total gel disruption.

5.4 Incorporation of Chiral Additives

It has previously been shown that enantiopure materials can form enantioselective interactions with other chiral molecules.²⁵⁹ This is of particular interest, as many bioactive molecules, including APIs, have one or more chiral centres. The effect of chiral additives on the hydrogels of the two DBS-CONH₂ enantiomers was therefore investigated.

The additives chosen for investigation were (*R*)-naproxen (**118b**) and (*S*)-naproxen (**118a**) (Figure 135). Naproxen (NPX) is a non-steroidal anti-inflammatory drug (NSAID), with the *S* form being both a more effective anti-inflammatory, and less toxic than the *R* form.²⁶⁰ The drug is used as a single enantiomer, however, other drugs in the same class (e.g. ibuprofen, ketoprofen etc.) are generally used as racemic mixtures. In previous work, interactions between D-DBS-CONH₂ and (*S*)-NPX have been investigated, and hydrogels containing the drug investigated as possible drug delivery vehicles.^{109, 174} As a result, there is already a good understanding of the hydrogen bonding interactions between the carboxylic acid of (*S*)-NPX and the gel fibres formed by D-DBS-CONH₂. For this reason, and as both enantiomers of naproxen are readily available, the interactions between the gels formed from the two DBS-CONH₂ enantiomers, and the two enantiomers of naproxen were investigated.

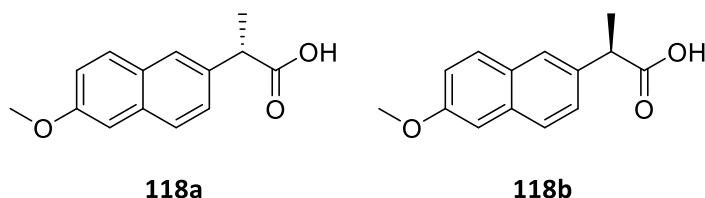


Figure 135. (*S*)-naproxen (**118a**) and (*R*)-naproxen (**118b**).

5.4.1 Gelation Studies with Chiral Additives

Initially, the four different combinations of the two gelator enantiomers, and the two naproxen enantiomers, were investigated to determine if a gel was still formed in all cases. To prepare the samples, the gelator was weighed into a vial, and NPX added as a solid. Water was then added, followed by 15 minutes of sonication to disperse the solid. The suspension was then heated until all of the solid was dissolved. Once the solution was cooled, gelation was determined using the tube inversion test (Table 20).

Table 20. Gelation testing for different combinations of DBS-CONH₂ and naproxen enantiomers. Gelator loading is 0.28% wt/vol, with one equivalent of NPX.

	(S)-naproxen	(R)-naproxen
D-DBS-CONH ₂	G	G
L-DBS-CONH ₂	G	G

In all combinations of the enantiomers, gels were still formed. Following this initial testing, the resulting hydrogels were tested in more detail for thermal stability by determination of the T_{gel} values. The hydrogels were prepared at a gelator concentration of 0.28% wt/vol, with one equivalent of NPX. The method for preparation was as discussed previously. Once hydrogels had been formed, these were heated in a thermoregulated oil bath, at a rate of 1 °C min⁻¹. The temperature at which the hydrogels were broken down was determined by the tube inversion test (Table 21).

Table 21. T_{gel} values for D-DBS-CONH₂ and L-DBS-CONH₂ hydrogels, with (S)-NPX or (R)-NPX. Hydrogels have gelator loading of 0.28% wt/vol, with 1 equivalent of NPX.

Gelator	(S)-naproxen	(R)-naproxen	None
D-DBS-CONH ₂	98	100+	100+
L-DBS-CONH ₂	100+	81	100+

For D-DBS-CONH₂ with (R)-NPX, and L-DBS-CONH₂ with (S)-NPX, the addition of NPX did not have a notable impact on the T_{gel} value – for hydrogels, T_{gel} values are only measured to 100 °C, as above this temperature, any breakdown of the gel network may be a result of the solvent evaporating. It is notable that these two combinations have an enantiomeric relationship with one another, and should therefore behave in the same way. The other two combinations, D-DBS-CONH₂ with (S)-NPX, and L-DBS-CONH₂ with (R)-NPX, showed a drop in the T_{gel} value – greater for L-DBS-CONH₂ than for D-DBS-CONH₂ – however, both clearly converting to a sol below 100 °C. Once again these two combinations have an enantiomeric relationship with one another, and would be expected to behave in the same way. However, they have a diastereomeric relationship with the other two combinations, and therefore it is plausible that they would exhibit different physical properties, such as T_{gel} value. These results would therefore suggest that the different diastereomeric combinations of gelator and NPX enantiomers may give rise to hydrogels with slightly different thermal stabilities, which could indicate the importance of chiral information in the self-assembly and drug binding process.

5.4.2 Rheology of Hydrogels with Chiral Additives

Following the investigation of the thermal stability of the DBS-CONH₂ hydrogels with the NPX additives, their mechanical properties were also investigated. Samples, of the different combinations of gelator and NPX enantiomers, were prepared as described previously, until the heat/cool cycle. At this point, while still hot, and the solid still dissolved, the solution was transferred to a bottomless vial, attached to a petri dish. Once the solution had cooled, the vial could be removed, and the gel disc transferred to the rheometer for analysis.

For each sample, an amplitude sweep was carried out first – to both determine the LVR for the gels, and to give information regarding the stiffness and resistance to strain of the material. This was carried out for D-DBS-CONH₂ with both NPX enantiomers (Figure 136), and for L-DBS-CONH₂ with both NPX enantiomers (Figure 137), with amplitude strain varied 0.01-100%, and frequency kept constant at 1 Hz.

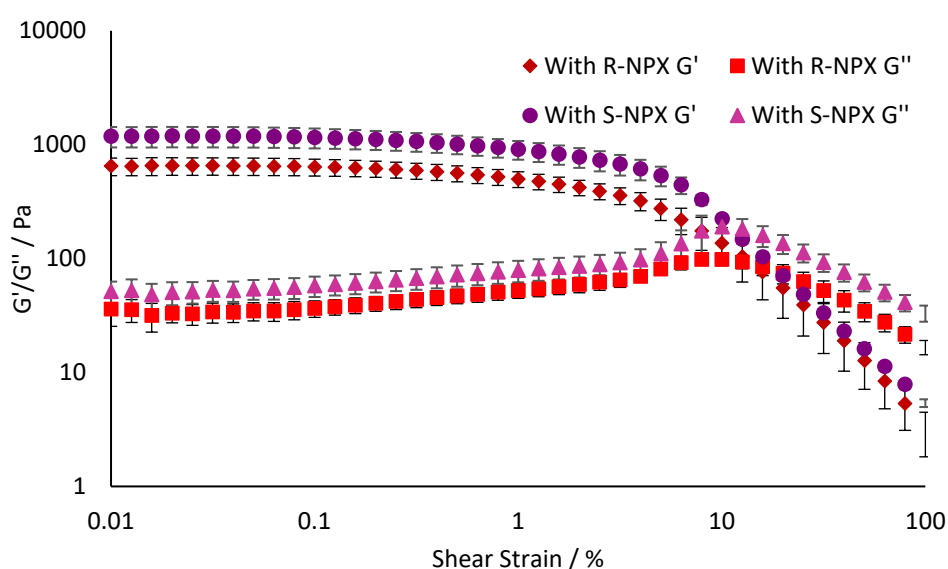


Figure 136. Amplitude sweep (0.01%-100%) for D-DBS-CONH₂ hydrogels with (R)- or (S)-NPX. Gelator loading 0.28% wt/vol, one equivalent NPX. Temperature 25 °C, frequency Hz.

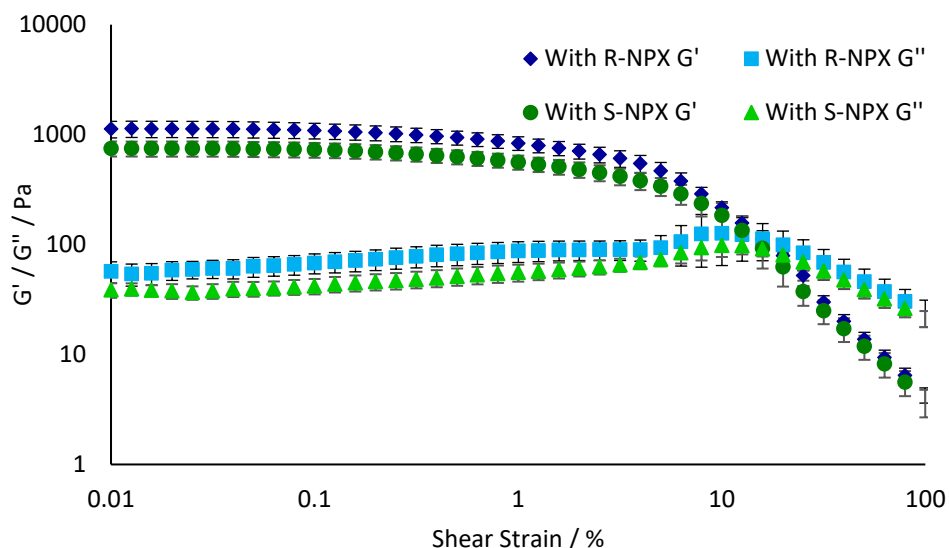


Figure 137. Amplitude sweep (0.01%-100%) for L-DBS-CONH₂ hydrogels with (R)- or (S)-NPX. Gelator loading 0.28% wt/vol, one equivalent NPX. Temperature 25 °C, frequency 1 Hz.

All of the gels tested showed a clear LVR, but with some variation in the stiffness. For each of D-DBS-CONH₂ and L-DBS-CONH₂, one additive gave a hydrogel with a G' value broadly similar to that of the gel without additive, and the second gave an increase in stiffness of ca. 400 Pa (Table 22). For each enantiomer of the gelator, the opposite enantiomer of naproxen gave these effects. For D-DBS-CONH₂, the addition of (S)-NPX gave the increase in stiffness, while for L-DBS-CONH₂ it was (R)-NPX that gave the increase. In agreement with the thermal studies, this indicates that enantiomeric systems behave the same, whereas systems with a diastereomeric relationship do have a difference in their physical properties. This suggests that the interactions between the chiral additives and the gel fibres do differ when chirality is changed, and this has some impact on the material properties of the hydrogels. Interestingly, the enantiomers of naproxen that decreased the thermal stability of the gels are those that increase the stiffness of the gels. This might suggest that certain enantiomers cause a stiffening of the gel network, that decreases its thermal stability. Despite the differences in stiffness of the gels, all had a similar crossover point of around 12%, indicating all have a similar resistance to strain.

Table 22. The effect of the addition of NPX to the DBS-CONH₂ hydrogels. Gelator concentration 0.28% wt/vol, with one equivalent of NPX.

Gel	Additive	G' / Pa
D-DBS-CONH₂	None	740 ± 300
D-DBS-CONH₂	(R)-NPX	630 ± 110
D-DBS-CONH₂	(S)-NPX	1190 ± 240
L-DBS-CONH₂	None	610 ± 280
L-DBS-CONH₂	(R)-NPX	1130 ± 190
L-DBS-CONH₂	(S)-NPX	750 ± 120

In summary, these observations, along with the reduced thermal stability of the gel, indicates that the two different enantiomers of NPX impact the two hydrogels differently, suggestive of a degree of chiral recognition between gelator and drug, and that this then has an impact on the physical materials properties of the gel.

5.4.3 NMR Studies of the Hydrogels with Additives

To try and further understand the interactions between the hydrogel fibres and the NPX additives, ¹H NMR studies were carried out. As discussed in section 5.3.1, NMR can be used to determine the amount of gelator incorporated within the network, due to the long relaxation times and subsequent broadening of peaks when the molecules have self-assembled. The same method can be used to determine if there are interactions between the gel network and any additives – if the additives are interacting with the gel network, the corresponding signals will also be broadened. Any signal that is observed is a result of ‘free’ molecules, within the pores of the hydrogel, and can be quantified by use of an internal standard.

For NMR analysis, DBS-CONH₂ hydrogels were prepared by adding the relevant enantiomer of gelator, along with the NPX additive, to a vial, along with D₂O and a DMSO internal standard (2 μl). This was then sonicated, followed by heating to dissolve the solid. While the solution was hot, it was transferred to a warm NMR tube, and the gel formed within the tube. The integrations of the DMSO standard, and the signal at 1.46 ppm corresponding to the methyl group of NPX, can be compared, and the amount of unbound NPX calculated (Table 23). There are very small differences in the amounts of NPX bound to the gel fibres, with each having around roughly 70% interacting with the fibres. There are however some small differences, and once again there appears to be a diastereomeric relationship, with the D/S and L/R systems (those that formed less

thermally stable, stiffer gels) appearing to have slightly less NPX bound to the gel than the D/R and L/S analogues.

Table 23. The percentage of (R)-NPX and (S)-NPX not bound to the gel network, as determined by use of a DMSO internal standard. Gelator loading 0.28% wt/vol, with one equivalent of NPX.

Gelator	(S)-NPX Unbound / %	(R)-NPX Unbound / %
D-DBS-CONH ₂	32 ± 0.4	26 ± 1.5
L-DBS-CONH ₂	27 ± 0.18	28 ± 0.6

For both gels, when there is a greater proportion of NPX is interacting with the fibres, the gel is less stiff. This effect is more pronounced for the D-DBS-CONH₂, with a greater difference between the amount of each NPX enantiomer bound to the fibres, and a greater difference in stiffness between the two gels formed. The difference in interactions of NPX with the L-DBS-CONH₂ hydrogels is much smaller – as is the difference in the stiffness of the gels. Overall, however, these NMR differences are close to error levels, and it is important not to place too much emphasis on them.

This further indicates that the two enantiomers of NPX may interact slightly differently with the fibres of the two hydrogels – and that these differences can have some influence on the material properties.

5.4.4 Release of Chiral Additives

Following the investigations into the impact of additives of different chiralities, the release of the two different NPX enantiomers was then considered. pH-dependent release of NPX from D-DBS-CONH₂ has been previously demonstrated,^{109, 174} and given the differing effects on the material properties of the hydrogels, it was reasoned that a change in chirality may also impact on the release of NPX.

Samples were prepared as previously, with the two solids weighed into a vial, water added, and this mixture sonicated, followed by a heat/cool cycle. This resulted in the formation of translucent hydrogels. The gels used a gelator concentration of 0.28% wt/vol, with one equivalent of NPX. Once the gels had formed, pH 7 buffer (6 ml) was added, and the samples placed in a 37 °C incubator. The release of NPX into the buffer was then monitored by UV-vis spectroscopy. A wavelength of 329 nm was used – NPX has a distinct absorbance at this wavelength, while any absorbance from DBS-CONH₂ is minimal.

Release was monitored for both (S)-NPX and (R)-NPX, from both D-DBS-CONHNH₂ (Figure 138) and L-DBS-CONHNH₂ (Figure 139). A sample containing no NPX was also monitored in each case, to allow any absorbance from the gelator to be accounted for.

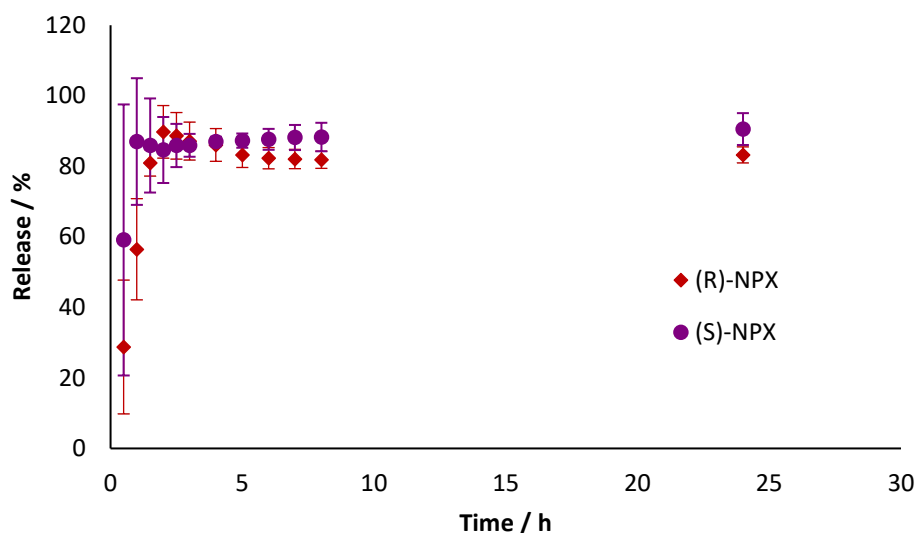


Figure 138. Release of (R)-NPX and (S)-NPX from D-DBS-CONHNH₂ hydrogels (1 ml), into pH 7 buffer (6 ml) at 37 °C. Gelator loading is 0.28% wt/vol, with one equivalent of NPX.

For D-DBS-CONHNH₂ hydrogels, release of both NPX enantiomers was very rapid, with the majority of the release occurring within the first 90 minutes. For both enantiomers, a maximum release of around 90% was reached.

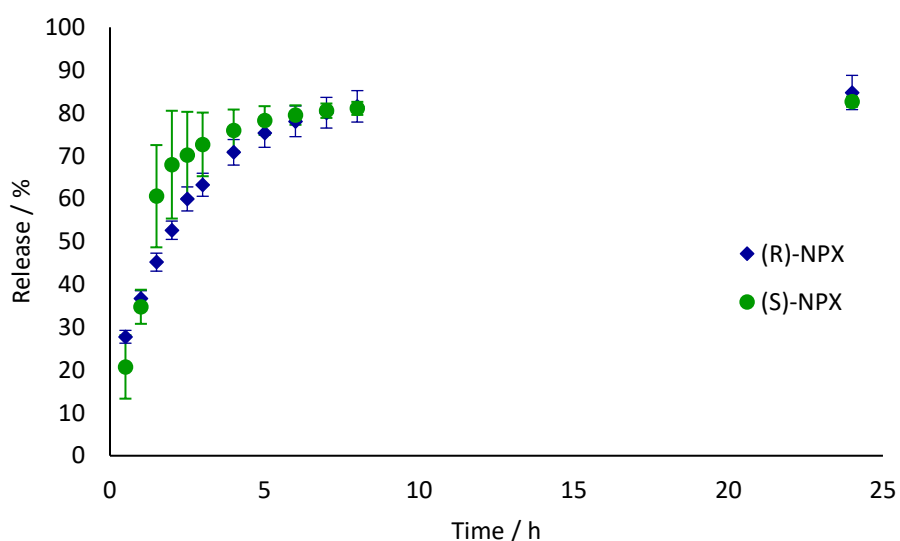


Figure 139. Release of (R)-NPX and (S)-NPX from L-DBS-CONHNH₂ hydrogels (1 ml), into pH7 buffer (6 ml) at 37 °C. Gelator loading is 0.28% wt/vol, with one equivalent of NPX.

For L-DBS-CONHNH₂ hydrogels, release of both enantiomers of NPX was again rapid, with the majority of the additive being released after 2-3 hours – maximum release in this case was around 85%. Overall, despite some small differences, the release of the two NPX enantiomers from the two hydrogels was very similar. For both enantiomers of NPX, slower release is observed from the L-DBS-CONHNH₂ hydrogels. The reason for this is not yet understood, and would require further investigation. As observed previously for DBS-CONHNH₂ hydrogels and NPX at pH 7, most release occurs rapidly, and around 90% of the total drug is released. This was the case for all combinations of enantiomers tested here, despite some small differences. This suggests that, although there are likely to be some small differences in how the two enantiomers of NPX interact with the gel fibres, as evidenced by the rheological and NMR studies carried out, these differences do not have a significant impact on the release profiles of the NPX from the hydrogels.

Similar studies were also carried out using (R)-(-)-2-phenylbutyric acid and (S)-(+)-2-phenylbutyric acid as the chiral additives. The results from these studies were broadly in line with those obtained with the two enantiomers with NPX. The main difference was observed in release studies – due to overlap between the UV signals from the DBS-CONHNH₂ and the acid additives. For these reasons these studies have not been included in the thesis.

5.5 Biological Studies

As discussed in the Introduction, it has been previously reported that using different enantiomers of a gelator led to differences in cell differentiation. Initial investigations into any differences between the two enantiomers of DBS-CONHNH₂ in cell culture were therefore carried out. D-DBS-CONHNH₂ has previously been used for cell culture, both alone¹⁷³ and in combination with polymer gelators.^{217, 261} However, no investigation into L-DBS-CONHNH₂ has previously been carried out. The two hydrogels were therefore investigated using cell proliferation and viability studies. All cell culture experiments were carried out by Dr Carmen Piras working in the laboratory of Prof Paul Genever (Department of Biology, University of York).

5.5.1 Cytotoxicity Studies

To test the impact of the two enantiomers on cells, a cytotoxicity assay was carried out. Gels formed from both enantiomers were prepared in a 6 well plate, with hot gelator solution transferred into bottomless vials (diameter 1 cm) attached to this plate. For both enantiomers, gelator loading was 0.4% wt/vol. Once the gels were formed, the vials could be removed to leave a gel disc in each well (Figure 140).

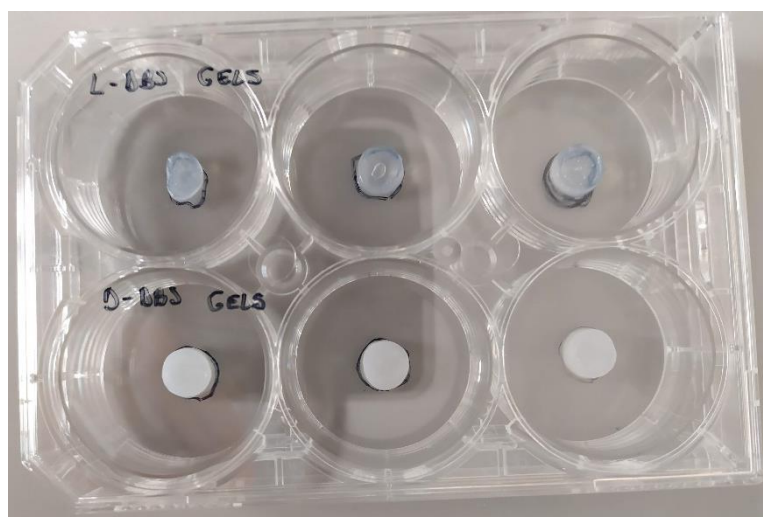


Figure 140. Hydrogels of L-DBS-CONHNH₂ (top) and D-DBS-CONHNH₂ (bottom), prepared in a 6 well plate. Gelator concentration for all hydrogels is 0.4% wt/vol.

The cells used were Y201 immortalised human mesenchymal stem cells (MSCs).²⁶² These were grown in Dulbecco's Modified Eagle Medium (DMEM) with fetal bovine serum (FBS, 10%) and penicillin/streptomycin (P/S, 1%). Once grown, these cells were seeded (100,000 per well) in the bottom of the wells around each gel, and covered with DMEM.

After 48 hours, DMEM was removed and the cells washed with PBS. The cells were then stained with crystal violet methanol solution. The stain was collected after 20 minutes, the plates washed in water multiple times, and left to dry. The plates were then imaged, to determine how the gels had influenced the cells (Figure 141).

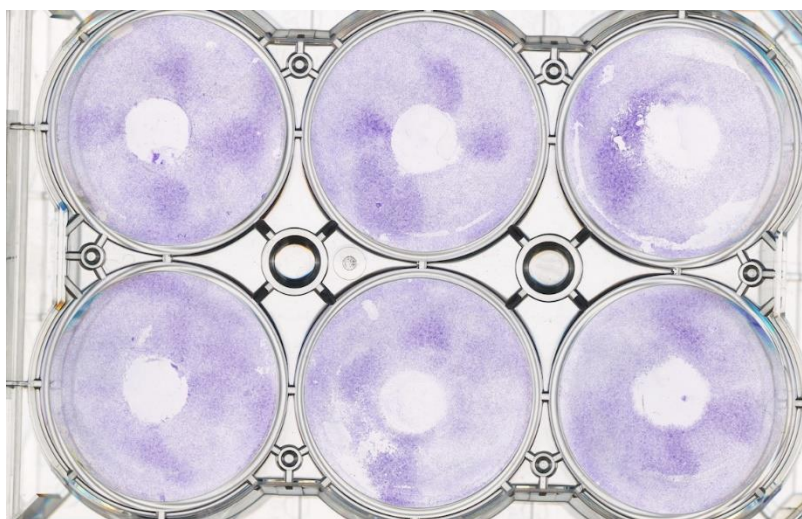


Figure 141. The plate after 48 hours, following treatment with crystal violet methanol solution. Purple indicates viable cells. Top: L-DBS-CONHNH₂; Bottom: D-DBS-CONHNH₂.

The images show that the cells, stained violet, are still present right up to the boundary of the hydrogels. This indicates that any cytotoxicity caused by the gels is very low. Additionally, there

was no difference between the two enantiomers – therefore the change in chirality does not have an effect on cytotoxicity.

5.5.2 Viability Studies

Cell viability studies were also carried out, to determine if both enantiomers would be equally suitable for cell culture. Hydrogels were prepared in a 96 well plate. Each well contained 50 μ l of gel, with a gelator concentration of 0.3% wt/vol. Once formed, the gels were soaked with DMEM (containing FBS and P/S). These gels were then seeded with Y201 immortalised human mesenchymal stem cells (25,000 per well). Both the gels and the cells were then covered with DMEM. Cell viability was measured at days 0, 3, 6 and 10 using the Alamar Blue assay. Alamar Blue (10% in DMEM) was added to each well, and the plates incubated for 4 hours at 37 °C. Aliquots (20 μ l) were then removed from each well, and these diluted with DMEM in a second well plate. Hydrogels without cells were also treated in the same way at each timepoint, to control for any effects from the gels themselves. The fluorescence was then measured (excitation 530-570 nm, emission 600 nm). This indicates the number of viable cells for each sample (Figure 142).

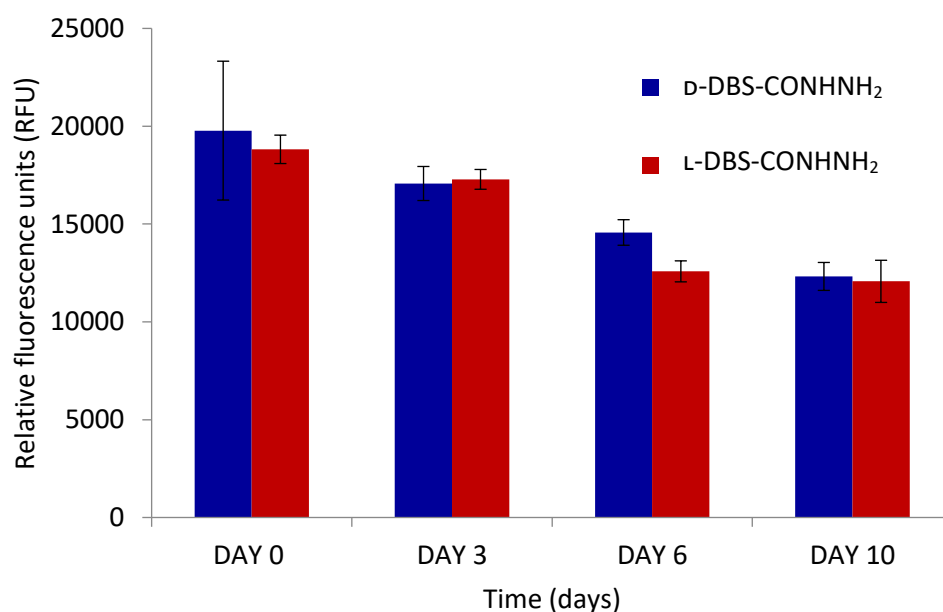


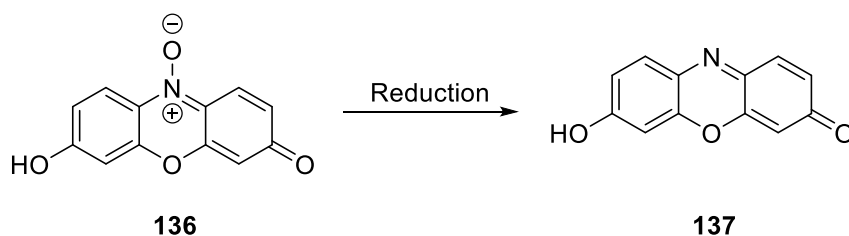
Figure 142. Cell viability for D-DBS-CONH₂ and L-DBS-CONH₂ hydrogels (0.3% wt/vol) at days 0, 3, 6, 10.

There is no significant difference in cell viability between the two enantiomers of DBS-CONH₂. Over time there is a small decrease in viability across both of the gels – this has previously been observed for D-DBS-CONH₂ hydrogels.

Although there is no difference in cell viability between the two enantiomers of the gel, this does not rule out the possibility that there may be differences in cell development or differentiation, however, such studies were beyond the scope of this preliminary investigation. There is no doubt that the potential impact of materials chirality on cells is a current hot topic,²⁶³ and these simple enantiomeric gelators may be worthy of further investigation in this regard.

5.5.3 Alamar Blue Test

Although no significant difference in cell viability was observed between the two enantiomers, an interesting difference in the control gels, with no cells present, was observed in response to the Alamar Blue assay. In this assay, the dye resazurin (**136**) is reduced by the processes that occur in viable cells, to give the fluorescent form, resorufin (**137**) (Scheme 24). More viable cells therefore lead to greater fluorescence.²⁶⁴



Scheme 24. Reduction of resazurin (weakly fluorescent) to give resorufin (highly fluorescent).

However, DBS-CONH₂ is also capable of reducing Alamar Blue – hence the importance of the control gels. These control experiments indicated that there was a difference in the reduction of Alamar Blue between the different gels formed by the two enantiomers of DBS-CONH₂, with fluorescence from the D-DBS-CONH₂ hydrogels being almost twice that from with L-DBS-CONH₂ hydrogels. Alamar blue itself is not a chiral substrate, and so there should be no difference in the way it interacts with the two gelator enantiomers. It therefore seemed possible that the ability of DBS-CONH₂ to reduce Alamar Blue was being impacted by an interaction with some component of the cell media, which contains many chiral compounds. One or more of these might be interacting with the gel fibres (differently for each enantiomer), and this in turn may impact the reduction. A preliminary study was therefore carried out to investigate which of the components might be causing this effect.

A selection of amino acids that are present in the cell culture medium were therefore investigated for their impact on the reduction of Alamar Blue by DBS-CONH₂. Hydrogels were prepared in a 96 well plate (gelator loading 0.3% wt/vol), as for the cell viability experiment. A selection of L- amino acids, along with D-glucose, were added in solution to the gels, and left overnight for

diffusion into the gels to take place. After this time, the additive solution was removed from the hydrogels. Alamar Blue solution (10 μ l in 90 μ l pH 7 sodium phosphate buffer) was then added, and the plate incubated at 37 °C for 4 hours. The Alamar Blue solution was then transferred to a second well plate, diluted with further buffer, and the absorbance measured. Absorbance was used in this case as the reduced, fluorescent form of Alamar Blue is not stable in buffer or water – only cell media.²⁶⁵ However, the reduction of Alamar Blue does also lead to an increase in absorbance. The values for each amino acid, as well as glucose and the control gels, could then be compared (Figure 143).

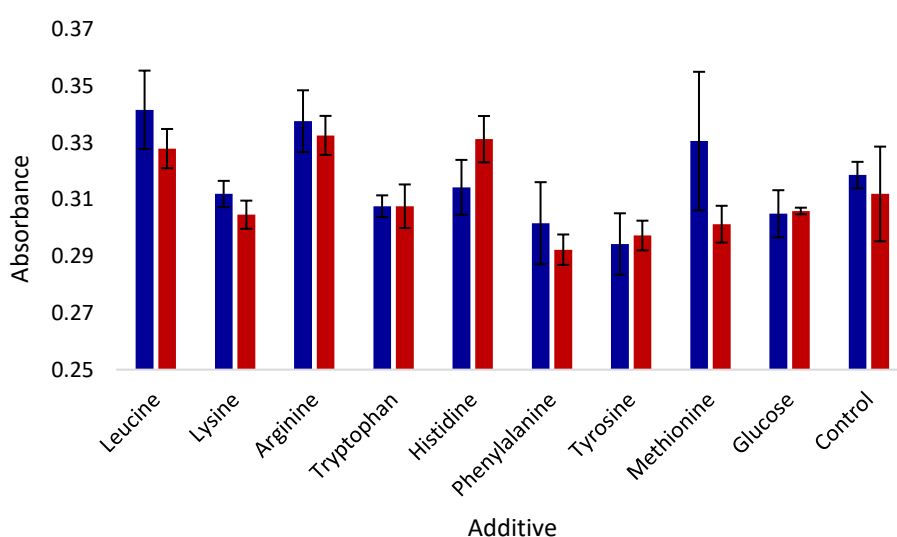


Figure 143. Impact of different amino acids, and glucose, on the reduction of Alamar Blue. Absorbance measured following incubation of gels with Alamar Blue at 37 °C for 4 hours. Solution was then removed, and absorbance measured.

For all of the amino acids investigated, there was no significant difference in absorbance between the two enantiomers – although some did give significant variation across the three samples. This suggests that it is likely to be another component of the cell media that is impacting the reduction of Alamar Blue - perhaps an amino acid that was not included in this study, or a protein present in the FBS that is also present, however we were unable to determine what underpinned this effect at this point.

5.6 Conclusions

Here, L-DBS-CONHNH₂ has been synthesised, its properties as a gelator investigated, and these compared to D-DBS-CONHNH₂. The two gelators were found to perform in an equivalent way with regard to both mechanical and thermal properties. Furthermore, electron microscopy imaging suggested similar nanostructures that could not easily be distinguished in terms of helicity. The

key differences were observed in CD spectra, which clearly indicated that the nanostructures formed by the two enantiomers had mirror image chirality.

Mixtures of the two enantiomers were also investigated, and these gels were found to be considerably weaker than those formed by a single enantiomer, indicating disruptive interactions. Additionally, chirality on the nanoscale was lost even with addition of only a small proportion of a second enantiomer. This further indicates disruptive interactions are established between the two enantiomers. This suggestion is supported by electron microscopy imaging of the racemic mixture which indicated the presence of some fragmented and poorly defined aggregates.

The gels from the two enantiomers were then tested for encapsulation of two enantiomers of NPX. Both gels could incorporate both NPX enantiomers and retain the characteristics of a gel. There was an impact on the thermal stability and stiffness of the two gels with different combinations of the two enantiomers, along with some small differences in interactions between the gel fibres and the NPX additive. This suggested there was some difference in the establishment of diastereomeric complexes. However, when release of the NPX was tested, the small changes in stiffness and level of interaction did not have a significant effect on drug release.

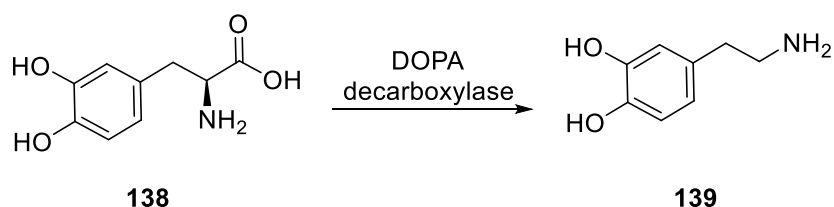
The gels were also tested with cells – for both cytotoxicity and viability. There were no differences observed in the behaviour of the cells with the two enantiomeric gels. Some interesting enantio-derived effects on the reduction of Alamar Blue were observed for the two hydrogels with no cells. However, we were unable to delineate a clear mechanism for this effect, with the preliminary studies using different amino acids present in the medium failing to indicate that any of them were the chiral species responsible for leading to this effect.

Further work in this area would focus on determining if the different gels have any impact on cell differentiation, now that initial cell viability studies have been carried out. Further investigations could also be undertaken to determine what components of cell media lead to the difference in reducing ability of the DBS-CONH₂ hydrogels. Increased understanding of how the gel fibres interact with additives could help guide future applications of these hydrogels.

6. Chapter 6 – Glutamine Amide Derivatives

As the population ages, society faces a number of challenges, including an increase in the prevalence of age-related diseases.²⁶⁶ This has implications for healthcare systems, with more people being affected by such diseases, even if the number of years spent in good health is also increasing.²⁶⁷ These diseases include Parkinson's disease (PD), a degenerative neurological disorder. There has been a significant increase in the global prevalence of Parkinson's since 1990,²⁶⁸ and this increase is projected to continue.²⁶⁹ The disease has significant impacts, both financial and otherwise, on patients and their families,²⁷⁰ as well as on healthcare systems.²⁷¹

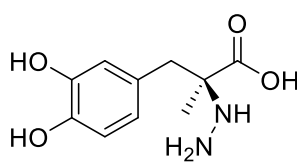
In Parkinson's, neurons in the brain that produce dopamine are broken down, leading to the characteristic symptoms of the disease, including tremors, slowness of movement, and muscle stiffness,²⁷² along with a range of non-motor symptoms.²⁷³ These can severely impact the ability of a patient to live independently. At present, there is no cure for Parkinson's – the neurons cannot be repaired or replaced. Current treatment therefore focusses on pharmaceutically replacing the dopamine that is no longer being produced. However, dopamine (**139**) itself is not capable of crossing the blood brain barrier, and therefore L-DOPA (**138**), a metabolic precursor to dopamine, is administered. L-DOPA is then converted by DOPA decarboxylase enzymes *in vivo*, to give dopamine (Scheme 25).



Scheme 25. Conversion of L-DOPA to dopamine, that occurs in vivo, by the action of DOPA decarboxylase.

However, there are a number of issues with this method of treatment. The first is the low bioavailability of L-DOPA in the brain. Only around 30% of administered L-DOPA ever reaches systematic circulation, with a mere 1% of a typical oral dose reaching the brain.²⁷⁴ This is due to significant first pass liver metabolism, with decarboxylation occurring not just in the brain, but around the whole body. Given that once L-DOPA has been converted to dopamine, it can no longer cross the blood brain barrier, any conversion prior to blood-brain barrier passage will mean it is unable to reach the brain. This early metabolic conversion of L-DOPA also leads to side effects as a result of off-target action, including nausea and hypotension.²⁷⁵ To reduce the proportion of L-DOPA converted before crossing the blood brain barrier, L-DOPA is typically administered with

an inhibitor of DOPA decarboxylase, carbidopa (**140**) (Figure 144).²⁷⁶ This carbidopa is metabolised by DOPA decarboxylase in preference to L-DOPA and therefore acts as a sacrificial additive. This improves the bioavailability of L-DOPA, and hence allows the dose of L-DOPA to be lowered, and this lowering of the required dose leads to a reduction in side effects.²⁷⁷ It is believed that carbidopa inhibits L-DOPA conversion primarily through binding to the active site of DOPA decarboxylase.²⁷⁸ Although this is not thought to be an irreversible interaction, the dissociation constant is small, and therefore the inhibition is highly effective.²⁷⁹ Carbidopa can also bind permanently to pyridoxal 5'-phosphate (PLP), an important co-enzyme in the decarboxylation – this further contributes to inhibition.²⁸⁰ This binding can also occur once the PLP has bound to the DOPA decarboxylase.²⁸¹ As PLP is also important for numerous other enzymes, significant inhibition of this can lead to side effects.²⁸²



140

Figure 144. The structure of carbidopa, the additive administered with L-DOPA.

Although the poor bioavailability and off-target effects of L-DOPA are problematic, the key issue with L-DOPA treatment is that, on prolonged treatment, metabolism of the drug is upregulated, and bioavailability is therefore lowered even further. Given Parkinson's is an incurable lifelong condition, with treatment for many years being required, this is a significant problem. This leads to unpredictability around the impact of the drug, with patients experiencing 'off-time' where the symptoms of Parkinson's are not reduced.²⁸³ Patients therefore require an ever-increasing dose of drug, with increasingly little impact on the symptoms. This can eventually lead to delivery of L-DOPA by an intestinal gel, delivered directly into the jejunum.²⁸⁴ This method is intrusive, unsuitable for many patients, and problems with the pump are common.²⁸⁵ These kind of problems typically begin 10-15 years after treatment with L-DOPA begins.

Despite these issues with L-DOPA, it has remained the gold standard for treatment of Parkinson's since the 1960s, with relatively little progress being made to improve things.²⁸⁶ There is therefore a clear need for enhanced delivery of L-DOPA, in either a slow-release formulation suitable for injection or implantation, or in a manner that may bypass the problematic first pass metabolism.

Work in this chapter therefore aimed to develop methods that might be capable of improving delivery of L-DOPA to the brain, either by developing a formulation for slow, controlled systemic release, or a system that might allow more direct delivery of L-DOPA to the brain.

6.1 Release of L-DOPA from DBS-CONH₂

DBS-CONH₂ hydrogels have previously been shown to form interactions with carboxylic acid containing compounds, including a number of non-steroidal anti-inflammatories, giving pH responsive release.¹⁰⁹ As L-DOPA also contains a carboxylic acid group, it was considered possible that this would also form interactions with the DBS-CONH₂ gel fibres (Figure 145), possibly leading to controlled release of the drug.

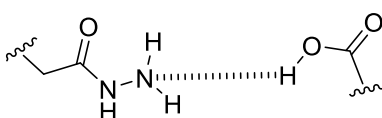


Figure 145. The potential interaction between L-DOPA and the DBS-CONH₂ gel fibres.

The incorporation of L-DOPA into DBS-CONH₂ hydrogels was therefore investigated, along with release of the drug. Initially, the best method for incorporation of L-DOPA into the hydrogels was explored.

Three methods for drug incorporation were investigated. The first used a solution of L-DOPA, which was then added to the gelator. This was sonicated, then the solids dissolved by heating. The second approach suspended DBS-CONH₂ in water, with this then being added to L-DOPA in a vial. Again, the solids were dissolved by heating. In both these methods although in some cases hydrogels were formed, gelation was not particularly reproducible. A third method, with the gelator and L-DOPA mixed as solids, in a 1:1 molar ratio, was therefore tried. Following sonication, the solids were dissolved by heating, and on cooling, hydrogels were reliably formed. This method was therefore used for the formation of all further DBS-CONH₂ hydrogels containing L-DOPA. Although the reasons for this method being more reliable were not further investigated, solvation is an important factor in gelation, and so changing the order in which the two solids were added to water may impact gelation.⁹⁴ In these studies, we had a preference for all the L-DOPA incorporated to be solubilised, to facilitate the analysis carried out. This required relatively low loadings of L-DOPA. In pharmaceutical formulations, it might be more desirable to formulate L-DOPA as a powder within the gel, to allow for higher loadings of the drug. This would be in equilibrium with the dissolved L-DOPA also present.

6.1.1 NMR Studies for DBS-CONHNH₂ Hydrogels with L-DOPA

Following the incorporation of L-DOPA into the DBS-CONHNH₂ hydrogels, the interactions between the drug and the gel fibres were investigated by ¹H NMR. Any gelator that is immobilised within the self-assembled 'solid-like' gel network will not appear in the NMR spectrum, as a result of a long relaxation time, and subsequent broadening of the peaks.²⁸⁷ This is also the case for any soluble additives that are interacting with the gel fibres. However, soluble drug additives that are mobile within the gel and capable of rapid diffusion, will be visible in the NMR spectrum and can hence be quantified. Through use of an internal standard, the proportion of an additive that is bound to the gel fibres can therefore be determined.

DBS-CONHNH₂ hydrogels with L-DOPA were therefore prepared for NMR studies. The same method as previously was used, with H₂O replaced with D₂O, and a DMSO internal standard (2 µl, 0.0282 mmol) was added. On heating, once the solid was dissolved, the solution was transferred, while hot, to a warm NMR tube, and the gel formed within the tube.

These studies indicated that around 59% of the L-DOPA included in the gel was immobilised, and hence potentially bound to the solid-like self-assembled gel fibres. This was promising, as such interactions can slow diffusion out of the gel, and therefore may be helpful in achieving controlled release of the drug.

6.1.2 Release of L-DOPA from DBS-CONHNH₂ Hydrogels

As DBS-CONHNH₂ has been shown to achieve pH-mediated release of naproxen,¹⁰⁹ as well as of rosuvastatin (see Chapter 2), the release of L-DOPA from these hydrogels was investigated at different pH values (Figure 146). Hydrogels were prepared as previously described, and buffer (6 ml) placed on top of the gel. The samples then placed in an incubator at 37 °C. At each timepoint, an aliquot (2 ml) of buffer was removed, and the amount of L-DOPA that had been released was quantified by UV-vis, with absorbance measured at 288 nm. The buffer was then returned to the gel. A sample containing no L-DOPA was also monitored, to account for the release of any DBS-CONHNH₂ into the solution and hence normalise the data.

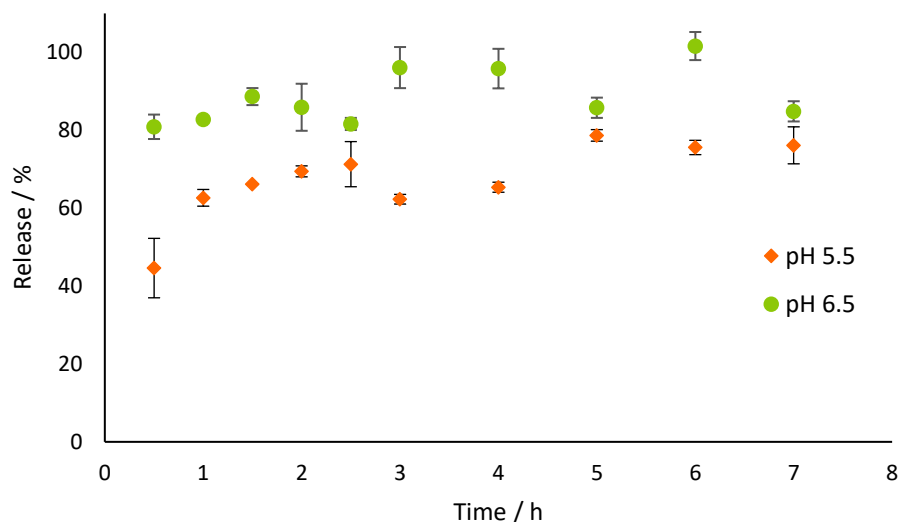


Figure 146. Release of L-DOPA from DBS-CONH₂ hydrogels (1 ml), into pH 5.5 or pH 6.5 buffer (6 ml) at 37 °C. Gelator loading 0.28% wt/vol, L-DOPA one molar equivalent.

As has been seen previously with DBS-CONH₂ hydrogels, there is some variation in release at different pH values, with lower release observed at lower pH. In this case, release is only slightly reduced at pH 5.5 compared to pH 6.5 – this is not surprising, given there is only a relatively small difference in pH. Furthermore, unlike previous carboxylic acid functionalised drugs studied with DBS-CONH₂, L-DOPA also contains an amine group. This directly impacts on the pKa values, which are 2.3, 8.7, 9.7 and 13.4.²⁸⁸ There are four pKa values as there are four ionisable groups (CO₂H, NH₂, and two OH). The pKa values mean that between pH 2.3 and 8.7, L-DOPA is predominantly present in the zwitterionic form, in which the amine group is protonated and the carboxylic acid is deprotonated. Changing the pH from 6.5 to 5.5 will therefore only slightly increase the level of protonation in this case. At both pH values, the majority of the total release occurred with the first 2-3 hours of the study, with relatively little further L-DOPA being released after this point.

Although there was evidence of some limited pH control over release, in both cases, the total amount of L-DOPA released still reaches its maximum rapidly – this is therefore not considered to be useful for a slow release formulation. It is also only of limited use to be able to obtain release at differing pH for L-DOPA – in any case, this would only have been really useful for oral delivery, which would not help bypass the problematic first pass metabolism.

6.2 Release of L-DOPA from MBS-CO₂Me

MBS-CO₂Me is a hydrogelator based on monobenzylidene sorbitol (MBS), that forms hydrogels at a gelator concentration of 0.75% wt/vol and above. As discussed in Chapter 2, it has properties

quite distinct from DBS-CONHNH₂, with greater mechanical strength, but reduced thermal stability and instability with respect to aqueous media. When tested for release of NPX, release was rapid, and primarily driven by gel erosion on addition of buffer.

Although this is not a useful property for slow, controlled, long term release, there are modes of delivery where rapid release of a drug from the gel would be desirable, including dermal and nasal delivery. Nasal delivery is of particular interest for delivery of drugs for Parkinson's. By administering the drug to the nasal cavity, not only can rapid systematic delivery be achieved via the nasal epithelia, but delivery directly to the brain can occur along the olfactory and/or trigeminal nerve, bypassing the blood brain barrier completely.²⁸⁹ One key issue for consideration with nasal delivery is the need to keep contact between the delivery vehicle and the nasal epithelium, to maximise uptake of the drug. It is here that hydrogels have potential to improve nasal delivery systems – the presence of the gel may help maintain this contact longer, as well as enhancing the intimacy of contact with nasal mucosa.

It was therefore considered that MBS-CO₂Me, with its rapid breakdown, and the resulting fast release of incorporated drugs, might have some potential for this application. Incorporation and release of L-DOPA from MBS-CO₂Me hydrogels was therefore investigated.

MBS-CO₂Me hydrogels containing L-DOPA were prepared by weighing a known mass of gelator into a vial, along with L-DOPA in a molar ratio of 0.5:1 drug: gelator. Water (1 ml) was added, and this was sonicated for 5 minutes to aid dispersion of the solid. The resulting suspension was heated until all the solid was dissolved, and the resulting solution allowed to cool. On cooling, transparent gels were formed.

The thermal stability of the gels was then investigated, with the concentration of MBS-CO₂Me at 0.9% wt/vol. The stability of the hydrogels was monitored by the tube inversion method, and the T_{gel} values determined (Table 24). The presence of the L-DOPA additive made very little difference to the T_{gel} value, which indicates that the presence of the drug does not significantly disturb the self-assembled gel, and may suggest that interactions between the drug and the gel network are limited in this case.

Table 24. T_{gel} values for MBS-CO₂Me hydrogels with and without L-DOPA.

MBS-CO ₂ Me / wt/%	L-DOPA Equivalents	T_{gel} / °C
0.90	-	57
0.90	0.5	56

Attempts were then made to quantify the release of L-DOPA from the MBS-CO₂Me hydrogels. MBS-CO₂Me gels containing L-DOPA were prepared in the manner described above, and 6 ml of buffer placed on top. The vials were then placed in a 37 °C incubator. The release of L-DOPA was then monitored by taking aliquots (2 ml) of the buffer at regular timepoints, and the concentration of L-DOPA determined by UV-vis absorbance at 288 nm. The aliquots were then returned to the sample. Control hydrogel samples, which did not contain any L-DOPA, were also prepared and treated in the same manner.

As demonstrated in Chapter 2, MBS-CO₂Me hydrogels break down rapidly on the addition of buffer, leading to burst release of incorporated drug. With NPX, the drug and the gelator have maximum absorbances at wavelengths that differ enough for release of the drug to be quantified. However, L-DOPA has a maximum absorbance at 288 nm – as does MBS-CO₂Me. It was found that both with and without L-DOPA, a significant signal was observed at ca. 290 nm, indicating release. Indeed, there was very little difference in absorption between the control gels, containing only MBS-CO₂Me, and the gels containing L-DOPA, and the overlap can be seen clearly (Figure 147). There was also significant variation in absorption for different control gels, adding to the difficulty in correcting for the overlap. This overlap gives significant problems with quantifying the release of L-DOPA.

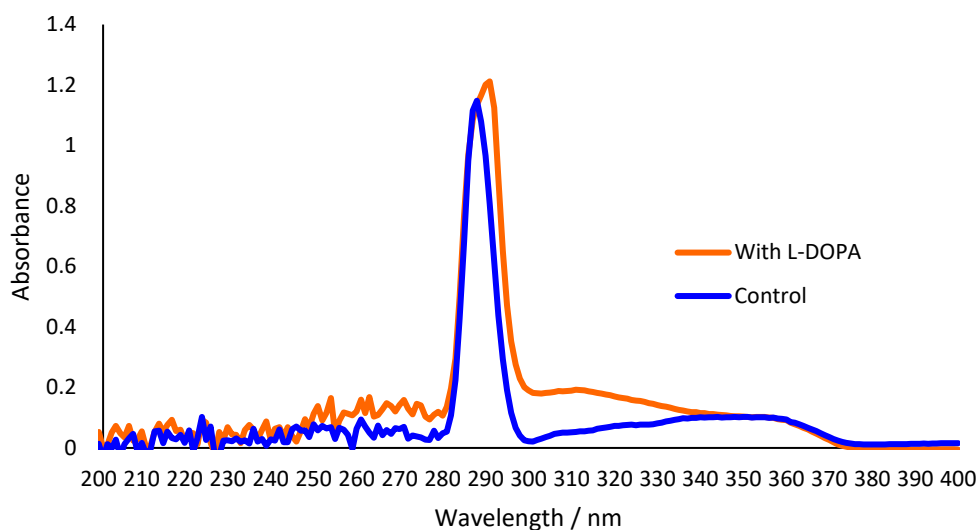


Figure 147. UV-vis spectra for release from MBS-CO₂Me hydrogels, both with and without L-DOPA.

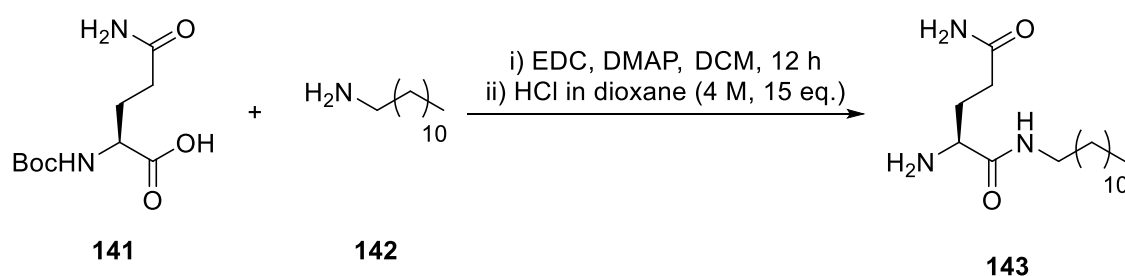
This problem is increased by the rapid breakdown of the MBS-CO₂Me hydrogels, a result of the relatively high water solubility of this gelator. This leads to more gelator being present in solution, further increasing the corresponding UV-vis signal. Indeed, within two hours of the supernatant being added, there is very little remaining gel. This suggests that, despite the issues with precise

quantification of L-DOPA release, all of the drug will have been released once the gel has broken down.

Despite the fast release of additives from MBS-CO₂Me hydrogels, they are not an especially suitable vehicle for nasal delivery. Ideally, for this application, rather than a bulk gel, it would be desirable to have a thin film, that could form on the inside of the nasal cavity. MBS-CO₂Me hydrogels are not especially well suited to this given their relatively high degree of rheological robustness – this gelator forms hydrogels that are fairly stiff, but have relatively low resistance to strain (see Chapter 2). It is likely that using this material for nasal delivery would cause discomfort to a patient. Furthermore, this gel has limited capacity to ‘self-heal’ which makes it poorly suited for delivery into the nasal cavity followed by thin film formation. It was therefore decided to focus attention on other possible candidate gels for L-DOPA delivery.

6.3 Development of Glutamine Amide Based Hydrogels

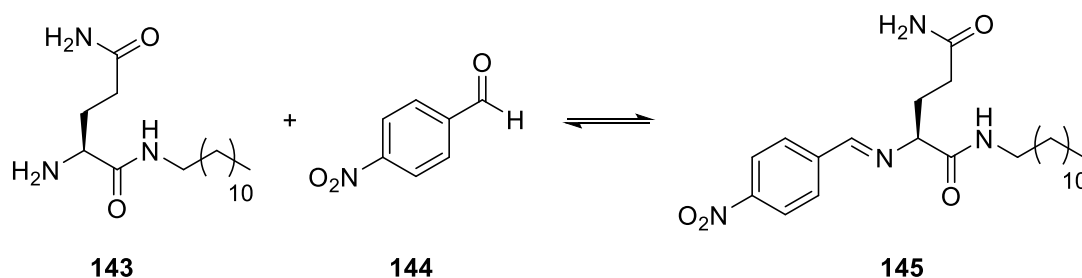
Previously, within our group, Dr Kirsten Hawkins investigated a group of molecules based on modified amino acids, for both the ability to form hydrogels, and catalysis of prebiotic reactions.²⁹⁰ Although a number of modified amino acids were synthesised, one in particular, based on glutamine, showed some promise – this amide-functionalised glutamine derivative was capable of forming hydrogels, albeit not especially reproducibly. This compound was synthesised by a straightforward two-step process (Scheme 26). First, dodecylamine (**142**) and Boc-protected glutamine (**141**) were coupled using 1-ethyl-3-(3-dimethylaminopropyl)carbodiimide (EDC) and dimethylaminopyridine (DMAP). This was followed by removal of the Boc protecting group with HCl. The resulting product was converted to the free base using NaOH (1 M).



Scheme 26. Synthesis of glutamine amide.

While glutamine amide (**143**) was found to be capable of forming hydrogels, this process was inconsistent, with gels not being formed in every case. However, it was found that further reaction between the glutamine amide (**143**) and aromatic aldehydes (e.g. **144**) resulted in the reversible formation of a Schiff base (eg. **145**) (Scheme 27). The product acted as a gelator, with

hydrogels being formed in a highly reproducible way. Two component hydrogels of this nature are relatively rare.^{177, 291}



Scheme 27. Formation of the Schiff base responsible for gelation, from glutamine amide and 4-nitrobenzaldehyde.

This novel hydrogel was investigated further by Hawkins, with the most effective method for gelation found to be a heat/cool cycle. The gelator had a very low MGC of 0.074% wt/vol (total loading, including both components) – low enough to be classed as a “supergelator”. Gels were still formed with even lower equivalents of 4-nitrobenzaldehyde used – as low as 0.7 equivalents. As the formation of the Schiff base requires 1:1 stoichiometry, this suggests that not all of the two starting materials need to be converted to the Schiff base for gelation to occur. This was further backed up by ¹H NMR studies of the gel with the components in a 1:1 ratio. These studies indicated that 0.3 equivalents of aldehyde were mobile in solution.

The Schiff base responsible for gelation is formed in a reversible reaction. As a result, it was considered plausible that the gel may be capable of self-healing behaviour. Tests were therefore carried out by Hawkins to determine if the gel behaved in a thixotropic manner. A hydrogel, with glutamine amide at 0.1% wt/vol, and 1 equivalent of 4-nitrobenzaldehyde, was formed in a syringe. This was then injected into a vial, and left to stand, without the application of any other stimuli. After 4-12 hours of standing, the hydrogel was shown to have re-formed, as demonstrated by the tube inversion test. Re-formation following injection is an attractive property for hydrogels, with potential applications in drug delivery in particular, as it indicates that the gel can be injected, and then reform in the desired location.²⁹² Although in this case the self-healing was relatively slow, it is worth noting that this was to form a full sample-spanning gel in a vial – very different to the formation of a thin film on a support.

Following this initial work with 4-nitrobenzaldehyde, an aldehyde screen was carried out, to determine how general this mechanism for gel formation might be. A number of aldehydes were screened, all in a 1:1 molar ratio with glutamine amide. These tests showed that for gelation to occur, the aldehyde was required to contain an aromatic group. The nature of this group was also

important, with electron-poor substituents typically giving hydrogels, and more electron-donating substituents not forming gels.

This screen indicated that the combination of glutamine amide and benzaldehyde led to the formation of a gel. Benzaldehyde, as the simplest aromatic aldehyde, was of particular interest.²⁹³ Notably, benzaldehyde is used both as a flavouring and in some fragrances,²⁹⁴ and is generally regarded as safe.²⁹⁵ This is in contrast to many other aromatic aldehydes, which are considered to be more toxic. This made the glutamine amide and benzaldehyde based gelator (**144**) (Figure 148) attractive for further investigation.

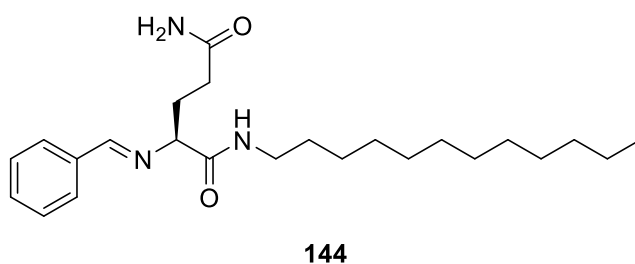


Figure 148. The Schiff base gelator formed from glutamine amide and benzaldehyde.

6.3.1 Rheology of Glutamine Amide Based Hydrogels

When considering applications for a hydrogel, it is important to understand the material properties in detail – how a gel behaves in response to an application of force can be particularly important. These properties influence what applications a hydrogel might be suitable for. The rheological properties of the glutamine amide and benzaldehyde hydrogels were therefore investigated in detail as a part of this PhD, as this feature had not previously been studied by Hawkins. In particular, we were interested in the self-healing characteristics, as these are particularly relevant in the application of nasal drug delivery where the gel should ideally enter the nasal cavity in liquid form and then rapidly assemble into a gel.

Firstly, an amplitude sweep was carried out – this allows the LVR of the hydrogel to be determined, and gives information on the stiffness and resistance to strain of the material. Hydrogels were prepared with glutamine amide at a concentration of 0.3% wt/vol, and 1 equivalent of benzaldehyde. These were prepared by addition of the gelator to a vial, followed by a heat/cool cycle. At this point, once the solid had been dissolved by heating, the hot solution was transferred quickly to a warmed bottomless vial, attached to a petri dish. Without warming the vial, the hydrogel formed very rapidly once transferred, and the hydrogels formed were not homogenous. This therefore gave very weak gels that could not be transferred to the rheometer. With a pre-warmed vial, the rate of cooling was slowed, and the gels therefore formed more

slowly, giving more homogenous gels. The gel discs could then be transferred to the rheometer for analysis. The amplitude sweep (Figure 149) was then carried out, with the amplitude varied from 0.001-100% strain, and frequency kept constant at 1 Hz.

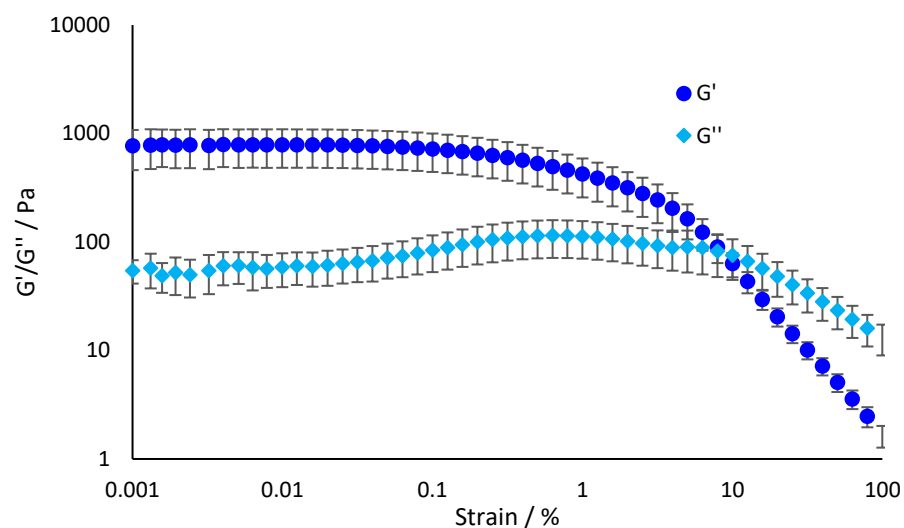


Figure 149. Amplitude sweep (0.001%-100%) for glutamine amide gels (0.3% wt/vol) formed with benzaldehyde (1 equivalent). Temperature 25 °C, frequency 1 Hz.

The glutamine amide and benzaldehyde hydrogel has a clear LVR, indicating that at lower strain, the material is behaving as a viscoelastic material. The LVR extends to around 0.065% strain – at this point, G' drops by 5% of its original value. The G' in the LVR is around 780 Pa, reasonably stiff for a LMWG – although this is at a relatively low strain. The crossover point, where $G'=G''$ is at just under 8% - indicating a reasonable resistance to strain.

As well as the amplitude sweep, a frequency sweep was also carried out (Figure 150). Frequency was varied from 0.1-100 Hz, with strain kept constant at 0.00787%. For a viscoelastic material such as a gel, G' should remain independent of frequency. This was indeed the case, with G' remaining constant to around 5 Hz. At very high frequencies, where gel dynamics are being studied over very short timescales, there is an increase in G' and G'' , indicative of hardening and breakage being induced, under these extreme conditions.^{174, 296}

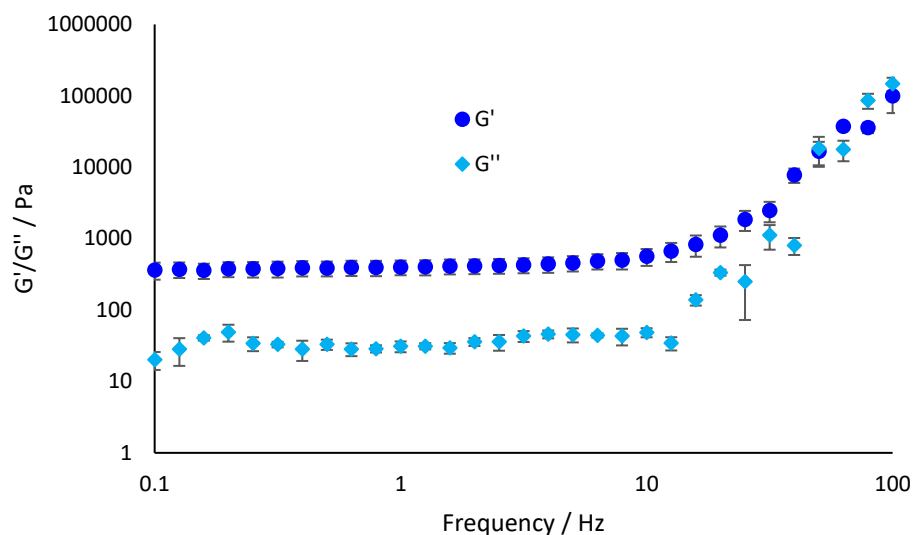


Figure 150. Frequency sweep (0.1 Hz-100 Hz) for glutamine amide (0.35 wt/vol) hydrogels with benzaldehyde (1 equivalent). Temperature 25 °C, amplitude 0.0078%.

A key consideration was whether the self-healing properties, observed visually for a macroscopic sample of the 4-nitrobenzaldehyde based gel by Hawkins were maintained in the benzaldehyde based system. This was initially tested using the same visual method as previously. A hydrogel of glutamine amide (0.35% wt/vol) with benzaldehyde (1 equivalent) was prepared. This followed the same method as previously until the heat-cool cycle. At this point, while the solution was hot, it was drawn up into a syringe. On cooling, the hydrogel was formed within the syringe barrel. Following gel formation, the gel was injected into a vial – at this point, the gel was broken down (Figure 151). The vial was then left to stand overnight, and gelation then tested by the tube inversion test.

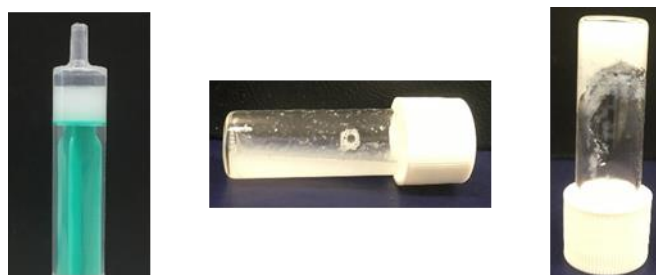


Figure 151. Left: Glutamine amide and benzaldehyde hydrogel (0.5 ml, 0.35% wt/vol, 1 equivalent benzaldehyde) formed in a syringe. Centre: The solution immediately after injection of the hydrogel into a vial. Right: The reformed hydrogel, following standing overnight.

Pleasingly, as for the 4-nitrobenzaldehyde based system, the glutamine amide and benzaldehyde hydrogels did reform after standing – with no further application of external stimuli. This is promising – as previously discussed, injectable hydrogels are attractive for pharmaceutical applications.

Self-healing of this nature would be of particular interest for nasal delivery. If the gel applied to the nasal cavity (with the gel breaking down in the process) can rapidly reform into a thin film, this offers potential for maintaining contact between the drug delivery vehicle (in this case the hydrogel) and the nasal cavity. This in turn allows more time for any incorporated drug to be delivered through the nasal epithelium.

The self-healing properties of the hydrogel were therefore investigated further. Particularly important are the kinetics of the process – to be useful for the desired application, the gel must reform relatively rapidly. The reformation process was therefore monitored by parallel plate rheology. Samples for rheology were prepared as previously, with glutamine amide at a concentration of 0.35% wt/vol, with one equivalent of benzaldehyde.

Once the gel had been transferred to the rheometer, a shear strain of 0.0126% was applied – this strain is within the LVR of the hydrogel, and therefore will not break it down. For the first 200 seconds, the frequency was maintained at 2 Hz. The frequency was then increased to 100 Hz for 30 seconds, resulting in the gel being broken down. The frequency was then returned to 2 Hz, and the recovery of the hydrogel monitored over time (Figure 152). In a nasal delivery device, it is likely that a mixture of both shear strain and frequency would contribute to the breakdown of the gel. This frequency method was therefore chosen, as it helped reduce artifacts in the data produced, and both the viscosity and G'/G'' were measured. This allowed the kinetics of gel reformation to be studied.

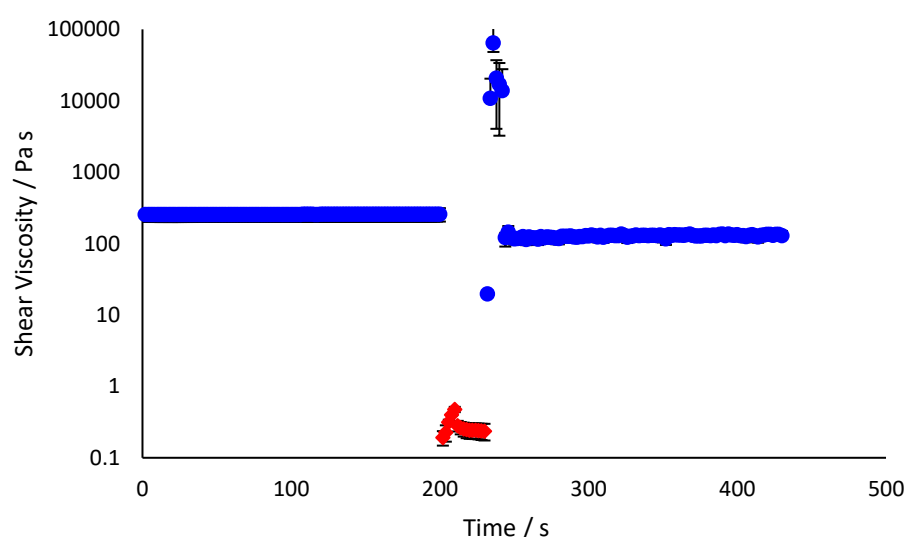


Figure 152. Shear viscosity of glutamine amide hydrogels (0.35% wt/vol, 1 equivalent benzaldehyde) with changing frequency. Blue: frequency is 2 Hz. Red: frequency is 100 Hz. Temperature 25 °C, shear strain 0.012%.

As expected, on the increase in frequency, the hydrogel broke down immediately – indicated by the significant reduction in viscosity. Pleasingly, once the frequency was returned to 2 Hz, the hydrogel quickly recovered to close to the original viscosity – within around 10 seconds. This indicated that although the larger bulk sample took longer to fully recover, under rheometry conditions designed to mimic those of nasal delivery, the majority of the recovery occurs rapidly. This was also observed in the G'/G'' measurements for the hydrogel (Figure 153). This shows the rapid recovery of the gel, within around 15 seconds, to close to the original G' value following the application of increased frequency. This is positive for the potential application of nasal drug delivery – as the material should be capable of forming the desired thin film inside the nasal cavity upon application by a spraying device or similar.

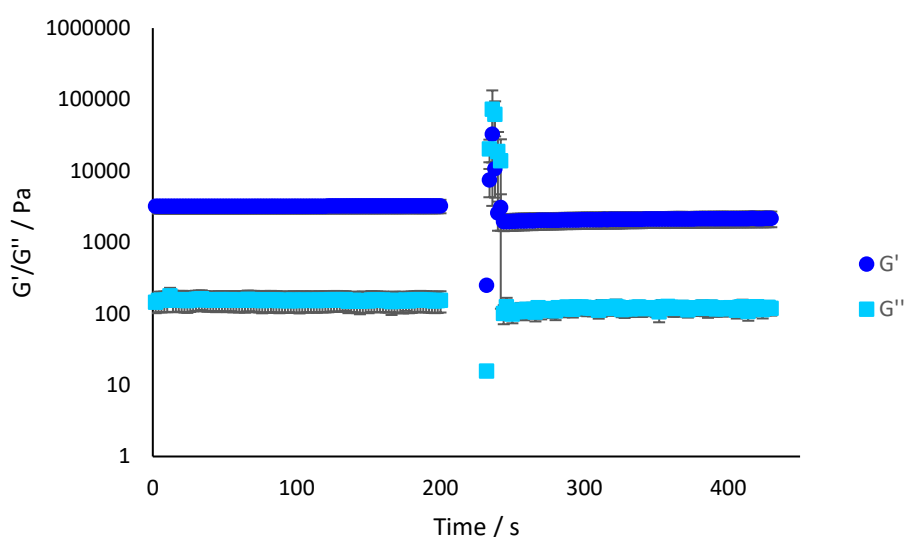


Figure 153. G' and G'' for the reformation of glutamine amide hydrogels (0.35% wt/vol, 1 equivalent benzaldehyde). The gap at 200-230 s is the time at which the frequency was increased. Temperature 25 °C, shear strain 0.012%.

6.4 Glutamine Amide Hydrogels with L-DOPA

Following confirmation that glutamine amide and benzaldehyde hydrogels undergo self-healing after the application of a force, the inclusion of L-DOPA as an additive was tested. Hydrogels with glutamine amide (0.35% wt/vol) and benzaldehyde (1 equivalent) were tested, with varying equivalents of L-DOPA. The hydrogels were formed as previously, with the components added to a vial, before addition of water, and dissolution of the solids by heating. On cooling, gelation was tested by the tube inversion test (Table 25).

Table 25. Gelation testing for glutamine amide hydrogels (0.35% wt/vol, 1 equivalent benzaldehyde) with L-DOPA. Equivalentents are molar equivalentents. G=Gel, P=Precipitate.

L-DOPA / equivalentents	Gel
0.25	G
0.5	G
0.75	G
1	G
2	G
3	G
4	G
4.5	G, P
5	G, P
10	G, P

Gels were still formed in the presence of L-DOPA. At up to 4 equivalentents of L-DOPA, all of the solid was still dissolved. At loadings above this, not all of the solid was dissolved, so although hydrogels were still formed with up to 10 equivalentents of L-DOPA, these gels also contained clumps of undissolved L-DOPA. This meant the samples were not homogenous. Such gels may, nonetheless be useful for practical drug delivery, but for the ease of characterisation and the purposes of this study, we elected to focus on gels in which all of the L-DOPA was fully dissolved.

6.4.1 Rheology for Glutamine Amide Hydrogels with L-DOPA

The effect of the addition of L-DOPA on the rheological properties was then investigated. Initially, an amplitude sweep was carried out, to confirm that a hydrogel was still being formed, and determine the LVR of the material. Glutamine amide hydrogels were prepared for rheology as previously, with glutamine amide at a concentration of 0.35% wt/vol, and 1 equivalent of each of benzaldehyde and L-DOPA. The amplitude sweep (Figure 154) was carried out with amplitude 0.001-100%, and a constant frequency of 1 Hz.

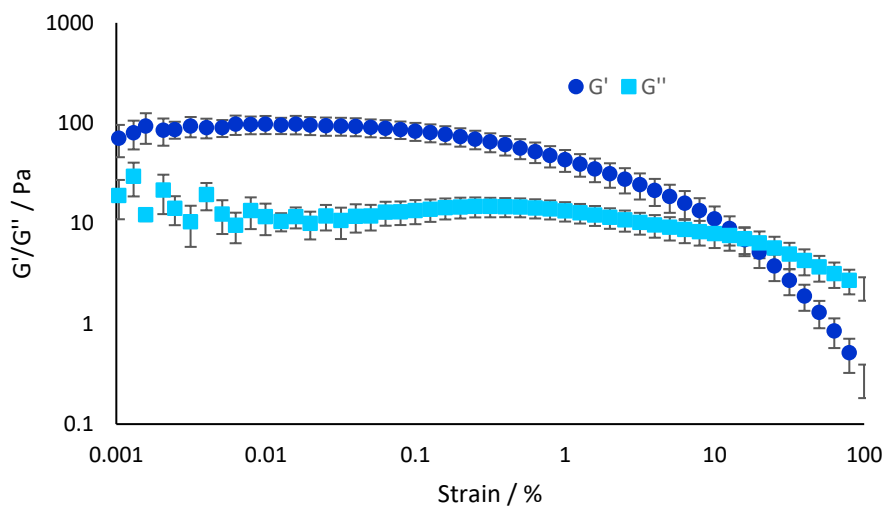


Figure 154. Amplitude sweep for glutamine amide and benzaldehyde hydrogels (0.35% wt/vol, 1 equivalent benzaldehyde) with L-DOPA (1 equivalent). Temperature 25 °C, frequency 1 Hz.

With addition of L-DOPA, the hydrogels still had a clear LVR. Although the G' , and therefore stiffness of the gel, was significantly reduced in comparison to the hydrogels without L-DOPA, to around 100 Pa. However, for the desired application of nasal drug delivery this is not too problematic, as a softer material would be preferable as it will be more suited to thin film formation.

The key characteristic which needed to be maintained for this application is the self-healing properties of the hydrogels. This was therefore tested for the glutamine amide hydrogels with one equivalent of L-DOPA, using the same method as described in section 6.3.1, with frequency first at 2 Hz, then increased to 100 Hz to break down the hydrogel, then returned to 2 Hz, at which point the recovery of the hydrogel was monitored (Figure 155).

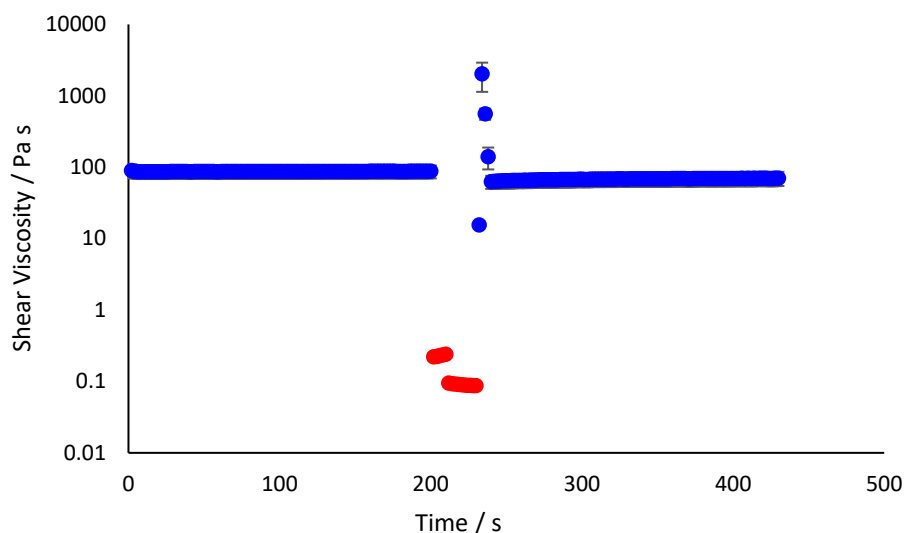


Figure 155. Shear viscosity of glutamine amide and benzaldehyde hydrogels (0.35% wt/vol, 1 equivalent benzaldehyde) with L-DOPA (1 equivalent). Blue: frequency is 2 Hz. Red: Frequency is 100 Hz. Temperature 25 °C, shear strain 0.012%.

As with glutamine amide hydrogels without L-DOPA, once the frequency returned to 2 Hz, the gel recovered quickly, within around 10 seconds. Once again, this was also observed in the G'/G'' values (Figure 156). This confirms that, on incorporation of L-DOPA into the hydrogel, the self-healing properties are maintained, and so this material still has potential for nasal drug delivery.

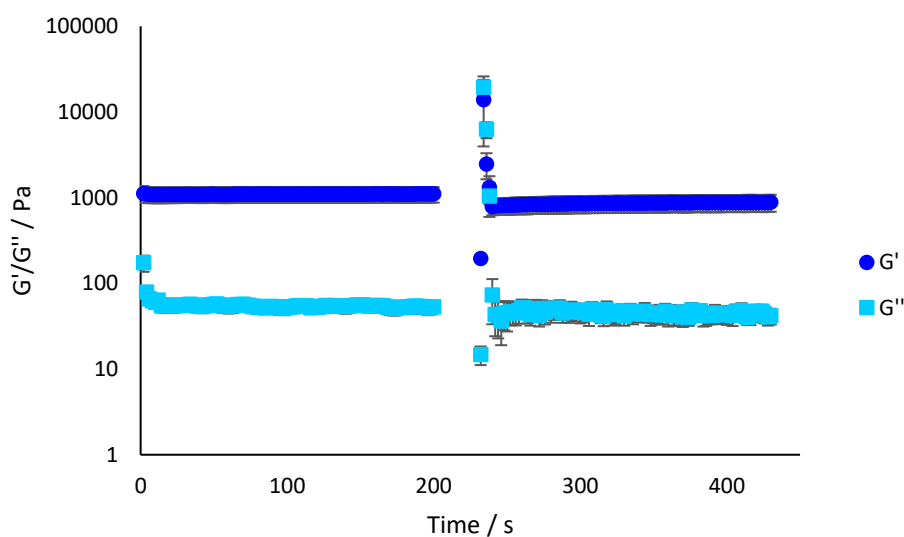


Figure 156. The G' and G'' for the reformation of glutamine amide hydrogels with L-DOPA (0.35% wt/vol, 1 equivalent benzaldehyde, 1 equivalent L-DOPA). The gap at 200-230 s is when the frequency was increased. Temperature 25 °C, shear strain 0.012%.

6.4.2 Imaging of Glutamine Amide Hydrogels with L-DOPA

To further investigate any impact of adding L-DOPA to the glutamine amide hydrogels, TEM and SEM imaging was carried out. As discussed in previous chapters, these techniques do have limitations associated with sample drying, but are nonetheless useful for comparing chemically related samples that have been prepared for imaging in the same way. Samples were prepared with a glutamine amide concentration of 0.35% wt/vol, and one equivalent of benzaldehyde, with the loading of L-DOPA being varied (Figure 157).

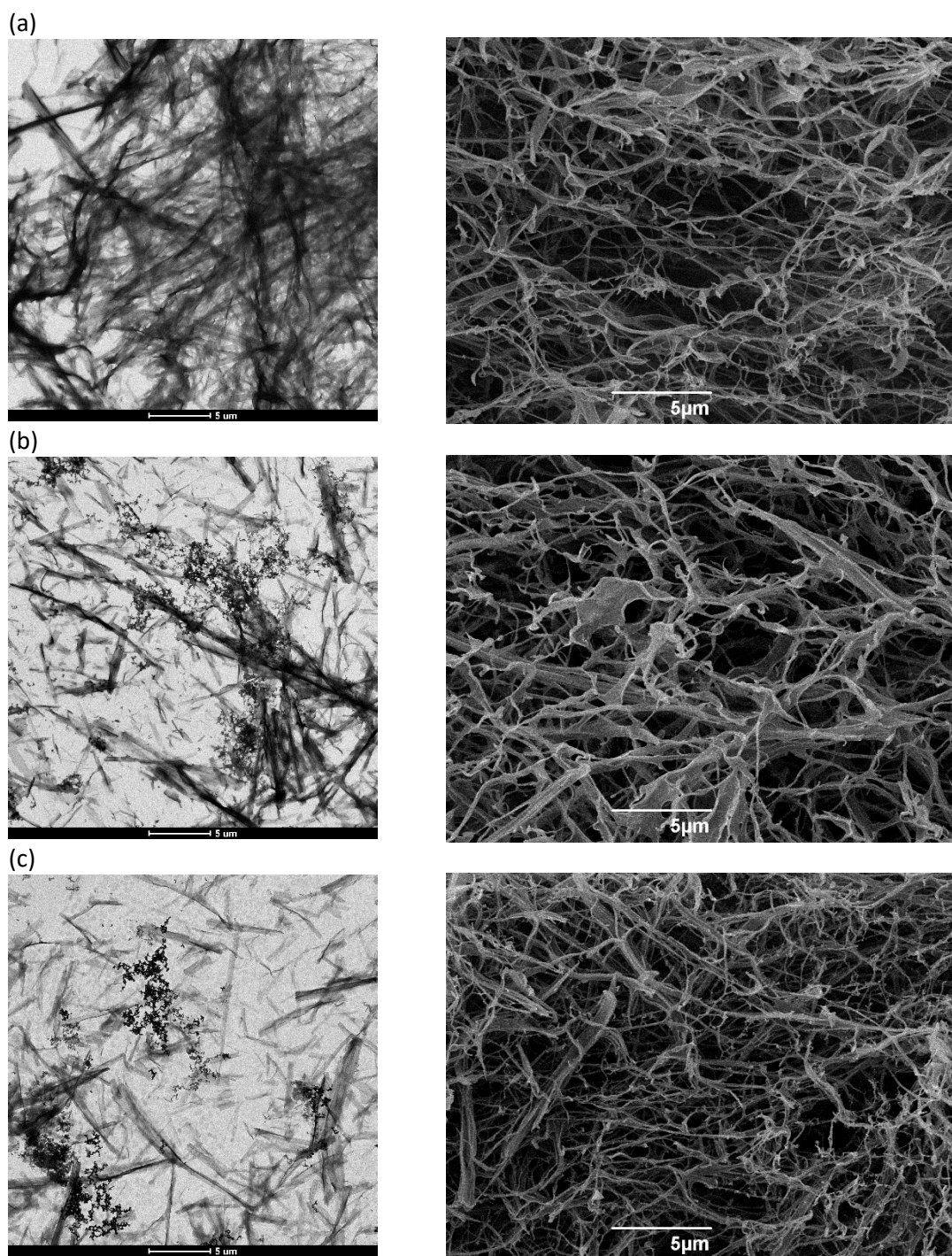


Figure 157. TEM (left) and SEM (right) images for glutamine amide hydrogels with L-DOPA. (a) benzaldehyde:L-DOPA 1:1 (b) benzaldehyde:L-DOPA 1:4 (c) benzaldehyde:L-DOPA 1:10. All scale bars 5 μm .

The images indicate that increasing the loading of L-DOPA has little impact on the nanostructured network of the hydrogel, with nanofibres clearly visible at all loadings. However, the TEM images for the samples at higher L-DOPA loadings do indicate that some aggregates have formed – most likely these are a result of L-DOPA that has not completely dissolved within the gel. In terms of drug delivery, in this work we generally ensured that all of the L-DOPA was soluble wherever possible for the studies, however, it is possible that for clinical application the presence of some

solid L-DOPA may not be problematic, and may actually enhance the total amount of L-DOPA that can be delivered using these gels, enhancing therapeutic performance.

6.4.3 NMR Studies for Glutamine Amide Hydrogels with L-DOPA

Given that the reaction for the formation of the Schiff base is reversible, it was important to determine how much benzaldehyde was 'free' at any point. Although benzaldehyde is generally regarded as safe, especially at low concentrations, there is some evidence of nasal irritation being caused on inhalation of benzaldehyde. While it is worth noting that this was observed under relatively extreme conditions, with volatilised benzaldehyde, at a concentration of 500 ppm, inhaled for multiple six hour periods,²⁹⁷ it is clearly still important to understand the nature of a system that may be used for drug delivery. The proportion would be determined by ¹H NMR, as discussed in Section 6.1.1.²⁸⁷

Hydrogels were therefore prepared of glutamine amide (0.35% wt/vol) and benzaldehyde (1 equivalent), in the same manner as for the samples with L-DOPA. Once the hydrogels had formed within the NMR tube, they were analysed by ¹H NMR, and the amount of 'free' benzaldehyde could be quantified.

It was determined that around 35% of the benzaldehyde added was not bound within the gel network. This equates to 0.4 mmol of benzaldehyde, or 0.04% wt/vol. This is considerably lower than the concentration of benzaldehyde used in other applications such as perfumes.

Additionally, it has been shown that these hydrogels can be formed successfully with only 0.7 equivalents of benzaldehyde. In this case, a greater proportion of the benzaldehyde would be bound within the gel network, further minimising any impact. We come back to this point at the end of the Chapter.

When considering a hydrogel for drug delivery, as noted previously, it is important to understand the level of interaction between the drug and the gel network – this can have an impact on the rate at which the drug is released.

Glutamine amide hydrogels (0.35% wt/vol), with benzaldehyde (1 equivalent) and L-DOPA (1 equivalent) were prepared in D₂O, with a DMSO internal standard. The standard method was followed to the point of the heat/cool cycle. At this point, once the solid was dissolved, the hot solution was transferred to a warm NMR tube. On cooling, a gel was formed within the NMR tube. The amount of unincorporated benzaldehyde was also calculated.

On analysis of the hydrogel by ^1H NMR, it was found that 92% of the L-DOPA was mobile within the hydrogel, rather than precipitated or bound to the gel fibres in a 'solid-like' form. This indicates there is little interaction between L-DOPA and the gel network in this case. This is likely to lead to rapid release of the drug – there are no interactions to slow the diffusion of the L-DOPA out of the gel network. For some applications, requiring slow, controlled release, this would be a disadvantage. However, for nasal delivery, rapid diffusion out of the gel is desirable once the gel has been applied, as residence times in the nose might be expected to be on the timescale of minutes (not hours). The amount of benzaldehyde that was unbound was also slightly reduced, to around 30%.

6.5 Release of L-DOPA from Glutamine Amide Hydrogels

Following the characterisation of the properties of the glutamine amide hydrogels, both with and without L-DOPA, the ability of the gel to release L-DOPA, both *in vitro* and *in vivo*, was investigated. Studies were also carried out to assess the cytotoxicity of the hydrogels.

6.5.1 *In vitro* Release

Initially, the release of L-DOPA *in vitro* was quantified. These studies were carried out by Dr Ana Campo-Rodrigo using the method for L-DOPA release previously developed by me. Glutamine amide hydrogels were prepared as previously, in sample vials, with a total volume of 1 ml, and a depth of around 0.5 cm. These were then exposed to pH 7 buffer solution (6 ml). Control samples, containing no L-DOPA, were also prepared and monitored. At each timepoint, aliquots (2 ml) were removed from the supernatant, and the concentration of L-DOPA determined by UV-vis spectroscopy (Figure 158). The aliquots were then returned to the sample.

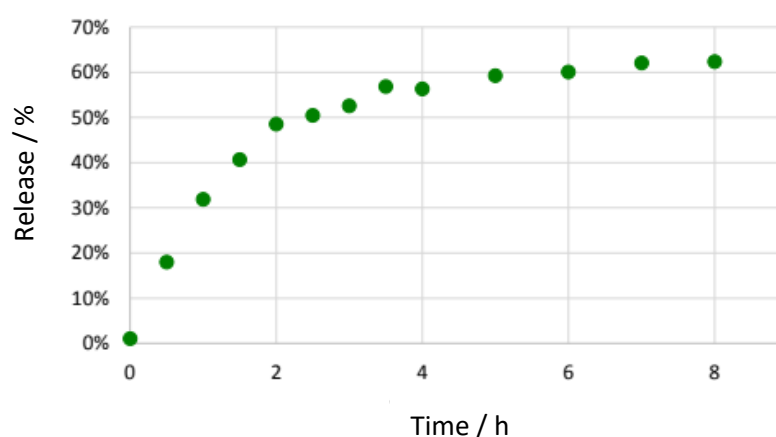


Figure 158. Release of L-DOPA (0.8 mM) from glutamine amide hydrogels (1 ml, 0.35% wt/vol) with benzaldehyde (1 equivalent), into pH 7 buffer (6 ml).

Release of L-DOPA from these bulk hydrogels was rapid, with the majority occurring within the first 2 hours. This is consistent with evidence from the ^1H NMR studies that indicated that the majority of the L-DOPA is free to move within the “liquid-like” part of the gel, and hence can rapidly diffuse out. Release of L-DOPA plateaued at around 60% of the total incorporated, although with replacement of the supernatant, greater release may have been achieved. However, for rapid nasal delivery, 60% release of the drug is sufficient. We also note that in this study, the release is from a bulk gel, somewhat different to the thin films expected on nasal delivery, that would be expected to have even faster drug release kinetics with the bulk of the gel being much closer in physical terms to the nasal epithelium.

6.5.2 *In vitro* Cytotoxicity Studies

As this system was being developed with nasal delivery in mind, the hydrogels, both with and without L-DOPA, were then tested for cytotoxicity. These studies were carried out by Dr Julie T. Wang at King’s College London.

To determine the cytotoxicity of the hydrogels, they were exposed to nasal epithelial cells *in vitro*. A glutamine amide hydrogel without L-DOPA, at a gelator loading of 0.35% wt/vol, and a second gel containing L-DOPA (4.8 mM) were prepared. Human nasal septum tumour RPMI 2650 cells were incubated with culture medium, that contained gels at concentrations of up to 10%, for both 24 and 48 hours. Additionally, cells were monitored with a mixture of ungelled glutamine amide (1780 μM) and L-DOPA (480 μM), as well as L-DOPA solution (480 μM) in water.

For both the gel alone, and the gels containing L-DOPA, some concentration-dependent cytotoxicity was observed (Figure 159). This was not the case for L-DOPA solution only, with cell viability only decreasing at the highest concentrations. This indicates that toxicity can be mainly attributed to the gel. It is possible this is a result of the gelator disassembling in the cell culture medium – the gelator is formed in a reversible process. The glutamine amide component can then act as an amphiphile, disrupting the cells.

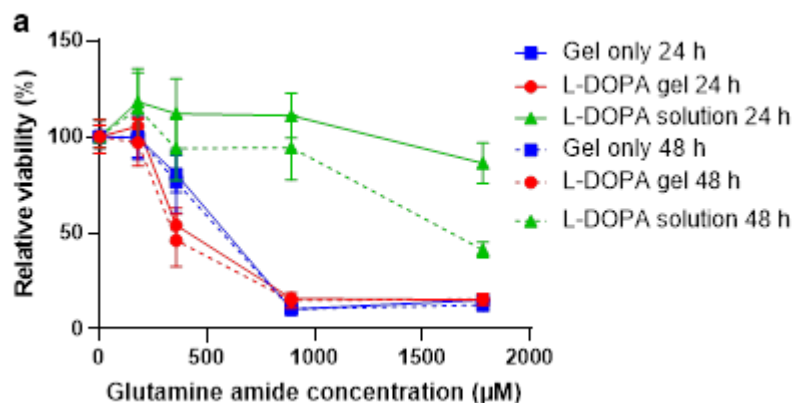


Figure 159. Cytotoxicity of the glutamine amide hydrogel alone, and with L-DOPA, in human nasal septum tumour RPMI 2650 cells. Cells were incubated with culture media, containing up to 10% gel alone, gel with L-DOPA, or L-DOPA solution for 24 and 48 h.

The results for glutamine amide in solution were therefore compared with two other surfactant amphiphiles (Figure 160), Tween® 80, a widely used surfactant considered safe,²⁹⁸ and cetyltrimethylammonium bromide (CTAB), used commonly as a surface coating agent, but highly toxic.²⁹⁹

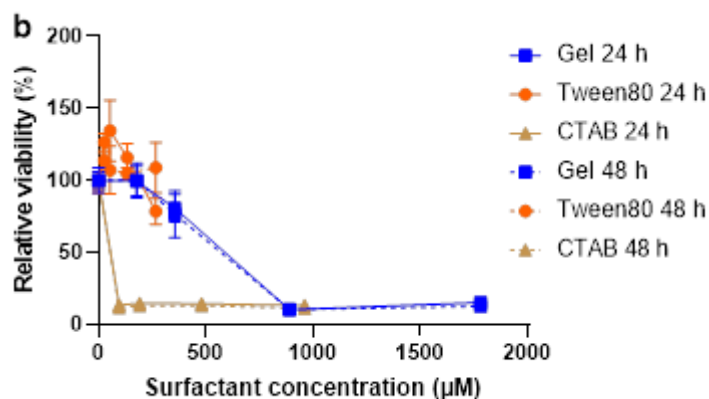


Figure 160. Viability of cells with varying concentrations of the glutamine amide hydrogel, Tween® 80 and CTAB for 24 and 48 h.

This comparison indicated that, at low concentrations, around 200 µM, the glutamine amide has comparable toxicity to Tween® 80. Cell viability in the presence of glutamine amide does decrease significantly at increased concentrations, but is not comparable to CTAB until concentrations of almost 1000 µM. In the case of CTAB, severe toxicity is apparent at even very low concentrations – this is not the case for glutamine amide.

This therefore indicates that the hydrogel has reasonable biocompatibility, particularly at low concentrations. It should also be noted that, in the application of nasal delivery, the gel will not be

immersed in solution such as cell media. There should be less disassembly of the gel, and therefore there is likely to be less glutamine amide in solution. This should further improve the biocompatibility.

6.5.3 *In vivo* Release and Biodistribution Studies

There has been increasing interest in drug delivery via the nasal route.³⁰⁰ This route offers the opportunity for rapid systematic uptake, by absorption into the bloodstream through the nasal epithelia.³⁰¹ However, the key attraction is to achieve uptake into the brain, via the olfactory or trigeminal nerves.³⁰² This is considered especially important for neurological diseases such as Parkinson's or Alzheimer's, in which delivery to the brain is vital.³⁰³ Active agents that have been investigated for delivery in this way include insulin,³⁰⁴ morphine,³⁰⁵ rivastigmine,³⁰⁶ and leptin.³⁰⁷ Often polymers are used as mucoadhesive agents, to increase the residence time of the drug within the nasal cavity,³⁰⁸ including polymer hydrogels.³⁰⁹ The use of a gel can also help to prevent mucosal clearance of the drug – this is a significant barrier in delivery of drugs to the brain.³¹⁰ To determine if this system had potential for use in intranasal drug delivery, *in vivo* studies were carried out, to determine the uptake and biodistribution of L-DOPA following application of the hydrogel. These studies were carried out by Dr Julie T. Wang at King's College London.

To allow the distribution of L-DOPA to be followed, radiolabelled [³H] L-DOPA was used. This was administered intranasally to anaesthetised naïve Balb/c mice, either in the hydrogel formulation, or in solution for comparison (L-DOPA 0.95 mg/kg, 1.5 µCi per mouse). At set timepoints (10 minutes, 20 minutes, 1 hour), blood samples were taken, followed by terminal anaesthesia and transcardiac perfusion. The brain tissue, other major organs, and the nasal cavity were then removed. The amount of L-DOPA in each organ, at each timepoint, was calculated by liquid scintillation counting. Of particular interest were the brain, nasal cavity, blood and liver (Figure 161).

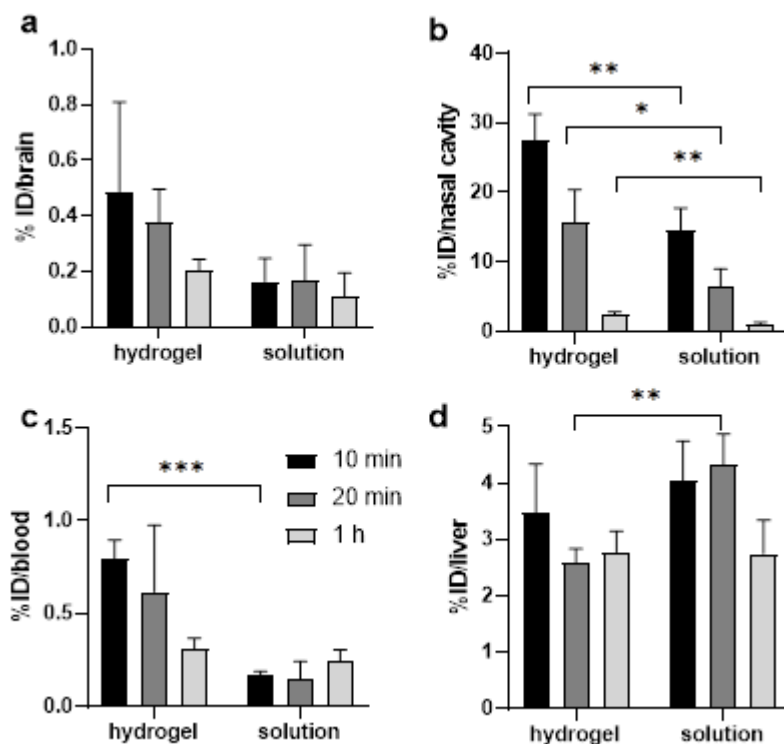


Figure 161. Uptake of [^3H] L-DOPA from hydrogel or solution in (a) the brain, (b) the nasal cavity, (c) the blood and (d) the liver, at 10 minutes, 20 minutes and 1 hour after administration. Results are %ID per tissue, with data expressed as the mean \pm SD. Statistical significance is compared between each timepoint. * $p < 0.05$, ** $0.01 < p < 0.05$, *** $p < 0.01$ (one-way ANOVA).

Delivery of L-DOPA via the hydrogel gave more L-DOPA both within the nasal cavity, and in the brain, when compared to L-DOPA in solution. This was particularly significant for the nasal cavity, with $27.55 \pm 3.73\%$ of L-DOPA in the nasal cavity ten minutes after delivery in the hydrogel, compared to $14.60 \pm 3.17\%$ when delivered in solution. This translates to a greater proportion of L-DOPA in the brain after ten minutes for hydrogel delivery, $0.49 \pm 0.32\%$, than for injection in solution, at $0.16 \pm 0.08\%$. This does suggest that the presence of the gel helps to keep the L-DOPA in the nasal cavity, hence giving more time for effective uptake of the drug. The level of L-DOPA in the blood after ten minutes was also much higher for the hydrogel delivery – this further supports that, with greater time in the nasal cavity, there is greater opportunity for effective uptake of L-DOPA. Although the dose per mouse is a relatively low 0.95 mg kg^{-1} , another study, with L-DOPA administered nasally to rats, found that a dose of 0.35 mg kg^{-1} was actually sufficient to show an improvement in motor symptoms – although this study did not quantify the amount of L-DOPA in the brain.³¹¹ This suggests that the dose used here could be effective in relieving symptoms in a disease model. It is also important to note that there is scope to increase the loading of L-DOPA in the hydrogel, giving an increased therapeutic dose.

Although nasal delivery can, to an extent, bypass the liver and gastrointestinal (GI) tract, and therefore avoid first pass metabolism, this route cannot be avoided completely. Some of the administered drug may be swallowed, or otherwise transported to the GI tract.³¹² From here, there will be transport to, and accumulation in, the liver. Interestingly, in these studies, there was a noticeable decrease in L-DOPA in the liver when the hydrogel application was used. It is possible that, when L-DOPA was administered in solution, it is more likely to enter the GI tract, and then the liver. This is in agreement with there being less L-DOPA in the nasal cavity when the solution is delivered – the hydrogel helps to keep the L-DOPA within the nasal cavity, which both increases delivery to the brain and blood, and reduces loss to the GI tract by swallowing or other routes.

The delivery of L-DOPA in an intranasal gel formulation was also compared to intravenous injection of L-DOPA – this method of delivery is sometimes required for late stage PD patients. Pleasingly, nasal delivery of the gel formulation again showed higher levels of L-DOPA both within the brain, and in the blood, while uptake in the liver was reduced (Figure 162).

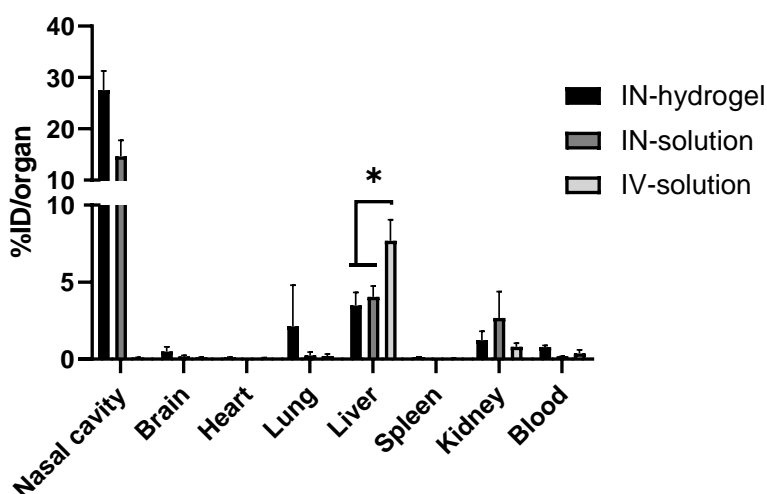


Figure 162. Distribution of L-DOPA in selected organs, following delivery by either intranasal hydrogel formulation, intranasal solution, or intravenous solution. Results are %ID per tissue, with data expressed as the mean \pm SD. Statistical significance is compared between each timepoint. * $p < 0.05$, ** $0.01 < p < 0.05$, *** $p < 0.01$ (one-way ANOVA).

As well as investigating the distribution of L-DOPA in different organs, the distribution in the brain was also studied more closely, following intranasal administration of the hydrogel formulation. Currently, the exact route of delivery from the nose to the brain is not fully understood. However, there are a number of possible pathways, and it is generally believed that which of these is taken depends on the nature of the drug and the delivery system. The inside of the nasal cavity has a relatively high level of blood flow, and this can result in the drug being absorbed into systemic

circulation. While this does not result in direct delivery to the brain, first pass metabolism by the liver is avoided.³¹³

Of greater interest are routes that allow for bypassing the blood brain barrier. There are thought to be two key routes for this. The first is via the olfactory nerves – these are the nerves that connect the olfactory region of the nasal cavity to the brain.^{289b} The olfactory bulb is the only part of the central nervous system (CNS) that is in contact with the environment,³¹⁴ and the route taken by active agents along this route has been followed by monitoring the progress of a fluorescent dye along the nerves.³¹⁵ The second route is via the trigeminal nerves. These are present in the respiratory region of the nasal cavity. As with the olfactory nerves, the progress of active agents along the trigeminal nerves has been monitored by use of a dye.³¹⁶ Transport via the nerves is believed to be both perineuronal and intraneuronal.³¹⁷ Perineuronal transport occurs in the perineural spaces. Nerves have bundles of axons, which originate from the brainstem or spinal cord. There are multiple types of axon bundles – some more closely associated with cells, and others more closely associated with the CNS. The space that is sometimes present between these two types of axon is the perineural space.³¹⁸ It is through these spaces that drug transport can occur.³¹⁹ Intraneuronal transport occurs within the axons themselves, along microtubules within the axon.³²⁰ This system exists as axons cannot produce proteins, and therefore rely on this transport around the structure.³²¹

The area of the brain to which the drug will be delivered depends on which of these nerves are followed – the olfactory nerves lead to areas including the hypothalamus and the amygdala, while the trigeminal nerves enter the brain in the rostral and caudal regions. Therefore, we aimed to gain a greater understanding of what areas of the brain the L-DOPA would be delivered to. Levels of radioactivity were determined in different segments of the brain – the olfactory bulbs (OB), the cerebrum (CB), the trigeminal nerves (TN), the brain stem (BS), the cerebellum (CE) and the spinal cord (SC) (Figure 163).

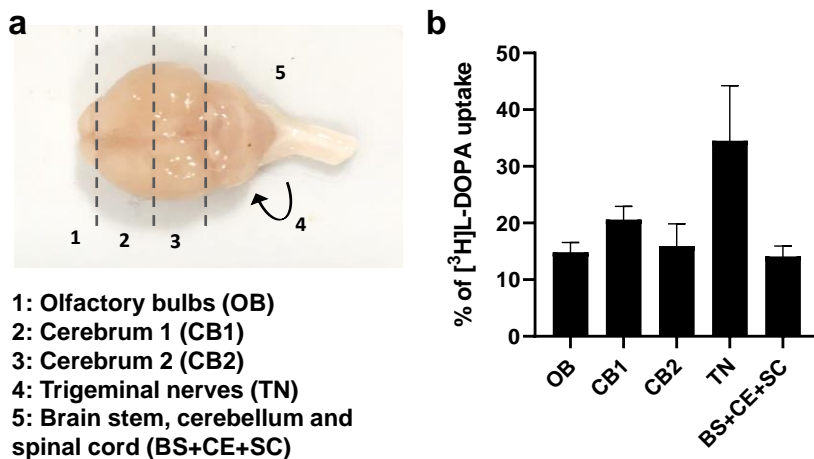


Figure 163. Distribution of [³H] L-DOPA in the brain, 10 minutes from intranasal delivery of the hydrogel formulation. (a) View of a mouse brain, with different sections indicated. (b) [³H] L-DOPA uptake in different brain sections.

Following liquid scintillation analysis, the highest level of [³H] L-DOPA was observed in the trigeminal nerves, with more than a third of the detected radioactivity. L-DOPA was, however, distributed across the entire brain. These results indicated that there is good delivery of L-DOPA to the brain upon intranasal application of the hydrogel formulation, with good distribution of L-DOPA throughout the brain achieved.

6.6 Conclusions

This chapter aimed to develop a delivery system with the potential to give improved delivery of L-DOPA, either via a slow release formulation, or by exploiting an alternative route of delivery.

Initially, the sorbitol derivatives DBS-CONHNH₂ and MBS-CO₂Me were tested, and although both were capable of encapsulating L-DOPA, neither gave a release profile that was suitable for the applications in mind. Both gave rapid drug release, meaning slow, controlled release of L-DOPA was not likely to be achieved. Despite rapid release being useful for some modes of delivery, these two hydrogels do not have the required material properties for such applications. Future work may focus on the incorporation of large amounts of solid L-DOPA, that would not be dissolved. The extra step of dissolution before the drug can be taken up may give slower release.

An alternative gel system, recently developed with the research group by Dr Kirsten Hawkins, was therefore investigated for drug encapsulation and release. This system, based on a modified amino acid and benzaldehyde, showed promising material properties, particularly the ability to self-heal following breakdown of the gel network. This ability is believed to be due to the reversible nature of the gelator formation.

Testing of the material properties indicated that this hydrogel could have potential for nasal delivery, with the gel being broken down on administration, and reforming within the nasal cavity. This allows for bypassing of the blood brain barrier, as well as first pass metabolism – these are key factors in the low bioavailability of L-DOPA in the brain.

Following this, *in vitro* release studies showed the gel rapidly release L-DOPA on addition of buffer – this is desirable for nasal delivery. This was followed by toxicity studies, which indicated the hydrogel system had toxicity comparable to surfactants that are considered safe, at appropriate concentrations.

Preliminary *in vivo* studies were carried out, to assess the distribution of L-DOPA following intranasal application. These indicated that delivery of L-DOPA in the hydrogel formulation did increase the amount of L-DOPA in the brain, compared to delivery intranasally in solution, and intravenous injection. Additionally, the gel formulation gave increased L-DOPA in the blood, and reduced levels in the liver. The results for the liver in particular indicate that this form of nasal delivery does indeed help to avoid first pass metabolism.

In addition to the distribution of L-DOPA in multiple organs, particular attention was given to the distribution of L-DOPA within the brain. These studies indicated that there was good distribution of L-DOPA throughout the whole brain, with the highest levels observed in the trigeminal nerves, which may suggest an uptake mechanism dominated by the trigeminal nerve pathway.

Overall, this system shows some potential for nasal delivery of L-DOPA, with improved delivery to the brain and blood observed. The ability of the hydrogel to reform within the nasal cavity following application allows for longer contact time, and therefore more time for L-DOPA to be transported to the brain, or absorbed into the bloodstream. This is very clearly observed in the *in vivo* studies. Combined with other work that indicates nasal delivery of L-DOPA to be a promising route,³²² these initial studies are very promising.

Further work would focus on optimisation of the system, to allow use with a nasal spray device. Some minor changes to the gelation system may also be tested, to minimise the amount of free benzaldehyde – for example, using only 0.7 equivalents in the formation of the hydrogel to minimise the presence of any excess aldehyde in the drug delivery formulation. Further preclinical trials would also be carried out, with a disease model, to determine the efficacy of the delivery system in treating the symptoms of PD as well as the ability of the system to deliver L-DOPA to the brain. It would also be worthwhile to investigate a formulation with a higher loading of L-DOPA (which would be in a powder form within the gel). This could allow for more L-DOPA to be

delivered, further increasing the concentration within the brain. An increased loading might also give increased application for slow release, as the requirement for solubilisation would provide some increased control over release rate. In this case, interactions with DBS-CONH₂ might also influence the release.

Given the promising nature of these results, it would be interesting to investigate other drugs used for the treatment of neurodegenerative disorders, such as rivastigmine for the treatment of Alzheimer's disease. Many of these therapies present similar challenges to the use of L-DOPA for Parkinson's disease.

7. Conclusions and Future Work

This project aimed to explore the modification of hydrogels, from the design of the gelator, to the components in the final material, to tune the properties with specific applications in mind. Applications for drug delivery were of particular interest over the course of the project.

In Chapter 2, a novel MBS derivative, MBS-CO₂Me, was synthesised, and investigated as a hydrogelator. This was capable of forming hydrogels. While these had good mechanical strength, they did not have good chemical stability, breaking down rapidly in the presence of any supernatant. This led to the very rapid release of any drug additive. While this can be useful for selected applications, other qualities of the gel, such as the very limited self-healing properties, mean that use in these areas would still be limited.

This relatively rigid and stiff hydrogel was therefore combined with the known gelator DBS-CONHNH₂, capable of interactions with additives, and crucially, which is stable in the presence of supernatant across a wide range of pH values. It was hoped that this combination would lead to a hybrid hydrogel, combining the most desirable properties of the two individual gelators.

On combining the two gelators, a novel hybrid hydrogel was formed. This could be formed even with both gelators below their individual MGCs. NMR studies indicated that the assembly of the two gelators was sequential as a result of their different thermal properties. The tuneability of the material was then investigated by varying the proportions of the two gelators making up the gel. When more of the stiffer MBS-CO₂Me was included, the hybrid gel was stiffer. When more of the more thermally-stable DBS-CONHNH₂ was included, the T_{gel} was higher. This tuning of macroscopic properties could be achieved even with the total concentration of gelator remained constant.

Following investigations into the tuning of the material, the ability of the MBS-CO₂Me/DBS-CONHNH₂ hybrid hydrogel to encapsulate APIs was investigated. Initially, naproxen was incorporated within the hydrogel, and release at different pH values investigated. In agreement with previous results obtained for hydrogels with DBS-CONHNH₂, lower release of naproxen was observed at the acidic pH, with higher release at neutral pH. This is desirable for oral release, with release minimised in acidic environments such as the stomach, and maximised in the intestine. Release of atorvastatin was also tested. In this case, release continued over the course of several days, although the relatively low solubility of atorvastatin was an important factor in this slow release.

Further work in this area would focus on the impact of changing the material properties on the release of active additives. This would include tuning the material for specific applications – with other drugs also investigated for encapsulation. The hydrogels would also be tested for other biomedical applications, such as tissue engineering or wound healing.

In Chapter 3, three-component beads, made up of the two LMWGs, DBS-CONH₂ and DBS-CO₂H, and the polymer gelator calcium alginate, were investigated as vehicles for statin release. In these multicomponent gels, the alginate provides a robust network which allows the shaping into beads on exposure to calcium ions. The two LMWGs provided responsiveness, with sensitivity to pH in particular. These could also be combined to give DBS-CONH₂/alginate beads, DBS-CO₂H/alginate beads, and alginate beads, along with the three-component beads.

Following the formation of the beads, they were loaded with rosuvastatin. Release of this drug molecule from beads of varying compositions was investigated. It was found that both the composition of the beads and pH of the receiving solution were important in determining the rate of release. This is a result of both interactions between the gel network and the drug additive, and the solubility of the drug in the receiving solution. These preliminary studies showed that the hybrid gel beads have potential for controlling the delivery of drugs.

Further work in this area will focus on fabricating nanosized beads, based on work previously carried out within the group. These will have greater potential applications, as they can be injected, and may therefore be highly useful for biomedical applications.

In Chapter 4, the synthesis of MBS and DBS derivatives was investigated. Following the synthesis of MBS-CO₂Me, other MBS derivatives were synthesised. The same general method was used, with the aldehyde being varied. While in some cases the MBS derivative could not be formed and isolated, in a number of cases the desired MBS derivative could be obtained.

These were then tested for gelation ability, with one, MBS-SMe, being able to form hydrogels. This formed very weak hydrogels, with characterisation indicating that a mix of gel nanofibres and microcrystals were present. Other successfully synthesised MBS derivatives were not capable of forming gels in any of the solvents tested. This was in agreement with work published by Amabilino and co-workers soon after the completion of our own work.²⁴²

The synthesis of non-symmetric DBS derivatives was also investigated – aiming to combine the properties of different DBS-based gelators. While there was some evidence that these could be synthesised, low yields and poor solubility made purification highly challenging, and none were successfully isolated. Control of the selectivity of the reactions was also very difficult. Use of DBS

derivatives in industry would require these to have a reliable synthesis, along with relatively simple purification. The difficulty of forming these systems led us to question some of the non-symmetric DBS derivatives that are reported with little comment or characterisation in the patent literature.

In Chapter 5, the impact of chirality on the properties and applications of DBS-CONHNH₂ was investigated. Initially the two enantiomers of DBS-CONHNH₂ were investigated separately, showing identical gelation behaviour and properties, with the exception of the CD spectra being equal and opposite. Mixtures of the two enantiomers were then investigated, and while hydrogels were still formed, these were considerably weaker than those formed by the individual enantiomers. This suggested the interactions between the two enantiomers were disruptive. Chirality on the nanoscale was also lost with only a small proportion of the second enantiomer present, further indicating disruptive interactions.

The two gels were also investigated following the encapsulation of two enantiomers of NPX. Both gelators could form hydrogels in the presence of either enantiomer of NPX. Some small impacts on the rheological and thermal properties of the gels were observed on addition of the enantiomers which suggested that those gelator: drug materials having a diastereomeric relationship had somewhat different properties. However, when release of each enantiomer of NPX from each of the gels was observed, no significant difference in overall drug release was observed, suggesting that the differences did not directly impact on drug delivery.

Cell studies were also carried out, with these indicating that changing the gelator enantiomer did not impact cell viability or proliferation. However, during these tests, a difference in the reduction of Alamar Blue, used for cell quantification, was observed. Alamar Blue itself is not chiral, and it was therefore reasoned that some interaction between the hydrogel and a chiral component of the cell culture media was impacting the reduction of Alamar Blue.

Future work in this area would focus on investigating whether the two enantiomers have any impact on the differentiation of stem cells, following indication that changing the enantiomer does not significantly impact cell proliferation. Further investigations would also be carried out to determine what component of cell culture media caused the change in interaction with Alamar Blue – a greater understanding of the interactions between the gel nanofibres and chiral additives might also inform future applications of this class of gelator in different areas where chirality plays an important role, such as catalysis.

In Chapter 6, hydrogels were investigated as release vehicles for L-DOPA, used in treatment of Parkinson's disease. Initially, the hydrogels DBS-CONHNH₂ and MBS-CO₂Me were investigated, and although both were able to encapsulate and release L-DOPA, neither had properties suitable for the desired mode of delivery, by nasal application.

A previously reported hydrogel, based on glutamine amide, was therefore investigated for this application. Rheological studies confirmed that this hydrogel had self-healing properties, both with and without L-DOPA incorporated. This would mean that the hydrogel could potentially reform within the nasal cavity following administration, improving the delivery of L-DOPA to the brain by enhancing residence times in the nose.

As part of a collaboration with Professor Khuloud Al Jamal, *in vivo* studies investigating the ability of this hydrogel to delivery L-DOPA to the brain were carried out. These studies indicated that the use of the hydrogel formulation did improve uptake of L-DOPA into the brain, in comparison to an intranasal solution or intravenous administration, as well as achieving good distribution of L-DOPA throughout the brain. This indicates that this method of delivery could be useful for improved delivery of L-DOPA to the brain.

Future work in this area would focus on optimising the glutamine amide based hydrogels for delivery of L-DOPA. In particular this would involve use of the gels in a disease model, to determine if intranasal delivery using this gel formulation could reduce Parkinson's symptoms. Some further optimisation of the gel system could also be carried out, perhaps reducing the amount of aldehyde used in forming the gel (to try and further lower any toxicity of the delivery gel), or increasing the drug loading (and therefore the potential dose to the brain). Additionally, other drugs for the treatment of neurological diseases could be incorporated within the hydrogels, and delivery to the brain investigated.

8. Experimental

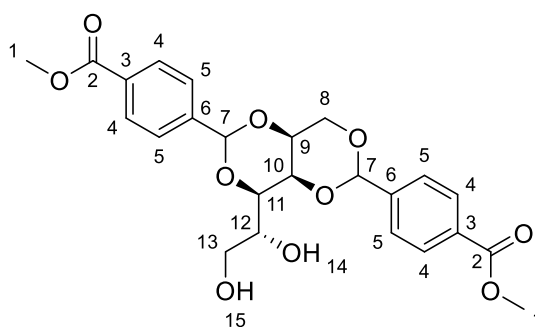
8.1 General Experimental Methods

All compounds required for synthesis and analysis were purchased from standard chemical suppliers and used without further purification. ¹H and ¹³C NMR were recorded on a Jeol 400 spectrometer (¹H 400 MHz, ¹³C 100 MHz), with the exception of the variable temperature NMR, or if stated otherwise, were recorded on a Bruker 500 (¹H 500 MHz). Coupling constants (*J*) are recorded in Hz. Mass spectrometry was performed by the University of York Mass Spectrometry Service. IR were recorded on a ThermoNicolet Avatar 370 FT-IR spectrometer. Melting points

were recorded using a Stuart SMP3 apparatus. All rheological measurements were carried out using a Malvern Instruments Kinexus Pro+ rheometer, at 25 °C unless otherwise stated. T_{gel} values were recorded using a high precision thermoregulated oil bath. Circular dichroism (CD) measurements were carried out using a Jasco J810 CD Spectrophotometer. UV-vis absorbance was measured on a Shimadzu UV-2401 PC spectrophotometer. TEM images were taken on a FEI Technai 12 G2. SEM images were taken on either a JEOL JSM-7600f field emission SEM, or a JEOL JSM-6490LV. $[\alpha]_D$ values recorded on a Bellingham and Stanley Single Wavelength Polarimeter ADP450.

8.2 Synthetic Procedures

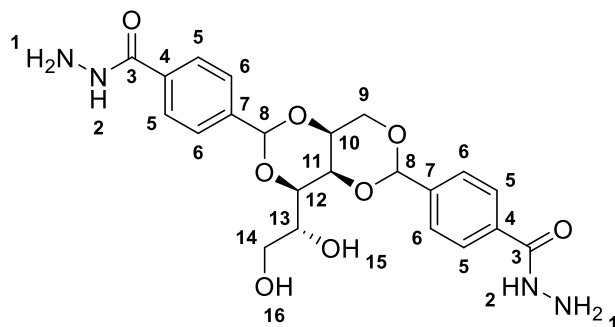
8.2.1 Synthesis of DBS-CO₂Me



D-Sorbitol (5.1 g, 27.0 mmol) was added to a three-necked round bottomed flask fitted with Dean-Stark apparatus. Methanol (30 ml) and cyclohexane (50 ml) were added and the mixture was stirred, under N₂, at 50°C for 20 minutes. 4-methylcarboxybenzaldehyde (7.1 g, 43.0 mmol) and *p*-TsOH (1.00 g, 5.59 mmol) were dissolved in methanol (20 ml) and stirred for 20 minutes at room temperature. This solution was then added dropwise to the D-sorbitol suspension. This was then heated to 70°C. After 1 hour, further methanol (15 ml) and cyclohexane (35 ml) were added. The mixture was heated for a further hour, until most of the solvent was removed. The resulting white paste was filtered and left to air dry overnight. The powder was washed with boiling DCM (3x50 ml) and boiling water (3x50 ml). The powder was then dried under high vacuum to a constant mass. Yield: 4.26 g (8.98 mmol, 43%); M.p: 226-229 °C; ¹H NMR (500 MHz, DMSO-*d*₆): δ 8.00-7.97 (m, 4H, H₄), 7.63-7.59 (m, 4H, H₅), 5.76 (s, 2H, H₇) 4.91 (d, *J*=5.9 Hz, 1H, H₁₄), 4.46 (dd, app. t, *J*=5.7, 5.7 Hz, 1H, H₁₅), 4.26-4.18 (m, 3H, H₈, H₉), 4.01-4.00 (app. d, *J*=1.6 Hz, 1H, H₁₀), 3.90 (dd, *J*= 9.3, 1.6 Hz, H₁₁), 3.86 (s, 6H, H₁), 3.79 (dddd, *J*=9.3, 5.9, 5.7, 2.3 Hz, 1H, H₁₂), 3.62 (ddd, *J*=11.6, 5.6, 2.3 Hz, 1H, H₁₃), 3.47 (ddd, ap. quin., *J*=11.6, 5.7, 5.7 Hz, 1H, H₁₃); ¹³C NMR (125 MHz, DMSO-*d*₆), 166.00 (C₂), 165.98, (C₂), 143.32 (C₆), 143.06 (C₆), 129.77 (C₃), 129.72 (C₃), 129.02 (C₄), 128.93 (C₄), 126.49 (C₅), 98.53 (C₇), 98.45 (C₇), 77.59 (C₁₁), 70.17 (C₁₀), 69.31 (C₈), 68.52 (C₉), 67.59 (C₁₂), 62.55

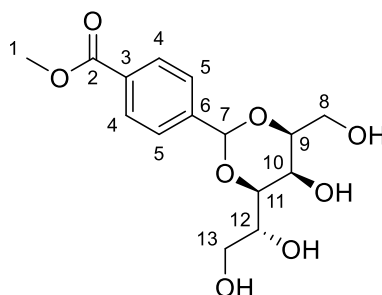
(C₁₃), 52.19 (C₁); [α]_D²⁵ (deg cm³ g⁻¹ dm⁻¹) 46.3 ± 0.2 (c=1, DMSO); ESI-MS (m/z) calc. for [M+Na]⁺, C₂₄H₂₇O₁₀Na⁺, 497.1424; found 497.1412 (100% [M+Na]⁺); ν_{max} (cm⁻¹) (solid): 3245w, 2955w, 2865w, 1723s, 1614w, 1578w, 1435w, 1414w, 1398m, 1368w, 1341w, 1376s, 1219w, 1198w, 1166w, 1093s, 1065m, 1050m, 1018s, 981m, 963m, 906w, 882w, 855m, 835m, 815w, 763m, 750s, 708m, 656w, 603w, 588m, 551m, 525w.

8.2.2 Synthesis of DBS-CONHNH₂



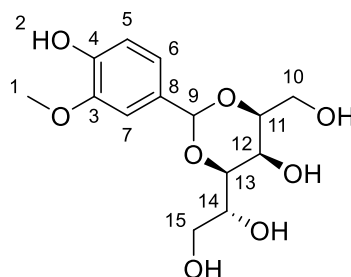
DBS-CO₂Me (1.10 g, 2.32 mmol) was dissolved in THF (50 ml). Hydrazine monohydrate (6 ml, 123.7 mmol) was added, and the mixture heated to reflux. The reaction was monitored by TLC. The white paste obtained was washed with water (6 x 50 ml). The resulting white paste was dried first under high vacuum, and then to a constant mass in a vacuum oven. Yield: 1.00 g (2.11 mmol, 91%). M.p: 292-294 °C, ¹H NMR (400 MHz, DMSO-*d*₆): δ 9.8 (s, 2H, H₂), 7.84-7.81 (m, 4H, H₅), 7.54-7.49 (m, 4H, H₆), 5.71 (s, 2H, H₈), 4.93 (d, *J*=6 Hz, 1H, H₁₅), 4.52 (br. s, 4H, H₁), 4.45 (m, 1H, H₁₆), 4.20-4.18 (m, 3H, H₉, H₁₀), 3.98 (br. s, 1H, H₁₁), 3.88-3.86 (m, 1H, H₁₂), 3.80-3.75 (m, 1H, H₁₃), 3.63-3.59 (m, 1H, H₁₄), 3.47-3.42 (m, 1H, H₁₄); ¹³C NMR (100 MHz, DMSO-*d*₆): 165.63 (C₃), 141.28 (C₄), 133.56 (C₇), 126.71 (C₅), 126.08 (C₆), 98.79 (C₈), 98.72 (C₈), 77.60 (C₁₂), 70.15 (C₁₁), 69.35 (C₉), 68.50 (C₁₀), 67.69 (C₁₃), 62.64 (C₁₄); [α]_D²⁵ (deg cm³ g⁻¹ dm⁻¹) 55.5 ± 0.16 (c=1, DMSO); ESI-MS (m/z) calc for [M+Na]⁺, C₂₂H₂₆N₄O₈Na⁺, 497.1649; found 497.1629 (100% [M+Na]⁺); ν_{max} (cm⁻¹) (solid): 3290m, 2934w, 2865w, 1655m, 1632m, 1594m, 1568m, 1541m, 1505m, 1448w, 1399m, 1369m, 1338m, 1309m, 1264m, 1221m, 1164m, 1091s, 1039m, 1020m, 1006m, 977m, 950m, 904w, 887w, 847m, 829m, 797w, 753m, 683m, 644m, 619m, 585m, 546m, 522m.

8.2.3 Synthesis of MBS-CO₂Me



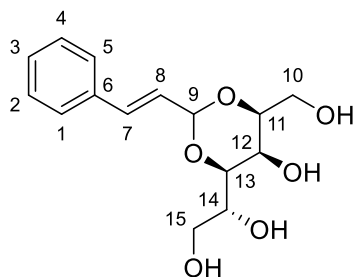
D-Sorbitol (15.9 g, 87 mmol) was added to a three-necked round bottomed flask fitted with Dean-Stark apparatus. Methanol (20 ml) and cyclohexane (40 ml) were added, and the mixture was stirred, under N₂, at 50°C for 20 minutes. 4-methylcarboxybenzaldehyde (3.5 g, 21.3 mmol) and *p*-TsOH (0.55 g, 2.89 mmol) were dissolved in methanol (20 ml) and stirred for 20 minutes at room temperature. This solution was then added dropwise to the D-sorbitol mixture. This was then heated to 70°C. After two to three hours, most of the solvent was removed, giving a white paste. The paste was washed with methanol, and cold water. The white solid was dissolved in boiling water, and filtered while hot. The filtrate was left to cool, to give a white solid. If necessary, this was then washed with further cold water. Yield: 2.11 g (6.4 mmol, 30%), M.p: 198-201 °C; ¹H NMR (400 MHz, DMSO-*d*₆): δ 7.98-7.96 (m, 2H, H₄), 7.64-7.62 (m, 2H, H₅), 5.64 (s, 1H, H₇), 4.74-4.70 (m, 2H, C-OH), 4.48-4.44 (m, 2H, C-OH), 3.85-3.82 (m, 4H, H₁, H_{10/12}), 3.71-3.69 (m, 3H, H₉, H_{10/12}, H₁₁), 3.60-3.55 (m, 3H, H_{8/13}), 3.43-3.42 (m, 1H, H_{8/13}); ¹³C NMR (100 MHz, DMSO-*d*₆): δ 166.11 (C₂), 143.53 (C₃), 129.75 (C₄), 128.94 (C₅), 126.89 (C₆), 99.27 (C₇), 81.09 (C_{10/12}), 79.46 (C_{10/12}), 69.11 (C_{9/11}), 62.72 (C_{8/13}), 61.62 (C_{9/11}), 61.01 (C_{8/13}), 52.27 (C₁); [α]_D²⁵ (deg cm³ g⁻¹ dm⁻¹) 16.5 ± 0.17 (c=1, DMSO); ESI-MS (*m/z*) calc. for [M+Na]⁺, C₁₅H₂₀O₈Na⁺ 351.1056; found 351.1049 (100% [M+Na]⁺); ν_{max} (cm⁻¹) (solid): 3293s, 2949w, 2877w, 1722s, 1616w, 1402m, 1340w, 1278s, 1218w, 1198w, 1151m, 1091s, 1077m, 1061m, 1031s, 1017s, 977m, 881m, 847m, 835m, 794m, 761s, 712s, 657m, 593m, 507m, 456w.

8.2.4 Synthesis of MBS-Van



D-Sorbitol (6.8 g, 37.3 mmol) was added to a three necked flask, fitted with a Dean-Stark apparatus, and suspended in cyclohexane/methanol (80 ml/50 ml). This was stirred, under N₂, for 20 minutes at 50 °C. Vanillin (1.8 g, 11.8 mmol) was dissolved in methanol (25 ml) with *p*-TsOH (1 g, 5.26 mmol). This solution was then added dropwise to the sorbitol suspension, and the resulting suspension heated to 70 °C. The reaction was allowed to proceed for 2 hours, after which time a white solid had been formed. This white solid was washed first with methanol (150 ml), then water (150 ml), to remove excess starting materials. A recrystallisation, using water, was then carried out. Yield: 1.75 g (5.54 mmol, 47%); M.p: 162.5-164.4 °C; ¹H NMR (400 MHz, DMSO-*d*₆): δ 9.01 (s, 1H, H₂), 7.05 (d, *J*=1.5 Hz, 1H, H₇), 8.86 (dd, *J*=1.5 Hz, 8.4, 1H, H₆), 6.72 (d, *J*=8.4 Hz, 1H, H₅), 5.41 (s, 1H, H₉), 4.69 (d, *J*=6.1 Hz, 1H, CHOH), 4.66 (dd, app. t, *J*=5.3, 5.3 Hz, 1H, CH₂OH), 4.41 (dd, app. t, *J*=6.1, 6.1 Hz, 1H, CH₂OH), 4.35 (d, *J*=8.4 Hz, 1H, CHOH), 3.76-3.74 (m, 4H, H₁, H_{12/14}), 3.71-3.64 (m, 2H, H_{11/13}), 3.61-3.48 (m, 4H, H_{12/14}, H_{10/15}), 3.41-3.39 (m, 1H, H_{10/15}); ¹³C NMR (100 MHz, DMSO-*d*₆) δ 147.07 (C₃/C₄), 146.78 (C₃/C₄), 130.07 (C₈), 119.38 (C₆), 114.62 (C₅), 110.81 (C₇), 100.58 (C₉), 80.96 (C₁₂/C₁₄), 79.46 (C₁₂/C₁₄), 69.12 (C₁₁/C₁₃), 62.75 (C₁₀/C₁₅), 61.58 (C₁₁/C₁₃), 60.97 (C₁₀/C₁₅), 55.70 (C₁); [α]_D²⁵ (deg cm³ g⁻¹ dm⁻¹) 7.5 ± 0.3 (c=1, DMSO); ESI-MS (*m/z*) calc. for [M+Na]⁺, C₁₄H₂₀O₈Na⁺ 339.1059; found 339.1051 (100% [M+Na]⁺); ν_{max} (cm⁻¹) (solid): 3252*m*, 2930*w*, 1605*w*, 1516*m*, 1458*w*, 1430*m*, 1390*w*, 1335*m*, 1269*m*, 1212*m*, 1165*m*, 1145*m*, 1093*s*, 1055*m*, 1044*m*, 1014*s*, 959*w*, 943*m*, 888*m*, 861*m*, 845*m*, 822*m*, 803*m*, 769*m*, 672*m*, 625*m*, 582*m*, 565*m*, 487*m*, 464*m*.

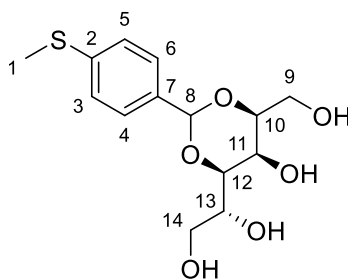
8.2.5 Synthesis of MBS-Cin



D-Sorbitol (7.6 g, 41.7 mmol) added to a three-necked flask, fitted with Dean-Stark apparatus, and suspended in cyclohexane/methanol (90 ml/50 ml). This was stirred under N₂, at 50 °C for 20 minutes. Cinnamaldehyde (1.57 ml, 12.5 mmol) was dissolved in methanol with *p*-TsOH (1 g, 5.26 mmol). This was added dropwise to the sorbitol suspension, and the resulting suspension heated to 70 °C. The reaction was allowed to proceed for 1.5 hours, at which point a mix of white and purple solids had been formed. This solid was washed with methanol (150 ml) and water (150 ml), to yield a white solid. Yield: 1.17 g (3.94 mmol, 32%); 130.8-131.9 °C; ¹H NMR (400 MHz, DMSO-

d_6): δ 7.48-7.46 (m, 2H, H₁, H₅), 7.37-7.33 (m, 2H, H₂, H₄), 7.30-7.26 (m, 1H, H₃), 6.72 (d, $J=16$ Hz, 1H, H₇), 6.22 (dd, $J=16$ Hz, 4.6 Hz, 1H, H₈), 5.17 (d, $J=4.6$ Hz, 1H, H₉), 4.96 (d, $J=6.1$ Hz, 1H, CHOH), 4.66 (dd, app. t, $J=5.7, 5.7$ Hz, 1H, CH₂OH), 4.43 (dd, app. t, $J=5.3, 5.3$ Hz, 1H, CH₂OH), 4.37 (d, $J=7.6$ Hz, 1H, CHOH), 3.71-3.64 (m, 3H, H₁₁, H_{12/14}, H₁₃), 3.59-3.48 (m, 4H, H_{10/15}, H_{12/14}), 3.43-3.37 (m, 1H, H_{10/15}); ¹³C NMR (100 MHz, DMSO- d_6): δ 135.73 (C₆), 132.49 (C₇), 128.71 (C₂, C₄), 128.18 (C₃), 126.60 (C₁, C₅), 126.30 (C₈), 99.76 (C₉), 80.48 (C_{12/14}), 78.91 (C_{12/14}), 69.14 (C_{11/13}), 62.62 (C_{10/15}), 61.48 (C_{11/13}), 60.88 (C_{10/15}); $[\alpha]_D^{25}$ (deg cm³ g⁻¹ dm⁻¹) 7.2 ± 0.5 (c=1, DMSO); ESI-MS (m/z) calc. for [M+Na]⁺, C₁₅H₂₀O₆Na⁺ 319.1158; found 319.1152 (100% [M+Na]⁺); ν_{\max} (cm⁻¹) (solid): 3291m, 2863w, 1449w, 1395m, 1312m, 1168m, 1124w, 1098m, 1061m, 1004s, 983m, 967s, 887m, 828m, 797w, 747m, 691m, 596m, 537m, 500m.

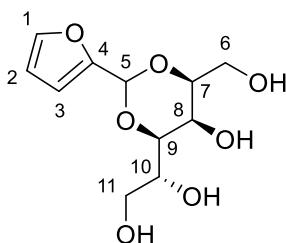
8.2.6 Synthesis of MBS-SMe



D-Sorbitol (9.37 g, 51 mmol) was added to a three necked flask, fitted with Dean-Stark apparatus, and suspended in a cyclohexane/methanol mix (90/50 ml), and stirred at 50 °C, under N₂, for 20 minutes. 4-methylthiobenzaldehyde (2.7 ml, 20.3 mmol) was dissolved in methanol (50 ml), with *p*-TsOH (1.1 g, 5.78 mmol). This solution was then added dropwise to the sorbitol suspension, and the resulting suspension heated to 70 °C. This was then heated for 2 hours, with additional cyclohexane added as necessary. The resulting white paste was washed with methanol (2 x 100 ml) and water (2 x 100 ml). The white solid was then washed with further methanol (400 ml), to give a white powder. Yield: 3.3 g (20.3 mmol, 52%), M.p. 174.8-179.0 °C; ¹H NMR (400 MHz, DMSO- d_6): δ 7.42-7.40 (m, 2H, H₄, H₆), 7.25-7.22 (m, 2H, H₃, H₅), 5.51 (s, 1H, H₈), 4.70 (d, $J=5.3$ Hz, 1H, CHOH), 4.67 (t, $J=5.3$ Hz, 1H, CH₂OH) 4.42 (t, $J=5.3$ Hz, 2H, CH₂OH) 4.39, (d, $J=7.6$ Hz, 1H, CHOH), 3.80-3.77 (m, 1H, H_{11/13}), 3.68-3.65 (m, 3H, H₁₀, H_{11/13}, H₁₂), 3.58-3.52 (m, 3H, H_{9/14}), 3.41-3.39 (m, 1H, H_{9/14}), 2.47 (s, 3H, H₁); ¹³C NMR (100 MHz, DMSO- d_6): δ 138.55 (C₂), 135.52 (C₇), 127.16 (C₄, C₆), 125.31 (C₃, C₅), 99.85 (C₈), 80.95 (C_{11/13}), 79.41 (C_{11/13}), 69.16 (C_{10/12}), 62.74 (C_{9/14}), 61.60 (C_{10/12}), 61.01 (C_{9/14}), 14.75 (C₁); $[\alpha]_D^{25}$ (deg cm³ g⁻¹ dm⁻¹) 18.3 ± 0.9 (c=1, DMSO); ESI-MS (m/z) calc. for [M-NH]⁻, C₁₄H₁₉O₆S⁻ 315.0903; found 315.0902 (100% [M-H]⁻); ν_{\max} (cm⁻¹) (solid):

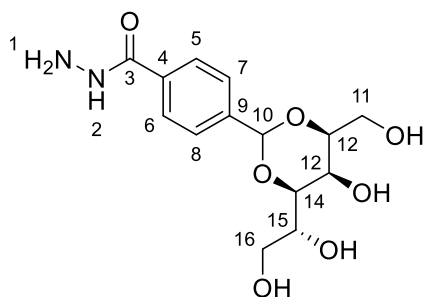
3273s, 2945w, 2868w, 1604w, 1502w, 1414m, 1397m, 1304m, 1224m, 1180w, 1149m, 1134w, 1089s, 1057s, 1020s, 1004s, 972m, 883m, 827m, 802m, 661m, 642m, 594m, 557m, 510m, 464w.

8.2.7 Synthesis of MBS-Fur



Water (2.29 ml) and H₂SO₄ (conc., 0.21 ml) were added to a flask, which was then purged with N₂. Sorbitol (7.1 g, 39.0 mmol) was dissolved in the minimum amount of water, and added slowly to the water in the flask. Furfural (2.7 ml, 32.6 mmol) was then added slowly, and the reaction stirred for 19 hours. 2-propanol was added, and the solvent removed *in vacuo* to give a dark brown solid. This was washed first with water, followed by acetone, to leave a mix of brown and black solid. Yield: 41.8 mg (0.16 mmol, 0.5%); 134.4-135.9 °C; ¹H NMR (400 MHz, DMSO-*d*₆): δ 7.63 (dd, app. t, *J*=1.3 Hz, 1H, *H*₁), 6.45-6.43 (m, 2H, *H*₂, *H*₃), 5.62 (s, 1H, *H*₅), 4.725 (d, *J*=5.5 Hz, 1H, OH), 4.68 (dd, *J*=5.7, 5.7, Hz, 1H, OH). 4.44-4.41 (m, 2H, OH), 3.80-3.77 (m, 1H, *H*₇), 3.68-3.65 (m, 3H, *H*₈, *H*₉, *H*₁₀), 3.56 (m, 4H, *H*₆, *H*₁₁); ¹³C NMR (100 MHz, DMSO-*d*₆): δ 151.57 (C₄), 143.00 (C₁), 110.75 (C₂/C₃), 108.19 (C₂/C₃), 95.23 (C₅), 81.39 (C₇), 79.76 (C₈/C₉/C₁₀), 69.61 (C₈/C₉/C₁₀), 63.05 (C₆/C₁₁), 62.06 (C₈/C₉/C₁₀), 61.34 (C₆/C₁₁); ESI-MS (*m/z*) calc for [M+Na]⁺, C₁₁H₁₆O₇Na⁺, 283.0788; found 283.0779 (100% [M+Na]⁺); *v*_{max} (cm⁻¹) (solid): 3264m, 2943w, 2884w, 1424m, 1361w, 1333w, 1294w, 1266w, 1216m, 1158m, 1149m, 1104s, 1067s, 1030s, 1008s, 973m, 956m, 935m, 885m, 874m, 815w, 800w, 786m, 761m, 743m, 682m, 646m, 597m, 542w, 498s, 458w.

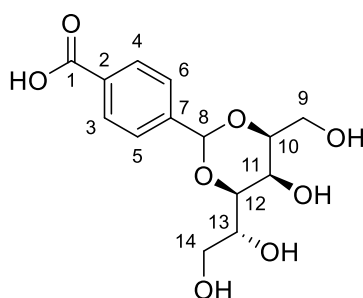
8.2.8 Synthesis of MBS-CONHNH₂



MBS-CO₂Me (0.7 g, 2.13 mmol) was suspended in THF (50 ml), and N₂H₄·H₂O (3 ml, 61.8 mmol). The suspension was heated to reflux, and the reaction allowed to proceed overnight. On cooling,

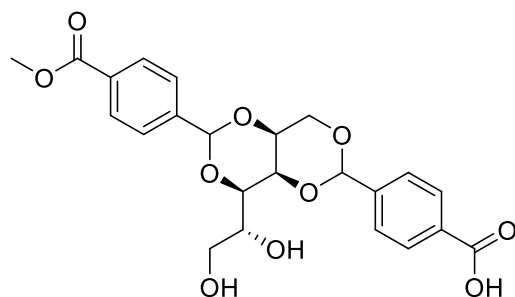
a white solid was obtained- this was isolated by filtration and washed with methanol (50 ml). Yield: 0.125 g (0.383 mmol, 18%); M.p: 184.9-187.8 °C; ^1H NMR (400 MHz, DMSO- d_6): δ 9.79 (s, 1H, H₂), 7.82-7.80 (m, 2H, H₅, H₆), 7.56-7.54 (m, 2H, H₇, H₈), 5.59 (s, 1H, H₁₀), 4.73 (dd, $J=8$, 8 Hz, 1H, CH₂OH), 4.50 (br. s, 2H, H₂), 4.46-4.42 (m, 2H, OH), 3.83-3.80 (m, 1H, H₁₃/H₁₅), 3.67-3.65 (m, 3H, H₁₂, H₁₃/H₁₅, H₁₄), 3.58-3.55 (m, 3H, H₁₁/H₁₆), 3.44-3.41 (m, 1H, H₁₁/H₁₆); ^{13}C NMR (100 MHz, DMSO- d_6): δ 165.74 (C₃), 141.40 (C₄), 133.48 (C₉), 126.72 (C₅, C₆), 126.47 (C₇, C₈), 99.51 (C₁₀), 80.98 (C₁₃/C₁₅), 79.35 (C₁₃/C₁₅), 69.06 (C₁₂/C₁₄), 62.74 (C₁₁/C₁₆), 61.57 (C₁₂/C₁₄), 61.03 (C₁₁/C₁₆); $[\alpha]_{\text{D}}^{25}$ (deg cm³ g⁻¹ dm⁻¹) 13.0 \pm 0.6 ($c=1$, DMSO); ESI-MS (m/z) calc for $[\text{M}+\text{Na}]^+$, C₁₄H₂₀N₂O₇Na⁺, 351.1169; found 351.1158 (100% $[\text{M}+\text{Na}]^+$); ν_{max} (cm⁻¹) (solid): 3559w, 3260m, 2961w, 1621s, 1569m, 1548m, 1505w, 1398m, 1340m, 1264m, 1215m, 1126w, 1153w, 1126m, 1093s, 1084s, 1063s, 1034s, 1003s, 982s, 959m, 903w, 843s, 767m, 699m, 659s, 565m, 496m, 456m.

8.2.9 Synthesis of MBS-CO₂H



MBS-CO₂Me (248 mg, 0.755 mmol) was suspended in methanol, and an excess of NaOH (1 M, 30 ml) added. The was heated to reflux, and left overnight. On cooling, a colourless solution was present. The solvent was removed *in vacuo* to leave a colourless oil. This was redissolved in water, and acidified with NaHSO₄. The solvent was then removed again, and the resulting white solid was washed with a small amount of cold water. This left a white solid. Yield: 103.34 mg (0.329 mmol, 44%); M.p: 181.8-183.2 °C; ^1H NMR (400 MHz, DMSO- d_6): δ 7.94-7.92 (m, 2H, H₅, H₆), 7.61-7.59 (m, 2H, H₃, H₄), 5.62 (s, 1H, H₈), 4.75-4.72 (m, 2H, OH), 4.49-4.46 (m, 2H OH), 3.85-3.82 (m, 1H, H₁₁/H₁₃), 3.72-3.67 (m, 3H, H₁₀, H₁₁/H₁₃, H₁₂), 3.62-3.53 (m, 3H, H₉/H₁₄), 3.43-3.40 (m, 1H, H₉/H₁₄); ^{13}C NMR (100 MHz, DMSO- d_6): δ 167.66 (C₁), 143.58 (C₇), 131.37 (C₂), 129.53 (C₃, C₄), 127.18 (C₅, C₆), 99.04 (C₈), 81.58 (C₁₁/C₁₃), 79.95 (C₁₁/C₁₃), 69.54 (C₁₀/C₁₂), 63.19 (C₉/C₁₄), 62.13 (C₁₀/C₁₂), 61.46 (C₉/C₁₄); $[\alpha]_{\text{D}}^{25}$ (deg cm³ g⁻¹ dm⁻¹) 12.5 \pm 0.6 ($c=1$, DMSO); ESI-MS (m/z) calc for $[\text{M}+\text{Na}]^+$, C₁₄H₁₈O₈Na⁺, 337.0894; found 337.0895 (100% $[\text{M}+\text{Na}]^+$); ν_{max} (cm⁻¹) (solid): 3321m, 2946w, 1694s, 1616w, 1580w, 1515w, 1401m, 1343m, 1317m, 1301m, 1218m, 1139m, 1094s, 1077s, 1015s, 938m, 893m, 869m, 839m, 826m, 761s, 704m, 655m, 586m, 512m, 480m.

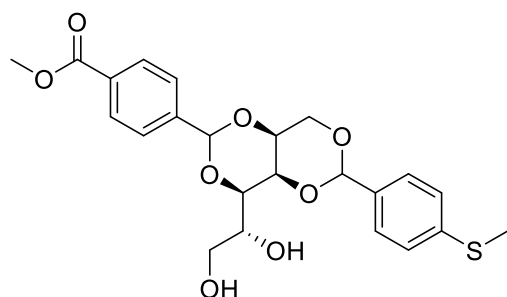
8.2.10 Synthesis of DBS-CO₂H/CO₂Me



4-methylcarboxybenzaldehyde (0.107 g, 0.65 mmol) was dissolved in methanol (30 ml).

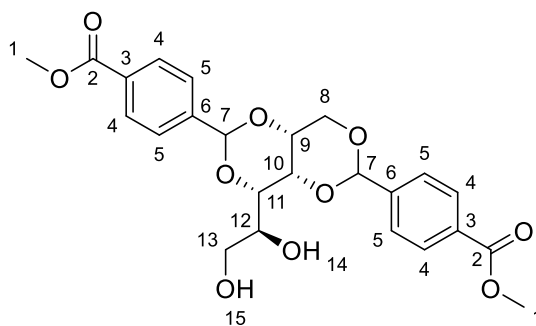
MBS-CO₂H (0.199 g, 0.61 mmol) was suspended in water, and added to the solution. Further methanol (20 ml) was added, and the mixture cooled to 0 °C. HCl (conc., 1 ml) was added slowly. The reaction was allowed to warm slowly to room temperature. The reaction was monitored by TLC, and when no reaction occurred at room temperature, the reaction was heated to reflux. After 3 hours, TLC indicated that a reaction had occurred. The reaction was cooled, and a white precipitate formed, which was isolated by filtration. This was a mix of products, and could not be purified further.

8.2.11 Synthesis of DBS-CO₂Me/SMe



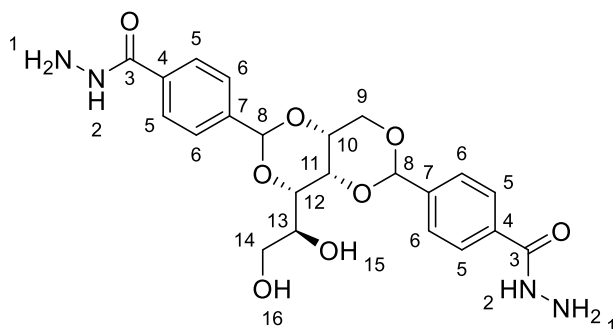
MBS-CO₂Me (0.1 g, 0.305 mmol) was added to a three-necked flask and suspended in cyclohexane/methanol (20/5 ml). The suspension was stirred, at 50 °C, under N₂, under Dean-Stark conditions for 20 minutes. 4-methylthiobenzaldehyde (0.05 ml, 0.376 mmol) was dissolved in methanol (25 ml) along with *p*-TsOH (0.1 g). This solution was then added dropwise to the MBS-CO₂Me suspension, and the temperature of the reaction increased to 70 °C. The reaction left to proceed for 1.5 hours, with more cyclohexane added as needed. After this time, a green oil had been formed. This was removed by filtration, and the solid washed sequentially with methanol, hot water, DCM and ethyl acetate. This left a white solid that could not be further purified.

8.2.12 Synthesis of L-DBS-CO₂Me



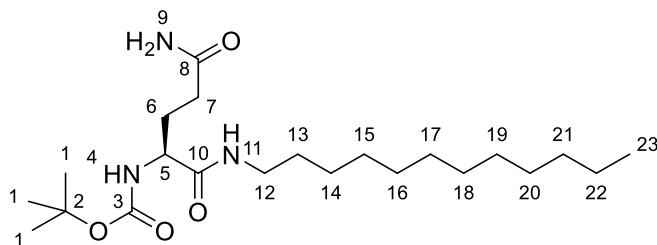
L-sorbitol (1.49 g, 2.69 mmol) was added to a three-necked flask, fitted with Dean-Stark equipment. Cyclohexane (30 ml) and methanol (20 ml) were added, and the suspension stirred, at 50 °C and under N₂, for 20 minutes. 4-methylcarboxybenzaldehyde (0.90 g, 5.48 mmol) was dissolved in methanol (20 ml) along with *p*-TsOH (0.8 g, 4.21 mmol), and this solution added dropwise to the L-sorbitol suspension. The temperature was then increased to 70 °C. The reaction was allowed to continue for two hours, with additional cyclohexane added as required. The resulting white powder was removed by filtration, then washed with cold methanol (150 ml). The white solid was then washed with hot water (3x50 ml) followed by hot DCM (3x50 ml). The white powder was then dried under a high vacuum. Yield: 725 mg (1.528 mmol, 57%); M.p: 186.6-87.9 °C; ¹H NMR (400 MHz, DMSO-*d*₆): δ 8.00-7.97 (m, 4H, H₄), 7.63-7.58 (m, 4H, H₅), 5.76 (s, 2H, H₇), 4.93 (d, *J*=8 Hz, 1H, H₁₄), 4.47 (dd, app. t, *J*=6, 6 Hz, 1H, H₁₅), 4.26-4.17 (m, 3H, H₈, H₉), 4.01 (ap. s, 1H, H₁₀), 3.91-3.88 (m, 1H, H₁₁), 3.85 (s, 6H, H₁), 3.81-3.75 (m, 1H, H₁₂), 3.64-3.59 (m, 1H, H₁₃), 3.49-3.43 (m, 1H, H₁₃); ¹³C NMR (100 MHz, DMSO-*d*₆), 166.00 (C₂), 165.98, (C₂), 143.32 (C₆), 143.06 (C₆), 129.77 (C₃), 129.72 (C₃), 129.02 (C₄), 128.93 (C₄), 126.49 (C₅), 98.53 (C₇), 98.45 (C₇), 77.59 (C₁₁), 70.17 (C₁₀), 69.31 (C₈), 68.52 (C₉), 67.59 (C₁₂), 62.55 (C₁₃), 52.19 (C₁); [α]_D²⁵ (deg cm³ g⁻¹ dm⁻¹) -31.8 ± 0.16 (c=1, DMSO); ESI-MS (m/z) calc. for [M+Na]⁺, C₂₄H₂₇O₁₀Na⁺, 497.1424; found 497.1431 (100% [M+Na]⁺); ν_{max} (cm⁻¹) (solid): 3246w, 2955w, 1723s, 1615w, 1579w, 1435w, 1414w, 1399m, 1368w, 1342w, 1277s, 1220w, 1193w, 1167w, 1090s, 1065m, 1051m, 1018s, 982m, 964m, 906w, 883w, 856m, 836m, 816w, 764m, 750s, 708s, 657m, 603w, 588m, 551m, 525w.

8.2.13 Synthesis of L-DBS-CONHNH₂



L-DBS-CONHNH₂ (498 mg, 1.05 mmol) was suspended in THF (50 ml), and N₂H₂.H₂O (5 ml, 103 mmol) added slowly. This was heated to reflux and left overnight. On cooling, a white precipitate was formed. This was removed by filtration, and washed with water (3x50 ml). The resulting white paste was dried first under high vacuum, then to a constant mass in a vacuum oven. Yield: 449.5 mg (0.947 mmol, 90%); 294.9-296.6 °C; ¹H NMR (400 MHz, DMSO-*d*₆): δ 9.81 (s, 2H, H₂) 7.84-7.81 (m, 4H, H₅), 7.54-7.49 (m, 4H, H₆), 5.71 (s, 2H, H₈), 4.93 (d, *J*=6, 1H, H₁₅), 4.50-4.46 (m, 5H, H₁, H₁₆), 4.24-4.15 (m, 3H, H₉, H₁₀), 3.98 (br. s, 1H, H₁₁), 3.88-3.86 (m, 1H, H₁₂), 3.80-3.74 (m, 1H, H₁₃), 3.63-3.58 (m, 1H, H₁₄), 3.48-3.45 (m, 1H, H₁₄); ¹³C NMR (100 MHz, DMSO-*d*₆): 165.71 (C₃), 141.33 (C₄), 141.06 (C₄) 133.58 (C₇), 133.50 (C₇), 126.84 (C₅), 126.76 (C₅), 126.15 (C₆), 126.13 (C₆) 98.83 (C₈), 98.76 (C₈), 77.62 (C₁₂), 70.18 (C₁₁), 69.39 (C₉), 68.53 (C₁₀), 67.72 (C₁₃), 62.66 (C₁₄); [α]_D²⁵ (deg cm³ g⁻¹ dm⁻¹) -55.5 ± 0.4 (c=1, DMSO); ESI-MS (m/z) calc for [M+Na]⁺, C₂₂H₂₆N₄O₈Na⁺, 497.1649; found 497.1643 (100% [M+Na]⁺); ν_{max} (cm⁻¹) (solid): 3290m, 1631m, 1594m, 1568m, 1541m, 1506w, 1399m, 1369w, 1338m, 1164w, 1091s, 1039m, 1006m, 977m, 904w, 847m, 829m, 753w, 683m, 644m, 622m, 545m.

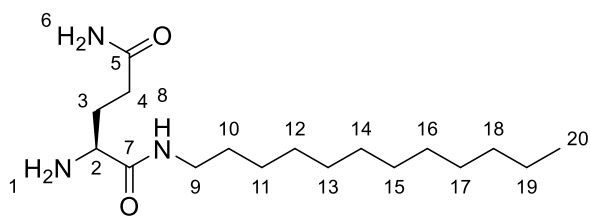
8.2.14 Synthesis of L-Boc glutamine dodecylamine



Boc-Gln-OH (491 mg, 1.99 mmol) was dissolved in DCM, and stirred for 5 minutes at 0 °C. Following this, DMAP (243 mg, 1.99 mmol), EDC (654 mg, 3.41 mmol) and dodecylamine (380 mg, 2.05 mmol) were added, and the solution stirred at room temperature overnight. The reaction mixture was then washed with HCl (2 M, 20 ml), water, NaOH (1 M, 20 ml) and brine (20 ml).

solvent was then removed from the organic layer *in vacuo* to give a white solid. Yield: 709 mg (1.71 mmol, 86%); M.p: 101.3-103.6 °C; ¹H NMR (400 MHz, DMSO-*d*₆): δ 7.73 (t, *J*=5.5 Hz, 1H, H₁₁), 7.27 (br. s, 1H, H₄), 6.81-6.76 (m, 2H, H₉), 3.84-3.78 (m, 1H, H₅), 3.06-2.98 (m, 2H, H₁₂), 2.09-2.03 (m, 2H, H₇), 1.81-1.74 (m, 1H, H₆), 1.70-1.62 (m, 1H, H₆), 1.37 (br. s, 9H, H₁), 1.23 (br. s, 20H, H₁₃-H₂₂), 0.85 (t, *J*=6 Hz, 3H, H₂₃); ¹³C NMR (100 MHz, DMSO-*d*₆): 173.81 (C₁₀), 171.62 (C₈), 155.25 (C₃), 77.97 (C₂), 54.21 (C₅), 38.42 (C₇), 31.63 (C₆), 31.36 (C₁₂), 29.13 (C₁), 29.08 (C₁₃-C₂₁), 28.84 (C₁₃-C₂₁), 28.79 (C₁₃-C₂₁), 28.19 (C₁₃-C₂₁), 27.89 (C₁₃-C₂₁), 26.32 (C₆), 22.16 (C₂₂), 13.99 (C₂₃); [α]_D²⁵ (deg cm³ g⁻¹ dm⁻¹) 2.47 ± 0.12 (c=1, chloroform); ESI-MS (m/z) calc for [M+Na]⁺, C₂₂H₄₄N₃O₄Na⁺, 436.3146; found 436.3142 (100% [M+Na]⁺); ν_{max} (cm⁻¹) (solid): 3381w, 3322w, 3201w, 3077w, 2921m, 2852m, 1689m, 1651s, 1548m, 1516s, 1454m, 1415w, 1392m, 1364m, 1319w, 1273m, 1245m, 1168s, 1090w, 1061m, 1027m, 999w, 863w, 785m, 720m, 637m, 594m, 553m.

8.2.15 Synthesis of L-glutamine dodecylamine



To deprotect, L-Boc glutamine dodecylamine (mass, moles) was added to a HCl in dioxane (4 M, 6 ml), and this stirred for 2 hours. The solvent was then removed *in vacuo* to give a white solid. The solid is then redissolved in NaOH (1 M, 50 ml) to deprotonate, and extracted with DCM. The solvent was then removed *in vacuo* to give a white solid. Yield: 372.6 mg (1.19 mmol, 59%); 103.4-104.6 °C; ¹H NMR (400 MHz, DMSO-*d*₆): δ 7.79 (t, *J*=5.5 Hz, 1H, H₈) 7.25 (br. s, 1H, H₆), 6.70 (br. s, 1H, H₆), 3.07-3.00 (m, 2H, H₂, H₉), 2.10-2.05 (m, 2H, H₄), 1.78-1.69 (m, 1H, H₃), 1.57-1.48 (m, 1H, H₃), 1.41-1.34 (m, 2H, H₁₀), 1.23 (s, 18H, H₁₁-H₁₉), 0.85 (t, *J*=6.7 Hz, 3H, H₂₀); ¹³C NMR (100 MHz, DMSO-*d*₆): 174.78 (C₅), 174.31 (C₇), 54.47 (C₃), 38.29 (C₄), 31.76 (C₂), 31.34 (C₉), 31.18 (C₁₀-C₁₉), 29.21 (C₁₀-C₁₉), 29.11 (C₁₀-C₁₉), 28.81 (C₁₀-C₁₉), 28.77 (C₁₀-C₁₉), 26.43 (C₁₀-C₁₉), 22.14 (C₂₀), 14.00 (C₁₉); [α]_D²⁵ (deg cm³ g⁻¹ dm⁻¹) 1059 ± 17 (c=1, DMSO); ESI-MS (m/z) calc for [M+H]⁺, C₁₇H₃₆N₃O₂, 314.2802; found 314.2799 (40% [M+H]), (m/z) calc for [M+Na]⁺, C₁₇H₃₅N₃O₂Na⁺, 336.2621; found 336.2621 (100% [M+Na]⁺); ν_{max} (cm⁻¹) (solid): 3401m, 3358w, 3317m, 3192m, 2956w, 2918s, 2851m, 1702w, 1642s, 1518m, 1471m, 1422m, 1344w, 1267w, 1237w, 1189w, 1152w, 1103w, 876w, 823w, 748m, 719m, 666m, 618m, 593m, 494w, 467w.

8.3 Standard Procedures for Preparing Hydrogels in Sample Vials

Generally, hydrogels were prepared the day before testing, to ensure that gelation was complete.

8.3.1 DBS-CONHNH₂ Hydrogels

A known mass of DBS-CONHNH₂ was added to a 7 ml sample vial, and H₂O (1 ml) added. This was then sonicated for 15 minutes, to give a suspension. The solid was then dissolved by heating with a heat gun, with dissolution being observed visually. The solution was cooled on the bench overnight, and a translucent gel was formed. The same method was used for both D-DBS-CONHNH₂ and L-DBS-CONHNH₂.

For DBS-CONHNH₂ hydrogels with additives, a known mass of the additive ((*R*)-naproxen, (*S*)-naproxen or L-DOPA), was added as a solid along with the gelator. The same procedure as for without additives was then followed. For (*R*)-(-)-2-phenylbutyric acid or (*S*)-(+)-2-phenylbutyric acid, a stock solution of known concentration was prepared, and this added to the gelator in place of water. The standard procedure for dissolution and cooling was then followed.

8.3.2 MBS-CO₂Me Hydrogels

A known mass of MBS-CO₂Me was added to a 7 ml sample vial, and H₂O (1 ml) added. This was then sonicated for 5 minutes, to give a suspension. The solid was then dissolved by heating with a heat gun, with dissolution observed visually. The solution was cooled on the bench overnight, and a transparent gel was formed.

For MBS-CO₂Me hydrogels with additives, a known mass of the additive (naproxen or L-DOPA), was added as a solid along with the gelator. The same procedure as for without additives was then followed.

8.3.3 DBS-CONHNH₂ and MBS-CO₂Me Hybrid Hydrogels

Known masses of both DBS-CONHNH₂ and MBS-CO₂Me were added to a 7 ml sample vial, and H₂O (1 ml) added. This was then sonicated for 10 minutes to give a suspension. The solids were then dissolved by heating with a heat gun, with dissolution observed visually. The solution was cooled on the bench overnight, and a translucent gel was formed.

For DBS-CONHNH₂ and MBS-CO₂Me hybrid hydrogels with additives, a known mass of the additive (naproxen or atorvastatin), was added as a solid along with the gelator. The same procedure as for without additives was then followed.

8.3.4 D-DBS-CONHNH₂ and L-DBS-CONHNH₂ Hydrogels

Known masses of both D-DBS-CONHNH₂ and L-DBS-CONHNH₂ were added to a 7 ml sample vial, and H₂O (1 ml) added. This was sonicated for 15 minutes to give a suspension. The solids were dissolved by heating with a heat gun, with dissolution observed visually. The solution was cooled overnight on the bench, and a translucent gel was formed.

8.3.5 MBS-SMe Hydrogels

A known mass of MBS-SMe was added to a 7 ml sample vial, and H₂O (1 ml) added. The suspension was heated with a heat gun until the solvent was beginning to boil. This was cooled on the bench overnight and white gel was formed.

8.3.6 Glutamine Amide Hydrogels

A known mass of L-glutamine dodecylamine was added to a 7 ml sample vial, along with benzaldehyde (1 equivalent), and H₂O (1 ml) added. The solid was dissolved by heating with a heat gun, with dissolution observed visually. The solution was cooled on the bench, and a white gel was formed.

For glutamine amide hydrogels with L-DOPA, a known mass of the L-DOPA was added as a solid along with the gelator. The same procedure as for without additives was then followed.

8.4 Procedure for Determination of T_{gel} Values

To determine T_{gel} values, hydrogels were first prepared as described in section 8.3, with the only difference being that the volume of water used was reduced to 0.5 ml. Once the gels had been formed, they were placed into a thermoregulated oil bath, and the temperature increased at a rate of 1 °C min⁻¹. The vials were removed every minute, gelation tested by the tube inversion test, and the vial replaced. This was continued until a gel-sol transition occurred.

8.5 Procedures for Rheology

For the preparation of samples for rheology, specially prepared vials, with the bottom removed, were used. These vials can be attached to a flat glass surface, using sealant, and the gel formed within this vial. The vial can then be removed, leaving a gel disc that can be transferred to the rheometer.

To prepare samples for rheology, hydrogels (all 1 ml) were prepared as described in section 8.3, with the following differences. In each case, following the heating of the suspension, the resulting solution was transferred to a warmed bottomless vial (described above). Once transferred, these were cooled overnight on the bench, and gels formed within the bottomless vial.

All rheology was carried out at 25 °C. For each amplitude sweep, frequency was kept constant at 1 Hz, and for each frequency sweep, shear strain was kept constant at a value determined by the amplitude sweep for that hydrogel. All rheology experiments were carried out in triplicate, with results presented as the mean of the values obtained. Error bars indicate standard error.

8.6 Procedures for Preparing Hydrogel Samples for NMR

To prepare samples for NMR studies, hydrogels (0.7 ml) both with and without additives, were prepared as described in section 8.3, with the following differences. In place of H₂O, D₂O was added as the solvent. At the same stage a DMSO internal standard (2 µl) was also added. This was then sonicated, for the appropriate time for each type of hydrogel. Once the suspension had been heated, this was quickly transferred to a warmed NMR tube while still hot. This was then cooled overnight on the bench, resulting in the formation of a hydrogel within the NMR tube.

8.7 Variable Temperature NMR Experiments

DBS-CONHNH₂ and MBS-CO₂Me hybrid hydrogels were prepared as described in section 8.3.3. Starting at 40 °C, spectra were recorded at intervals of 5 °C, up to 90 °C.

8.8 Procedures for Preparing Gels for CD

To prepare samples for circular dichroism, hydrogels (all 0.5 ml) were prepared as described in section 8.3, with the following differences. In each case, following the heating of the suspension, the resulting solution was transferred to a warmed quartz cuvette (pathlength=1 mm) while still hot. Once transferred, these were cooled overnight on the bench, and gels formed within the cuvette.

8.9 CD Experiments

CD experiments were carried out using the following settings: Data Pitch = 0.5 nm, Scanning Mode = continuous, Scan Speed = 100 nm min⁻¹, Response = 1 s, Bandwidth = 2 nm, Accumulation = 5. Quartz cuvettes (pathlength 1 mm) were used. For variable temperature experiments, measurements were carried out at 5 °C intervals, from 20-90 °C.

8.10 UV-vis Drug Release Experiments

For UV-vis experiments, gels were prepared in 7 ml vials as in section 8.3, to a volume of 1 ml. Each experiment was carried out in duplicate or triplicate, with a control gel with no additive also monitored. The reported values are the mean and error bars represent standard error. To each sample, buffer (6 ml) was added. This amount of buffer was used to maximise the volume of media into which the drug could be released. Although sink conditions were not always achieved, these quantities provided a balance between limiting the impact of drug solubility on release, and having the drug present at concentrations suitable for analysis. At regular intervals, a portion of the buffer (2 ml) was removed from the sample, and the absorbance at λ_{\max} measured. This portion of buffer was then returned to the gel. For all drug release experiments, samples were maintained in an incubator at 37 °C throughout the experiment.

8.11 HPLC Drug Release Experiments

For the quantification of atorvastatin release from DBS-CONHNH₂ and MBS-CO₂Me hybrid gels, HPLC was used. This used a C18 column, dimensions 150 x 4.6 mm. The HPLC method was developed by Dr Scott Hicks.

Conditions for separation were determined, with each of the two gelators and atorvastatin run, along with a mixed sample. To prepare the samples, 1 mg of the relevant solid was added to a sample vial, and methanol (1 ml) added. Any undissolved solid was removed by filtration, before the samples were run on the column. The solvent system developed for separation of these components was acetonitrile (45%) and pH 4 buffer (55%) (0.01 M, 1 L, ammonium hydroxide solution (33%, 0.75 ml), adjust to desired pH using formic acid (98%)). The run time was 30 minutes, oven temperature 30 °C, the flow rate 1 ml min⁻¹, and the detection UV at 247 nm.

A calibration curve was prepared. For each point, a known mass of atorvastatin was dissolved in methanol (1 ml). These samples were run using the previously described method, and the resulting peak areas plotted to give a calibration curve, shown in Figure 164.

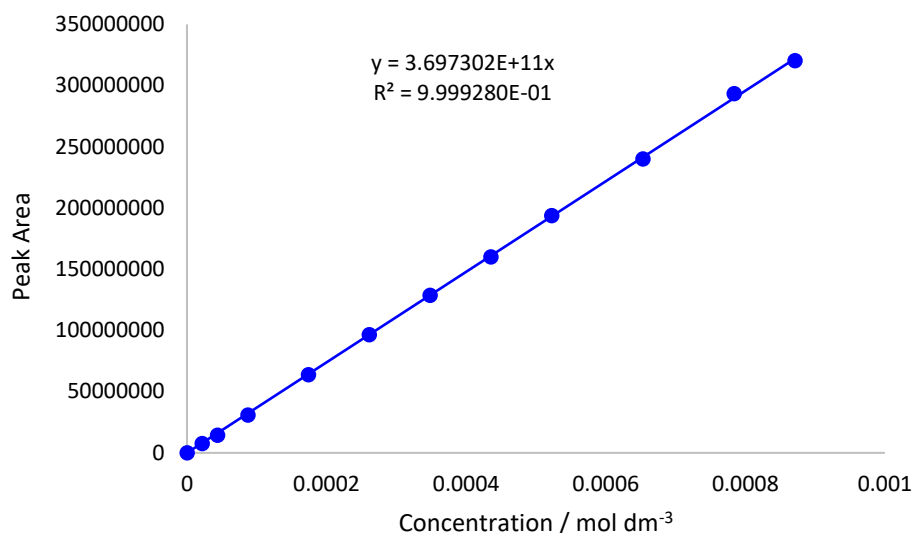


Figure 164. Calibration curve for the quantification of atorvastatin.

The quantification of release from the hybrid hydrogels (each 1 ml) was carried out in triplicate, with an additional control sample containing no atorvastatin also monitored. The reported values are the mean and error bars represent standard error. Initially, pH 7 buffer (6 ml) was added to each hydrogel. At each time point (every hour for the first eight hours, at 24 hours and at 24 hour intervals thereafter), a portion (1 ml) of buffer was removed from the sample, and replaced with fresh buffer (1 ml). The solvent was removed *in vacuo*, and methanol (1 ml) added to the remaining solid. The sample was then filtered to remove any undissolved solid, and analysed by HPLC. The amount of atorvastatin in each sample was then calculated by comparison to the calibration curve. Samples were maintained in an incubator at 37 °C throughout the experiment.

8.12 TEM Sample Preparation

All TEM imaging was carried out using the following method: A small portion of gel was transferred, by drop-casting, to a heat-treated copper support. Excess material was removed using a filter paper, and the samples air-dried for 20 minutes. Sample preparation and imaging was carried out by Meg Stark or Karen Hodgkinson at the at the Biology Technology Facility, Department of Biology, University of York.

8.13 SEM Sample Preparation

All SEM images were obtained using the following method: A small portion of gel was transferred to a copper support, then freeze-dried by plunging into liquid nitrogen. The samples were then lyophilised for 12 hours, and any excess material removed. The dried sample was then sputter coated with a thin layer of gold/palladium, to prevent sample charging, and imaging carried out.

Sample preparation and imaging was carried out by Meg Stark or Karen Hodgkinson at the at the Biology Technology Facility, Department of Biology, University of York.

8.14 Preparation of Buffers

8.14.1 Tris Buffer

For 100 ml of pH 7.4 buffer, Tris solution (1 ml) and NaCl (0.876 g) were dissolved in deionised water (99 ml).

8.14.2 HEPES Buffer

For 100 ml of buffer, HEPES prepared solution (1 M) was diluted with deionised water to the required concentration.

8.14.3 Phosphate Buffered Saline

For 1 L of buffer, one packet of premade PBS powder (Sigma Aldrich) was dissolved in deionised water (1 L).

8.14.4 pH 7.5 Phosphate Buffer

For 100 ml of buffer (0.1 M), Na_2HPO_4 (1.19 g) and NaH_2PO_4 (0.22 g) were dissolved in 100 ml deionised water.

8.14.5 pH 7 Phosphate Buffer

For 100 ml of buffer (0.1 M), Na_2HPO_4 (1.55 g) and NaH_2PO_4 (0.58 g) were dissolved in 100 ml deionised water.

8.14.6 pH 6.5 Phosphate Citrate Buffer

For 100 ml of buffer (0.1 M), Na_2HPO_4 (35.5 ml, 0.2 M) and citric acid (14.5 ml, 0.1 M) were combined, and the solution diluted with deionised water (50 ml).

8.14.7 pH 5.5 Phosphate Citrate Buffer

For 100 ml buffer (0.1 M), Na_2HPO_4 (28.4 ml, 0.2 M) and citric acid (21.6 ml, 0.1 M) were combined, and the solution diluted with deionised water (50 ml).

8.14.8 Sodium Acetate Buffer

For 100 ml of buffer (0.1 M, pH 4), sodium acetate (0.18 g) and acetic acid (0.46 g) were dissolved in deionised water (100 ml).

8.14.9 Sodium Citrate Buffer

For 100 ml of buffer (0.1 M, pH 4), sodium citrate dihydrate (0.99 g) and citric acid (1.27 g) were dissolved in deionised water (100 ml).

9. Abbreviations

Ala	Alanine
Anthra	9-anthraldehyde
ap. d	Apparent doublet (NMR)
ap. Quin.	Apparent quintet (NMR)
API	Active pharmaceutical ingredient
Arg	Arginine
Asp	Aspartic acid
BAP	Bacterial alkaline phosphatase
Boc	Tert-butyloxycarbonyl
br	Broad (NMR)
BS	Brain stem
Bzl	Benzoyl
CB	Cerebrum
CD	Circular dichroism
CE	Cerebellum
Cin	Cinnamaldehyde
CIP	Ciprofloxacin
CNS	Central Nervous System
COSY	Homonuclear correlation spectroscopy sequence
COX	Cyclooxygenase
CTAB	Cetyltrimethylammonium bromide
d	Doublet (NMR)
DBS	1,3:2,4-dibenzylidene-D-sorbitol

DBS-CO ₂ H	1,3:2,4-dibenzylidene-D-sorbitol- <i>p,p'</i> -dicarboxylic acid
DBS-CO ₂ Me	1,3:2,4-dibenzylidene-D-sorbitol- <i>p,p'</i> -dimethyl ester
DBS-CONHNH ₂	1,3:2,4-dibenzylidene-D-sorbitol- <i>p,p'</i> -diacylhydrazide
DCM	Dichloromethane
dd	Double doublet (NMR)
ddd	Double double doublet (NMR)
dddd	Double double double doublet (NMR)
DMAP	dimethylaminopyridine
DMEM	Dulbecco's Modified Eagle Medium
DMSO	Dimethyl sulfoxide
DMSO- <i>d</i> ₆	Deuterated dimethyl sulfoxide
DOX	Doxorubicin
DSC	Differential Scanning Calorimetry
EDC	1-ethyl-3-(3-dimethylaminopropyl)carbodiimide
ESI	Electrospray ionisation
FBS	Fetal bovine serum
Fmoc	Fluorenylmethyloxycarbonyl
FT-IR	Fourier transform infrared
Fur	Furfural
G'	Storage modulus
G''	Loss modulus
GdL	Glucono- δ -lactone
GI	Gastrointestinal
Gln	Glutamine
Gly	Glycine
HEPES	4-(2-hydroxyethyl)-1-piperazineethanesulfonic acid
Hexcin	Hexylcinnamaldehyde
HGF	Hepatocyte growth factor
HPLC	High-performance liquid chromatography
HSQC	Heteronuclear single quantum coherence
HT	High tension
ID	Injected dose
IgG	Immunoglobulin G
Ile	Isoleucine

IN	Intranasal
IV	Intravenous
LC-MS	Liquid chromatography-mass spectrometry
LC-MS	Liquid chromatography
Leu	Leucine
LMWG	Low molecular weight gelator
LVR	Linear viscoelastic region
Lys	Lysine
m	Multiplet (NMR)
<i>m</i>	Medium (IR)
M.p.	Melting point
MBA	Methylbenzylamine
MBS	2,4-monobenzylidene-D-sorbitol
MBS-CO ₂ Me	2,4-monobenzylidene-D-sorbitol- <i>p</i> -methyl ester
Met	Methionine
MGC	Minimum gelation concentration
MS	Mass spectrometry
MSC	Mesenchymal stem cell
NMR	Nuclear magnetic resonance
NPX	Naproxen
NSAID	Non-steroidal anti-inflammatory drug
OB	Olfactory bulbs
P/S	Penicillin/streptomycin
PBS	Phosphate buffered saline
PD	Parkinson's disease
PEG	Poly(ethyleneglycol)
PEGDM	Poly(ethyleneglycol dimethylacrylate)
PEI	Percutaneous ethanol injection therapy
PG	Polymer gelator
Phe	Phenylalanine
PLP	Pyridoxal 5'-phosphate
<i>p</i> -TsOH	<i>para</i> -Toluene sulfonic acid (monohydrate)
s	Singlet (NMR)
s	Strong (IR)

SC	Spinal cord
SEM	Scanning electron microscopy
SMe	4-(methylthio)benzaldehyde
t	Triplet (NMR)
TEM	Transmission electron microscopy
T_{gel}	Gel-sol transition temperature
THF	Tetrahydrofuran
TLC	Thin layer chromatography
TN	Trigeminal nerves
TNF	Tumour necrosis factor
Tris	Trisaminomethane
Trp	Tryptophan
Try	Tyrosine
UV	Ultraviolet
UV-vis	Ultraviolet-visible
Val	Valine
Van	Vanillin
w	Weak (IR)
β -gal	β -galactosidase

10. References

- ¹ J. W. Steed, *Chem. Commun.*, 2011, **47**, 1379-1383
- ² P. Terech and R. G. Weiss, *Chem. Rev.*, 1997, **97**, 3133-3160
- ³ M. Suzuki, S. Owa, M. Kimura, A. Kurose, H. Shirai and K. Hanabusa, *Tetrahedron Lett.*, 2005, **46**, 303-306
- ⁴ Z. Xie, A. Zhang, L. Ye and Z-G. Feng, *Soft Matter*, 2009, **5**, 1474-1482
- ⁵ J. Le Bideau, L. Viau and A. Vioux, *Chem. Soc. Rev.*, 2011, **40**, 907-925
- ⁶ P. C. Marr and A. C. Marr, *Green Chem.*, 2016, **18**, 105-128
- ⁷ B. Joos, T. Vranken, W. Marchal, M. Safari, M. K. Van Bael and A. T. Hardy, *Chem. Mater.*, 2018, **30**, 655-662
- ⁸ J. Ruiz-Olles, P. Slavik, N. K. Whitelaw and D. K. Smith, *Angew. Chem. Int. Edit.*, 2019, **58**, 4173-4178

- ⁹ S-K. Ahn, R. M. Kasi, S-C. Kim, N. Sharma and Y. Zhou, *Soft Matter*, 2008, **4**, 1151-1157
- ¹⁰ T. Graham, *Philos. Trans.*, 1861, **151**, 183-224
- ¹¹ N. M. Sangeetha and U. Maitra, *Chem. Soc. Rev.*, 2005, **34**, 821-836
- ¹² L. A. Estroff and A. D. Hamilton, *Chem. Rev.*, 2004, **104**, 1201-1218
- ¹³ A. R. Hirst, I. A. Coates, T. R. Boucheteau, J. F. Miravet, B. Escuder, V. Castelletto, I. W. Hamley and D. K. Smith, *J. Am. Chem. Soc.*, 2008, **130**, 9113-9121
- ¹⁴ V. Jayawarna, M. Ali, T. A. Jowitt, A. F. Miller, A. Saiani, J. E. Gough and R. V. Ulijn, *Adv. Mater.*, 2006, **18**, 611-614
- ¹⁵ G. Ben Messaoud, P. Le Griel, D. Hermida-Merino, S. L. K. W. Roelants, W. Soetaert, C. Victor Stevens and N. Baccile, *Chem. Mater.*, 2019, **31**, 4817-4830
- ¹⁶ D. J. Adams, M. F. Butler, W. J. Frith, M. Kirkland, L. Mullen and P. Sanderson, *Soft Matter*, 2009, **5**, 1856-1862
- ¹⁷ (a) T. Naota and H. Koori, *J. Am. Chem. Soc.*, 2005, **127**, 9324-9325; (b) G. Cravotto and P. Cintas, *Chem. Soc. Rev.*, 2009, **38**, 2684-2697; (c) I. Maity, D. B. Rasale and A. K. Das, *Soft Matter*, 2012, **8**, 5301-5308; (d) M. Yamanaka, *J. Incl. Phenom. Macro.*, 2013, **77**, 33-48
- ¹⁸ E. R. Draper and D. J. Adams, *Chem. Commun.*, 2016, **52**, 8196-8206
- ¹⁹ (a) Z. Yang, H. Gu, D. Fu, P. Gao, J. K. Lam and B. Xu, *Adv. Mater.*, 2004, **19**, 1440-1444; (b) S. Toledano, R. J. Williams, V. Jayawarna and R. V. Ulijn, *J. Am. Chem. Soc.*, 2006, **128**, 1070-1071; (c) Z. Yang, G. Liang and B. Xu, *Acc. Chem. Res.*, 2008, **41**, 315-326; (d) R. J. Williams, R. J. Mart and R. V. Ulijn, *Peptide Science*, 2010, **94**, 107-117; (e) S. C. Bremmer, A. J. McNeil and M. B. Soellner, *Chem. Commun.*, 2014, **50**, 1691-1693; (f) J. Baillet, A. Gaubert, J. Verget, L. Latqague and P. Barthélémy, *Soft Matter*, 2020, **16**, 7648-7651
- ²⁰ D. B. Amabilino, D. K. Smith and J. W. Steed, *Chem. Soc. Rev.*, 2017, **46**, 2404-2420
- ²¹ R. G. Weiss, *J. Am. Chem. Soc.*, 2014, **136**, 7519-7530
- ²² (a) B. O. Okesola and D. K. Smith, *Chem. Soc. Rev.*, 2016, **45**, 4226-4251; (b) J. Y. C. Lim, S. S. Goh, S. S. Liow, K. Xue and X. J. Loh, *J. Mater. Chem. A*, 2019, **7**, 18759-18791
- ²³ (a) C. Yuan, J. Guo, M. Tan, M. Guo, L. Qiu and F. Yan, *ACS Macro Lett.*, 2014, **3**, 271-275; (b) J-D. Decoppet, T. Moehl, S. S. Babkair, R. A. Alzubaydi, A. A. Ansari, S. S. Habib, S. M. Zakeeruddin, H-W. Schmidt and M. Grätzel, *J. Mater. Chem. A.*, 2014, **2**, 15972-15977; (c) M. Bielejewski, A. Rachocki, J. Kaszyńska and J. Tritt-Goc, *Phys. Chem. Chem. Phys.*, 2018, **20**, 5803-5817; (d) P. Guo, A. Su, Y. Wei, X. Liu, Y. Li, F. Guo, J. Li, Z. Hu and J. Sun, *ACS Appl. Mater. Inter.*, 2019, **11**, 19413-19420

- ²⁴ (a) B. Escuder, F. Rodríguez-Llansola and J. F. Miravet, *New J. Chem.*, 2010, **34**, 1044-1054; (b) W. Fang, Y. Zhang, J. Wu, C. Liu, H. Zhu and T. Tu, *Chem.-Asian J.*, 2018, **13**, 712-729
- ²⁵ K. J. Skilling, F. Citossi, T. D. Bradshaw, M. Ashford, B. Kellam and M. Marlow, *Soft Matter*, 2014, **10**, 237-256
- ²⁶ O. Wichterle, D. Lim, *Nature*, 1960, **185**, 117-118
- ²⁷ (a) W. C. Frazier, *J. Infect Dis.*, 1926, **39**, 302-309; (b) H. L. Smith and K. Goodner, *J Bacteriol.*, 1958, **76**, 662-665
- ²⁸ X. Li, H. Bai, Y. Yang, J. Yoon, S. Wang and X. Zhang, *Adv. Mater.*, 2019, **31**, 1805092
- ²⁹ S. Marchesan, Y. Qu, L. J. Waddington, C. D. Easton, V. Glattauer, T. J. Lithgow, K. M. McLean, J. S. Forsythe and P. G. Hartley, *Biomaterials*, 2013, **34**, 3678-3687
- ³⁰ T. Simon, C-S. Wu, J-C. Liang, C. Cheng and F-H. Ko, *New J. Chem.*, 2016, **40**, 2036-2043
- ³¹ C. C. Piras, C. S. Mahon and D. K. Smith, *Chemistry*, 2020, **26**, 8452-8457
- ³² Y. Li, F. Zhou, Y. Wen, K. Liu, L. Chen, Y. Mao, S. Yang and T. Yi, *Soft Matter*, 2014, **10**, 3077-3085
- ³³ A. Baral, S. Roy, S. Ghosh, D. Hermida-Merino, I. W. Hamley and A. Banerjee, *Langmuir*, **32**, 1836-1845
- ³⁴ A. P. McCloskey, S. M. Gilmore, J. Zhou, E. R. Draper, S. Porter, B. F. Gilmore, B. Xu and G. Laverty, *RSC Adv.*, 2016, **6**, 114738-114749
- ³⁵ (a) G. Laverty, S. P. Gorman and B. F. Gilmore, *Int. J. Mol. Sci.*, 2011, **12**, 6566-6596; (b) C. D. Fjell, J. A. Hiss, R. E. W. Hancock and G. Schneider, *Nat. Rev. Drug Discov.*, 2012, **11**, 37-51
- ³⁶ F. E. Silverstein *et al.*, *JAMA*, 2000, **284**, 1247-1255
- ³⁷ Z. Yang, G. Liang, Z. Guo, Z. Guo and B. Xu, *Angew. Chem. Int. Edit.*, 2007, **46**, 8216-8219
- ³⁸ Z. Yang, G. Liang, M. Ma, A. S. Abbah, W. W. Lu and B. Xu, *Chem. Commun.*, 2007, 843-845
- ³⁹ (a) M. F. McCarty, *Med. Hypotheses*, 1996, **47**, 273-275; (b) S. Shaunak, S. Thomas, E. Gianasi, A. Godwin, E. Jones, I. Teo, K. Mireskandari, P. Luthert, R. Duncan, S. Patterson P. Khaw and S. Brocchini, *Nat. Biotechnol.*, 2004, **22**, 977-984
- ⁴⁰ J. Gao, W. Zheng, J. Zhang, D. Guan, Z. Yang, D. Kong, Q. Zhao, *Chem. Commun.*, 2013, **49**, 9173-9175
- ⁴¹ (a) B. V. Khan, D. G. Harrison, M. T. Olbrych, R. W. Alexander and R. M. Medford, *Proc. Natl. Acad. Sci. USA*, 1996, **93**, 9114-9119; (b) A. Wolf, C. Zalpour, G. Theilmeyer, B-Y. Wang, A. Ma, B. Anderson, P. S. Tsao and J. P. Cooke, *J. Am. Coll. Cardiol.*, 1997, **29**, 479-485; (c) N. W. Rajapakse and D. L. Mattson, *Clin. Exp. Pharmacol. P.*, 2009, **36**, 249-255; (d) J. Kim, B. C. Yung, W. J. Kim and X. Chen, *J. Control. Release*, 2017, **263**, 223-230

- ⁴² (a) H. Chakrapani, T. C. Wilde, M. L. Citro, M. M. Goodblatt, L. K. Keefer and J. E. Saavedra, *Bioorgan. Med. Chem.*, 2008, **16**, 2657-2664; (b) X. Jia, Y. Zhang, Y. Zou, Y. Wang, D. Niu, Q. He, Z. Huang, W. Zhu, H. Tian, J. Shi and Y. Li, *Adv. Mater.*, 2018, **30**, 1704490
- ⁴³ V. A. Kumar, N. C. Wickremasinghe, S. Shi and J. D. Hartgerink, *ACS Biomater. Sci. Eng.*, 2015, **1**, 1300-1305
- ⁴⁴ (a) K. Stocker and G. H. Barlow, *Method. Enzymol.*, 1976, **45**, 214-223; (b) S. Braud, C. Bon and A. Wisner, *Biochimie*, 2000, **82**, 851-859
- ⁴⁵ S. M. T. Serrano, *Toxicon*, 2013, **62**, 19-26
- ⁴⁶ D. M. Ryan and B. L. Nilsson, *Polym. Chem.*, 2012, **3**, 18-33
- ⁴⁷ (a) K. Y. Lee and D. J. Mooney, *Chem. Rev.*, 2001, **101**, 1869-1880; (b) M. W. Tibbit and K. S. Anseth, *Biotechnol. Bioeng.*, 2009, **103**, 655-663; (c) S. R. Caliari and J. A. Burdick, *Nat. Methods*, 2016, **13**, 405-414
- ⁴⁸ (a) G. M. Abouna, *Transpl. P.*, 2008, **40**, 34-38; (b) O. Jawoniyi, K. Gormley, E. McGleenan and H. R. Noble, *J. Clin. Nurs.*, 2017, **27**, 726-738; (c) B. Bastani, *J. Nephrol.*, 2020, **33**, 277-288; (d) K. Bambha, A. Shingina, J. L. Dodge, K. O'Connor, S. Dunn, J. Prinz, M. Pabst, K. Nilles, L. Sibulesky and S. W. Biggins, *Am. J. Transplant.*, 2020, **20**, 1642-1649
- ⁴⁹ (a) P. E. Morrissey, M. L. Flynn and S. Lin, *Drugs*, 2007, **67**, 1463-1481; (b) B. L. Kasiske, M. G. Zeier, J. R. Chapman, J. C. Craig, H. Ekberg, C. A. Garvey, M. D. Green, V. Jha, M. A. Josephson, B. A. Kiberd, H. A. Kreis, R. A. McDonald, J. M. Newmann, G. T. Obrador, F. G. Vincenti, M. Cheung, A. Earley, G. Raman, S. Abariga, M. Wagner and E. M. Balk, *Kidney Int.*, 2010, **77**, 299-311; (c) C. Duvoux and G. P. Pageaux, *J. Hepatol.*, 2011, **54**, 1041-1054; (d) C. R. Ensor, J. Trofe-Clark, S. Gabardi, L. M. McDevitt-Potter and M. A. Shullo, *Pharmacotherapy*, 2011, **31**, 1111-1129
- ⁵⁰ (a) K. D. Yoo, J. Noh, H. Lee, D. K. Kim, C. S. Lim, Y. H. Kim, J. P. Lee, G. Kim and Y. S. Kim, *Sci. Rep.*, 2017, **7**, 8904; (b) A. Loupy and C. Lefucheur, *New Engl. J. Med.*, 2018, **379**, 1150-1160
- ⁵¹ G. A. Silva, C. Czeisler, K. L. Niece, E. Beniash, D. A. Harrington, J. A. Kessler and S.I. Stupp, *Science*, 2004, **303**, 1352-1355
- ⁵² (a) K. Tashiro, G. C. Sphel, B. Weeks, M. Sasaki, G. R. Martin, H. K. Kleinman and Y. Yamada, *J. Biol. Chem.*, 1989, **264**, 16174-16182; (b) M. Nomizu, B. S. Weeks, C. A. Weston, W. H. Kim, H. K. Kleinman and Y. Yamada, *FEBS Lett.*, 1995, **365**, 227-231; (c) S. K. Powell, J. Rao, E. Roque, M. Nomizu, Y. Kuratomi, Y. Yamada and H. K. Kleinman, *J. Neurosci. Res.*, 2000, **61**, 302-312
- ⁵³ V. M. Tysseling-Mattiace, V. Sahni, K. L. Niece, D. Birch, C. Czeisler, M. G. Fehlings, S. I. Stupp and J. A. Kessler, *J. Neurosci.*, 2008, **28**, 3814-3823

- ⁵⁴ R. G. Ellis-Behnke, Y-X. Liang, S-W. You, D. K. C. Tay, S. Zhang, K-F. So and G. E. Schneider, *Proc. Natl. Acad. Sci. USA*, 2006, **103**, 5054-5059
- ⁵⁵ (a) S. Zhang, T. Holmes, C. Lockshin and A. Rich, *Proc. Natl. Acad. Sci. USA*, 1993, **90**, 3334-3338; (b) S. Zhang, T. C. Holmes, C. M. DiPersio, R. O. Hynes, X. Su and A. Rich, *Biomaterials*, 1995, **16**, 1385-1393
- ⁵⁶ T. C. Holmes, S. de Lacalle, X. Su, G. Liu, A. Rich and S. Zhang, *Proc. Natl. Acad. Sci. USA*, 2000, **97**, 6728-6733
- ⁵⁷ M. Zhou, A. M. Smith, A. K. Das, N. W. Hodson, R. F. Collins, R. V. Ulijn and J. E. Gough, *Biomaterials*, 2009, **30**, 2523-2530
- ⁵⁸ (a) R. J. Pelham and Y-L. Wang, *Proc. Natl. Acad. Sci. USA*, 1997, **94**, 13661-13665; (b) A. J. Engler, S. Sen, H. L. Sweeney and D. E. Discher, *Cell*, 2006, **126**, 677-689; (c) A. S. Rowlands, P.A. George and J. J. Cooper-White, *Am. J. Physiol-Cell Ph.*, 2008, **295**, 1037-1044; (d) J. H. Wen, L. G. Vincent, A. Fuhrmann, Y. S. Choi, K. C. Hribar, H. Taylor-Weiner, S. Chen and A. J. Engler, *Nat. Mater.*, 2014, **13**, 979-987
- ⁵⁹ Y. Hu, W. Gao, F. Wu, H. Wu, B. He and J. He, *J. Mater. Chem. B*, 2016, **4**, 3504-3508
- ⁶⁰ J. Liu, F. Yuan, X. Ma, D. Y. Auphedeous, C. Zhao, C. Liu. C. Shen and C. Feng, *Angew. Chem. Int. Edit.*, 2018, **57**, 6475-6479
- ⁶¹ (a) R. K. Verma, D. M. Krishna and S. Garg, *J. Control. Release*, 2002, **79**, 7-27; (b) G. Pilcer and K. Amighi, *Int. J. Pharm.*, 2010, **392**, 1-19; (c) B. Mishra, B. B. Patel and S. Tiwari, *Nanomed-Nanotechnol.*, 2010, **6**, 9-24; (d) C. Paderni, D. Compilato, L. I. Giannola and G. Campisi, *Or. Surg. Or. Med. Or. Pa.*, 2012, **114**, 25-34; (e) S. Mazzaferro, K. Bouchemal and G. Ponchel, *Drug Discov. Today*, 2013, **18**, 99-104; (f) S. Basavaraj and G. V. Betageri, *Acta. Pharm. Sin. B*, 2014, **4**, 3-17; (g) F. L. Lopez, T. B. Ernest. C. Tuleu and M. O. Gul, *Expert Opin. Drug Del.*, 2015, **12**, 1727-1740
- ⁶² (a) M. L. MacDonald, J. Lamerdin, S. Owens, B. H. Keon, G. K. Bilter, Z. Shang, Z. Huang, H. Yu, J. Dias, T. Minami, S. W. Michnick and J. K. Westwick, *Nat. Chem. Biol.*, 2006, **2**, 329-337; (b) S. Liu and R. Kurzrock, *Cancer Treat. Rev.*, 2014, **40**, 883-891; (c) S. L. Garon, R. K. Pavlos, K. D. White, N. J. Brown, C. A. Stone and E. J. Phillips, *Brit. J. Clin. Pharmacol.*, 2017, **83**, 1896-1911; (d) Z. Sa, J. Zhou, Y. Zou, Z. Su and X. Gu, *Genomics Proteomics Bioinformatics*, 2017, **15**, 246-254; (e) A. Lin, C. J. Giuliano, A. Palladino, K. M. John, C. Abramowicz, M. L. Yuan, E. L. Sausville, D. E. Lukow, L. Liu. A. R. Chait, Z. C. Galluzzo, C. Tucker and J. M. Sheltzer, *Sci. Transl. Med.*, 2019, **11**; (f) C. W. McAleer, C. J. Long, D. Elbrecht, T. Sassrath, L. R. Bridges, J. W. Rumsey, C. Martin, M. Schnepfer, Y. Wang, F. Schuler, A. B. Roth, C. Funk, M. L. Shuler and J. J. Hickman, *Sci. Transl. Med.*, 2019, **11**

- ⁶³ (a) S. M. Paul, D. S. Mytelka, C. T. Dunwiddie, C. C. Persinger, B. H. Munos, S. R. Lindborg and A. L. Schacht, *Nat. Rev. Drug Discov.*, 2010, **9**, 203-214; (b) J. W. Scannell, A. Blanckley, H. Boldon and B. Warrington, *Nat. Rev. Drug Discov.*, 2012, **11**, 191-200; (c) T. J. Hwang, D. Caprenter, J. C. Lauffenburger, B. Wang, J. M. Franklin and A. S. Kesselheim, *JAMA Intern. Med.*, 2016, **176**, 1826-1833
- ⁶⁴ X. Yu, L. Chen, M. Zhang and T. Yi, *Chem. Soc. Rev.*, 2014, **43**, 5346-5371
- ⁶⁵ D. K. Smith, in *Molecular Gels*, ed. R. G. Weiss, Royal Society of Chemistry, Cambridge, 2018, ch. 9, pp 300-358
- ⁶⁶ J. J. Panda, A. Mishra, A. Basu and V. S. Chauhan, *Biomacromolecules*, 2008, **9**, 2244-2250
- ⁶⁷ S. Koutsopoulos, L. D. Unsworth, Y. Nagai and S. Zhang, *P. Natl. Acad. Sci. USA*, 2009, **106**, 4623-4628
- ⁶⁸ Y. Nagai, L. D. Unsworth, S. Koutsopoulos and S. Zhang, *J. Control. Release*, 2006, **115**, 18-25
- ⁶⁹ S. Liu, M. Zhao, Y. Zhou, L. Li, C. Wang, Y. Yuan, L. Li, G. Liao, W. Bresette, Y. Chen, J. Cheng, Y. Lu and J. Liu, *Acta Biomater.*, 2020, **103**, 102-114
- ⁷⁰ S. Liu, L. Zhang, J. Cheng, Y. Lu and J. Liu, *Int. J. Nanomed.*, 2016, **11**, 4875-4890
- ⁷¹ D. Limón, E. Amirthalingam, M. Rodrigues, L. Halbaut, B. Andrade, M. L. Garduño-Ramírez, D. B. Amabilino, L. Pérez-García and A. Calpena, *Eur. J. Pharm. Biopharm.*, 2015, **96**, 421-436
- ⁷² J. Mayr, C. Saldías and D. Díaz Díaz, *Chem. Soc. Rev.*, 2018, **47**, 1484-1515
- ⁷³ (a) T. Vermonden, R. Censi and W. E. Hennink, *Chem. Rev.*, 2012, **112**, 2853-2888; (b) Y. Wang, E. Delgado-Fukushima, R. X. Fu, G. S. Doerk and J. K. Monclare, *Biomacromolecules*, 2020, **21**, 3608-3619
- ⁷⁴ M. Ikeda, T. Tanida, T. Yoshii and I. Hamachi, *Adv. Mater.*, 2011, **23**, 2819-2822
- ⁷⁵ V. Leskovac, S. Trivić, G. Wohlfahrt, J. Kandrač and D. Peričin, *Int. J. Biochem. Cell B.*, 2005, **37**, 731-750
- ⁷⁶ N. Tao, G. Li, M. Liu, W. Gao and H. Wu, *Tetrahedron*, 2017, **73**, 3173-3180
- ⁷⁷ M. G. F. Angelero, R. Markus, V. Paraskevopoulou, R. Foralosso, P. Clarke, C. V. Alvarez, M. Chenlo, L. Johnson, C. Rutland, S. Allen, C. Brasnett, A. Seddon, M. Zelzer and M. Marlow, *J. Control. Release*, 2020, **317**, 118-129
- ⁷⁸ K. J. Skilling, B. Kellam, M. Ashford, T. D. Bradshaw and M. Marlow, *Soft Matter*, 2016, **12**, 8950-8957
- ⁷⁹ J. B. Matson and S. I. Stupp, *Chem. Commun.*, 2011, **47**, 7962-7964
- ⁸⁰ J. Majumder, P. Yedoti and P. Dastidar, *Org. Biomol. Chem.*, 2015, **13**, 2300-2309
- ⁸¹ J. A. Sáez, B. Escuder and J. F. Miravet, *Tetrahedron*, 2010, **66**, 2614-2618

- ⁸² (a) K. K. Jain, in *Drug Delivery Systems*, ed. K. K. Jain, Springer, New York, 1st edn, 2008, ch. 1, pp. 1-50; (b) L. Liu, W. D. Yao, Y. F. Rao, X. Y. Lu and J. Q. Gao, *Drug Deliv.*, 2017, **24**, 569-581; (c) B. Homayun, X. Lin and H-J. Choi, *Pharmaceutics*, 2019, **11**, 129
- ⁸³ (a) H. Zhang, J. Zhang and J. B. Streisand, *Clin. Pharmacokinet.*, 2012, **41**, 661-680; (b) G. Tiwari, R. Tiwari, B. Sriwastawa, L. Bhati, S. Pandey, P. Pandey and S. K. Banerjee, *Int. J. Pharm. Investig.*, 2012, **2**, 2-11; (c) A. R. Khan, M. Liu, M. W. Khan and G. Zhai, *J. Control. Release*, 2017, **268**, 364-389; (d) B. Iqbal, J. Ali and S. Baboota, *Int. J. Dermatol.*, 2018, **57**, 646-660; (e) Y. L. Mato, *Int. J. Pharm.*, 2019, **572**, 118813; (f) D. Ramadan, M. T. C. McCrudden, A. J. Courtenay and R. F. Donnelly, *Drug Deliv. Transl. Re.*, 2021
- ⁸⁴ (a) S. M. Pond and T. N. Tozer, *Clin. Pharmacokinet.*, 1984, **9**, 1-25; (b) D. J. Morgan and R. A. Smallwood, *Clin. Pharmacokinet.*, 1990, **18**, 61-76; (c) B. Agoram, W. S. Woltoz and M. B. Bolger, *Adv. Drug Deliver. Rev.*, 2001, **50**, 41-67; (d) S. Ghosh, S. Ghosh and P. C. Sil, *Toxicol. Rep.*, 2019, **6**, 358-368
- ⁸⁵ (a) Y. Mateo, E. A. Budygin, D. Morgan, D. C. S. Roberts and S. R. Jones, *Eur. J. Neurosci.*, 2004, **20**, 2838-2842; (b) K. Venkatakrishnan, K. E. Culm, B. L. Ehrenberg, J. S. Harmatz, K. E. Corbett, J. C. Fleishaker and D. J. Greenblatt, *J. Clin. Pharmacol.*, 2005, **45**, 529-537; (c) R. N. Upton, A. A. Somogyi, A. M. Martinez, J. Colvill and C. Grant, *Brit. J. Anaesth.*, 2010, **105**, 798-809; (d) W. F. Peacock, D. E. Hilleman, P. D. Levy, D. J. Rhoney and J. Varon, *Am. J. Emerg. Med.*, 2012, **30**, 981-993; (e) Å. Norberg, P. Koch, S. J. Kanés. M. A. Bjornsson, S. Barassin, K. Ahlén and S. Kalman, *Anesth. Analg.*, 2015, **121**, 894-903; (f) M. Mahmoud and K. P. Mason, *F1000Res.*, 2018, **7**, 470
- ⁸⁶ (a) A. Bernkop-Schnürch, *Eur. J. Pharm. Sci.*, 2013, **49**, 272-277; (b) B. Hens, M. Corsetti, R. Spiller, L. Marciani, T. Vanuytsel, J. Tack, A. Talattof, G. L. Amidon, M. Koziolk, W. Weitschies, C. G. Wilson, R. J. Bennick, J. Brouwers and P. Augustijns, *Int. J. Pharm.*, 2017, **519**, 79-97; (c) H. Shahdadi Sardo, F. Saremnejad, S. Bagheri, A. Akhgari, H. Afrasiabi Garekani and F. Sadeghi, *Int. J. Pharm.*, 2019, **558**, 367-379
- ⁸⁷ (a) D. J. Kellerman, M. Ameri and S. J. Tepper, *Pain Manag.*, 2017, **7**, 559-567; (b) J. Woo Lee and M. R. Prausnitz, *Expert Opin. Drug Del.*, 2018, **15**, 541-543; (c) J. A. Bartlett and K. van der Voort Maarschalk, *AAPS Pharmscitech*, 2012, **13**, 1110-1115; (d) S. Hua, *Front. Pharmacol.*, 2019, **10**, 1-9
- ⁸⁸ (a) L. H. Nicoll and A. Hesby, *Appl. Nurs. Res.*, 2002, **15**, 149-162; (b) G. Bertelli, M. Venturini, L. del Mastro, M. Bergaglio, P. Sismondi. N. Biglia, S. Venturini, G. Porcile, P. Pronzato, M. Constantini and R. Rosso, *Ann. Oncol.*, 2002, **13**, 883-888; (c) E. MacLachlan, L. M. Atuyambe, T. Millogo, G. Guiella, S. Yaro, S. Kasasa, J. Bukenya, A. Nyabigambo, F. Mubiru, J. Tumusiime, Y.

- Onadja, L. Moussa Zan, C. Coeum/Sanon, S. Kouanda and A. Namagembe, *Contraception*, 2018, **98**, 423-429; (d) M. Reid Groseclose and S. Castellino, *Int. J. Mass Spectrom.*, 2019, **437**, 92-98
- ⁸⁹ E. Kisak and J. Singh, *US. Pat.*, 20080300311, 2008
- ⁹⁰ (a) M. Singh, S. Kundu, A. Reddy M, V. Sreekanth, R. K. Motiana, S. Sengupta, A. Srivastava and A. Bajaj, *Nanoscale*, 2014, **6**, 12849-12855; (b) C. Martin, E. Oyen, J. Mangelschots, M. Bibian, T. Ben Haddou, J. Andrade, J. Gardiner, B. van Mele, A. Madder, R. Hoogenboom, M. Spetea and S. Ballet, *Med. Chem. Commun.*, 2016, **7**, 542-549; (c) M. Kurbasic, C. D. Romano, A. M. Garcia, S. Kralj and S. Marchesan, *Gels*, 2017, **3**, M. E. Roth-Konforti, M. Comune, M. Halperin-Sternfeld, I. Grigoriants, D. Shabat and L. Adler-Abramovich, *Macromol. Rapid Comm.*, 2018, **39**, 1800588; (d) C-G. Wu, X. Wang, Y-F. Shi, B-C. Wang, W. Xue and Y. Zhang, *Biomater. Sci.*, 2020, **8**, 6190-6203; (e) R. Chen, C. Xu, Y. Lei, H. Liu, Y. Zhu, J. Zhang and L. Xu, *RSC Adv.*, 2021, **11**, 12641-12648
- ⁹¹ P. McCrorie, J. Mistry, V. Taresco, T. Lovato, M. Fay, I. Ward, A. A. Ritchie, P. A. Clarke, S. J. Smith, M. Marlow and R. Rahman, *Eur. J. Pharm. Biopharm.*, 2020, **157**, 108-120
- ⁹² L. Xu, Y. Liang, C. Sun. N. Hao, J. Yan. W. Gao and B. He, *Nanotheranostics*, 2017, **1**, 313-325
- ⁹³ (a) J. H. Van Esch and B. L. Feringa, *Angew. Chem. Int. Edit.*, 2000, **39**, 2263-2266; (b) C. D. Jones and J. W. Steed, *Chem. Soc. Rev.*, 2016, **45**, 6546-6596; (c) M. Liu, G. Ouyang, D. Niu and Y. Sang, *Org. Chem. Front.*, 2018, **5**, 2885-2900; (d) P. Dastidar, *Gels*, 2019, **5**, 15
- ⁹⁴ Y. Lan, M. G. Corradini, R. G. Weiss, S. R. Raghavan and M. A. Rogers, *Chem. Soc. Rev.*, 2015, **44**, 6035-6058
- ⁹⁵ (a) B. Xing, C-W. Yu, K-H. Chow, P-L. Ho, D. Fu and B. Xu, *J. Am. Chem. Soc.*, 2002, **124**, 14846-14847; (b) W. Deng, H. Yamauchi, Y. Takashima and A. Harada, *Angew. Chem. Int. Edit.*, 2007, **46**, 5144-5147; (c) N. E. Shi, H. Dong, G. Yin, Z. Yu and S. H. Li, *Adv. Funct. Mater.*, 2007, **17**, 1837-1843; (d) G. O. Lloyd and J. W. Steed, *Nat. Chem.*, 2009, **1**, 437-442; (e) T. Luan, M. Ma, P. Xing, Y. Wang, M. Yang, Y. Zhang, W. An, Q. Cheng and A. Hao, *Soft Matter*, 2018, **14**, 1753-1758; (f) D. Blasco, J. M. López-de-Luzuriaga, M. Monge, M. E. Olmos, D. Pascual and M. Rodríguez-Castillo, *Inorg. Chem.*, 2018, **57**, 3805-3817
- ⁹⁶ H. Kobayashi, A. Friggeri, K. Koumoto, M. Amaike, S. Shinkai and D. N. Reinhoudt, *Org. Lett.*, 2002, **4**, 1423-1426
- ⁹⁷ M. J. Meunier, *Ann. Chim. Phys.*, 1891, **22**, 412
- ⁹⁸ R. M. C. Douglas, J. Brecknell, J. J. Kibby and L. T. Nicholas, *Aust. J. Chem.*, 1976, **29**, 1859-1863
- ⁹⁹ (a) R. B. Kasat, W. Lee, D. R. McCarthy and N. G. Telyan, *US Pat.*, 1994; (b) J. Mattai, C. Ortiz, E. P. Guenin and J. Afflitto, *Hungarian Pat.*, HU0401078, 2002; (c) G. Malle, T Luukas, *US Pat.*, 20130039862, 2010

- ¹⁰⁰ (a) H. Uchiyama, *US Pat.*, 4483952, 1983; (b) J. Xu, X. Zhao, J. Li and K. Lake, *US Pat.*, 20060270766, 2005; (c) C. Xie, L. R. Rieth and T. D. Danielson, *US Pat.*, 2007
- ¹⁰¹ B. O. Okesola, V. M. P. Vieira, D. J. Cornwell, N. K. Whitelaw and D. K. Smith, *Soft Matter*, 2015, **11**, 4768-4787
- ¹⁰² (a) R. Stan, S. Roşca, C. Ott, S. Roşca, E. Perez, I. Rico-Lattes and A. Lattes, *Rev. Roum. Chem.*, 2006, **51**, 609-613; (b) R. Feng, L. Chen, Z. Hou and J. Song, *Trans. Tianjin. Univ.*, 2007, **13**, 35-41; (c) P. Aduri and P. V. Uppara, *US. Pat.*, 20130296581, 2013, (d) T-T. Huang, C-P. Tsou and W-C. Wei, *EP. Pat.*, 2940023, 2015
- ¹⁰³ T. Furuishi, K. Tomono, T. Suzuki, T. Fukami and K. Kunimasu, *US. Pat.*, 20120264742, 2012
- ¹⁰⁴ C. R. King, D. W. Bristol and M. L. English, *US. Pat.* 20140178480, 2014
- ¹⁰⁵ D. J. Cornwell, B. O. Okesola and D. K. Smith, *Soft Matter*, 2013, **9**, 8730-8736
- ¹⁰⁶ B. O. Okesola and D. K. Smith, *Chem. Commun.*, 2013, **49**, 11164-11166
- ¹⁰⁷ S. J. Beckers, S. Parkinson. E. Wheeldon and D. K. Smith, *Chem. Commun.*, 2019, **55**, 1947-1950
- ¹⁰⁸ B. O. Okesola and D. K. Smith, *Chem. Commun.*, 2013, **49**, 11164-11166
- ¹⁰⁹ E. J. Howe, B. O. Okesola and D. K. Smith, *Chem. Commun.*, 2015, **51**, 7451-7454
- ¹¹⁰ L. V. Vargha, *Eur. J. Inorg. Chem.*, 1935, **68**, 1377-1384
- ¹¹¹ T. Saito, T. Teshigawara, M. Reger, H. Hoffman, Y. Sugiyama and M. Kitajima, *US Pat.*, 20150134255
- ¹¹² S. Sun, J. Song, Z. Shan and R. Feng, *J. Electroanal. Chem.*, 2012, **676**, 1-5
- ¹¹³ K. Fan, J. Song, J. Li, X. Guan, N. Tao, C. Tong. H. Shen and L. Niu, *J. Mater. Chem. C*, 2013, **1**, 7479-7482
- ¹¹⁴ R. Vegners, I. Shestakova, I. Kalvinsh, R. M. Ezzell and P. A. Janmey, *J. Pept. Sci.*, 1995, **1**, 371-378
- ¹¹⁵ Z. Yang and B. Xu, *Chem. Commun.*, 2004, 2424-2425
- ¹¹⁶ S. Fleming and R. V. Ulijn, *Chem. Soc. Rev.*, 2014, **43**, 8150-8177
- ¹¹⁷ (a) S. Debnath, A. Shome, D. Das and P. K. Das, *J. Phys. Chem. B*, 2010, **114**, 4407-4415; (b) D. M. Ryan, S. B. Anderson, F. T. Senguen, R. E. Youngman and B. L. Nilsson, *Soft Matter*, 2010, **6**, 475-479; (c) H. Zhang, H. Wang, G. Xu and S. Yuan, *Colloid. Surface. A*, 2013, **417**, 217-223
- ¹¹⁸ Y-Y. Xie, Y-W. Zhang, X-T. Qin, L-P. Liu, F. Wahid, C. Zhong and S-R. Jia, *Colloid. Surface. B.*, 2020, **193**, 111099
- ¹¹⁹ E. R. Draper, K. L. Morris, M. A. Little, J. Raeburn, C. Colquhoun, E. R. Cross, T. O. McDonald, L. C. Serpell and D. J. Adams, *CrystEngComm*, 2015, **17**, 8047-8057

- ¹²⁰ (a) S. Chen, A. Zhou, B. He, W. Zhao, X. Chen and D. Jiang, *Int. J. Mol. Med.*, 2017, **40**, 679-688; (b) M. Garton, S. Nim, T. A. Stone, K. E. Wang, C. M. Deber and P. M. Kim, *Proc. Natl. Acad. Sci. USA*, 2018, **115**, 1505-1510; (c) W. K. Restu, S. Yamamoto, Y. Nishida, H. Ienaga, T. Aoi and T. Maruyama, *Mater. Sci. Eng. C*, 2020, **11**, 110746
- ¹²¹ K. Basu, A. Baral, S. Basak, A. Dehsorki, J. Nanda, D. Bhunia, S. Ghosh, V. Castelletto, I. W. Hamley and A. Banerjee, *Chem. Commun.*, 2016, **52**, 5045-5048
- ¹²² (a) C. F. Thorn, C. Oshiro, S. Marsh, T. Hernandez-Boussard, H. McLeod, T. E. Klein and R. B. Altman, *Pharmacogenet. Genom.*, 2012, **21**, 440-446; (b) F. S. Carvalho, A. Burgeiro, R. Garcia, A. J. Moreno, R. A. Carvalho and P. J. Oliveira, *Med. Res. Rev.*, 2014, **34**, 106-135; (c) A. Pugazhendhi, T. N. J. I. Edison, B. K. Velmurugan, J. A. Jacob and I. Karuppusamy, *Life Sci.*, 2018, **200**, 26-30
- ¹²³ (a) W-F. Ma, K-Y. Wu, J. Tang, D. Li, C. Wei, J. Guo, S-L. Wang and C-C. Wang, *J. Mater. Chem.*, 2012, **22**, 15206-15214; (b) J. Zhu, L. Liao, X. Bian, J. Kong, P. Yang and B. Liu, *Small*, 2012, **8**, 2715-2720; (c) K-I. Joo, L. Xiao, S. Liu, Y. Liu, C-L. Lee, P. S. Conti, M. K. Wong, Z. Li, and P. Wang, *Biomaterials*, 2013, **34**, 3098-3109; (d) Q. Zeng, P. N. Prasad, B. A. Pfeifer and C. Cheng, *Langmuir*, 2014, **30**, 4111-4119; (e) N. Amreddy, R. Muralidharan, A. Babu, M. Mehta, E. V. Johnson. Y. D. Zhao, A. Munshi and R. Ramesh, *Int. J. Nanomed.*, 2015, **10**, 6773-6788
- ¹²⁴ (a) H. T. Ta, C. R. Dass, I. Larson, P. F. M. Choong and D. E. Dunstan, *Biomaterials*, 2009, **30**, 3605-3613; (b) M. Dadsetan, Z. Liu, M. Pumberger, C. V. Giraldo, T. Ruesink, L. Lu and M. J. Yaszemski, *Biomaterials*, 2010, **31**, 8051-8062; (c) L. Mei, K. Xu, Z. Zhai, S. He, T. Zhu and W. Zhong, *Org. Biomol. Chem.*, 2019, **17**, 3853-3860; (d) K. Baek, A. D. Noblett, P. Rena and L. J. Suggs, *Biomater. Sci.*, 2020, **8**, 3130-3137; (e) E. Gallo, C. Diaferia, E. Rosa, G. Smaldone, G. Morelli and A. Accardo, *Int. J. Nanomed.*, 2021, **16**, 1617-1630
- ¹²⁵ J. Naskar, G. Palui and A. Banerjee, *J. Phys. Chem. B*, 2009, **113**, 11787-11792
- ¹²⁶ G. M. Peters and J. T. Davis, *Chem. Soc. Rev.*, 2016, **45**, 3188-3206
- ¹²⁷ (a) I. Bang, *Biochem. Z.*, 1910, **26**, 293; (b) M. Gellert, M. N. Lipsett and D. R. Davis, *Proc. Natl. Acad. Sci. USA*, 1962, **48**, 2013-2018
- ¹²⁸ R. Iwauru, K. Yoshida, M. Masuda, K. Yase and T. Shimizu, *Chem. Mater.*, 2002, **14**, 3047-3053
- ¹²⁹ M. A. Ramin, L. Latxague, K. R. Sindhu, O. Chassande and P. Barthélémy, *Biomaterials*, 2017, **145**, 72-80
- ¹³⁰ (a) H. B. Bosmann and T. C. Hall, *Proc. Natl. Acad. Sci. USA*, 1974, **71**, 1833-1837; (b) S. D. Szajda, A. Jankowska and K. Zwierz, *Dis. Markers*, 2008, **25**, 233-242
- ¹³¹ (a) T. Legigan, J. Clarhaut, I. Tranoy-Opalinski, A. Monviosin, B. Renoux, M. Thomas, A. le Pape, S. Lerondel and S. Papot, *Angew. Chem. Int. Edit.*, 2012, **51**, 11606-11610; (b) T. Nishihara, S.

- Kuno, H. Nonaka, S. Tabata, N. Saito, S. Fukuda, M. Tomita, S. Sando and T. Soga, *Chem. Commun.*, 2018, **54**, 11745-11748; (c) Y. Wang, J. Liu, X. Ma, C. Cui, P. R. Deenik, P. K. P. Henderson, A. L. Sigler and L. Cui, *Sci. Rep.*, 2019, **9**, 2102
- ¹³² R. Tian, J. Chen and R. Niu, *Nanoscale*, 2014, **6**, 3474-3482
- ¹³³ H. Wang, L. Lv, G. Xu, C. Yang, J. Sun and Z. Yang, *J. Mater. Chem.*, 2012, **22**, 16933-16938
- ¹³⁴ P. K. Vemula, G. A. Cruikshank, J. M. Karp and G. John, *Biomaterials*, 2009, **30**, 383-393
- ¹³⁵ J. Nanda and A. Banerjee, *Soft Matter*, 2012, **8**, 3380-3386
- ¹³⁶ (a) FDA Inactive Ingredient Search for Approved Drug Products, <https://www.accessdata.fda.gov/scripts/cder/iig/index.cfm?event=BasicSearch.page>, (accessed June 2021); (b) I. Mitrus, A. Smagur, W. Fidyk, M. Czech, M. Prokop, A. Chwieduk, M. Glowala-Kosinska, T. Vzerw, M. Sobczyk-Kruszelnicka, W. Mendrek, K. Michalak, M. Sados-Wojciechowska, J. Najda, J. Holowieki and S. Giebel, *Bone Marrow Transpl.*, 2018, **53**, 274-280
- ¹³⁷ L. Zhang, Q. Jin and M. Liu, *Chem. Asian J.*, 2016, **11**, 2642-2649
- ¹³⁸ X. Dou, N. Mehwish, C. Zhao, J. Liu, C. Xing and C. Feng, *Accounts Chem. Res.*, 2020, **53**, 852-862
- ¹³⁹ D. Gambhir, S. Kumar, G. Dey, V. Krishnan and R. R. Koner, *Chem. Commun.*, 2018, **54**, 11407-11410
- ¹⁴⁰ G. Liu, X. Li, J. Sheng, P-Z. Li, W. K. Ong, S. Z. F. Phua, H. Agren, L. Zhu and Y. Zhao, *ACS Nano*, 2017, **11**, 11880-11889
- ¹⁴¹ M. Maity and U. Maitra, *Eur. J. Org. Chem.*, 2017, **2017**, 1713-1720
- ¹⁴² B. O. Okesola and A. Mata, *Chem. Soc. Rev.*, 2018, **47**, 3721-3736
- ¹⁴³ L. E. Buerkle and S. J. Rowan, *Chem. Soc. Rev.*, 2012, **41**, 6089-6102
- ¹⁴⁴ M. A. Ramin, K. R. Sindhu, A. Appavoo, K. Oumzil, M. W. Grinstaff, O. Chassande and P. Barthélémy, *Adv. Mater.*, 2017, **29**, 1605227
- ¹⁴⁵ G-F. Liu, W. Ji, W-L. Wang and C-L. Feng, *ACS. Appl. Mater. Interfaces*, 2015, **7**, 301-307
- ¹⁴⁶ M. D. Pierschbacher and E. Ruoslahti, *Nature*, 1984, **309**, 30-33
- ¹⁴⁷ (a) N. Sreenivasachary and J-M. Lehn, *Proc. Natl. Acad. Sci. USA*, 2005, **102**, 5938-5943; (b) J. Wu, L. Tang, K. Chen, L. Yan, F. Li and Y. Wang, *J. Colloid Interf. Sci.*, 2007, **307**, 280-287; (c) K. V. Rao, K. Jayaramulu, T. K. Maji and S. J. George, *Angew. Chem. Int. Edit.*, 2010, **49**, 4218-4222; (d) S. R. Nelli, J-H. Lin, T. N. A. Nguyen, D. T-H. Tseng, S. K. Talloj and H-C. Lin, *New J. Chem.*, 2017, **41**, 1229-1234; (e) S. R. Nelli, R. D. Chakravarthy, M. Mohiuddin and H-C. Lin, *RSC Adv.*, 2018, **8**, 14753-14759

- ¹⁴⁸ K. Hanabusa, T. Miki, Y. Taguchi, T. Koyama and H. Shirai, *J. Chem. Soc., Chem. Commun.*, 1993, 1382-1384
- ¹⁴⁹ M. Suzuki, Y. Makajima, M. Yumoto, M. Kimura, H. Shirai and K. Hanabusa, *Langmuir*, 2003, **19**, 8622-8624
- ¹⁵⁰ M. M. Smith, W. Edwards and D. K. Smith, *Chem. Sci.*, 2013, **4**, 671-676
- ¹⁵¹ C. B. Minkenberg, W. E. Hendriksen, F. Li, E. Mendes, R. Eelkema and J. H. van Esch, *Chem. Commun.*, 2012, **48**, 9837-9839
- ¹⁵² C. B. Minkenberg, F. Li, P. van Rijn, L. Florusse, J. Boekhoven, M. C. A. Stuart, G. J. M. Koper, R. Eelkema and J. H. van Esch, *Angew. Chem. Int. Edit.*, 2011, **50**, 3421-3424
- ¹⁵³ M. A. Khalily, M. Goktas and M. O. Guler, *Org. Biomol. Chem.*, 2015, **13**, 1983-1987
- ¹⁵⁴ (a) M. M. Green, M. P. Reidy, R. D. Johnson, G. Darling, D. J. O'Leary and G. Wilson, *J. Am. Chem. Soc.*, 1989, **111**, 6452-6554; (b) M. M. Green, B. A. Garetz, B. Munoz, H. P. Chang, S. Hoke and R. G. Cooks, *J. Am. Chem. Soc.*, 1995, **117**, 4181-4182; (c) P. Duan, H. Cao, L. Zhang and M. Liu, *Soft. Matter*, 2014, **10**, 5428-5448
- ¹⁵⁵ (a) P. Xing and Y. Zhao, *Acc. Chem. Res.*, 2018, **51**, 2324-2334; (b) B. Yue and L. Zhu, *Chem. Asian J.*, 2019, **14**, 2172-2180
- ¹⁵⁶ S. Zhang, S. Yang, J. Lan, S. Yang and J. You, *Chem. Commun.*, 2008, 6170-6172
- ¹⁵⁷ F. Rodríguez-Llansola, D. Hermida-Merino, B. Nieto-Ortega, F. J. Ramírez, J. T. López Navarrete, J. Casado, I. W. Hamley, B. Escuder, W. Hayes and J. F. Miravet, *Chem. Eur. J.*, 2012, **18**, 14725-14731
- ¹⁵⁸ Z. Shen, T. Wang and M. Liu, *Langmuir*, 2014, **30**, 10772-10778
- ¹⁵⁹ D. K. Smith, *Chem. Soc. Rev.*, 2009, **38**, 684-694
- ¹⁶⁰ (a) Z. Liu, J. Sun, Y. Zhang, Y. Wu, S. K. M. Nalluri, Y. Wang, A. Samanta, C. A. Mirkin, G. C. Schatz and F. J. Stoddart, *J. Org. Chem.*, 2016, **81**, 2581-2588; (b) D. A. Tomászon, D. Ghosh, Z. Kržišnik, L. H. Fasolin, A. A. Vincente, A. D. Martin, P. Thordarson and K. K. Damodaran
- ¹⁶¹ (a) A. R. Hirst, D. K. Smith, M. C. Feiters and H. P. M. Geurts, *Chem. Eur. J.*, 2004, **10**, 5901-5910; (b) Z. Yang, G. Liang, M. Ma, Y. Ga and B. Xu, *J. Mater. Chem.*, 2007, **17**, 850-854; (c) J-S. Shen, G-J. Mao, Y-H. Zhou, Y-Bao. Jiang and H-W. Zhang, *Dalton Trans.*, 2010, **39**, 7054-7058; (d) V. Singh, R. K. Rai, A. Arora, N. Sinha and A. K. Thakur, *Sci. Rep.*, 2014, **4**, 3875; (e) K. Nagy-Smith, P. J. Beltramo, E. Moore, R. Tycko, E. M. Furst and J. P. Schneider, *ACS Cent. Sci.*, 2017, **3**, 586-597
- ¹⁶² L. Wang, X. Jin, L. Ye, A-Y. Zhang, D. Bezuidenhout and Z-G. Feng, *Langmuir*, 2017, **33**, 13821-13827
- ¹⁶³ B. Sharma, A. Singh, T. K. Sarma, N. Sardana and A. Pal, *New J. Chem.*, 2018, **42**, 6427-6432

- ¹⁶⁴ C. Guilbaud-Chéreau, B. Dinesh, R. Schurhammer, D. Collin, A. Bianco and C. Ménard-Moyon, *ACS Appl. Mater. Inter.*, 2019, **11**, 13147-13157
- ¹⁶⁵ P. Dastidar, R. Roy, R. Parveen and K. Sarkar, *Adv. Ther.*, 2019, **2**, 1800061
- ¹⁶⁶ R. Parveen, B. Sravanthi and P. Dastidar, *Chem. Asian J.*, 2017, **12**, 792-803
- ¹⁶⁷ E. V. Alakpa, V. Jayawarna, K. E. V. Burgess, C. C. West, B. Péault, R. V. Ulijn and M. J. Dalby, *Sci. Rep.*, 2017, **7**, 6895
- ¹⁶⁸ D. J. Cornwell and D. K. Smith, *Mater. Horiz.*, 2015, **2**, 279-293
- ¹⁶⁹ J. Wang, Z. Wang, J. Gao, L. Wang, Z. Yang, D. Kong and Z. Yang, *J. Mater. Chem.*, 2009, **19**, 7892-7896
- ¹⁷⁰ V. M. P. Vieira, L. L. Hay and D. K. Smith, *Chem. Sci.*, 2017, **8**, 6981-6990
- ¹⁷¹ B. O. Okesola, S. K. Suravaram, A. Parkin and D. K. Smith, *Angew. Chem. Int. Edit.*, 2016, **55**, 183-187
- ¹⁷² P. Slavík, D. W. Kurka and D. K. Smith, *Chem. Sci.*, 2018, **9**, 8673-8681
- ¹⁷³ V. M. P. Vieira, A. C. Lima, M. de Jong and D. K. Smith, *Chem-Eur. J.*, 2018, **24**, 15112-15118
- ¹⁷⁴ P. R. A. Chivers and D. K. Smith, *Chem. Sci.*, 2017, **8**, 7218-7227
- ¹⁷⁵ P. R. A. Chivers and D. K. Smith, *Nat. Rev. Mater.*, 2019, **4**, 463-478
- ¹⁷⁶ P. R. A. Chivers, J. A. Kelly, M. J. S. Hill and D. K. Smith, *React. Chem. Eng.*, 2020, **5**, 1112-1117
- ¹⁷⁷ E. R. Draper and D. J. Adams, *Chem. Soc. Rev.*, 2018, **47**, 3395-3405
- ¹⁷⁸ A. Sarkar, R. Sasmal, C. Empereur-Mot, D. Bochicchio, S. V. K. Kompella, K. Sharma, S. Dhiman, B. Sundaram, S. S. Agasti, G. M. Pavan and S. J. George, *J. Am. Chem. Soc.*, 2020, **142**, 7606-7617
- ¹⁷⁹ (a) J. R. Moffat and D. K. Smith, *Chem. Commun.*, 2009, 316-318; (b) S. Onogi, H. Shigemitsu, T. Yoshii, T. Tanida, M. Ikeda, R. Kubota and I. Hamachi, *Nat. Chem.*, 2016, **8**, 743-752; (c) E. R. Draper, B. Dietrich and D. J. Adams, *Chem. Commun.*, 2017, **53**, 1864-1867
- ¹⁸⁰ (a) D. M. Ryan, T. M. Doran and B. L. Nilsson, *Langmuir*, 2011, **27**, 11145-11156; (b) C. Colquhoun, E. R. Draper, E. G. B. Eden, B. N. Cattoz, K. L. Morris, L. Chen, T. O. McDonald, A. E. Terry, P. C. Griffiths, L. C. Serpell and D. J. Adams, *Nanoscale*, 2014, **6**, 13719-13725
- ¹⁸¹ C. Diaferia, G. Morelli and A. Accardo, *J. Mater. Chem. B*, 2019, **7**, 5142-5155
- ¹⁸² K. L. Morris, L. Chen, J. Raeburn, O. R. Sellick, P. Contanda, A. Paul, P. C. Griffiths, S. M. King, R. K. O'Reilly, L. C. Serpell and D. J. Adams, *Nat. Commun.*, 2013, **4**, 848-852
- ¹⁸³ N. Singh, Z. Zhang, C. A. Angulo-Pachón, E. Mendes, J. H. van Esch and B. Escuder, *Chem. Sci.*, 2016, **7**, 5568-5572

- ¹⁸⁴ (a) F. Rodríguez-Llansola, J. F. Miravet and B. Escuder, *Chem. Commun.*, 2009, 7303-7305; (b) M. Fontanillo, C. A. Angulo-Pachón, B. Escuder and J. F. Miravet, *J. Colloid Interf. Sci.*, 2013, **412**, 65-71
- ¹⁸⁵ H. Shigemitsu, T. Fujisaku, W. Tanaka, R. Kubota, S. Minami, K. Urayama and I. Hamachi, *Nat. Nanotechnol.*, 2018, **13**, 165-172
- ¹⁸⁶ H. Komatsu, S. Matsumoto, S. Tamaru, K. Kaneko, M. Ikeda and I. Hamachi, *J. Am. Chem. Soc.*, 2009, **131**, 5580-5585
- ¹⁸⁷ C. Rendondo-Gómez, S. Padilla-Lopategui, H. S. Azevedo and A. Mata, *ACS Biomater. Sci. Eng.*, 2020, **6**, 4870-4880
- ¹⁸⁸ K. Fan, H. Kong, X. Wang, X. Yang and J. Song, *RSC Adv.*, 2016, **6**, 80934-80938
- ¹⁸⁹ J. Song, H. Sun, S. Sun and R. Feng, *Trans. Tianjin Univ.*, 2013, **19**, 319-325
- ¹⁹⁰ (a) J. Boekhoven, J. M. Poolman, C. Maity, F. Li, L. van der Mee, C. B. Minkenberg, E. Mendes, J. H. van Esch and R. Eelkema, *Nat. Chem.*, 2013, **5**, 433-431; (b) A. Baral, S. Basak, K. Basu, A. Dehsorkhi, I. W. Hamley and A. Banerjee, *Soft Matter*, 2015, **11**, 4944-4951
- ¹⁹¹ (a) J. Raeburn, G. Pont, L. Chen, Y. Cesbron, R. Lévy and D. J. Adams, *Soft Matter*, 2012, **8**, 1168-1174; (b) E. R. Draper, T. O. McDonald and D. J. Adams, *Chem. Commun.*, 2015, **51**, 6595-6597
- ¹⁹² V. J. Nebot and D. K. Smith, in *Functional Molecular Gels*, ed. B. Escuder and J. F. Miravet, RSC, Cambridge, 1st edn, 2013, ch. 2, pp. 30-66
- ¹⁹³ F. van de Manakker, L. M. J. Kroon-Batenburg, T. Vermonden, C. F. van Nostrum and W. E. Nennink, *Soft Matter*, 2010, **6**, 187-194
- ¹⁹⁴ R. W. Woody, *Methods Enzymol.*, 1995, **246**, 34-71
- ¹⁹⁵ D. J. Adams, *Gels*, 2018, **4**
- ¹⁹⁶ M. Adrian, J. Dubochet, J. Lepault and A. W. McDowell, *Nature*, 1984, **308**, 32-36
- ¹⁹⁷ N. Bhala, J. Emberson, *et al.*, *Lancet*, 2013, **382**, 769-779
- ¹⁹⁸ E. Sabadini, T. Cosgrove and F. do Carmo Egídio, *Carbohydr. Res.*, 2006, **341**, 270-274
- ¹⁹⁹ (a) I. Broutin, M. Ries-Kautt and A. Ducuix, *J. Appl. Crystallogr.*, 1995, **28**, 614-617, (b) C. Gripon, L. Legrand, I. Roseman, O. Vidal, M. C. Robert and F. Boué, *J. Cryst. Growth*, 1991, **177**, 238-247
- ²⁰⁰ M. Jelińska-Kazimierczuk and J. Szydlowski, *J. Solution Chem.*, 1996, **25**, 1175-1184
- ²⁰¹ M. V. C. Cardoso, L. V. C. Carvalho and E. Sabadini, *Carbohydr. Res.*, 2012, **353**, 57-61
- ²⁰² (a) F. Barbato, M. I. La Rotonda and F. Quaglia, *J. Pharm. Sci.*, 1997, **86**, 225-229; (b) F. Paesani, *Phys. Chem. Chem. Phys.*, 2011, **13**, 19865-19875; (b) T. Clark, J. Heske and T. D. Kühne, *ChemPhysChem.*, 2019, **20**, 2461-2465

- ²⁰³ B. Escuder, M. Llusar and J. F. Miravet, *J. Org. Chem.*, 2006, **71**, 7747-7752
- ²⁰⁴ F. Barbato, M. I. La Rotonda and F. Quaglia, *J. Pharm. Sci.*, 1997, **86**, 225-229
- ²⁰⁵ S. Audi, D. R. Burrage, D. O. Lonsdale, S. Pontefract, J. J. Coleman, A. W. Hitchings and E. H. Baker, *Br. J. Clin. Pharmacol.*, 2018, **84**, 2563-2571
- ²⁰⁶ S. Korani, M. Korani, S. Bahrami, T. P. Johnson, A. E. Butler, M. Banach and A. Sahebkar, *Drug Discov. Today*, 2019, **24**, 567-574
- ²⁰⁷ N. Xiang, X. Zhou, X. He, Y. Zhang, J. Zhang, Z-R. Zhang, X. Sun, T. Gong and Y. Fu, *J. Pharm. Sci.*, 2016, **105**, 1148-1155
- ²⁰⁸ H. Lennernäs, *Clin. Pharmacokinet.*, 2003, **42**, 1141-1160
- ²⁰⁹ A. D. Augst, H. J. Kong and D. J. Mooney, *Macromol. Biosci.*, 2006, **6**, 623-633
- ²¹⁰ B. B. Lee, P. Ravindra and E. S. Chan, *Chem. Eng. Technol.*, 2013, **36**, 1627-1642
- ²¹¹ (a) F. Chen, Z. Deng, Z. Zhang, R. Zhang, Q. Xu, G. Fan, T. Luo and D. J. McClements, *J. Food Eng.*, 2018, **238**, 156-163; (b) M. Fathi, Á. Martín and D. J. McClements, *Trends Food Sci. Tech.*, 2014, **39**, 18-39; (c) G. A. Martău, M. Mihai and D. C. Vodnar, *Polymers*, 2019, **11**, 1837; (d) K. F. C. De Silva, A. G. da Silva Carvalho, R. S. Rabelo and M. D. Hubinger, *Food Bioprod. Tech.*, 2019, **116**, 118-129
- ²¹² (a) H. H. Tønnesen and J. Karlsen, *Drug Dev. Ind. Pharm.*, 2002, **6**, 621-630; (b) D. Jain and D. Bar-Shalom, *Drug Dev. Ind. Pharm.*, 2014, **40**, 1576-1584; (c) R. G. Puscaselu, A. Lobiuc, M. Dimian and M. Covasa, *Polymers*, 2020, **12**, 2417 (d) R. A. Raus, W. M. F. W. Nawawi and R. R. Nasaruddin, *Asian J. Pharm. Sci.*, 2020, *In Press*; (d) C. C. Piras and D. K. Smith, *J. Mater. Chem. B.*, 2020, **8**, 8171-8188
- ²¹³ (a) X. Wang, E. Wenk, X. Zhang, L. Meinel, G. Vunjak-Novakovic and D. L. Kaplan, *J. Control. Release*, 2009, **134**, 81-90; (b) D. Wei, W. Xiao, J. Sun, M. Zhong, L. Guo, H. Fan and X. Zhang, *J. Mater. Chem. B.*, 2015, **3**, 2753-2763; (c) E. Quinlan, A. López-Noriega, E. M. Thompson, A. Hibbitts, S. A. Cryan and F. J. O'Brien, *J. Tissue Eng. Regen. M.*, 2017, **11**, 1097-1109; (d) J. P. Newsom, K. A. Payne and M. D. Krebs, *Acta Biomater.*, 2019, **88**, 32-41
- ²¹⁴ C. C. Piras, P. Slavík and D. K. Smith, *Angew. Chem. Int. Edit.*, 2020, **59**, 853-859
- ²¹⁵ (a) J. K. Oh, R. Drumright, D. J. Siegwart and L. Matyjaszewski, *Prog. Polymer Sci.*, 2008, **33**, 448-477; (b) X. Zhang, S. Malhotra, M. Marina and R. Haag, *Chem. Soc. Rev.*, 2015, **44**, 1948-1973; (c) H-Q. Wu and C-C. Wang, *Langmuir*, 2016, **32**, 6211-6225; (d) K.S. Soni, S. S. Desale and T. K. Bronich, *J. Control. Release*, 2016, **240**, 109-126; (e) G. Agrawal and R. Agrawal, *Small*, 2018, **14**, 1801724; (f) G. Choe, J. Park, H. Park and J. Y. Lee, *Polymers*, 2018, **10**, 997; (g) Y. Wang, L. Guo, S. Dong, J. Cui and J. Hao, *Adv. Colloid Interfac.*, 2019, **266**, 1-20; (h) X. Luo, P. Su, W. Zhang and C. L.

- Raston, *Adv. Mater. Technol.*, 2019, **4**, 1900488; (i) B. Kupikowska-Stobba and D. Lewińska, *Biomater. Sci.*, 2020, **8**, 1536-1574; (j) Y. Yin, B. Hu, X. Yuan, L. Cai, H. Gao and Q. Yang, *Pharmaceutics*, 2020, **12**, 290
- ²¹⁶ C. Echeverria, S. N. Fernandes, M. H. Godinho, J. P. Borges and P. I. P. Soares, *Gels*, 2018, **4**, 54
- ²¹⁷ C. C. Piras, A. G. Kay, P. G. Genever and D. K. Smith, *Chem. Sci.*, 2021, **12**, 3958-3965
- ²¹⁸ (a) P. S. Damus, M. Hicks and R. D. Rosenberg, *Nature*, 1973, **246**, 355-357; (b) M. Kim, Y. H. Kim and G. Tae, *Acta Biomater.*, 2013, **9**, 7833-7844; (c) M. Quade, S. Knaack, D. Weber, U. König, B. Paul, A. Rösen-Wolff, R. Schwartz-Albiez, M. Gelinsky and A. Lode, *Eur. Cells Mater.*, 2017, **33**, 105-120; (d) A. Maslow, A. Chambers, T. Cheves and J. Sweeney, *J. Cardiothor. Vasc. An.*, 2018, **32**, 1603-1608
- ²¹⁹ (a) D. J. Cornwell, B. O. Okesola and D. K. Smith, *Angew. Chem. Int. Edit.*, 2014, **53**, 12461-12465; (b) D.J. Cornwell, O. J. Daubney and D. K. Smith, *J. Am. Chem. Soc.*, 2015, **137**, 15486-15492; (c) V. M. P. Vieira, L. L. Hay and D.K. Smith, *Chem. Sci.*, 2017, **8**, 6981-6990;
- ²²⁰ C. C. Piras and D. K. Smith, *Chem-Eur. J.*, 2019, **25**, 11318-11326
- ²²¹ L. Schlichter, C. C. Piras and D.K. Smith, *Chem. Sci.*, 2021, **12**, 4162-4172
- ²²² (a) A. G. Olsson, J. Pears, J. McKellar, J. Mizen and A. Raza, *Am. J. Cardiol.*, 2001, **88**, 504-508; (b) C. I. Carswell, G. L. Plosker and B. Jarvis, *Drugs*, 2002, **62**, 2075-2085; (c) P. M. Ridker *et. Al.*, *New Engl. J. Med.*, 2009, **360**, 1851-1861
- ²²³ (a) C. M. White, *J. Clin. Pharmacol.*, 2002, **42**, 963-970; (b) M. B. Clearfield, J. Amerena, J-P. Bassand, H. R. Hernández García, S. S. Miller, F. F. M. Sosef, M. K. Palmer and B. S. Bryzinski, *Trials*, 2006, **7**, 35
- ²²⁴ L. P. Zeng, X. F. Liu, T. Yang, B. M. Zhao, and H. S. Tuo, *Pak. J. Pharm. Sci.*, 2018, **31**, 2203-2208
- ²²⁵ (a) H. K. Trivedi and M. C. Patel, *Sci. Pharm.*, 2012, **80**, 393-406; (b) M. Lopes Ângelo, F. de Lima Moreira, A. L. Morais Ruela, A. L. Araújo Santos, H. R. Nunes Salgado and M. B. de Araújo, *Crit. Rev. Anal. Chem.*, 2018, **48**, 317-329; (c) N. M. Sweed, A. M. Fayez, S. Z. El-Emam and M. H. S. Dawoud, *J. Pharm. Investig.*, 2021, **51**, 85-101
- ²²⁶ (a) B. Skoglund, C. Forslund and P. Aspenberg, *J. Bone Miner. Res.*, 2002, **17**, 2004-2008; (b) T. Fukui, M. Ii, T. Shoji, T. Matsumoto, Y. Mifune, Y. Kawakami, H. Akimaru, A. Kawamoto, T. Kuroda, T. Saito, Y. Tabata, R. Kuroda, M. Kurosaka and T. Asahara, *J. Bone Miner. Res.*, 2012, **27**, 1118-1131; (c) E. Roca-Millan, B. González-Navarro, K. Izquierdo-Gómez, A. Marí-Roig, E. Jané-Salas, J. López-López and E. Velasco-Ortega, *Materials*, 2019, **12**, 2992
- ²²⁷ (a) O. Lindy, K. Suomalainen, M. Mäkelä and S. Lindy, *BMC Oral Health*, 2008, **8**; (b) I. M. Gomes Estanislau, I. R. Colares Terceiro, M.R. Pontes Lisboa, P. de Barros Teles, R. de Sousa

- Carvalho, R. Souza Martins and M. M. S. Mendes Moreira, *Brit. J. Clin. Pharmacol.*, 2015, **79**, 877-885; (c) F. W. M. Gomes Muniz, K. Taminski, J. Cavagni, R. K. Celeste, P. Weidlich and C. K. Rösing, *Clin. Oral. Invest.*, 2018, **22**, 671-687; (d) C. Petit, F. Batool, I. M. Bugueno, P. Schwinté, N. Benkirane-Jessel and O. Huck, *Mediat. Inflamm.*, 2019 (e) E. Pająk-Łysek, M. Polak, G. Kopeć, M. Podolec, M. Desvarieux, A. Pająk and J. Zarzecka, *Int. J. Environ. Res. Public Health*, 2021, **18**, 770
- ²²⁸ E. L. Roehl and H. B. Tan, *US Pat.*, 4154816, 1979
- ²²⁹ A. U. Gutierrez, J. J. Albanese, R. J. Bianchini and S. L. Fantano, *US Pat.*, 5871720, 1997
- ²³⁰ M. Kauffmann, N. Gregoire and E. Quemin, *US Pat.*, 5286755, 1992
- ²³¹ T. D. Danielson, J. Rockwood and N. A. Mehl, *US Pat.*, 8653165, 2006
- ²³² W-C. Lai, *J. Phys. Chem. B*, 2011, **115**, 11029-11037
- ²³³ Y. Kawai, K. Sasagawa, M. Maki, H. Ueda, M. Miyamoto, *US Pat.*, 4314039A
- ²³⁴ Y. S. Oh, P. S. Junega, D. S. Connor, *US Pat.*, 5609855A
- ²³⁵ D. L. Dotson and W. A. Scrivens, *US Pat.*, 6121332, 1999
- ²³⁶ A. Gandini and M. N. Belgacem, *Prog. Polym. Sci.*, 1997, **22**, 1203-1379
- ²³⁷ R. Mariscal, P. Maireles-Torres, M. Ojeda, I. Sádaba and M. López Granados, *Energy Environ. Sci.*, 2016, **9**, 1144-1189
- ²³⁸ (a) S. L. Ruskin and R. C. Hockett, *US Pat.*, 2853495A, 1954; (b) P. Ciuffreda, A. Brizzolari, S. Casati, I. Eberini, L. Palazzolo, C. Parravicini and E. Santaniello, *Arkivoc*, 2016, 50-68
- ²³⁹ D. K. Smith, *Chem. Commun.*, 2018, **54**, 4743-4760
- ²⁴⁰ (a) Y. Miyako, N. Khalef, K. Matsuzaki and R. Pinal, *Int. J. Pharm.*, 2010, **393**, 48-54 (b) A. Grenier and D. N. Carrara, *WO Pat.*, 2014009241, 2014 (c) J. J. Hobson, S. Edwards, R. A. Slater, P. Martin, A. Owen and S. P. Rannard, *RSC Adv.*, 2018, **8**, 12984-12991
- ²⁴¹ C. Fruijtjer-Pöllth, *Toxicology*, 2005, **214**, 1-38
- ²⁴² G. C. Dizon, G. Atkinson, S. P. Argent, L. T. Santu and D. B. Amabilino, *Soft Matter*, 2020, **16**, 4640-4654
- ²⁴³ N. K. Whitelaw, PhD Thesis, University of York, 2016
- ²⁴⁴ B. K. Chun, R. F. Schinazi, Y-C. Cheng and C. K. Chu, *Carbohydr. Res.*, 2000, **328**, 49-59
- ²⁴⁵ D. L. Dotson, B. M. Burkhart, J. D. Anderson, J. R. Jones and S. R. Sheppard, *US Pat.*, 6555696, 2001
- ²⁴⁶ J. R. Jones, N. A. Mehl, *US Pat.*, 6495620, 2001
- ²⁴⁷ (a) J. Xu, J. Li, B. Bolt, K. Lake, J. Sprinkle, B. Burkhart and K. Keller, *US Pat.*, 2005, 20060173108; (b) C. Xie, J. Li and J. Xia, *US Pat.*, 2005, 20060079720

- ²⁴⁸ (a) X. Yan, P. Zhu and J. Li, *Chem. Soc. Rev.*, 2010, **39**, 1877-1890; (b) E. K. Johnson, D. J. Adams and P. J. Cameron, *J. Mater. Chem.*, 2011, **21**, 2024-2027; (c) X. Du, J. Zhou, J. Shi and B. Xu, *Chem. Rev.*, 2015, **115**, 13165-13307; (d) S. Mondal, S. Das and A. K. Nandi, *Soft Matter*, 2020, **16**, 1404-1454;
- ²⁴⁹ S. Datta and Bhattacharya, *Chem. Soc. Rev.*, 2015, **44**, 5596-5637
- ²⁵⁰ G. Gottarelij, S. Lena, S. Masiero, S. Pieraccini, G. P. Spada, *Chirality*, 2008, **20**, 471-485
- ²⁵¹ N. Sanabria-DeLong, S. K. Agrawal, S. R. Bhatia, G. N. Tew, *Macromolecules*, 2006, **39**, 1308-1310
- ²⁵² (a) J. Makarević, M. Jokić, Z. Raza, Z. Štefanić, B. Kojić-Prodić, M. Žinić, *Chem. -Eur. J.*, 2003, **9**, 5567-5580; (b) W. Edwards and D. K. Smith, *Gels*, 2018, **4**
- ²⁵³ G-F. Liu, D. Zhang, C-L. Feng, *Angew. Chem. Int. Edit.*, 2014, **53**, 7789-7793
- ²⁵⁴ G. Liang, Z. Yang, R. Zhang, L. Li, Y. Fan, Y. Kuang, Y. Gao, T. Wang, W. W. Lu and B. Xu, *Langmuir*, 2009, **25**, 8419-8422
- ²⁵⁵ H. Wang, Z. Feng, Y. Wang, R. Zhou, Z. Yang and B. Xu, *J. Am. Chem. Soc.*, 2016, **138**, 16046-16055
- ²⁵⁶ N. Mehwish, X. Dou, Y. Zhao and C-L. Feng, *Mater. Horiz.*, 2019, **6**, 14-44
- ²⁵⁷ (a) X. Li, X. Du, J. Li, Y. Gao, Y. Pan, J. Shi, N. Zhou and B. Xu, *Langmuir*, 2012, **28**, 13512-13517; (b) R. D. Mahapatra, J. Dey and R. G. Weiss, *Langmuir*, 2017, **33**, 12989-12999
- ²⁵⁸ S. Yamasaki, Y. Ohashi, H. Tsutsumi, K. Tsujii, *B. Chem. Soc. Jpn.*, 1995, **68**, 146-151
- ²⁵⁹ (a) X. Wang, H. Gan and T. Sun, *Adv. Funct. Mater.*, 2011, **21**, 3276-3281; (b) M. Zhang, G. Quing and T. Sun, *Chem. Soc. Rev.*, 2012, **41**, 1972-1984; (c) K. Lv, L. Zhang, W. Lu and M. Liu, *ACS Appl. Mater. Inter.*, 2014, **6**, 18878-18884
- ²⁶⁰ L. Steenkamp and D. Brady, *Enzyme Microb. Tech.*, 2003, **32**, 472-477; (b) B. Petrie and D. Camacho-Muñoz, *Environ. Chem. Lett.*, 2021, **19**, 43-75
- ²⁶¹ P. R. A. Chivers, PhD Thesis, University of York, 2019
- ²⁶² S. James, J. Fox, F. Afsari, J. Lee, S. Clough, C. Knight, J. Ashmore, P. Ashton, O. Preham, M. Hoogduijn, R. De Almeida Rocha Ponzoni, Y. Hancock, M. Coles and P. Genever, *Stem Cell Rep.*, 2015, **4**, 1004-1015
- ²⁶³ X. Yao, X. Wang and J. Dong, *Acta Biomater.*, 2021, **126**, 92-108
- ²⁶⁴ M. V. Lancaster and R. D. Fields, US Pat. 5501959, 1995
- ²⁶⁵ Alamar Blue Manual, https://tools.thermofisher.com/content/sfs/manuals/PI-DAL1025-1100_TI%20alamarBlue%20Rev%201.1.pdf, (accessed June 2021)

- ²⁶⁶ (a) T. Fulop, A. Larbi, J. M. Witkowski, J. McElhaney, M. Loed, A. Mitnitski and G. Pawelec, *Biogerontology*, 2010, **11**, 547-563; (b) E. Jaul and J. Barron, *Front. Public Health*, 2017, **5**, 335; (c) Y. G. Kang, E. Suh, J-W. Lee, D. W. Kim, K. H. Cho, C-Y. Bae, *Clin. Interv. Aging*, 2018, **13**, 429-436
- ²⁶⁷ A. Y. Chang, V. F. Skirbekk, S. Tyrovolas, N. J. Kassebaum and J. L. Dieleman, *Lancet Public Health*, 2019, **4**, 159-167
- ²⁶⁸ R. N. Rees, A. P. Acharya, A. Schrag and A. J. Noyce, *F1000 Faculty Rev.*, 2018, **7**
- ²⁶⁹ J-P. Bach, U. Ziegler, G. Deuschl, R. Dodel and G. Doblhammer-Reiter, *Movement Disord.*, 2011, **26**, 2286-2290
- ²⁷⁰ N. Afentou, J. Jarl, U-G Gerdtham and S. Saha, *Mov. Disord. Clin. Pract.*, 2019, **6**, 282-290
- ²⁷¹ S. Weir, M. Samnaliev, T-C. Kuo, T. S. Tierney, S. Walleser Auteiro, R. S. Taylor and A. Schrag, *Movement Disord.*, 2018, **33**, 974-981
- ²⁷² (a) S. Sveinbjornsdottir, *J. Neurochem.*, 2016, **139**, 318-324; (b) J. E. Throp, P. G. Adamczyk, H-L. Ploeg and K. A. Pickett, *Front. Neurol.*, 2018, **9**
- ²⁷³ (a) R. F. Pfeiffer, *Parkinsonism Relat. D.*, 2016, **22**, 119-122; (b) A. H. V. Schapira, K. R. Chaudhuri and P. Jenner, *Nat. Rev. Neurol.*, 2017, **18**, 435-450
- ²⁷⁴ O. S. Gershanik, *Movement Disord.*, 2015, **30**, 103-113
- ²⁷⁵ (a) D. Salat and E. Tolosa, *J. Parkinson. Dis.*, 2013, **3**, 255-269; (b) E. Bézard et al, *Prog. Neurobiol.*, 2015, **132**, 96-168
- ²⁷⁶ S-P Khor and A. Hsu, *Curr. Clin. Pharmacol.*, 2007, **2**, 234-243
- ²⁷⁷ (a) A. Lieberman, A. Goodgold, S. Jonas and M. Leibowitz, *Neurology*, 1975, **25**; (b) P. S. Leppert, M. Cortese and J. A. Fix, *Pharm. Res.*, 1988, **5**, 587-591; (c) M. Contin and P. Martinelli, *J. Neurol.*, 2010, **257**, 253-261; (d) P. A. LeWitt, *Movement. Disord.*, 2014, **30**, 64-72
- ²⁷⁸ R. R. Bowsher and D. P. Henry, in *Neurotransmitter Enzymes*, ed. A. A. Boulton, G. B. Baker and P. H. Yu, Humana Press, New Jersey, 1st Edn, 1986, ch. 2, pp. 33-78
- ²⁷⁹ C. Borri-Voltattorni, A. Minelli and P. Borri, *FEBS Lett.*, 1977, **75**, 277-280
- ²⁸⁰ E. A. Rudd, W. C. Cunningham and J. W. Thanassi, *J. Med. Chem.*, 1979, **22**, 233-237
- ²⁸¹ M. J. Jung, *Bioinorg. Chem.*, 1986, **14**, 439-443
- ²⁸² F. Daidone, R. Montioli, A. Paiardini, B. Cellini, A. Macchiarulo, G. Giardina, F. Bossa and C. Borri-Voltattorni, *PLoS One*, 2012
- ²⁸³ E. L. Lane, *Eur. J. Neurosci.*, 2018, **49**, 384-398
- ²⁸⁴ (a) D. Nyholm, S. Asberg, R. Bolsoey and M. Tutschke-Saettler, *US Pat.*, 0051459, 2008; (b) F. Amjad, D. Bhatti, T. L. Davis, O. Oguh, R. Pahwa, P. Kukreja, J. Zamudio and L. Verhagen Metman, *Adv. Ther.*, 2019, **36**, 2233-2246

- ²⁸⁵ M.Sensi, G. Cossu, F. Mancini, M. Pilleri, M. Zibetti, N. Modugno, R. Quatrala, F. Tamma and A. Antonini, *Parkinsonism Relat. D.*, 2017, **38**, 90-92
- ²⁸⁶ (a) J. G. Goldman and D. Weintraub, *Movement Disord.*, 2015, **30**, 1471-1489; (b) S. H. Fox, R. Katzenschlager, S-Y. Lim, B. Barton, R. M. A. de Bie, K. Seppi, M. Coelho and C. Sampaio, *Movement Disord.*, 2018, **33**, 1248-1266; (c) K. J. Nagao and N. J. Patel, *Drugs Context*, 2019, **8**, 212592; (d) A. Iarkov, G. E. Barreto, J. A. Grizzell and V. Echeverria, *Front. Aging Neurosci.*, 2020, **12**
- ²⁸⁷ (a) F. M. Menger, Y. Yamasaki, K. K. Catlin and T. Nishimi, *Angew. Chem. Int. Edit.*, 1995, **34**, 585-586; (b) J. Makarević, M. Jokić, B. Perić, C. Tomišić, B. Kojić-Prodić and M. Žinic, *Chem.-Eur. J.*, 2001, **7**, 3328-3341; (c) B. Escuder, M. Llusar and J. F. Miravet, *J. Org. Chem.*, 2006, **71**, 7747-7752
- ²⁸⁸ J. Swarbrick, *Clarke's Isolation and Identification of Drugs*, Pharmaceutical Press, London, 1986
- ²⁸⁹ (a) R. G. Thorne, C. R. Emory, T. A. Ala and W. H. Frey, *Brain Res.*, 1995, **692**, 278-282; (b) A. Mistry, S. Stolnik and L. Illum, *Int. J. Pharm.*, 2009, **379**, 146-157; (c) S. Gänger and K. Schindowski, *Pharmaceutics*, 2018, **10**, 116
- ²⁹⁰ (a) K. Hawkins, *PhD Thesis*, 2019; (b) K. Hawkins, A. K. Patterson, P. A. Clarke and D. K. Smith, *J. Am. Chem. Soc.*, 2020, **142**, 4379-4389
- ²⁹¹ A. R. Hirst and D. K. Smith, *Chem. -Eur. J.*, 2005, **11**, 5496-5508
- ²⁹² (a) M. Norouzi, B. Nazari and D. W. Miller, *Drug Discov. Today*, 2016, **21**, 1835-1849; (b) X. Zhao, H. Wu, B. Guo, R. Dong, Y. Qiu and P. X. Ma, *Biomaterials*, 2017, **122**, 34-47; (c) V. Pertici, C. Pin-Barre, C. Rivera, C. Pellegrino, J. Laurin, D. Gígmes and T. Trimaille, *Biomacromolecules*, 2019, **20**, 149-163
- ²⁹³ C. Menor-Salván and M. R. Marín-Yaseli, *Chem. Soc. Rev.*, 2012, **41**, 5404-5415
- ²⁹⁴ (a) R. S. Verma, R. C. Padalia, V. R. Singh, P. Goswami, A. Chauhan and B. Bhukya, *Int. J. Food Prop.*, 2017, **20**, 1259-1263; (b) A. M. Api et. al., *Food Chem. Toxicol.*, 2019, **134**, 110878
- ²⁹⁵ A. Andersen, *Int. J. Toxicol.*, 2006, **25**, 11-27
- ²⁹⁶ (a) E. R. Draper, L. L. E. Mears, A. M. Castilla, S. M. King, T. O. McDonald, R. Akhtar and D. J. Adams, *RSC Adv.* 2015, **5**, 95369-95378; (b) Y. Abidine, V. M. Laurent, R. Michel, A. Duperray, L. I. Palade and C. Verdier, *Europhys. Lett.*, 2015, **109**, 38003
- ²⁹⁷ S. Laham, B. Broxup, M. Robinet, M. Potvin and K. Schrader, *Am. Ind. Hyg. Assoc. J.*, 1991, **52**, 503-510
- ²⁹⁸ E. V. Brovč, J. Mravljak, R. Šink and S. Pajk, *Int. J. Pharm.*, 2020, **581**, 119285
- ²⁹⁹ Y. Zhang, B. Newton, E. Lewis, P. P. Fu, R. Kafoury, P. C. Ray and H. Yu, *Toxicol. in vitro*, 2015, **29**, 762-768

- ³⁰⁰ (a) L. Illum, *J. Control. Release*, 2003, **87**, 187-198; (b) C. V. Pardeshi and V. S. Belgamwar, *Expert. Opin. Drug. Del.*, 2013, **10**, 957-972; (c) P. P. Martins, H. D. C. Smyth and Z. Cui, *Int. J. Pharm.*, 2019, **570**, 118635
- ³⁰¹ (a) C. Prego, M. García, D. Torres and M. J. Alonso, 2005, **101**, 151-162; (b) A. Sosnik, J. das Neves and B. Sarmeto, *Prog. Polym. Sci.*, 2014, **39**, 2030-2075
- ³⁰² (a) S. V. Dhuria, L. R. Hanson and W. H. Frey, *J. Pharm. Sci.*, 2010, **99**, 1654-1673; (b) J. J. Lochhead and R. G. Thorne, *Adv. Drug. Deliver. Rev.*, 2012, **64**, 614-628
- ³⁰³ (a) Y. Fan, M. Chen, J. Zhang, P. Maincent, X. Xia and W. Wu, *Crit. Rev. Ther. Drug.*, 2018, **35**, 433-467; (b) M. Agrawal, S. Saraf, S. Saraf, S. G. Antimisiaris, M. B. Chougule, S. A. Shoyele and A. Alexander, *J. Control. Release*, 2018, **281**, 139-177
- ³⁰⁴ (a) D. R. Owens, B. Zinman and G. Bolli, *Diabetic Med.*, 2003, **20**, 886-898; (b) M. A. Reger, G. S. Watson, W. H. Frey, L. D. Baker, B. Cholerton, M. L. Keeling, D. A. Belongia, M. A. Fishel, S. R. Plymate, G. D. Schellenberg, M. M. Cherrier and S. Craft, *Neurobiol. Aging*, 2006, **27**, 451-458
- ³⁰⁵ U. Westin, E. Piras, B. Jansson, U. Bergdström, M. Dahlin, E. Brittebo and E. Björk, *Eur. J. Pharm. Sci.*, 2005, **24**, 565-573
- ³⁰⁶ Z-Z. Yang, Y-Q. Zhang, Z-Z. Wang, K. Wu, J-N. Lou and X-R. Qi, *Int. J. Pharm.*, 2013, **452**, 344-354
- ³⁰⁷ C. Schulz, K. Paulus, O. Jöhren and H. Lehnert, *Endocrinology*, 2012, **153**, 143-153
- ³⁰⁸ (a) S. Horvát, A. Fehér, H. Wolburg, P. Sipos, S. Veszelka, A. Tóth, L. Kis, A. Kurunczi, G. Balogh, L. Kürti, I. Erős, P. Szabó-Révész and M. A. Deli, *Eur. J. Pharm. Biopharm.*, 2009, **72**, 252-259; (b) R. Jain, S. Nabar, P. Dandekar and V. Patravale, *Pharm. Res.*, 2010, **27**, 655-664; (c) A. Bernkop-Schnürch and S. Dünnhaupt, *Eur. J. Pharm. Biopharm.*, 2012, **81**, 463-469; (d) G. Rassu, E. Soddu, M. Cossu, A. Brundu, G. Cerri, N. Marchetti, L. Ferraro, R. F. Regan, P. Giunchedi, E. Gavini and A. Dalpiaz, *J. Control. Release*, 2015, **201**, 68-77;
- ³⁰⁹ (a) B. Jansson, H. Hägerström, N. Fransén, K. Edsman and E. Björk, *Eur. J. Pharm. Biopharm.*, 2005, **59**, 557-564; (b) P. Mura, N. Mennini, C. Nativi and B. Richichi, *Eur. J. Pharm. Biopharm.*, 2018, **122**, 54-61
- ³¹⁰ (a) S. Charlton, N. S. Jones, S. S. Davis and L. Illum, *Eur. J. Pharm. Sci.*, 2007, **30**, 295-302; (b) C. Karavasili and D. G. Fatouros, *Drug Deliv. Today*, 2016, **21**, 157-166; (c) B. Viganì, S. Rossi, G. Sandri, M. C. Bonferoni, C. M. Caramella and F. Ferrari, *Pharmaceutics*, 2020, **12**, 859
- ³¹¹ P. Y. Gambaryan, I. G. Kondrasheva, E. S. Severin, A. A. Guseva and A. A. Kamensky, *Exp. Neurobiol.*, 2014, **23**, 246-252
- ³¹² Y. C. Wong and Z. Zuo, *Pharm. Res.*, 2010, **27**, 1208-1223

- ³¹³ A. Fortuna, G. Alves, A. Serralheiro, J. Sousa and A. Falcão, *Eur. J. Pharm. Biopharm.*, 2014, **88**, 8-27
- ³¹⁴ M. van Woensel, N. Wauthoz, R. Rosière, K. Amighi, V. Mathieu, F. Lefranc, S. W. van Gool and S. de Vleeschouwer, *Cancers*, 2013, **5**, 1020-1048
- ³¹⁵ B. Jansson and E. Björk, *J. Drug. Target.*, 2002, **10**, 379-386
- ³¹⁶ N. J. Johnson, L. R. Hanson and W. H. Frey, *Mol. Pharmaceuticals.*, 2010, **7**, 884-893
- ³¹⁷ B. A. Aderibigbe, *Pharmaceutics*, 2018, **10**, 40
- ³¹⁸ I. S. Brown, *J. Neurol. Surg. B. Skull. Base.*, 2016, **77**, 124-130
- ³¹⁹ J. J. Lochhead and T. P. Davis, *Pharmaceutics*, 2019, **11**, 598
- ³²⁰ S. Millecamps and J-P. Julien, *Nat. Rev. Neurosci.*, 2013, **14**, 161-176
- ³²¹ G. Pigino, G. Morfini, Y. Atagi, A. Deshpande, C. Yu, L. Jungbauer, M. LaDu, J. Busciglio and S. Brady, *P. Natl. Acad. Sci. USA*, 2009, **106**, 5907-5912
- ³²² (a) M. A. de Souza Silva, C. Mattern, R. Häcker, P. J. C. Nogueira, J. P. Huston and R. K. W. Schwarting, *J. Neurochem.*, 1997, **68**, 233-239; (b) T. K. Kim, W. Kang, I. K. Chun, S. Y. Oh, Y. H. Lee and H. S. Gwak, *Eur. J. Pharm. Sci.*, 2009, **38**, 525-532 (c) O. Y. Chao, C. Mattern, A. M. de Souza Silva, J. Weßler, L. A. Ruocco, S. Nikolaus and J. P. Huston and M. E. Pum, *Brain Res. Bull.*, 2012, **87**, 340-345